L^1-Minimization for Space Mechanics

Zheng Chen

NNT: 2016SACLS229

UNIVERSITÉ PARIS-SACLAY

École doctorale de mathématiques Hadamard (EDMH, ED 574)

Établissement d'inscription : Université Paris-Sud

Laboratoire d'accueil : Laboratoire de mathématiques d'Orsay, UMR 8628 CNRS

THÈSE DE DOCTORAT DE MATHÉMATIQUES

Spécialité : Mathématiques appliquées

Zheng CHEN

Minimisation $\mathbf{L}^1$ en Mécanique Spatiale

$\mathbf{L}^1$-Minimization for Space Mechanics

Date de soutenance : 14 Septembre 2016

Après avis des rapporteurs :

HEINZ SCHAETTLER (Washington University, USA)
DANIEL J. SCHEERES (University of Colorado, USA)

Jury de soutenance :

JÉRÔME BOLTE	Université Toulouse Capitole	Examinateur
JEAN-BAPTISTE CAILLAU	Université Bourgogne	Co-directeur de thèse
YACINE CHITOUR	Université Paris-Saclay	Co-directeur de thèse
FRÉDÉRIC LAGOUTIÈRE	Université Paris-Saclay	Co-directeur de thèse
FRANCESCO TOPPUTO	Politecnico di Milano (Italie)	Examinateur
EMMANUEL TRÉLAT	Université Pierre et Marie Curie	Président

Thèse préparée au

Département de Mathématiques d'Orsay

Laboratoire de Mathématiques d'Orsay (UMR 8628), Bât. 425

Université Paris-Sud

91405 Orsay Cedex

France

Résumé

En astronautique, une question importante est de contrôler le mouvement d'un satellite soumis à la gravitation des corps célestes de telle sorte que certains indices de performance soient minimisés (ou maximisés). Dans cette thèse, nous nous intéressons à la minimisation de la norme L^1 du contrôle pour le problème circulaire restreint des trois corps. Les conditions nécessaires à l'optimalité sont obtenues en utilisant le principe du maximum de Pontryagin, révélant l'existence de contrôles bang-bang et singuliers. En s'appuyant sur les résultats de Marchal [53] et Zelikin *et al.* [95, 96], la présence du phénomène de Fuller est mise en évidence par l'analyse des es extrêmales singulières.

La contrôlabilité pour le problème à deux corps (un cas dégénéré du problème circulaire restreint des trois corps) avec un contrôle prenant des valeurs dans une boule euclidienne est caractérisée dans le chapitre 2. Le résultat de contrôlabilité est facilement étendu au problème des trois corps puisque le champ de vecteurs correspondant à la dérive est récurrent. En conséquence, si les trajectoires contrôlées admissibles restent dans un compact fixé, l'existence des solutions du problème de minimisation L^1 peut être obtenu par une combinaison du théorème de Filippov (voir [2, chapitre 10], par exemple) et une procédure appropriée de convexification (voir, par exemple, [31]).

En dimension finie, le problème de minimisation L^1 est bien connu pour générer des solutions où le contrôle s'annule sur certains intervalles de temps. Bien que le principe du maximum de Pontryagin soit un outil puissant pour identifier les solutions candidates pour le problème de minimisation L^1, il ne peut pas garantir que ces candidats sont au moins localement optimaux sauf si certaines conditions d'optimalité suffisantes sont satisfaites. En effet, il est une condition préalable pour établir (et pour être capable de vérifier) les conditions d'optimalité nécessaires et suffisantes pour résoudre le problème de minimisation L^1. Dans cette thèse, l'idée cruciale pour obtenir de telles conditions est de construire une famille paramétrée d'extrémales telle que l'extrémale de référence peut être intégrée dans un champ d'extrémales. Deux conditions de non-pliage pour la projection canonique de la famille paramétrée d'extrémales sont proposées. En ce qui concerne le cas de points terminaux fixés, ces conditions de non-pliage sont suffisantes pour garantir que l'extrémale de référence est localement minimisante tant que chaque point de commutation est régulier (cf. chapitre 3). Si le point terminal n'est pas fixe mais varie sur une sous-variété lisse, une condition suffisante supplémentaire impliquant la géométrie de variété de cible est établie (cf. chapitre 4).

Bien que diverses méthodes numériques, y compris celles considérées comme directes [58, 79], indirectes [17, 18, 31], et hybrides [67], dans la littérature sont en mesure de calculer des solutions optimales, nous ne pouvons pas attendre d'un satellite piloté par le contrôle optimal précalculé (ou le contrôle nominal) de se déplacer sur la trajectoire optimale précalculée (ou trajectoire nominale) en raison de perturbations et des erreurs inévitables. Afin d'éviter de recalculer une nouvelle trajectoire optimale une fois que la déviation de la trajectoire nominale s'est produite, le contrôle de rétroaction optimale voisin, qui est probablement

l'application pratique la plus importante de la théorie du contrôle optimal [82, Chapitre 5], est obtenu en paramétrant les extrémales voisines autour de la nominale (cf. chapitre 5). Étant donné que la fonction de contrôle optimal est bang-bang, le contrôle optimal voisin comprend non seulement la rétroaction sur la direction de poussée, mais aussi celle sur les instants de commutation. En outre, une analyse géométrique montre qu'il est impossible de construire un contrôle optimal voisin une fois que le point conjugué apparaisse ou bien entre ou bien à des instants de commutation.

Mots clés : poussée faible, minimisation L^1, fuel-optimal, problème circulaire restreint des trois corps, problème aux deux corps, condition d'optimalité suffisante, points conjugués, points focaux, guide optimal voisin, contrôle de rétroaction optimal voisin.

Abstract

In astronautics, an important issue is to control the motion of a satellite subject to the gravitation of celestial bodies in such a way that certain performance indices are minimized (or maximized). In the thesis, we are interested in minimizing the L^1-norm of control for the circular restricted three-body problem. The necessary conditions for optimality are derived by using the Pontryagin maximum principle, revealing the existence of bang-bang and singular controls. Singular extremals are analyzed, and the Fuller phenomenon shows up according to the theories developed by Marchal [53] and Zelikin *et al.* [95, 96].

The controllability for the controlled two-body problem (a degenerate case of the circular restricted three-body problem) with control taking values in a Euclidean ball is addressed first (cf. Chapter 2). The controllability result is readily extended to the three-body problem since the drift vector field of the three-body problem is recurrent. As a result, if the admissible controlled trajectories remain in a fixed compact set, the existence of the solutions of the L^1-minimizaion problem can be obtained by a combination of Filippov theorem (see [2, Chapter 10], e.g.) and a suitable convexification procedure (see, e.g., [31]).

In finite dimensions, the L^1-minimization problem is well-known to generate solutions where the control vanishes on some time intervals. While the Pontryagin maximum principle is a powerful tool to identify candidate solutions for L^1-minimization problem, it cannot guarantee that these candidates are at least locally optimal unless sufficient optimality conditions are satisfied. Indeed, it is a prerequisite to establish (as well as to be able to verify) the necessary and sufficient optimality conditions in order to solve the L^1-minimization problem. In this thesis, the crucial idea for establishing such conditions is to construct a parameterized family of extremals such that the reference extremal can be embedded into a field of extremals. Two no-fold conditions for the canonical projection of the parameterized family of extremals are devised. For the scenario of fixed endpoints, these no-fold conditions are sufficient to guarantee that the reference extremal is locally minimizing provided that each switching point is regular (cf. Chapter 3). If the terminal point is not fixed but varies on a smooth submanifold, an extra sufficient condition involving the geometry of the target manifold is established (cf. Chapter 4).

Although various numerical methods, including the ones categorized as direct [58, 79], indirect [17, 18, 31], and hybrid [67], in the literature are able to compute optimal solutions, one cannot expect a satellite steered by the precomputed optimal control (or nominal control) to move on the precomputed optimal trajectory (or nominal trajectory) due to unavoidable perturbations and errors. In order to avoid recomputing a new optimal trajectory once a deviation from the nominal trajectory occurs, the neighboring optimal feedback control, which is probably the most important practical application of optimal control theory [82, Chapter 5], is derived by parameterizing the neighboring extremals around the nominal one (cf. Chapter 5). Since the optimal control function is bang-bang, the neighboring optimal control consists of not only the feedback on thrust direction but also that on switching times. Moreover, a geometric analysis shows that it is impossible to construct the neighboring optimal control

once a conjugate point occurs either between or at switching times.

Keywords: Low-thrust, L^1-minimization, fuel-optimal, circular restricted three-body problem, two-body problem, sufficient optimality conditions, conjugate points, focal points, neighboring optimal guidance, neighboring optimal feedback control.

Acknowledgments

I wish to offer my sincerest acknowledgements to my advisors, Prof. Jean-Baptiste Caillau and Prof. Yacine Chitour, for guiding me step by step into the field of geometric (optimal) control with their patience, time, and kindness, for their guidance and supports over the course of my Ph.D study, for taking care of a bunch of little things of a non-French speaker, and for many other things else. I would also like to express my gratitude to Prof. Frédéric Lagoutiere for his prompt assistance whenever administrative difficulties cropped up.

I would like to express my gratitude to Dr. Olivier Cots (INP-ENSEEIHT-IRIT, Toulouse) for his prompt assistance whenever I encountered numerical difficulties ; it would have been impossible to compute all the numerical examples of the thesis without his help. Thanks also to Prof. Frédéric Jean (ENSTA, Paris-Saclay) for his assistance in providing me with an office at the very beginning when I arrived in France.

Thanks to Prof. Shuo Tang (Northwestern Polytechnical University, China) for his kind supports on pursuing my Ph.D degree abroad and for his guidance on the engineering topics in these years.

I would like to thank Mr. Maxime Chupin (Jussieu, Paris) for providing me with some initial conditions of the numerical examples in this thesis. Thanks also to Mr. Bo Xia (Paris-Sud, Orsay) for his patience and time on discussing the basic concepts of differential geometry.

I would like to express a special appreciate to Xiaohua Guo ; this venture in France would not have succeeded without her. Last but not the least, I cannot thank my parents enough for being there for me, always !

Contents

List of Figures

List of Tables

Abbreviations

AMP	Accessory Minimum Problem
COE	Classical Orbital Elements
CRTBP	Circular Restricted Three-Body Problem
DOP	De-orbit Problem
ESA	European Space Agency
FOP	Fuel-optimal problem
GICC	Geocentric inertial Cartesian coordinate
HJB	Hamilton-Jacobi-Bellman
ICCF	Inertial Cartesian Coordinate Frame
JAXA	Japan Aerospace Exploration Agency
JNC	Jacobi necessary condition
MEOE	Modified Equinoctial Orbital Elements
NASA	National Aeronautics and Space Administration
NOG	Neighboring optimal guidance
ODE	Ordinary Differential Equation
OIP	Orbital Insertion Problem
OTP	Orbital Transfer Problem
PMP	Pontryagin maximum principle
STO	Space Trajectory Optimization

Introduction française

Ce travail s'intéresse au contrôle optimal appliqué à la mécanique spatiale. Plus précisément, la détermination de trajectoires à consommation minimale est considérée ; comme expliqué dans ce qui suit, cette fonction coût (la plus importante pour la conception de missions spatiales) se traduit en termes de norme L^1 du contrôle. Le manuscrit est organisé en six chapitres. Après un premier chapitre introductif rappelant notamment le modèle circulaire restreint pour le problème des trois corps, la question de la contrôlabilité est étudiée au chapitre deux ; de nouveaux résultats y sont donnés dans le cas où des contraintes d'état supplémentaires sont prises en comptes lors des manœuvres d'orbitation ou de désorbitation d'un engin spatial. Le chapitre trois est consacré à la définition de conditions suffisantes d'optimalité pour des extrémales brisées en contrôle optimal, telles celles apparaîssant en minimisation L^1. Un résumé de cette contribution, basé sur l'article "L^1-minimization for mechanical systems" paru dans *SIAM J. Control Optim.* **54** (2016), no. 3, 1245–1265 (Chen, Z. ; Caillau, J.-B. ; Chitour, Y.) est proposé ci-après. Le chapitre quatre étend ces résultats au cas d'extrémales dont la cible n'est plus ponctuelle mais définie par une sous-variété propre de l'ensemble d'état. L'avant-dernier chapitre applique ces techniques au calcul d'extrémales voisines en détaillant l'implémentation numérique associée. Le sixième et dernier chapitre donne en conclusion les pistes de recherche laissées ouvertes par ce travail. Trois annexes complètent le texte ; la première définit les éléments équinoxiaux utilisés pour décrire la dynamique d'un engin spatial dans le champ de gravité d'un corps céleste, la deuxième détaille les conditions suffisantes de type point conjugué dans le cas lisse, la dernière précisant la méthode de calcul des champs de Jacobi intervenant dans ces conditions d'optimalité.

$$\therefore$$

On considère le problème du contrôle optimal de systèmes mécaniques de la forme suivante :

$$\ddot{q}(t) + \nabla V(q(t)) = \frac{u(t)}{M(t)}\,, \quad \dot{M}(t) = -\beta|u(t)|,$$

où q est à valeurs dans un ouvert Q de $\mathbf{R}^m$, $m \geqslant 2$, sur lequel le potentiel V est défini. la deuxième équation décrit la variation de la masse M du système quand un contrôle est appliqué (β est une constante positive). La norme en dimension finie est euclidienne,

$$|u| = \sqrt{u_1^2 + \cdots + u_m^2},$$

et on a une contrainte sur le contrôle :

$$|u(t)| \leqslant \varepsilon, \quad \varepsilon > 0. \tag{0.1}$$

Étant données des conditions aux deux bouts dans l'espace d'état n-dimensionel $X := TQ \simeq Q \times \mathbf{R}^m$ ($n = 2m$), le problème qui nous intéresse est la minimisation de la consommation, c'est-à-dire la maximisation de la masse finale $M(t_f)$, le temps final t_f étant fixé. Cela revient à minimiser la norme L^1 du contrôle,

$$\int_0^{t_f} |u(t)| \, \mathrm{d}t \to \min . \tag{0.2}$$

À un facteur positif près, on a deux cas : $\beta = 1$ ou $\beta = 0$. Dans le second, la masse est constante ; bien qu'alors maximiser la masse finale n'ait plus de sens, le coût de Lagrange (0.2) reste bien défini. De fait, dans la mesure où le carburant ne représente qu'une fraction limitée de la masse totale, on peut attendre de ce modèle idéalisé "à masse constante" qu'il capture les principaux traits du problème de départ. On supposera donc $\beta = 0$ dans la suite, si bien que l'état se réduit au couple $x := (q, v)$ avec $v := \dot{q}$.

Il est connu qu'en dimension finie la minimisation ℓ^1 engendre des solutions parcimonieuses ayant un grand nombre de coordonnées nulles ; cette propriété se traduit ici par l'existence de sous-intervalles du temps sur lesquels le contrôle s'annule, comme on le voit immédiatement lorsqu'on applique le principe du maximum. Intuitivement, cela semble en accord avec l'objectif recherché de minimisation de la consommation : il existe des valeurs privilégiées de l'état en lesquelles le contrôle est plus efficace et doit être allumé (arcs de poussée), tandis qu'il en existe d'autres en lesquelles il doit être éteint (arcs balistiques). (Voir aussi [5] pour une interprétation d'un autre type dans un contexte biologique, à nouveau en minimisation L^1.) La parcimonie de la solution qui en résulte est ajustée par le ratio du temps final fixé sur le temps minimum associé aux conditions aux limites : alors qu'une conséquence immédiate de la forme de la dynamique (et de la contrainte de boule sur le contrôle) est qu'un contrôle temps minimum doit être de norme constante et maximale partout,[1] le temps additionnel disponible autorise une optimisation dont l'effet est l'apparition d'arcs à contrôle nul. (Voir la Proposition 1.) Une particularité notable de la dimension infinie est l'existence d'arcs dits arcs singuliers sur lesquels la norme du contrôle prend des valeurs intérieures à l'intervalle de variation prescrit. L'analyse de ce phénomène remonte au papier séminal de Robbins [78] dans le cas du potentiel des deux corps, exemple qui illustre l'interaction si fructueuse entre mécanique spatiale et contrôle optimal dans les premières années de la discipline. La conséquence du fait que ces arcs singuliers soient d'ordre deux a été plus tard appréhendée par Marchal qui a étudié le phénomène de chattering [53] ; cet exemple est probablement le second après celui, historique, de Fuller [30], et a ensuite été étudié en profondeur par Zelikin et Borisov [95, 96].

[1] Voir par exemple [20] ; cette propriété reste vraie en temps minimum à masse variable à condition que la masse finale soit laissée libre [*ibid*].

Un exemple caractéristique de système du deuxième ordre contrôlé est le problème circulaire restreint des trois corps [17] pour lequel, en notation complexe ($\mathbf{R}^2 \simeq \mathbf{C}$),

$$V_\mu(t,q) := -\frac{1-\mu}{|q+\mu e^{it}|} - \frac{\mu}{|q-(1-\mu)e^{it}|}.$$

Dans ce cas, μ est le ratio des masses des deux primaires en rotation uniforme autour de leur centre de masse. Le troisième corps, contrôlé, est un engin spatial gravitant dans le potentiel engendré par les deux primaires, mais qui n'influence pas leur mouvement. Quand $\mu = 0$, le potentiel est autonome et on retrouve le problème des deux corps contrôlé. L'étude des stratégies de commande "continues" (par opposition à impulsionnelles) remonte aux années 60 ; voir par exemple les travaux de Lawden [46], ou le livre de Beletsky [4] où l'importance de la poussée faible (ε dans (0.1)) pour "spiraler" depuis une orbite initiale avait été anticipée. Il y a actuellement un fort intérêt pour ces missions à poussée faible avec, par exemple, la mission Lisa Pathfinder [60] de l'ESA[2] vers le point de Lagrange L_1 du système Soleil-Terre, ou encore la mission BepiColombo [59] de l'ESA et de la JAXA[3] vers Mercure.

Une question importante en contrôle optimal est la capacité à vérifier des conditions suffisantes d'optimalité. En minimisation L^1, les premiers candidats sont les contrôles dont la norme est bang-bang, commutant de zéro à la borne prescrite par (0.1) (les situations plus riches incluant les contrôles singuliers.) Les conditions du second ordre dans le cas bang-bang ont été assez largement étudiées ; citons les travaux de Sarychev [81], suivis par [3] et [54, 64, 65]. Dans la même direction, la notion plus forte de "state optimality" a été introduite par [71] pour le temps final libre. Plus récemment, un procédé de régularisation a été développé dans [85] pour des systèmes mono-entrée. Ces références traitent du cas de contrôles à valeurs dans des polyhèdres ; les hypothèses qui y sont faites permettent de définir un problème accessoire dont les seules inconnues sont les instants de commutation. Il s'avère dans ce cas qu'une vérification de conditions du deuxième ordre sur ce problème auxiliaire suffit à garantir l'optimalité locale des contrôles bang-bang. Un corollaire de cette analyse est que les temps conjugués, en lesquels l'optimalité locale est perdue, doivent être des instants de commutation. Une approche différente, basée sur Hamilton-Jacobi-Bellman et la méthode des caracteristiques en contrôle optimal, est proposée par Noble et Schättler dans [63]. (Voir aussi la référence plus récente [82].) Leurs résultats incluent le cas des extrémales brisées, avec des points conjugués apparaîssant soit en des temps de commutations, soit entre ceux-ci. Nous obtenons des résultats similaires en étendant la condition de disconjugaison des champs de Jacobi aux extrémales brisées, et en utilisant plutôt un point de vue hamiltonien dans l'esprit des travaux [27, 45]. Remarquons que les travaux de Maurer et Osmolovskii couvrent également le cas de la minimisation L^1 avec encore une autre approche ; voir [66, Chap. 5] sur les problèmes de contrôle où une partie du contrôle intervient linéairement dans la dynamique. (La vérification numérique des conditions suffisantes passant alors par l'étude d'une équation de Riccati analogue à celle de [82].) Traiter le cas des extrémales brisées est crucial

[2] European Space Agency
[3] Japan Aerospace Exploration Agency

pour la minimisation L^1 : Dans la mesure où la norme sur le contrôle intervenant à la fois dans la contrainte (0.1) et dans le coût (0.2) est une norme ℓ^2 (définissant ainsi un problème de minimisation "L^1-ℓ^2"), le contrôle est astreint à prendre ses valeurs dans une boule euclidienne de $\mathbf{R}^m$, pas dans un polyhèdre dès que $m > 1$. Pour $m = 1$, la situation est dégénérée, et on peut par exemple poser $u = u_+ - u_-$, avec $u_+, u_- \geqslant 0$. (Cette approche est également possible pour $m > 1$ quand une norme ℓ^1 ou ℓ^∞ est utilisée pour les valeurs du contrôle ; voir par exemple [92].) Quand $m > 1$, il apparaît clairement en passant en coordonnées sphériques que nonobstant la possibilité pour la norme du contrôle d'être bang-bang, les variations des composantes sur $\mathbf{S}^{m-1}$ de ce contrôle empêchent une réduction à un problème d'optimisation en dimension finie. (La même remarque vaut pour toute norme ℓ^p sur les valeurs du contrôle avec $1 < p < \infty$.) Un exemple de conjugaison ayant lieu entre les instants de commutation (et non en ceux-ci) est donné dans les tests numériques.

Analyse des singularités du flot extrémal

Quitte à renormaliser le temps et le potentiel, on peut supposer $\varepsilon = 1$ dans (0.1), on considère donc le contrôle L^1-minimum de

$$\ddot{q}(t) + \nabla V(q(t)) = u(t), \quad |u(t)| \leqslant 1,$$

avec $x(t) = (q(t), v(t)) \in X = TQ$ ($v(t) = \dot{q}(t)$), Q étant un ouvert de $\mathbf{R}^m$ ($m \geqslant 2$), et on fait les hypothèses suivantes sur les conditions aux limites :

$$x(0) = x_0 \quad \text{et} \quad x(t_f) \in X_f \subset X$$

où (i) x_0 n'appartient pas à la variété cible X_f, (ii) X_f est invariante par le flot de la dérive,[4]

$$F_0(q, v) = v\frac{\partial}{\partial q} - \nabla V(q)\frac{\partial}{\partial v},$$

et (iii) le temps final fixé t_f est supposé strictement plus grand que le temps minimum $\bar{t}_f(x_0, X_f) < \infty$ du problème. Comme le coût n'est pas différentiable pour $u = 0$, plutôt que d'utiliser un principe du maximum non-lisse (voir par exemple [5]), on fait une désingularisation élémentaire : en coordonnées sphériques, $u = \rho w$ où $\rho \in [0, 1]$ et $w \in \mathbf{S}^{m-1}$; ce changement de coordonnées revient à ajouter une fibre $\mathbf{S}^{m-1}$ au dessus de la singularité $u = 0$ du coût. Dans ces variables, la dynamique s'écrit

$$\dot{x}(t) = F_0(x(t)) + \rho(t)\sum_{i=1}^{m} w_i(t) F_i(x(t))$$

[4] Cette hypothèse peut être affaiblie ; son seul objet est de garantir qu'un contrôle temps minimal prolongé par zéro au delà du temps min reste admissible. (Voir la Proposition 1.)

avec des champs de vecteurs $F_i = \partial/\partial v_i$, $i = 1, \dots, m$ canoniques, et un critère linéarisé :

$$\int_0^{t_f} \rho(t)\,\mathrm{d}t \to \min\,.$$

Le hamiltonien du problème est

$$H(x, p, \rho, w) = p^0\rho + H_0(x, p) + \rho \sum_{i=1}^{m} w_i \psi_i(x, p)$$

où $H_0(x, p) := pF_0(x)$ et où les $\psi_i(x, p) := pF_i(x)$ sont les relèvements hamiltoniens des F_i, $i = 1, \dots, m$. Clairement, $H \leqslant H_0 + \rho H_1$ avec

$$H_1 := p^0 + \sqrt{\sum_{i=1}^{m} \psi_i^2}\,,$$

et l'égalité peut toujours être atteinte en un certain $w \in \mathbf{S}^{m-1}$: $w = \psi/|\psi|$ si $\psi := (\psi_1, \dots, \psi_m)$ n'est pas nul, w quelconque sinon. En vertu du principe du maximum, si (ρ, w) est un contrôle mesurable minimisant, alors la trajectoire associée est la projection d'une courbe intégrale $(x, p) : [0, t_f] \to T^*X$ de $H_0 + \rho H_1$ telle que, presque partout,

$$H_0(x(t), p(t)) + \rho(t) H_1(x(t), p(t)) = \max_{r \in [0,1]} H_0(x(t), p(t)) + r H_1(x(t), p(t)). \tag{0.3}$$

De plus, la constante p^0 est négative et $(p^0, p) \neq (0, 0)$. Soit $p^0 = 0$ (cas anormal), soit p^0 peut être fixé à -1 par homogénéité (cas normal).

Proposition 1 (Gergaud *et al.* [31])**.** *Il n'y a pas d'extrémales anormales.*

On pose donc $p^0 = -1$, et $H_1 := |\psi| - 1$. À la différence du cas du temps minimum, la singularité $\psi = 0$ ne joue pas de rôle en minimisation L^1. Au voisinage de t tel que $\psi(t) = 0$, H_1 est negatif, aussi $\rho = 0$. Localement, le contrôle s'annule et l'extrémale est lisse. Le seul effet de la singularité est une discontinuité dans la fibre $\mathbf{S}^{m-1}$ au dessus de $u = 0$ dans laquelle $w(t+) = -w(t-)$ (voir [20]).

La singularité importante est $H_1 = 0$. Contrairement au cas mono-entrée classique, H_1 n'est pas le relèvement d'un champ de vecteurs sur X ; les propriétés du flot dépendent de H_0, H_1, et de leur crochets de Poisson. On note H_{01} le crochet $\{H_0, H_1\}$, ainsi de suite. Le résultat ci-après est classique (voir par exemple [10]) et traduit l'entrelacement d'arcs le long desquels $\rho = 0$ (arcs γ_0) avec des arcs tels que $\rho = 1$ (arcs γ_+).

Proposition 2. *Au voisinage de z_0 dans $\{H_1 = 0\}$ tel que $H_{01}(z_0) \neq 0$, toute extrémale est localement bang-bang de la forme $\gamma_0\gamma_+$ ou $\gamma_+\gamma_0$, selon le signe de $H_{01}(z_0)$.*

De tels points de commutation sont dits *réguliers* et sont étudiés dans ce qui suit à l'aide de conditions d'optimalité du second ordre. Outre l'existence d'arcs γ_0 traduisant le caractère parcimonieux des solutions, la particularité du problème de contrôle (vu comme un problème

d'optimisation en dimension infinie) est l'existence d'arcs singuliers le long desquels H_1 s'annule identiquement. Sur de tels arcs, ρ peut prendre des valeurs arbitraires entre $[0, 1]$.

Théorème 1 (Robbins [78])**.** *Les extrémales singulières sont d'ordre au moins deux, et les singulières minimisantes d'ordre deux sont contenues dans*

$$\{z = (q, v, p_q, p_v) \in T^*X \mid V''(q)p_v^2 \geqslant 0,\ V'''(q)p_v^3 > 0\}.$$

Corollaire 1. *Dans le cas du potentiel des deux corps $V(q) = -1/|q|$ $(q \neq 0)$, le long d'une singulière d'ordre deux on a soit $\alpha \in (\pi/2, \alpha_0]$, soit $\alpha \in [-\alpha_0, -\pi/2)$, où α est l'angle que fait le contrôle avec la direction radiale, et où $\alpha_0 = \operatorname{acos}(1/\sqrt{3})$.*

L'existence de singulières d'ordre deux dans le cas de deux corps a pour conséquence le phénomène de Fuller ou "chattering" [53, 95]. Le même phénomène persiste pour le problème circulaire restreint comme cela est expliqué dans [96]. Bien que ces extrémales singulières soient contenues dans une sous-variété de codimension > 1 de l'espace cotangent, leur présence est une obstruction à l'existence de bornes globales sur le nombre de commutations des extrémales régulières décrites par la Proposition 2. Le paragraphe suivant établit des conditions d'optimalité suffisantes pour ces extrémales bang-bang.

Conditions suffisantes pour des extrémales avec des commutations régulières

Soient X un ouvert de $\mathbf{R}^n$, U une partie non-vide de $\mathbf{R}^m$, f un champ de vecteur sur X parametrisé par $u \in U$, et $f^0 : X \times U \to \mathbf{R}$ une fonction coût, toutes ces données étant lisses. On considère le problème de minimisation à temps final fixé suivant : trouver $(x, u) : [0, t_f] \to X \times U$, x absolument continu, u mesurable et borné, tel que

$$\dot{x}(t) = f(x(t), u(t)), \quad t \in [0, t_f] \text{ (p.p.)},$$

$$x(0) = x_0, \quad x(t_f) = x_f,$$

et que

$$\int_0^{t_f} f^0(x(t), u(t))\,\mathrm{d}t$$

soit minimisée. Le principe du maximum assure que, si $(\overline{x}, \overline{u})$ est une telle paire, il existe un relèvement absolument continu $(\overline{x}, \overline{p}) : [0, t_f] \to T^*X$ et un scalaire négatif $\overline{p}^0$, $(\overline{p}^0, \overline{p}) \neq (0, 0)$, tels que presque partout sur $[0, t_f]$

$$\dot{\overline{x}}(t) = \frac{\partial H}{\partial p}(\overline{x}(t), \overline{p}(t), \overline{u}(t))\,, \quad \dot{\overline{p}}(t) = -\frac{\partial H}{\partial x}(\overline{x}(t), \overline{p}(t), \overline{u}(t))\,,$$

et

$$H(\overline{x}(t), \overline{p}(t), \overline{u}(t)) = \max_U H(\overline{x}(t), \overline{p}(t), \cdot)$$

où $H : T^*X \times U \to \mathbf{R}$ est le hamiltonien du problème,

$$H(x,p,u) := p^0 f^0(x,u) + pf(x,u).$$

On suppose tout d'abord que

(A0) L'extrémale de référence est normale.

On fixe en conséquence p^0 à -1. Soient $H_1, H_2 : T^*X \to \mathbf{R}$ deux fonctions lisses, et soient $\Sigma := \{H_1 = H_2\}$, $\Omega_1 := \{H_1 > H_2\}$ ($\Omega_2 := \{H_2 > H_1\}$, *resp.*) On fait l'hypothèse que

$$\max_U H(z,\cdot) = H_i, \quad z \in \Omega_i, \quad i = 1,2, \tag{0.4}$$

et on adopte le point de vue de [27] selon lequel ces deux hamiltoniens sont en "compétition". Soit $(\overline{x},\overline{p},\overline{u})$ une extrémale de référence ayant un seul point de contact avec Σ en $\overline{z}_1 := \overline{z}(\overline{t}_1)$, $\overline{t}_1 \in (0,t_f)$ ($\overline{z} := (\overline{x},\overline{p})$). On note $H_{12} = \{H_1,H_2\}$ le crochet de Poisson de H_1 avec H_2, et on fait l'hypothèse suivante :

(A1) $H_{12}(\overline{z}_1) > 0$.

Dans la terminologie de [45], $\overline{z}_1$ est un point de commutation *régulier* (ou *normal*). Cette condition est encore appelée *condition de Legendre bang-bang stricte* dans [3]. L'analyse ci-après s'étend de façon directe au cas d'une extrémale possédant un nombre fini de telles commutations.

Lemme 1. *$\overline{z}$ est le concatenation des flots de H_1 puis H_2.*

En conséquence de (A1), Σ est une sous-variété de codimension un au voisinage de $\overline{z}_1$, et on peut définir localement une fonction $z_0 \mapsto t_1(z_0)$ telle que $z_1(t_1(z_0),z_0)$ appartient à Σ pour z_0 dans un voisinage de $\overline{z}_0 := \overline{z}(0)$. Comme cela vient d'être fait, on notera

$$z_i(t,z_0) = e^{t\overrightarrow{H}_i}(z_0), \quad i = 1,2,$$

les flots hamiltoniens de H_1 et H_2. Dans un souci de simplicité, ces flots sont supposés complets. On note $' = \partial/\partial z$.

Lemme 2.

$$t_1'(z_0) = \frac{(H_1 - H_2)'}{H_{12}}(z_1(t_1(z_0),z_0))z_1'(t_1(z_0),z_0).$$

On définit localement $z_0 \mapsto z(t,z_0) = (x(t,z_0),p(t,z_0)) := z_1(t,z_0)$ si $t \leqslant t_1(z_0)$ et $z(t,z_0) := z_2(t - t_1(z_0), z_1(t_1(z_0),z_0))$ si $t \geqslant t_1(z_0)$.

Lemme 3. *Pour $t > t_1(z_0)$,*

$$\frac{\partial z}{\partial z_0}(t,z_0) = z_2'(t - t_1(z_0), z_1(t_1(z_0),z_0))(I + \sigma(z_0))z_1'(t_1(z_0),z_0)$$

avec

$$\sigma(z_0) = \overrightarrow{H_1 - H_2}\frac{(H_1 - H_2)'}{H_{12}}(z_1(t_1(z_0), z_0)). \tag{0.5}$$

La fonction

$$\delta(t) := \det \frac{\partial x}{\partial p_0}(t, \overline{z}_0), \quad t \neq \overline{t}_1, \tag{0.6}$$

est continue par morceaux le long de l'extrémale de référence, et on fait l'hypothèse additionnelle que

(A2) $\delta(t) \neq 0$, $t \in (0, \overline{t}_1) \cup (\overline{t}_1, t_f]$, et $\delta(\overline{t}_1+)\delta(\overline{t}_1-) > 0$.

Cette condition signifie qu'on suppose la disconjugaison sur $(0, \overline{t}_1]$ et $[\overline{t}_1, t_f]$ le long des flots linéarisés de H_1 et H_2, respectivement, et que le saut (encodé par la matrice $\sigma(z_0)$) des champs des Jacobi est tel qu'il n'y a pas de changement de signe du déterminant associé. Il s'agit précisément de la condition qu'on est capable de vérifier numériquement en calculant ces champs de Jacobi (voir par exemple [10, 18]). Géométriquement, cette hypothèse est une condition d'absence de singularité pli ("no-fold condition") [63, 82] (absence de pli en dehors $\overline{t}_1$, de pli "brisé" en $\overline{t}_1$).

Théorème 2. *Sous les hypothèses (A0)-(A2), la trajectoire de référence est un minimiseur $\mathscr{C}^0$-local parmi toutes les trajectoires avec les mêmes extrémités.*

En vertu de (A2), $\partial x_1/\partial p_0(t, \overline{z}_0)$ est inversible pour $t \in (0, \overline{t}_1]$; on peut donc construire une perturbation lagrangienne $\mathscr{L}_0$ transverse à la fibre $T^*_{x_0}X$ contenant $\overline{z}_0$ et telle que $\partial x_1/\partial z_0(t, \overline{z}_0)$ soit inversible pour $t \in [0, \overline{t}_1]$, $t = 0$ inclus, $\partial/\partial z_0$ dénotant les n dérivées partielles par rapport à $z_0 \in \mathscr{L}_0$. Pour $\varepsilon > 0$ assez petit, on définit

$$\mathscr{L}_1 := \{(t, z) \in \mathbf{R} \times T^*X \mid (\exists z_0 \in \mathscr{L}_0) : t \in (-\varepsilon, t_1(z_0) + \varepsilon) \text{ t.q. } z = z_1(t, z_0)\}.$$

Quitte à restreindre $\mathscr{L}_0$, $\Pi : \mathbf{R} \times T^*X \to \mathbf{R} \times X$, $(t, z) \mapsto (t, x)$ induit un difféomorphisme de $\mathscr{L}_1$ sur son image. De même, (A2) implique que

$$\frac{\partial}{\partial p_0}\left[x_2(t - t_1(z_0), z_1(t_1(z_0), z_0))\right]|_{z_0=\overline{z}_0}$$

est inversible pour $t \in [\overline{t}_1, t_f]$; quitte à restreindre à nouveau $\mathscr{L}_0$, on peut supposer que Π induit également un difféomorphisme de

$$\mathscr{L}_2 := \{(t, z) \in \mathbf{R} \times T^*X \mid (\exists z_0 \in \mathscr{L}_0) : t \in (t_1(z_0) - \varepsilon, t_f + \varepsilon)$$

$$\text{t.q. } z = z_2(t - t_1(z_0), z_1(t_1(z_0), z_0))\}$$

sur son image. On définit ensuite $\Sigma_1 := \mathscr{L}_1 \cap (\mathbf{R} \times \Sigma)$. Comme $(t, z_0) \mapsto (t, x_1(t, z_0))$ est un difféomorphisme de $\mathbf{R} \times \mathscr{L}_0$ sur $\Pi(\mathscr{L}_1)$, il existe une fonction réciproque $z_0(t, x)$ telle que $\Pi(\Sigma_1) = \{\psi = 0\}$ avec

$$\psi(t, x) := t - t_1(z_0(t, x)).$$

On note $\psi(t) := \psi(t, \overline{x}(t))$ l'évaluation de cette fonction le long de la trajectoire de référence. Par construction, $\dot{\psi}(\bar{t}_1-) = 1 > 0$ et (voir aussi [63])

$$\dot{\psi}(\bar{t}_1+) = 1 + \frac{\partial t_1}{\partial z_0}(\overline{z}_0) \left(\frac{\partial x_1}{\partial z_0}(\bar{t}_1, \overline{z}_0) \right)^{-1} \nabla_p (H_1 - H_2)(\overline{z}_1).$$

Lemme 4.

$$\delta(\bar{t}_1+) = \delta(\bar{t}_1-) \left(1 + \frac{\partial t_1}{\partial p_0}(\overline{z}_0) \left(\frac{\partial x_1}{\partial p_0}(\bar{t}_1, \overline{z}_0) \right)^{-1} \nabla_p (H_1 - H_2)(\overline{z}_1) \right). \tag{0.7}$$

Comme $\delta(\bar{t}_1+)$ et $\delta(\bar{t}_1-)$ ont le même signe, l'expression entre parenthèses dans (0.7) doit être positive. Par conséquent, $\dot{\psi}(\bar{t}_1+) > 0$ puisque $\mathscr{L}_0$ peut être choisi arbitraitement proche de $T^*_{x_0} X$. Localement donc, $\Pi(\Sigma_1)$ est une sous-variété qui sépare $\mathbf{R} \times X$ en deux et, en restreignant au besoin $\mathscr{L}_0$, toute extrémale du champ $t \mapsto x(t, z_0)$ avec $z_0 \in \mathscr{L}_0$ intersecte $\Pi(\Sigma_1)$ transversalement. En définissant

$$\mathscr{L}_1^- := \{(t, z) \in \mathbf{R} \times T^*X \mid (\exists z_0 \in \mathscr{L}_0) : t \in [0, t_1(z_0)] \text{ t.q. } z = z_1(t, z_0)\}$$

et

$$\mathscr{L}_2^+ := \{(t, z) \in \mathbf{R} \times T^*X \mid (\exists z_0 \in \mathscr{L}_0) : t \in [t_1(z_0), t_f]$$
$$\text{t.q. } z = z_2(t - t_1(z_0), z_1(t_1(z_0), z_0))\},$$

on peut recoller les restrictions de Π à $\mathscr{L}_1^-$ et $\mathscr{L}_2^+$ en une bijection continue de $\mathscr{L}_1^- \cup \mathscr{L}_2^+$ sur $\Pi(\mathscr{L}_1^- \cup \mathscr{L}_2^+)$. En se restreignant à un voisinage compact du graphe de $\overline{z}$, on peut supposer que Π induit un homéomorphisme sur son image. (Voir Figure 0.1.) La fin de la preuve utilise les résultats classiques d'exactitude de la forme de Poincaré-Cartan convenablement restreinte en les étendant au cas d'extrémales brisées à l'aide du lemme ci-après :

Lemme 5.

$$I + \sigma(z_0) \in \mathrm{Sp}(2n, \mathbf{R}).$$

Application au potentiel des deux corps

Suivant [31], on considère le contrôle du problème des deux corps en dimension trois. À énergie strictement négative, les orbites du mouvement libre sont des ellipses, et le but est de réaliser un transfert à consommation minimale entre orbites non-coplanaires autour d'un centre de masse fixe. Le potentiel $V(q) := -\mu/|q|$ est défini sur $Q := \{q \in \mathbf{R}^3 \mid q \neq 0\}$, et on se restreint en fait à

$$X := \{(q, v) \in TQ \mid |v|^2/2 - \mu/|q| < 0,\ q \wedge v > 0\}.$$

(La dernière condition sur le moment cinétique permet d'éviter les trajectoires de collision et oriente les orbites elliptiques.) La constante μ est la constante gravitationnelle qui dépend

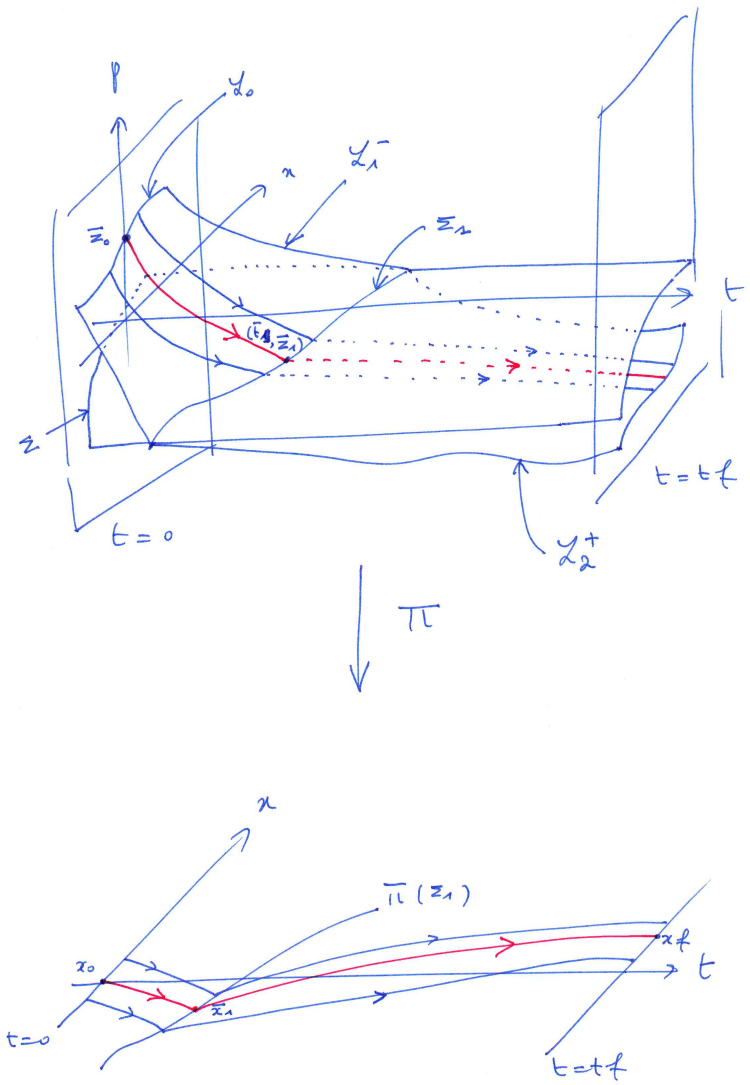

FIGURE 0.1 – Le champ d'extrémales.

du corps attracteur. Pour plus de clarté, deux transferts à poussées moyennes sont présentés ; le temps final est fixé à 1.6 fois le temps min (cas A), ou à 1.3 fois le temps min (cas B), approximativement, ce qui assure déjà un gain satisfaisant de consommation [31]. Afin d'avoir des extrémités fixées pour faire un test de point conjugué selon notre approche, les positions initiales et finales sur les orbites sont fixées (on fixe les longitudes[5]) initiales et finales). Un traitement plus réaliste consisterait à laisser libre la longitude finale ; cela demanderait de réaliser un test de point focal assez semblable (voir par exemple [18]). Les tableaux 1 et 2 résument les valeurs utilisées pour l'application numérique.

Comme expliqué précédemment, la minimisation L^1 correspond à la minimisation de la consommation pour un modèle idéal à masse constante. On a une compétition entre deux ha-

[5]La longitude l est définie comme la somme de trois angles brisés : $l = \Omega + \theta + \varpi$, où Ω est la longitude du nœud ascendant (premier angle d'Euler entre le plan de l'orbite avec le plan équatorial ; le deuxième angle d'Euler définit l'inclinaison de l'orbite), θ est l'argument du perigée (angle du demi-grand axe de l'ellipse, égal au troisième angle d'Euler du plan de l'orbite), et ϖ est l'anomalie vraie (angle polaire par rapport au demi-grand axe dans le plan de l'orbite). Ici, $\Omega = 0$ sur les orbites initiales et finales.

TABLE 1 – Cas A. Valeurs numériques utilisées pour le calcul.

Constante gravitationnelle μ de la Terre :			398600.47 Km^{3}s^{-2}
Masse de l'engin spatial :	1500 Kg	Poussée :	20 Newtons
Périgée initial :	6643 Km	Périgée final :	42165 Km
Apogée initial :	46500 Km	Apogée final :	42165 Km
Inclinaison intiale :	56 deg	Inclinaison finale :	0 deg
Longitude initiale :	π rad	Longitude finale :	56.659 rad
Temps minimum :	93.865 heures	Temps final fixé :	147.28 heures
L^1 Coût (normalisé) obtenu :			52.638

miltoniens : H_0 (qui provient de la dérive seule) et $H_0 + H_1$ (en supposant que la borne sur le contrôle est normalisée par une homothétie appropriée). Les deux hamiltoniens sont lisses de sorte qu'on est dans le bon cadre pour vérifier des conditions suffisantes d'optimalité. On se restreint aux extrémales bang-bang (en la norme du contrôle) ; la régularité des commutations est aisément vérifiable numériquement, tandis que la normalité des extrémales provient de la Proposition 1. Reste a vérifier la condition de disconjugaison sur les champs de Jacobi. Les solutions optimales (voir Figs. 0.2 et 0.4) et ces champs sont calculés à l'aide du code `hampath` [86]. À l'instar de [18, 31], une régularisation par homotopie est mise en œuvre pour capturer la structure de commutation et initialiser le calcul des extrémales bang-bang par une méthode de tir. On est alors capable de vérifier la condition (A2) par un simple test de signe (tenant compte des sauts sur les champs de Jacobi en les instants de commutations régulières) sur le déterminant de ces champs (voir Figures 0.3 et 0.5). Une alternative serait d'établir un résultat de convergence analogue à [85] puis de vérifier des conditions du second ordre sur les extrémales régularisées. Comme on l'a précédemment souligné, les temps conjugués peuvent apparaî tre soit entre deux instants de commutation, soit en ces instants. Sur les exemples traités, aucun point conjugué n'est détecté sur $[0, t_f]$, ce qui garantit l'optimalité locale forte des trajectoires calculées. Les extrémales sont prolongées jusqu'à $2\,t_f$ dans le cas A (*resp.* jusqu'à $3.5\,t_f$ dans le cas B), et un point conjugué est détecté vers $1.1\,t_f$ dans le cas A (*resp.* $3.2\,t_f$ dans le cas B), à chaque fois en un instant de commutation (le changement de signe du déterminant a lieu à la discontinuité). Un test sur une perturbation du cas B est proposé Figure 0.6 ; en changeant légèrement les conditions terminales, on observe une conjugaison intervenant non plus en un temps de commutation, mais le long d'un arc de poussée.

Remarque 1. Dans la mesure où H_0 est le relèvement d'un champ de vecteurs, le déterminant des champs de Jacobi est soit identiquement nul, soit sans zéro le long d'un arc balistique ($\rho = 0$). (Comparer au cas d'un ensemble de contrôle polyhédral ; voir aussi le Corollaire 3.9

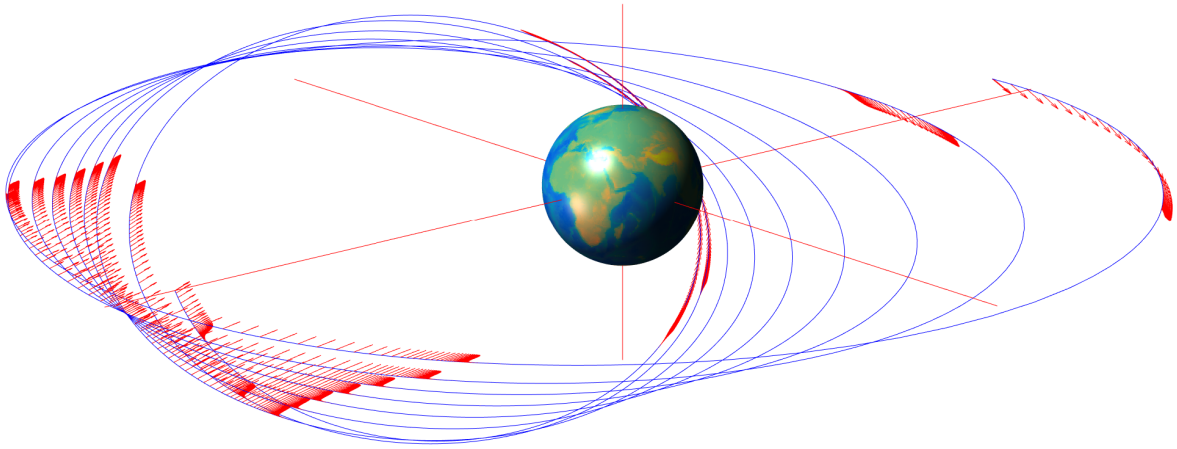

FIGURE 0.2 – Cas A. Trajectoire L^1-minimale. La figure montre la trajectoire (en bleu), ainsi que l'action du contrôle (en rouge). L'orbite initiale est fortement excentrique (0.75) et fortement inclinée $(56$ degrés). La cible géostationnaire est atteinte en $t_f \simeq 147.28$ heures. La structure creuse du contrôle est bien observée, avec des arcs de poussée concentrés autour des périgées et apogées (voir [31]). La minimisation permet de ne pousser que 35% du temps.

TABLE 2 – Cas B. Valeurs numériques utilisées pour le calcul.

Constante gravitationnelle μ de la Terre :			398600.47 Km^3s^{-2}
Masse de l'engin spatial :	1500 Kg	Poussée :	10 Newtons
Périgée initial :	6643 Km	Périgée final :	42165 Km
Apogée initial :	46500 Km	Apogée final :	42165 Km
Inclinaison initiale :	7 deg	Inclinaison finale :	0 deg
Longitude initiale :	π rad	Longitude finale :	56.659 rad
Temps minimum :	110.41 heures	Temps final fixé :	147.28 heures
L^1 Coût (normalisé) obtenu :			67.617

dans [63].) De plus, la dérive F_0 est le gradient symplectique d'une fonction d'énergie,

$$E(q,v) := \frac{1}{2}|v|^2 + V(q).$$

Par conséquent, la coordonnée $\delta x = (\delta q, \delta v)$ du champ de Jacobi le long d'une intégrale de $\overrightarrow{H}_0$ est solution de

$$\delta\dot{x}(t) = \overrightarrow{E}'(\overline{x}(t))\delta x(t),$$

de sorte que δx a un déterminant constant le long d'un tel arc puisque le flot associé est symplectique. En particulier, la condition de disconjugaison (A2) implique que la solution optimale débute par un arc de poussée.

FIGURE 0.3 – Cas A. Test de point conjugué sur l'extrémale bang-bang prolongée sur $[0, 2\,t_f]$. La valeur du déterminant des champs de Jacobi (0.6) le long de l'extrémale est représentée en fonction du temps. Le premier point conjugué apparaî t à $t_{1c} \simeq 171.20$ heures $> t_f$; on en déduit l'optimalité locale sur $[0, t_f]$ de l'extrémale de référence. Des sauts sur les champs de Jacobi sont observés en chaque instant de commutation, et la conjugaison a lieu en une commutation (changement de signe du déterminant).

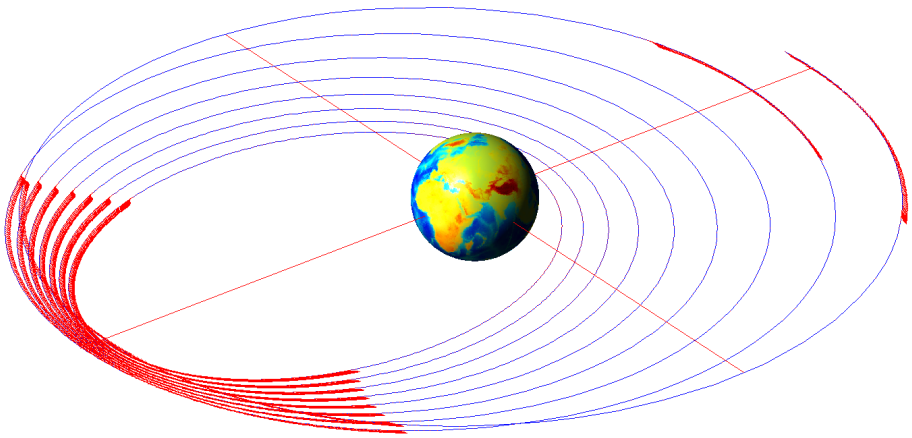

FIGURE 0.4 – Cas B. Trajectoire L^1 minimale. La figure montre la trajectoire (en bleu), ainsi que l'action du contrôle (en rouge). L'orbite initiale est fortement excentrique (0.75) et faiblement inclinée (7 degrés). La cible géostationnaire est atteinte en $t_f \simeq 147.28$ heures. La structure creuse du contrôle est clairement observée, avec des arcs de poussée à nouveau concentrés autour des périgées et apogées. La minimisation permet de ne pousser que 46% du temps. Ce pourcentage est supérieur à celui du cas A (voir Figure 0.2), ce qui est cohérent avec le fait que la ratio temps final fixé sur temps minimum est diminué dans le cas B.

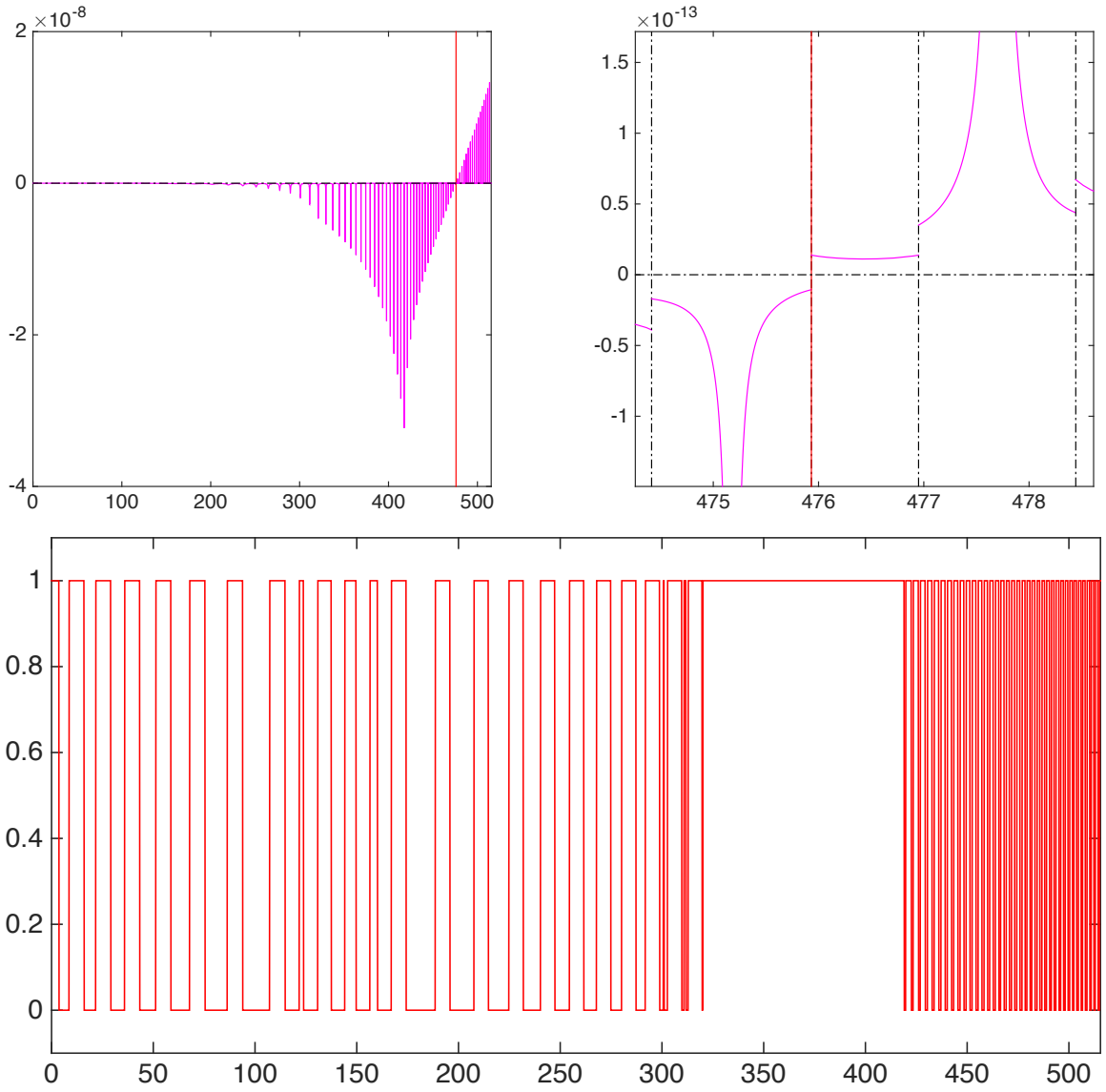

FIGURE 0.5 – Cas B. Test de point conjugué sur l'extrémale bang-bang prolongée sur $[0, 3.5t_f]$. La valeur du déterminant des champs de Jacobi (0.6) le long de l'extrémale est représentée en fonction du temps sur le graphe en haut à gauche. Le premier point conjugué apparaît à $t_{1c} \simeq 475.93$ heures $> t_f$; l'optimalité locale de l'extrémale de référence sur $[0, t_f]$ s'ensuit. Sur le graphe en haut à droite, un zoom permet de voir les sauts sur les champs de Jacobi (et donc sur leur déterminant) autour du premier temps conjugué ; plusieurs sauts sont observés, le premier conduisant à un changement de signe en l'instant de commutation. D'après la Remarque 1, le déterminant doit être constant le long des arcs balistiques ($\rho = 0$) quand les coordonnées symplectiques $x = (q, v)$ sont utilisées ; ce n'est pas le cas ici où les éléments équinoxiaux [20] sont employés pour l'état — d'où les légères variations du déterminant. La norme bang-bang du contrôle, rescalé pour appartenir à $[0, 1]$ puis prolongé jusqu'à $3.5\, t_f$, est représentée sur le graphe du dessous. Sur l'intervalle de temps étendu, on observe déjà plus de 70 commutations alors que la poussée est simplement moyenne. Dans le cas de poussées faibles, des centaines de commutation ont lieu.

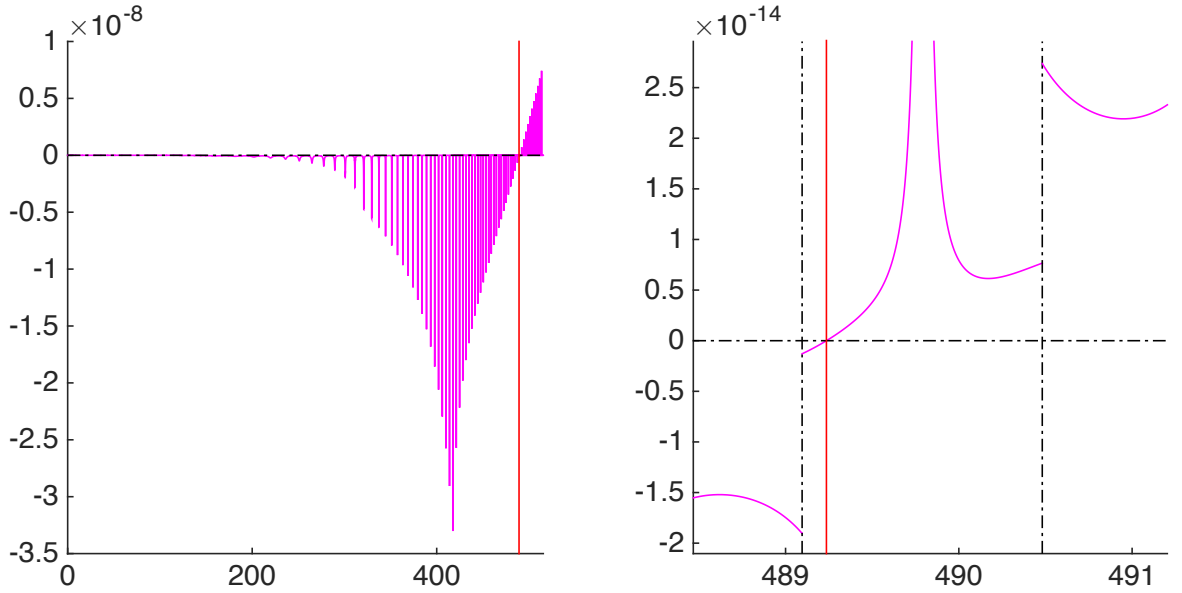

FIGURE 0.6 – Cas B (après perturbation). Test de point conjugué sur l'extrémale bang-bang prolongée sur $[0, 3.5\,t_f]$. La valeur du déterminant des champs de Jacobi (0.6) le long de l'extrémale est représentée en fonction du temps (détails sur le graphe en bas à droite). Les conditions aux deux bouts x_0, x_f données Tab. 2 sont perturbées selon $x \leftarrow x + \Delta x$, $|\Delta x| \simeq 1e-5$, conduisant à observer un point conjugué non pas en un instant de commutation mais entre deux instants de commutation — le long d'un arc de poussée ($\rho = 1$). Le premier temps conjugué intervient en $t_{1c} \simeq 489.23$ heures $> t_f$, garantissant à nouveau l'optimalité locale de l'extrémale de référence sur $[0, t_f]$.

Chapter 1

Introduction and preliminaries

1.1 Definitions and notations

1.1.1 Circular restricted three-body problem

In celestial mechanics, the three-body problem is a classical problem of predicting the individual motions of celestial bodies interacting with one another gravitationally. Once one body is light enough such that its influence on the other two is negligible, it is called the restricted three-body problem. Furthermore, once the two massive bodies move on circular orbits around their common center of mass, it is called the circular restricted three-body problem (CRTBP). Therefore, the CRTBP is an isolated dynamical system consisting of three gravitationally interacting bodies. Let P_1, P_2, and P_3 be the three bodies (considered as mass points) and denote their mass by m_1, m_2, and m_3, respectively. Then the following two properties hold:

1) the third mass m_3 is so small that its gravitational influence on the motions of the other two is negligible;

2) the two primaries, P_1 and P_2, move on circular orbits around their common center of mass.

Without loss of generality, we assume $m_1 > m_2$. Let us consider a rotating frame *OXYZ* whose origin is located at the barycenter of the two bodies P_1 and P_2 (see Fig. 1.1). The X-axis is oriented by the axis between the two primaries P_1 and P_2 and points toward P_2; the Z-axis is defined by the momentum vector of the motion of P_1 and P_2, and the Y-axis is defined to complete a right-hand coordinate system.

We consider that the third body is an artificial satellite or a spacecraft. It is advantageous to use non-dimensional parameters. Let us denote the distance between P_1 and P_2 by $d_* > 0$ and the initial mass of a spacecraft by $m_* > 0$. We then denote by d_* and m_* the unit of length and mass, respectively. We also define the unit of time $t_* > 0$ in such a way that the

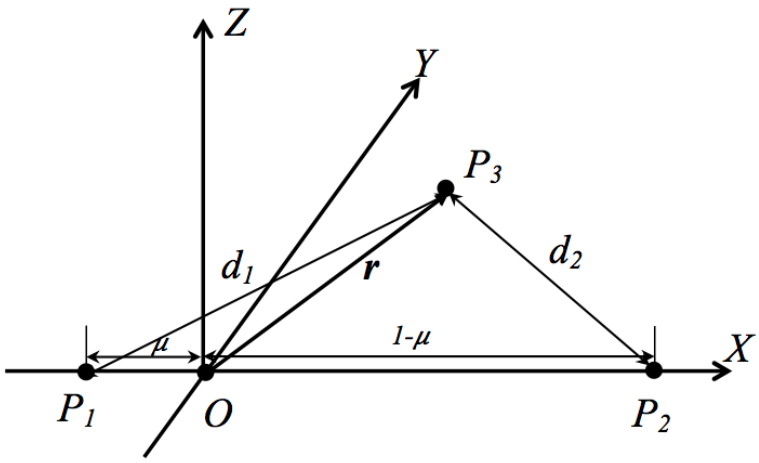

Figure 1.1 – Rotating frame *OXYZ* of the CRTBP.

gravitational constant $G > 0$ is equal to one. Accordingly, one can obtain

$$t_* = \sqrt{\frac{d_*^3}{G(m_1 + m_2)}}$$

according to Kepler's third law. If $\mu := m_2/(m_1 + m_2)$, the two constant vectors $\boldsymbol{r}_1 = (-\mu,\ 0,\ 0)$ and $\boldsymbol{r}_2 = (1 - \mu,\ 0,\ 0)$ denote the positions of P_1 and P_2 in the rotating frame *OXYZ*, respectively. The dynamics that governs the motion of a satellite in the Earth-Moon system can be approximately modelled by the CRTBP (see the physical parameters for the Earth-Moon system in Tab. 1.1).

Table 1.1 – Physical parameters for the Earth-Moon system

The average distance between Earth and Moon:	384400.00 km
The eccentricity of the orbits of Earth and Moon:	5.49×10^{-2}
The unit of time for Earth-Moon system t_*:	3.7521×10^{5} s (or 4.3427 days)
Earth's mass m_1: 5.972×10^{24} kg	Moon's mass m_2: 7.3477×10^{22} kg
The ratio of m_2 to $m_1 + m_2$, μ:	1.12153×10^{-2}

From the astronautical point of view, an important issue is to control the motion of the satellite subject to the gravitation of celestial bodies. In this thesis, we consider that the satellite is controlled by propulsion systems, which is detailed in the next paragraph.

1.1.2 Propulsion control systems

The control of the motion of a satellite is generally performed by propulsion systems. A propulsion system is a machine that produces thrust to push an object forward by ejecting propellants in a high speed to generate an opposite reaction force according to Newton's

third law of motion. Nowadays, there are various types of propulsion systems available, such as chemical engines (with high thrust) and electric engines (with low thrust). In this thesis, we are interested in the low-thrust propulsion systems. The study of low-thrust optimal space trajectories dates back to the 1960s (see, e.g., the work of Lawden [47] or Beletsky's book [4], where the importance of low thrust to spiral out from a given initial orbit was foreseen.) Currently, there is also a strong interest for low-thrust missions, such as the Lisa Pathfinder [60], an ESA mission toward the L_1 Lagrangian point of the Sun-Earth system; or BepiColombo [59], a mission of ESA and JAXA to Mercury.

Let us denote by $\boldsymbol{\tau} \in \mathbb{R}^3$ the thrust vector generated by the low-thrust engine; it takes values in an Euclidean ball

$$\mathcal{B}_\tau := \{\boldsymbol{\tau} \in \mathbb{R}^3 \mid \|\boldsymbol{\tau}\| \leqslant \tau_{\max}\}, \tag{1.1}$$

where the constant $\tau_{\max} > 0$ is the maximum magnitude of the thrust. An important parameter of a thruster is the value of specific impulse (usually abbreviated as I_{sp}), and it is a measure of the efficiency of rocket and jet engines. By definition, it is the total impulse (or change in momentum) delivered per unit of propellant consumed, and is dimensionally equivalent to the generated thrust divided by the propellant flow rate. Assuming that $g_0 = 9.81$ m/s^2 is the gravity of a unit mass at the see level of the Earth, the flow of propellant is therefore governed by

$$\dot{m}(t) = -\frac{1}{I_{sp} g_0} \|\boldsymbol{\tau}(t)\|, \tag{1.2}$$

where $t \in \mathbb{R}_+$ denotes time. Low-thrust systems are generally related to electrical propulsion systems. Compared with the chemical propulsion systems, the low-thrust ones have especially high specific impulse values but only can provide a few Newtons of thrust due to the power limitations of the spacecraft. There are several types of electrical propulsion devices available, including the ones classified as electrothermal, electrostatic, and electromagnetic. On one hand, the use of low-thrust control systems saves fuel thanks to their high values of specific impulse, ensuring a longer satellite lifetime for a given propellant mass; on the other hand, the possible maximum thrust provided by the electrical propulsion systems is very low, resulting in the challenge to control the motion of a satellite. Once the thrust is very low, an important problem is to know if the motion of a satellite can be controlled in some region of the state space. To address this problem, the controllability of the motion of a satellite in the two-body problem ($\mu = 0$ or 1) with a low-thrust control system is established in Chapter 2. It is shown that in some appropriate subregion of state space, the motion of a satellite is controllable for every $\tau_{\max} > 0$.

It is worth mentioning that the model for the propellant flow rate in Eq. (1.2) is also applicable to chemical propulsion systems only if $\tau_{\max}$ is finite (compared with the impulsive ones). Therefore, the results of this thesis can be straightforwardly applied to controlling the motion of a satellite with a high thrust.

1.1.3 Controlled equation for the CRTBP

Let $t \in \mathbb{R}_+$ be the non-dimensional time and let $\boldsymbol{r} \in \mathbb{R}^3$ and $\boldsymbol{v} \in \mathbb{R}^3$ be the non-dimensional position and velocity vectors of P_3 (or the satellite) in the rotating frame *OXYZ*. If $m := m_3/m_*$ is the non-dimensional mass of the spacecraft, the non-dimensional state $\boldsymbol{x} \in \mathbb{R}^n$ ($n = 7$) for the motion of the satellite consists of $\boldsymbol{r}$, $\boldsymbol{v}$, and m. Denote by $r_{m_1} > 0$ and $r_{m_2} > 0$ the radiuses of the two bodies P_1 and P_2, respectively, and denote by $m_c > 0$ the non-dimensional mass of the spacecraft without any fuel. Then we define the admissible subset for the state $\boldsymbol{x}$ by

$$\mathcal{X} = \big\{(\boldsymbol{r}, \boldsymbol{v}, m) \in \mathbb{R}^3 \times \mathbb{R}^3 \times \mathbb{R}_+ \mid \|\boldsymbol{r} - \boldsymbol{r}_1\| > r_{m_1},\ \|\boldsymbol{r} - \boldsymbol{r}_2\| > r_{m_2},\ m \geqslant m_c\big\},$$

where the notation " $\|\cdot\|$ " denotes the Euclidean norm. According to Newton's second law of motion, the differential equations for the controlled motion of the spacecraft in the CRTBP in the admissible set $\mathcal{X}$ for positive times can be written as

$$\Sigma : \begin{cases} \dot{\boldsymbol{r}}(t) = \boldsymbol{v}(t), \\ \dot{\boldsymbol{v}}(t) = \boldsymbol{h}(\boldsymbol{v}(t)) + \boldsymbol{g}(\boldsymbol{r}(t)) + \frac{\boldsymbol{\tau}(t)}{m(t)}, \\ \dot{m}(t) = -\beta \| \boldsymbol{\tau}(t) \|, \end{cases} \tag{1.3}$$

with

$$\begin{aligned} \boldsymbol{h}(\boldsymbol{v}) &= \begin{bmatrix} 0 & 2 & 0 \\ -2 & 0 & 0 \\ 0 & 0 & 0 \end{bmatrix} \boldsymbol{v}, \\ \boldsymbol{g}(\boldsymbol{r}) &= \begin{bmatrix} 1 & 0 & 0 \\ 0 & 1 & 0 \\ 0 & 0 & 0 \end{bmatrix} \boldsymbol{r} - \frac{1-\mu}{\|\boldsymbol{r} - \boldsymbol{r}_1\|^3}(\boldsymbol{r} - \boldsymbol{r}_1) - \frac{\mu}{\|\boldsymbol{r} - \boldsymbol{r}_2\|^3}(\boldsymbol{r} - \boldsymbol{r}_2), \end{aligned}$$

where $\beta = 1/(I_{sp} g_0) > 0$ (see Eq. (1.2)) is a scalar constant determined by the specific impulse I_{sp} of the engine.

Remark 1.1. *In Eq. (1.3), one has to multiply the ratio $\tau_{\max}/m$ – where $\tau_{\max}$ is expressed in Newtons and m in kilograms – by the normalization constant $d_*^3/(Gm_*)$ when performing numerical computations.*

1.1.4 Dynamics

Denote by $\rho \in [0, 1]$ the normalized magnitude of $\boldsymbol{\tau}$, i.e., $\rho = \|\boldsymbol{\tau}\|/\tau_{\max}$, and by $\boldsymbol{\omega}$ the unit-length vector equal to $\boldsymbol{\tau}/\|\boldsymbol{\tau}\|$. Then ρ and $\boldsymbol{\omega}$ are control variables. Let $\boldsymbol{u} := (\rho, \boldsymbol{\omega})$ be the control, so $\mathcal{U} := [0, 1] \times \mathbb{S}^2$ is the admissible set for $\boldsymbol{u}$. For the sake of notational clarity, let us define a smooth vector field $\boldsymbol{f}$ on $\mathcal{X} \times \mathcal{U}$ as

$$\boldsymbol{f} : \mathcal{X} \times \mathcal{U} \to T_{\boldsymbol{x}}\mathcal{X},\ \boldsymbol{f}(\boldsymbol{x}, \boldsymbol{u}) = \boldsymbol{f}_0(\boldsymbol{x}) + \rho \boldsymbol{f}_1(\boldsymbol{x}, \boldsymbol{\omega}),$$

where

$$\boldsymbol{f}_0(\boldsymbol{x}) \;=\; \begin{bmatrix} \boldsymbol{v} \\ \boldsymbol{h}(\boldsymbol{v}) + \boldsymbol{g}(\boldsymbol{r}) \\ 0 \end{bmatrix},$$

is the drift vector field and

$$\boldsymbol{f}_1(\boldsymbol{x}, \boldsymbol{\tau}) \;=\; \begin{bmatrix} 0 \\ \tau_{\max}\boldsymbol{\omega}/m \\ -\beta\tau_{\max} \end{bmatrix},$$

is the control vector field. According to Eq. (1.3), the following control-affine system,

$$\Sigma : \dot{\boldsymbol{x}}(t) = \boldsymbol{f}(\boldsymbol{x}(t), \rho(t), \boldsymbol{\omega}(t)) = \boldsymbol{f}_0(\boldsymbol{x}(t)) + \rho(t)\boldsymbol{f}_1(\boldsymbol{x}(t), \boldsymbol{\omega}(t)),\ t \in \mathbb{R}_+, \tag{1.4}$$

governs the controlled motion of a low-thrust spacecraft in the CRTBP.

Remark 1.2. *The drift vector field $\boldsymbol{f}_0$ describes the dynamics of the uncontrolled motion. It has five equilibrium points, namely the Lagrangian points or libration points. Their locations are calculated by solving $\boldsymbol{f}_0(\boldsymbol{x}) = 0$. We refer the readers to [91] for detailed properties of $\boldsymbol{f}_0$.*

1.1.5 L^1-minimization

In astronautics, a significant issue is to minimize (or maximize) some performance indices while controlling a satellite. The frequently used performance indices include, e.g., the transfer time, the fuel consumption, and/or a linear combination of them. In this thesis, we are interested in minimizing the L^1-norm of the control.

Given an integer $l \in \mathbb{N}$ such that $0 < l \leqslant n$, we define the l-codimensional constraint submanifold on the final state by

$$\mathcal{M} = \{\boldsymbol{x} \in \mathcal{X} \mid \phi(\boldsymbol{x}) = 0\}, \tag{1.5}$$

where $\phi : \mathcal{X} \to \mathbb{R}^l$ denotes a twice continuously differentiable function of $\boldsymbol{x}$ whose explicit expression depends on specific mission requirements.

Regarding the two-body case ($\mu = 0$ or 1), the system Σ in Eq. (1.4) is controllable in the region with negative energy for every positive $\tau_{\max}$ (cf. Chapter 2). For $\mu \in (0, 1)$, the controllability of Σ holds in an appropriate subregion of the state space $\mathcal{X}$ as well (see, e.g., [17]). As a consequence, if $\boldsymbol{x}_0 \notin \mathcal{M}$, there exists a well-defined time $t_m > 0$ that is minimum for all measurable controls $(\rho(\cdot), \boldsymbol{\omega}(\cdot)) \in \mathcal{U}$ to steer the system Σ from $\boldsymbol{x}_0$ to $\mathcal{M}$.

Assumption 1.1. *Let $t_m > 0$ be the minimum time to steer the system Σ from $\boldsymbol{x}_0$ to $\mathcal{M}$, the final time t_f is assumed to be strictly greater than t_m, i.e., $t_f > t_m$.*

Definition 1.1 (L^1-minimization)**.** *Given the final time $t_f > t_m$, the L^1-minimization problem consists of steering the system Σ in $\mathcal{X}$ by a measurable control $(\rho(\cdot), \boldsymbol{\omega}(\cdot)) : [0, t_f] \to \mathcal{U}$ from $\boldsymbol{x}_0$ to $\mathcal{M}$ such that the L^1-norm of control is minimized:*

$$\int_0^{t_f} \rho(t)dt \to \textit{min}. \tag{1.6}$$

Remark 1.3. *Note that minimizing the cost functional in Eq. (1.6) is equivalent to maximizing the final mass if $\beta > 0$ (see Eq. (1.2)). Thus, the L^1-minimization problem is related to the well-known fuel-optimal control problem in astronautics once the control is generated by propulsion systems.*

Assuming the admissible controlled trajectories of Σ remain in a fixed compact set, the existence of the L^1-solutions can be obtained by a combination of Filippov theorem [2] and a suitable convexification procedure(see, e.g., [31]).

1.2 Pontryagin Maximum Principle

Let us define by $\boldsymbol{p} \in T^*_{\boldsymbol{x}}\mathcal{X}$, as usual, the costate of $\boldsymbol{x}$. According to the Pontryagin Maximum Principle [76], if a trajectory $\boldsymbol{x}(\cdot) : [0, t_f] \to \mathcal{X}$ associated with a measurable control $\boldsymbol{u}(\cdot) = (\rho(\cdot), \boldsymbol{\omega}(\cdot)) : [0, t_f] \to \mathcal{U}$ is optimal, there exists a nonpositive real number p^0 and an absolutely continuous mapping $t \mapsto \boldsymbol{p}(\cdot) \in T^*_{\boldsymbol{x}(\cdot)}\mathcal{X}$ on $[0, t_f]$, satisfying $(\boldsymbol{p}(t), p^0) \neq 0$ for $t \in [0, t_f]$, such that almost everywhere on $[0, t_f]$ there holds

$$\begin{cases} \dot{\boldsymbol{x}}(t) = \frac{\partial H}{\partial \boldsymbol{p}}(\boldsymbol{x}(t), \boldsymbol{p}(t), p^0, \boldsymbol{u}(t)), \\ \dot{\boldsymbol{p}}(t) = -\frac{\partial H}{\partial \boldsymbol{x}}(\boldsymbol{x}(t), \boldsymbol{p}(t), p^0, \boldsymbol{u}(t)), \end{cases} \tag{1.7}$$

and

$$H(\boldsymbol{x}(t), \boldsymbol{p}(t), p^0, \boldsymbol{u}(t)) = \max_{\boldsymbol{\eta}(t) \in \mathcal{U}} H(\boldsymbol{x}(t), \boldsymbol{p}(t), p^0, \boldsymbol{\eta}(t)), \tag{1.8}$$

where

$$H(\boldsymbol{x}, \boldsymbol{p}, p^0, \boldsymbol{u}) = \boldsymbol{p}\boldsymbol{f}_0(\boldsymbol{x}) + \rho \boldsymbol{p}\boldsymbol{f}_1(\boldsymbol{x}, \boldsymbol{\tau}) + p^0\rho \tag{1.9}$$

is the Hamiltonian. Moreover, the boundary transversality conditions assert

$$\boldsymbol{p}(t_f) \perp T_{\boldsymbol{x}(t_f)}\mathcal{M}. \tag{1.10}$$

Every 4-tuple $t \mapsto (\boldsymbol{x}(\cdot), \boldsymbol{p}(\cdot), p^0, \boldsymbol{u}(\cdot)) \in T^*\mathcal{X} \times \mathbb{R} \times \mathcal{U}$ on $[0, t_f]$, if satisfying Eqs. (1.7–1.9), is called an extremal. Furthermore, an extremal is said normal if $p^0 \neq 0$ and abnormal if

$p^0 = 0$. Hereafter, define by $\boldsymbol{p}_r \in T^*_{\boldsymbol{r}}\mathbb{R}^3$, $\boldsymbol{p}_v \in T^*_{\boldsymbol{v}}\mathbb{R}^3$, and $p_m \in T^*_m\mathbb{R}$ the costates of $\boldsymbol{r}$, $\boldsymbol{v}$, and m, respectively, such that $\boldsymbol{p} = (\boldsymbol{p}_r,\ \boldsymbol{p}_v,\ p_m)$.

Proposition 1.1 (Gergaud et al. [31])**.** *There are no abnormal extremals if $t_f > t_m$.*

Lemma 1.1. *Either the vector $\boldsymbol{p}_v(\cdot)$ on $[0, t_f]$ along an extremal has isolated zeros or the extremal is normal.*

Proof. Assume that $\boldsymbol{p}_v(\cdot)$ has a non isolated zero t_* in $[0, t_f]$, i.e., there exists a sequence of distinct times (t_n) in $[0, t_f]$ such that $\boldsymbol{p}_v(t_n) = 0$ for $n \geqslant 0$ and $\lim_{n\to\infty} t_n = t_*$. By continuity, $\boldsymbol{p}_v(t_*) = 0$. Moreover, one has $\dot{\boldsymbol{p}}_r = -\boldsymbol{p}_v d\boldsymbol{g}(\boldsymbol{r})$ and $\dot{\boldsymbol{p}}_r = -\boldsymbol{p}_r - \boldsymbol{p}_v\widetilde{\boldsymbol{h}}$, where $\widetilde{\boldsymbol{h}}$ denotes a 3×3 matrix. Integrating the last equation between t_n and t_* yields that

$$\boldsymbol{p}_r(t_*) = \frac{1}{t_n - t_*}\int_{t_*}^{t_n} \boldsymbol{p}_v(s)\big((t_n - s)d\boldsymbol{g}(\boldsymbol{r}(s)) + \widetilde{\boldsymbol{h}}\big)ds,$$

which clearly tends to zero as n tends to infinity. Therefore $\boldsymbol{p}_r(t_*) = 0$ as well and, since $\boldsymbol{p}_r$ and $\boldsymbol{p}_v$ are governed by a set of linear differential equations, one gets that $\boldsymbol{p}_v(\cdot) = \boldsymbol{p}_r(\cdot) \equiv 0$ on $[0, t_f]$. Note that

$$\dot{p}_m(t) = \frac{\boldsymbol{p}_v(t)\boldsymbol{\tau}(t)}{m^2(t)}, \tag{1.11}$$

and $p_m(t_f) = 0$ according to the transversality condition. As a result, $\boldsymbol{p}(\cdot)$ on the whole interval $[0, t_f]$ vanishes identically. Since $(\boldsymbol{p}(\cdot), p^0) \neq 0$, one gets that p^0 is strictly negative and the corresponding extremal is normal. □

Proof of the proposition. According to Lemma 1.1, one may assume that $\boldsymbol{p}_v(\cdot)$ has only isolated zeros on $[0, t_f]$ along the extremal. The maximization condition implies therefore that $\boldsymbol{p}_v(\cdot)\boldsymbol{\tau}(\cdot) = \|\boldsymbol{p}_v(\cdot)\|\|\boldsymbol{\tau}(\cdot)\|$ almost everywhere on $[0, t_f]$. Eq. (1.11) implies $p_m(\cdot) \leqslant 0$ on $[0, t_f)$ since $p_m(t_f) = 0$ and $\dot{p}_m(\cdot) \geqslant 0$ on $[0, t_f]$. Assume now that $p^0 = 0$. It follows that

$$H_1 = \left(\frac{\|\boldsymbol{p}_v(\cdot)\|}{m(\cdot)} - p_m(\cdot)\beta\right)\tau_{\max} > 0$$

on $[0, t_f]$, except maybe in a finite number of times. Thus, there holds $\rho(\cdot) = 1$ on $[0, t_f]$, except maybe in a finite number of times, in accordance with the maximum condition. As a result, $\int_0^{t_f} \rho(t)dt = t_f > t_m$ by Assumption 1.1. Let us denote by $\widetilde{\boldsymbol{u}}(\cdot) : [0, t_m] \to \mathcal{U}$ the minimum time control; it follows that there exists a control $\boldsymbol{u}_*(\cdot) : [0, t_f] \to \mathcal{U}$ with $\boldsymbol{u}_*(t) = \widetilde{\boldsymbol{u}}(t)$ for $t \in [0, t_m]$ and $\boldsymbol{u}_*(t) = 0$ for $[t_m, t_f]$ such that a smaller performance index is reached. A contradiction is reached, which proves the proposition. □

Consequently, we normalize $(\boldsymbol{p}, p^0)$ such that $p^0 = -1$. Let us denote by $H(\boldsymbol{x}(\cdot), \boldsymbol{p}(\cdot))$ on $[0, t_f]$ the maximized Hamiltonian of the extremal $(\boldsymbol{x}(\cdot), \boldsymbol{p}(\cdot))$ on $[0, t_f]$. Then, we write the maximized Hamiltonian as

$$H(\boldsymbol{x}, \boldsymbol{p}) := H_0(\boldsymbol{x}, \boldsymbol{p}) + \rho(\boldsymbol{x}, \boldsymbol{p})H_1(\boldsymbol{x}, \boldsymbol{p}),$$

where $H_0(\boldsymbol{x},\boldsymbol{p}) = \boldsymbol{p}\boldsymbol{f}_0(\boldsymbol{x})$ is the drift Hamiltonian and $H_1(\boldsymbol{x},\boldsymbol{p}) = \boldsymbol{p}\boldsymbol{f}_1(\boldsymbol{x},\boldsymbol{\omega}(\boldsymbol{x},\boldsymbol{p})) - 1$ is the switching function. The maximum condition in Eq. (1.8) implies

$$\boldsymbol{\omega} = \boldsymbol{p}_v/\|\boldsymbol{p}_v\|, \text{ if } \|\boldsymbol{p}_v\| \neq 0, \tag{1.12}$$

and

$$\rho = \begin{cases} 1, \text{ if } H_1 > 0, \\ 0, \text{ if } H_1 < 0. \end{cases} \tag{1.13}$$

Thus, the optimal direction of the thrust is collinear to $\boldsymbol{p}_v$, a well known fact ("primer vector" theory of Lawden [47]). If the switching function H_1 has either none or only isolated zeros along an extremal $(\boldsymbol{x}(\cdot),\boldsymbol{p}(\cdot))$ on $[0,t_f]$, this extremal is called a nonsingular one.

Definition 1.2. *Along a nonsingular extremal $(\boldsymbol{x}(\cdot),\boldsymbol{p}(\cdot))$ on $[0,t_f]$, an arc on a finite interval $[t_1,t_f] \subset [0,t_f]$ with $t_1 < t_2$ is called a maximum-thrust (or burn) arc if $\rho = 1$, otherwise it is called a zero-thrust (or coast) arc.*

Given the extremal $(\boldsymbol{x}(\cdot),\boldsymbol{p}(\cdot))$ on $[0,t_f]$, if there holds $H_1(\boldsymbol{x}(\cdot),\boldsymbol{p}(\cdot)) \equiv 0$ on a finite interval $[t_1,t_2] \subseteq [0,t_f]$ with $t_1 < t_2$, the arc on $[t_1,t_2]$ is called a singular one.

1.3 Singular solutions

The minimizing value of ρ along a singular extremal can be calculated by differentiating the switching function H_1 until it explicitly appears [41].

Proposition 1.2. *Given a singular extremal $(\boldsymbol{x}(\cdot),\boldsymbol{p}(\cdot))$ on $[t_1,t_2] \subseteq [0,t_f]$ with $t_1 < t_2$, assume $\|\boldsymbol{p}_v(\cdot)\| \neq 0$ on $[t_1,t_2]$. Then, we have that the order of the singular extremal is at least two.*

Proof. Since $H_1 \equiv 0$ along a singular arc, differentiating H_1 with respect to time, one obtains

$$0 = H_{01} := \{H_0, H_1\} = -\tau_{max}\frac{\boldsymbol{p}_v(\boldsymbol{p}_r^T + d\boldsymbol{h}(\boldsymbol{v})\boldsymbol{p}_v^T)}{m \parallel \boldsymbol{p}_v \parallel}, \tag{1.14}$$

where the notation " $\{\cdot,\cdot\}$ " denotes the Poisson bracket. Using Leibniz's rule, Eq. (1.14) implies

$$\begin{aligned} H_{101} &:= \{H_1, H_{01}\} = 0, \\ H_{1001} &:= \{H_1, \{H_0, H_{01}\}\} \\ &= \{-H_{01}, H_{01}\} + \{H_0, H_{101}\} = 0. \end{aligned}$$

Then, the equality, $0 = H_{001} + \rho H_{101}$, implies $H_{001} = 0$, whose explicit expression is given

by

$$H_{001} = \tau_{\max}\frac{\boldsymbol{p}_v d\boldsymbol{g}(\boldsymbol{r})\boldsymbol{p}_v^T + [\boldsymbol{p}_r + 2\boldsymbol{p}_v d\boldsymbol{h}(\boldsymbol{v})][\boldsymbol{p}_r + \boldsymbol{p}_v d\boldsymbol{h}(\boldsymbol{v})]^T}{m \parallel \boldsymbol{p}_v \parallel}.$$

A direct calculation on this equation yields

$$\begin{aligned} H_{0001} &:= \{H_0, H_{001}\} \\ &= \frac{\tau_{max}}{m \parallel \boldsymbol{p}_v \parallel}\Big\{\big[\boldsymbol{p}_v d^2\boldsymbol{g}(\boldsymbol{r})\boldsymbol{p}_v^T\big]\boldsymbol{v} - \boldsymbol{p}_v d\boldsymbol{g}(\boldsymbol{r})[2\boldsymbol{p}_r + 3\boldsymbol{p}_v d\boldsymbol{h}(\boldsymbol{v})]^T \\ &- [2\boldsymbol{p}_v d\boldsymbol{g}(\boldsymbol{r}) + 3\boldsymbol{p}_r d\boldsymbol{h}(\boldsymbol{r}) + 4\boldsymbol{p}_v (d\boldsymbol{h}(\boldsymbol{v}))^2][\boldsymbol{p}_r + \boldsymbol{p}_v d\boldsymbol{h}(\boldsymbol{v})]^T\Big\}. \end{aligned}$$

Eventually, one has $0 = \dot{H}_{0001} = H_{00001} + \rho H_{10001}$. Let α_i $(i = 1, 2)$ be defined by

$$\cos(\alpha_i) = \frac{\boldsymbol{p}_v(\boldsymbol{r} - \boldsymbol{r}_i)}{\parallel \boldsymbol{p}_v \parallel\parallel \boldsymbol{r} - \boldsymbol{r}_i \parallel},$$

the explicit expression of $H_{10001} := \{H_1, H_{0001}\}$ is therefore

$$\begin{aligned} H_{10001} &= \tau_{max}\frac{\big[\boldsymbol{p}_v d^2\boldsymbol{g}(\boldsymbol{r})\boldsymbol{p}_v^T\big]\boldsymbol{p}_v^T}{m^2 \parallel \boldsymbol{p}_v \parallel^2} \\ &= 3\tau_{max}\frac{\parallel \boldsymbol{p}_v \parallel}{m^2}\left[\mu\cos\alpha_2\frac{3 - 5\cos^2\alpha_2}{\parallel \boldsymbol{r} - \boldsymbol{r}_2 \parallel^4} + (1-\mu)\cos\alpha_1\frac{3 - 5\cos^2\alpha_1}{\parallel \boldsymbol{r} - \boldsymbol{r}_1 \parallel^4}\right]. \end{aligned}$$

Note that the term H_{10001} does not vanish identically on a singular extremal. So the singular extremal is of order two according to Kelley's definition [41], which proves the proposition. □

This proposition for the 3-dimensional case expands the work in [96] where the motion of the spacecraft is restricted into a 2-dimensional plane and the work in [78] where the model of two-body problem ($\mu = 0$ or 1) is considered. Note that Kelley's second-order necessary condition [41] in terms of ρ on singular arcs is $H_{10001} \leqslant 0$. Let

$$\mathcal{S} := \big\{(\boldsymbol{x}, \boldsymbol{p}) \in T^*\mathcal{X} \mid H_1 = H_{01} = H_{001} = H_{0001} = 0,\ H_{10001} \leqslant 0\big\}$$

be the singular submanifold and denote by $\mathrm{int}(\mathcal{S})$ the interior of $\mathcal{S}$. Note that $\mathrm{int}(\mathcal{S})$ is not empty according to [96].

1.4 Fuller (or chattering) phenomena

The chattering phenomena originates from the Fuller problem (see [30]). In this paragraph, it will be shown that the chattering phenomena may occur in the L^1-minimization problem when concatenating a nonsingular extremal with a singular one.

Set

$$\begin{cases} z_1 = H_1, \\ z_2 = -H_{01}, \\ z_3 = -H_{001}, \\ z_4 = -H_{0001}. \end{cases} \tag{1.15}$$

According to the equations in the proof of Proposition 1.2, we have

$$\begin{cases} \dot{z}_1 = -z_2, \\ \dot{z}_2 = z_3, \\ \dot{z}_3 = z_4, \\ \dot{z}_4 = -\alpha(\boldsymbol{x}, \boldsymbol{p})\rho - \beta(\boldsymbol{x}, \boldsymbol{p}), \end{cases} \tag{1.16}$$

where $\alpha = H_{10001}$ and $\beta = H_{00001}$. By virtue of [96, Lemma 2.1], the functions (z_1, z_2, z_3, z_4) are functionally independent in the vicinity of the extremal $(\boldsymbol{x}, \boldsymbol{p})$ and we can complement the coordinates $\boldsymbol{z} := (z_1, z_2, z_3, z_4)$ by functions $\boldsymbol{w} = (w_1, w_2, \cdots, w_{2n-4}) \in \mathbb{R}^{2n-4}$ such that the Jacobian matrix of the mapping $(\boldsymbol{z}, \boldsymbol{w}) \to (\boldsymbol{x}, \boldsymbol{p})$ is nondegenerate, i.e.,

$$\det \left[\frac{d(\boldsymbol{z}, \boldsymbol{w})}{d(\boldsymbol{x}, \boldsymbol{p})} \right] \neq 0.$$

Hence, the variables $(\boldsymbol{x}, \boldsymbol{p})$ can be locally expressed as functions of $(\boldsymbol{z}, \boldsymbol{w})$. Substitution of these functions in Eq. (1.15) and letting $F(\boldsymbol{z}, \boldsymbol{w}) \in \mathbb{R}^{2n-4}$ be the differentiation of $\boldsymbol{w}$ with respect to time yields

$$\begin{cases} \dot{z}_1 = -z_2, \\ \dot{z}_2 = z_3, \\ \dot{z}_3 = z_4, \\ \dot{z}_4 = -\rho\alpha(\boldsymbol{z}, \boldsymbol{w}) - \beta(\boldsymbol{z}, \boldsymbol{w}), \\ \dot{\boldsymbol{w}} = F(\boldsymbol{z}, \boldsymbol{w}), \end{cases} \tag{1.17}$$

where

$$\rho = \begin{cases} 1, & \text{if } z_1 > 0, \\ 0, & \text{if } z_1 < 0, \\ -\beta/\alpha, & \text{if } z_1 = 0. \end{cases} \tag{1.18}$$

The choice of $(\boldsymbol{z}, \boldsymbol{w})$ is not unique and Eq. (1.17) is henceforth called *semi-canonical* form of the Hamiltonian system of Eq. (1.7). Next, we will show that the semi-canonical system is related to the well-known Fuller problem, defined as follow.

Problem 1.1 (Unsymmetrical Fuller problem)**.** *Minimize*

$$\int_0^1 \frac{x^2}{2} dt$$

subject to

$$\dot{x} = y, \quad \dot{y} = au + b, \quad u \in [0, 1], \ a > 0,$$

with the boundary conditions

$$x(0) = x_0, \quad y(0) = y_0, \quad x(1) = x_1, \quad y(1) = y_1.$$

The existence of the solution of the Fuller problem is proved by Zelikin and Borisov (see [95, Chapter 5]). The Hamiltonian for this problem is

$$H = p_x y + p_y(au + b) - x^2/2.$$

Then the variables (x, y, p_x, p_y) are governed by

$$\begin{cases} \dot{p}_y = -p_x, \\ \dot{p}_x = x, \\ \dot{x} = y, \\ \dot{y} = au + b, \end{cases} \tag{1.19}$$

where

$$u = \begin{cases} 1, & \text{if } p_y > 0, \\ 0, & \text{if } p_y < 0, \\ -b/a, & \text{if } p_y = 0. \end{cases} \tag{1.20}$$

Note that the Hamiltonian system Eq. (1.19) of the Fuller problem is the same as Eq. (1.16) once $\alpha(\boldsymbol{z}, \boldsymbol{w})$ and $\beta(\boldsymbol{z}, \boldsymbol{w})$ are constant. The solution to Eq. (1.19) has an infinite number of switching times on a finite time interval (see the typical picture for Fuller phenomenon in Fig. 1.2). This phenomenon is called *chattering*. Since the system in Eq. (1.17) is diffeomorphic to the original Hamiltonian system in Eq. (1.7), there may occur chattering phenomena for the extremal of L^1-minimization problem, as shown by the following remark.

Remark 1.4 (Zelikin and Borisov [95])**.** *Given every point* $(\boldsymbol{x}, \boldsymbol{p}) \in \mathrm{int}(\mathcal{S})$*, there exists a one parameter family of chattering solutions passing through the point* $(\boldsymbol{x}, \boldsymbol{p})$ *and another one parameter family of chattering solutions coming out from the point* $(\boldsymbol{x}, \boldsymbol{p})$.

Though the efficient computation of chattering solutions is an open problem (see, e.g., [32, 69]), Remark 1.4 gives some insights on the control structure of the L^1-minimization trajectory; there exists a chattering arc when concatenating a singular arc with a nonsingular arc if ρ is not saturating at the instant prior to the junction time.

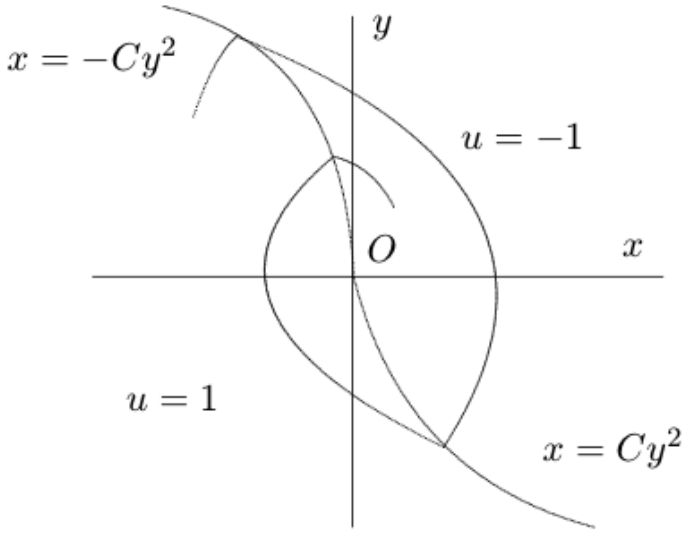

Figure 1.2 – Fuller phenomenon.

1.5 Computational method

Not considering the singular and chattering controls, even the computation the L^1-minimization solution with a bang-bang control structure is a challenging task. To address this problem, various numerical methods, e.g., direct methods [58, 79], indirect methods [17, 18, 31], and hybrid methods [67], have been developed in the literature in recent years. In this thesis, the indirect method, the most popular way to solve optimal control problems, is employed to compute the solutions for L^1-minimization. In the next paragraph, the indirect method will be detailed.

The PMP gives a Hamiltonian ODE (see Eq. (1.7)) of the state $\boldsymbol{x}$ and the adjoint state $\boldsymbol{p}$. Thus, let

$$\overrightarrow{H} := \left(\frac{\partial H}{\partial \boldsymbol{p}}, -\frac{\partial H}{\partial \boldsymbol{x}}\right)$$

be the Hamiltonian vector field defined by Eq. (1.7) and Eq. (1.8); we denote by

$$(\boldsymbol{x}(t, \boldsymbol{x}_0, \boldsymbol{p}_0), \boldsymbol{p}(t, \boldsymbol{x}_0, \boldsymbol{p}_0)) = e^{t\overrightarrow{H}}(\boldsymbol{x}_0, \boldsymbol{p}_0)$$

the Hamiltonian flow parameterized by $\boldsymbol{x}_0 \in \mathcal{X}$ and $\boldsymbol{p}_0 \perp T^*_{\boldsymbol{x}_0}\mathcal{X}$. The Hamiltonian flow $(\boldsymbol{x}(t, \boldsymbol{x}_0, \boldsymbol{p}_0), \boldsymbol{p}(t, \boldsymbol{x}_0, \boldsymbol{p}_0))$ is uniquely determined by $(t, \boldsymbol{x}_0, \boldsymbol{p}_0)$ and it can be computed numerically using more or less sophisticated integration schemes, e.g., Runge-Kutta. Since the initial state is fixed, i.e., $\boldsymbol{x}(0) = \boldsymbol{x}_0$, and the final time t_f is fixed, we define a shooting function

$$S : T^*_{\boldsymbol{x}_0}\mathcal{X} \times \mathbb{R}^l \to \mathbb{R}^{n+l},\ (\boldsymbol{p}_0, \boldsymbol{\nu}) \mapsto S(\boldsymbol{p}_0, \boldsymbol{\nu}), \tag{1.21}$$

such that

$$S(\boldsymbol{p}_0, \boldsymbol{\nu}) = \begin{bmatrix} \phi(\boldsymbol{x}(t_f, \boldsymbol{x}_0, \boldsymbol{p}_0)) \\ \boldsymbol{p}^T(t_f, \boldsymbol{x}_0, \boldsymbol{p}_0) - \nabla\phi^T(\boldsymbol{x}(t_f, \boldsymbol{x}_0, \boldsymbol{p}_0))\boldsymbol{\nu} \end{bmatrix}, \tag{1.22}$$

where $\boldsymbol{\nu} \in \mathbb{R}^l$ is the vector of the Lagrangian multipliers. In order to compute the solution of the L^1-minimization problem, it is sufficient to search a zero of the equation $S(\boldsymbol{p}_0, \boldsymbol{\nu}) = 0$.

A simple shooting method does not allow one to solve this problem because one does not know *a priori* the structure of the optimal control. Moreover, the numerical computation of the shooting function and its differential may be intricate, as the function may not even be differentiable (typically at points corresponding to a change in the structure of the control strategy, which is a change in the number of switching times here). We will employ a regularization procedure [31] that smoothes the control discontinuities and get an energy-optimal trajectory first, then use a homotopy method to find the real trajectory with a bang-bang control.

1.6 Contributions of the PhD

1.6.1 Controllability

To study the controllability of the system Σ is a prerequisite to design a mission or to compute an optimal trajectory. In this thesis, the controllability for the Keplerian motion ($\mu = 0$ or 1) with low-thrust control systems is addressed. Without taking into account state constraints, the controllability for Keplerian motion was derived in [8, 20], showing that there exists admissible controlled trajectories for orbital transfer problem (OTP) if the maximum thrust is positive. In the current thesis, the controllability for OTP is established using alternative techniques from geometric control (cf. [34, 87]). Considering the state constraint that the radius of the orbit of a satellite is larger than the radius of the surface of the atmosphere around the Earth, the orbital insertion problem (OIP) and the de-orbit problem (DOP) are defined. Some controllability properties for OIP's and DOP's are then addressed and we show that there exist admissible controlled trajectories for OIP and DOP if and only if the maximum thrust is bigger than a specific value (depending on the initial point or final point). It is worth mentioning that the techniques used to establish the controllability for Keplerian motion are applicable to establish the controllability of the CRTBP since the drift vector field $\boldsymbol{f}_0$ of the CRTBP is recurrent.

1.6.2 Sufficient optimality conditions

Though the above shooting method can be employed to compute candidate solutions, they cannot be guaranteed to be at least locally optimal unless sufficient optimality conditions are satisfied. In order to assess the optimality properties for the L^1-minimization problem, the sufficient optimality conditions for broken-extremals are established in this work.

Definition 1.3 (First conjugate point [9]). *Given the extremal $(\boldsymbol{x}(\cdot), \boldsymbol{p}(\cdot))$ on $[0, t_f]$, the first conjugate point is defined as the first point at which the extremal ceases to be locally optimal (essentially in L^∞ topology on the control).*

Consequently, the sufficient conditions are related to the first conjugate point.

In the classical calculus of variations, the sufficient conditions are usually established by ensuring that the second order variation of the cost functional is positive [13, 16], which yields the accessory minimum problem. Based on this variational idea, some verifiable conditions sufficient for the optimality of continuous-thrust problems were developed in [36, 77]. From the geometric point of view, the sufficient conditions have been studied as well (see, e.g., [2, 3, 22, 23, 28, 45, 71, 80] and the references therein). The key idea in those papers is to establish conditions ensuring the $\boldsymbol{x}$-part of the Jacobi fields (the nonconstant solution to the Jacobi equation with specific boundary conditions) is nonvanishing (see, e.g., [2, Chapter 21]); based on this method, a numerical procedure for testing conjugate points was proposed in [9] for smooth extremals.

However, once the specified transfer time is greater than the minimum transfer time for the same boundary conditions, the thrust is discontinuous [31], i.e., the optimal control function exhibits a bang-bang behavior. Second order conditions in the bang-bang case have received quite an extensive treatment; references include the paper of Sarychev [81], followed by [3] and [54, 64, 65]. On a similar line, the stronger notion of state optimality was introduced in [71] for free final time. More recently, a regularization procedure has been developed in [85] for single-input systems. These papers consider controls taking values in polyhedra; the standing assumptions allow one to define a finite dimensional accessory optimization problem in the switching times only. Then, checking a second order sufficient condition on this auxiliary problem turns out to be sufficient to ensure strong local optimality of the bang-bang controls. A by-product of the analysis is that conjugate points occur at switching times. A different approach, based on the Hamiltonian-Jacobi-Bellman equation and the method of characteristics in optimal control, has been proposed by Noble and Schättler in [63] (see also the more recent reference [82]). Their results encompass the case of broken extremals with conjugate points occurring at or between switching times. In this thesis, we will provide a similar analysis by requiring some generalized (with respect to the smooth case) disconjugacy condition on the Jacobi fields (cf. Chapter 3), and using instead a Hamiltonian point of view reminiscent of [27, 45]. Also note that the work of Maurer and Osmolovskii actually covers this situation with yet another approach; see [66, Chapter 5] on optimal control problems with a part of the controls linearly entering the dynamics. (For the purpose of numerical verification of their sufficient conditions, they devise a Riccati equation similar to the one in [82].) Treating the case of such broken extremals is crucial for L^1-minimization problem: As the finite dimensional norm of the control involved in the constraint Eq. (1.1) and in the cost Eq. (1.6) is an l^2-norm (defining a so-called L^1-l^2 minimization problem), the control is valued in the Euclidean ball of $\mathbb{R}^m$, not a polyhedron if $m > 1$. When $m = 1$, the situation is degenerate, and one can, for instance, set $u = u_+ - u_-$, with $u_+, u_- > 0$. (This approach also works for $m > 1$ when an l^1 or l^∞-norm is used for the values of the control; see, e.g., [92].)

When $m > 1$, it is clear using spherical coordinates that although the norm of the control might be bang-bang, the variations of the control component on $\mathbb{S}^{m-1}$ preclude the reduction to a finite dimensional optimization problem. (The same remark holds true for any l^p-norm of the control values with $1 < p < \infty$.) An example of conjugacy occurring between switching times is provided in Chapter 3.

Although the disconjugacy conditions, satisfying at or between switching times, are sufficient to guarantee an extremal with fixed endpoints to be locally optimal, a further second-order condition has to be formulated once the final point is not fixed but varies on a smooth submanifold (see [2, 15, 93], e.g.). In Chapter 4, the extra condition related to the geometry of the target manifold and the Jacobi fields is established. As a result, sufficient conditions for strong optimality can be tested by only computing Jacobi fields.

1.6.3 Neighboring optimal feedback control

Due to numerous perturbations and errors, one cannot expect a spacecraft controlled by a precomputed optimal control to exactly move on the corresponding precomputed optimal trajectory to a desired target. The precomputed optimal trajectory and the associated optimal control are generally referred to as the nominal trajectory and the nominal control, respectively. The guidance is a process that calculates a new control according to navigational data in each guidance cycle such that the spacecraft can be steered by the new control to track the nominal trajectory or to move on a new optimal trajectory [49]. Since the 1960s, various guidance schemes have been developed [7, 21, 25, 39, 40, 48, 50–52], among which there are two main categories: implicit and explicit ones. While the implicit guidance strategy generally compares the measured state with the nominal state to generate control corrections, the explicit guidance strategy solves the equations of motion and generates control corrections by onboard computers during its motion. To implement an explicit guidance strategy, numerical iterations are required to solve a highly nonlinear two-point boundary-value problem and the time required for convergence heavily depends on the merits of initial guesses. In recent years, through employing a multiple shooting method and the analytical property in a linear gravity field [35], an explicit closed-loop guidance has been developed by Lu *et al.* for exo-atmospheric ascent flights [50] and for deorbit problems [7]. This explicit type of guidance for endo-atmospheric ascent flights were investigated in [21, 51, 52] as well. However, the duration of a low-thrust orbital transfer is so long that the onboard computer can hardly afford the large amount of computational time for integrations and iterations once a shooting method is employed; this fact makes the explicit guidance strategy unattractive to low-thrust orbital transfer problems.

The neighboring optimal guidance (NOG) is an implicit and less demanding guidance scheme based on the neighboring optimal feedback control, and the neighboring optimal control is probably the most important application of the optimal control theory (see [82, Chapter 5], e.g.). Once the gain matrices associated with the nominal extremal are computed offline and stored in the onboard computer, the latter is able to compute the neighboring optimal feedback control in real time. Moreover, the neighboring optimal feedback control handles

disturbances well [61]. Assuming the optimal control function is totally continuous along the nominal trajectory, through minimizing the second variation of the cost functional subject to the variational state and adjoint equations, a linear feedback control was proposed independently by Breakwell *et al.* [14], Kelley [39, 40], Lee [48], Speyer *et al.* [88], Bryson *et al.* [16], and Hull [33]. Based on this variational idea, an increasing number of papers (see, e.g., [1, 62, 70, 83, 84] and the references therein) on the topic of the NOG for orbital transfer problems have been published. More recently, the variable-time-domain NOG was proposed by Pontani *et al.* [74, 75] to avoid the numerical difficulties arising from the singularity of the gain matrices while approaching the final time and it was applied to a continuous thrust space trajectories [73].

However, difficulties arise when we consider the L^1-minimization problem because the corresponding optimal control function exhibits a bang-bang behavior. Considering the control function as a discontinuous scalar, the corresponding neighboring optimal feedback control law was studied by Mcintyre [55] and Mcneal [56]. Then, Foerster *et al.* [29] extended the work of Mcintyre and Mcneal to problems with discontinuous vector control functions. Using a multiple shooting technique, the algorithm for computing the NOG of general optimal control problems with discontinuous control and state constraints was developed in [43], which was then applied to a space shuttle guidance in [44]. As far as the author knows, with the exception of Chuang *et al.* [25], few have made efforts on developing the NOG for low-thrust multi-burn orbital transfer problems. In the work [25] by Chuang *et al.*, without taking into account the feedback on thrust-on times, the second variation on each burn arc was minimized such that the neighboring optimal feedback on thrust direction and thrust off-times were obtained. In this thesis, through deriving the first order term of the Taylor expansion of the parameterized family of extremals, the neighboring optimal feedback on thrust direction and switching times (including not only the thrust on but also the thrust off times) are established.

Note that the existence of neighboring extremals around the nominal extremal is a prerequisite to implement the NOG (cf. e.g., [16, 33, 39, 48, 74]). For a smooth nominal extremal, it is well-known that there exist neighboring extremals if the Jacobi necessary condition is satisfied on the nominal extremal, as was readily obtained by Kelley [39], Lee [48], Kornhauser *et al.* [42], Chuang *et al.* [25], Pontani *et al.* [74, 75], and many others who minimize the AMP to derive the NOG. Once a nominal extremal exhibits a bang-bang behavior, it is however not clear that what conditions have to be satisfied in order to guarantee the existence of neighboring extremals [42]. In this thesis, a geometric interpretation will be given to show that, although the Jacobi necessary condition is satisfied, it is still impossible to construct the NOG if a transversality condition at switching times is not satisfied.

Chapter 2

Controllability of Keplerian Motion with Low-Thrust Control Systems

If $\mu = 0$ or 1, the CRTBP degenerates to the classical two-body problem. A common example of the two-body problem is the motion of an artificial body, i.e., spacecraft or satellite, around the Earth (see Fig. 2.1). Once the atmospheric effects are negligible and the Earth overwhelm-

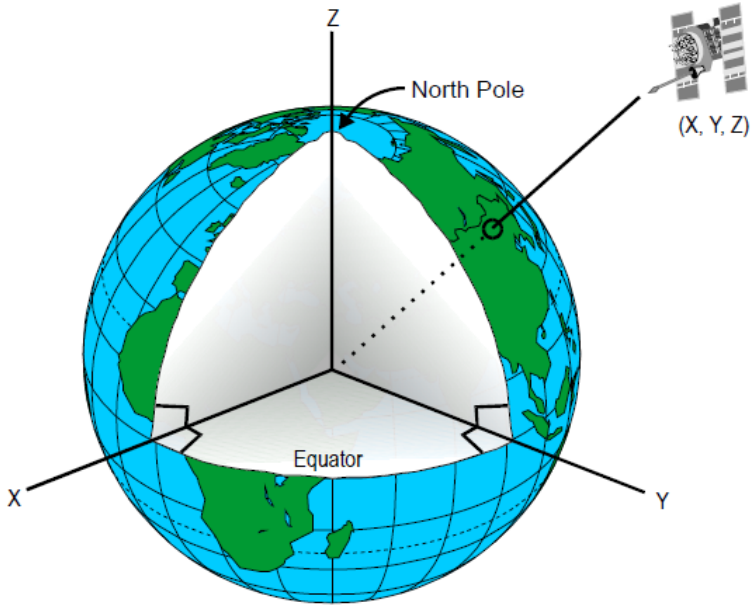

Figure 2.1 – The satellite moves in an Earth centered inertial Cartesian coordinate.

ingly dominates the gravitational influence, a satellite moves stably on a periodic orbit if the mechanical energy of the satellite is negative. We say the motion is the Keplerian motion. Although the low-thrust control systems can provide a fuel-efficient means to control the motion of a satellite (see Sect. 1.1.2), it is important to know if they have the ability to steer a satellite from one point to another one with some constraints being satisfied. This is actually related to the controllability property. The study of the controllability property is a prerequisite to analyze mission feasibility before designing a space mission or computing an optimal trajectory.

Restricting the mechanical energy of a satellite into negative region without any other state constraints, the controlled motion is related to the orbital transfer problem (OTP), and the controllability for OTP was derived in [8, 20] to show that there exist admissible controlled trajectories for every OTP if the maximum thrust is positive.

In this chapter[1], the controllability for OTP is established using alternative techniques from geometric control (see, e.g., [34, 87]). Taking into account the state constraint that the orbit of the radius of a satellite is larger than the radius of the surface of the atmosphere around the Earth, the orbital insertion problem (OIP) and de-orbit problem (DOP) are defined in this chapter. Some controllability properties for the OIP and the DOP are then addressed and we show that there exist admissible controlled trajectories for OIP's and DOP's if and only if the maximum thrust is greater than a specific value (depending on the initial point or final point).

2.1 Definitions and notations

2.1.1 Dynamics for controlled two-body problem

For the two-body case ($\mu = 0$ or 1), the dynamics in Eq. (1.4) is reduced to

$$\Sigma_{sat} : \begin{cases} \dot{\boldsymbol{r}}(t) = \boldsymbol{v}(t), \\ \dot{\boldsymbol{v}}(t) = -\frac{\mu_e}{\|\boldsymbol{r}(t)\|^3}\boldsymbol{r}(t) + \frac{\boldsymbol{\tau}(t)}{m(t)}, \\ \dot{m}(t) = -\beta\|\boldsymbol{\tau}(t)\|, \end{cases} \tag{2.1}$$

where $\mu_e > 0$ is a constant, a multiplication of the gravitational constant and the mass of the Earth. If $\mathcal{Y} = \mathbb{R}^3\backslash\{0\} \times \mathbb{R}^3$ and $\boldsymbol{y} = (\boldsymbol{r}, \boldsymbol{v})$, we define two vector fields $\widetilde{\boldsymbol{f}}_0$ and $\widetilde{\boldsymbol{f}}_1$ on $\mathcal{Y}$ by

$$\widetilde{\boldsymbol{f}}_0 : \mathcal{Y} \to \mathbb{R}^6,\ \widetilde{\boldsymbol{f}}_0(\boldsymbol{y}) = \begin{pmatrix} \boldsymbol{v} \\ -\frac{\mu_e}{\|\boldsymbol{r}\|^3}\boldsymbol{r} \end{pmatrix}, \tag{2.2}$$

$$\widetilde{\boldsymbol{f}}_1 : \mathcal{Y} \to \mathbb{R}^{6\times 3},\ \widetilde{\boldsymbol{f}}_1(\boldsymbol{y}) = \begin{pmatrix} 0 \\ I_3 \end{pmatrix}, \tag{2.3}$$

where $\mathbb{R}^{6\times 3}$ denotes the set of 6×3 matrices with real entries and I_3 denotes the identity matrix of $\mathbb{R}^3$. Let $\mathcal{B}_\varepsilon$ be the closed ball in $\mathbb{R}^3$ centered at the origin and of radius $\varepsilon > 0$. For every $\varepsilon > 0$, we consider the control-affine system Σ_ε given by

$$\Sigma_\varepsilon : \dot{\boldsymbol{y}}(t) = \widetilde{\boldsymbol{f}}_0(\boldsymbol{y}(t)) + \widetilde{\boldsymbol{f}}_1(\boldsymbol{y}(t))\boldsymbol{u}(t), \tag{2.4}$$

where the control vector $\boldsymbol{u} \in \mathbb{R}^3$ takes values in $\mathcal{B}_\varepsilon$. We will use in this chapter the vector field point of view of [38, 89, 90]. For every point $\boldsymbol{y} \in \mathcal{Y}$ and every $\boldsymbol{u} \in \mathcal{B}_\varepsilon$, we denote by

$$\widetilde{\boldsymbol{f}} : \mathcal{Y} \times \mathcal{B}_\varepsilon \to T_{\boldsymbol{y}}\mathcal{Y},\ (\boldsymbol{y}, \boldsymbol{u}) \mapsto \widetilde{\boldsymbol{f}}(\boldsymbol{y}, \boldsymbol{u}) = \widetilde{\boldsymbol{f}}_0(\boldsymbol{y}) + \widetilde{\boldsymbol{f}}_1(\boldsymbol{y})\boldsymbol{u}, \tag{2.5}$$

[1]This chapter is based on the paper "Controllability of Keplerian Motion with Low-Thrust Control Systems" (with Yacine Chitour) to appear in [24].

where $\widetilde{\boldsymbol{f}}_0$ and $\widetilde{\boldsymbol{f}}_1$ are referred to as the *drift vector field* and the *control vector field*, respectively. Note that trajectories of Σ_ε starting at any $\boldsymbol{y}_0 \in \mathcal{Y}$ associated with measurable controls $\boldsymbol{u} : \mathbb{R}_+ \to \mathcal{B}_\varepsilon$ are well-defined on an open interval of $\mathbb{R}_+$ containing 0, which depends in general on $\boldsymbol{y}_0$ and $\boldsymbol{u}(\cdot)$.

2.1.2 Study of the drift vector field in $\mathcal{Y}$

In this paragraph, we recall the main properties of the drift vector field $\widetilde{\boldsymbol{f}}_0$. For every $\boldsymbol{y} \in \mathcal{Y}$, we use $\gamma_{\boldsymbol{y}}$ to denote the restriction to $\mathbb{R}_+$ of the maximal trajectory of $\widetilde{\boldsymbol{f}}_0$ starting at $\boldsymbol{y}$, i.e. $\gamma_{\boldsymbol{y}}$ is defined on some interval $[0, t_f(\boldsymbol{y}))$ where $t_f(\boldsymbol{y}) \leqslant \infty$. Then the following holds true.

Property 2.1 (First integrals [6, 26])**.** *For every $\boldsymbol{y} \in \mathcal{Y}$, if $\gamma_{\boldsymbol{y}}(t) = (\widetilde{\boldsymbol{r}}(t), \widetilde{\boldsymbol{v}}(t))$ on $[0, t_f(\boldsymbol{y}))$, the quantities*

$$\boldsymbol{h}(t) \;=\; \widetilde{\boldsymbol{r}}(t) \times \widetilde{\boldsymbol{v}}(t), \tag{2.6}$$

$$\boldsymbol{L}(t) \;=\; \widetilde{\boldsymbol{v}}(t) \times \boldsymbol{h}(t) - \mu_e \frac{\widetilde{\boldsymbol{r}}(t)}{\| \widetilde{\boldsymbol{r}}(t) \|}, \tag{2.7}$$

$$E(t) \;=\; \frac{\| \widetilde{\boldsymbol{v}}(t) \|^2}{2} - \frac{\mu_e}{\| \widetilde{\boldsymbol{r}}(t) \|}, \tag{2.8}$$

are constant along $\gamma_{\boldsymbol{y}}$ and the corresponding constant values are the angular momentum vector $\boldsymbol{h} \in \mathbb{R}^3$, the Laplace vector $\boldsymbol{L} \in \mathbb{R}^3$, and the mechanical energy of a unit mass $E \in \mathbb{R}$, which is the sum of the relative kinetic energy $\| \widetilde{\boldsymbol{v}}(t) \|^2 /2$ and the potential energy $-\mu_e / \| \widetilde{\boldsymbol{r}}(t) \|$.

As a consequence of Eq. (2.6) and Eq. (2.7), we have the following two properties.

Property 2.2 (Straight line [6, 26])**.** *Let $\boldsymbol{y} \in \mathcal{Y}$ with $\boldsymbol{h} = 0$, i.e., $\boldsymbol{r}$ and $\boldsymbol{v}$ are collinear. Then the trajectory $\gamma_{\boldsymbol{y}}$ is a straight line.*

Property 2.3 (Conic section [6, 26])**.** *Let $\boldsymbol{y} \in \mathcal{Y}$ with $\boldsymbol{h} \neq 0$ i.e., $\boldsymbol{r}$ and $\boldsymbol{v}$ are not collinear. Then, $t_f(\boldsymbol{y})$ is infinite and the locus of trajectory $\gamma_{\boldsymbol{y}}$ defines a conic section lying in a two-dimensional plane perpendicular to $\boldsymbol{h}$ called the orbital plane.*

Let

$$\widetilde{\mathcal{Y}} = \{(\boldsymbol{r}, \boldsymbol{v}) \in \mathcal{Y} \mid \boldsymbol{r} \times \boldsymbol{v} = \boldsymbol{h} \neq 0\}. \tag{2.9}$$

Define on $\mathcal{Y}$ the function $e : \boldsymbol{y} \mapsto \| \boldsymbol{L} \| /\mu_e$. Along every trajectory of $\widetilde{\boldsymbol{f}}_0$ starting at $\boldsymbol{y} \in \widetilde{\mathcal{Y}}$, one gets, after multiplying Eq. (2.7) by $\widetilde{\boldsymbol{r}}(t)$, that

$$\| \widetilde{\boldsymbol{r}}(t) \| = \frac{\| \boldsymbol{h} \|^2}{\mu_e (1 + e(\boldsymbol{y}) \cos \theta(t, \boldsymbol{y}))}, \tag{2.10}$$

where the angle $\theta(t, \boldsymbol{y})$ is defined by $\cos\theta(t, \boldsymbol{y}) = \frac{\boldsymbol{L}^T \cdot \widetilde{\boldsymbol{v}}(t)}{\|\widetilde{\boldsymbol{r}}(t)\|\|\boldsymbol{L}\|}$. Note that the previous formula holds true if $\boldsymbol{L} = 0$ since in that case $e(\boldsymbol{y})\cos\theta(t, \boldsymbol{y})$ is equal to zero and the orbit is a circle.

Notice from Eq. (2.10) that an orbit $(\widetilde{\boldsymbol{r}}(t), \widetilde{\boldsymbol{v}}(t)) = \gamma_{\boldsymbol{y}}(t)$ with $\boldsymbol{y} \in \widetilde{\mathcal{Y}}$ on $\mathbb{R}^+$ is a parabola if $e(\boldsymbol{y}) = 1$ and a hyperbola if $e(\boldsymbol{y}) > 1$. Put a satellite on a parabolic or a hyperbolic orbit without any control, then it can escape to infinity $\lim\limits_{t\to+\infty} \widetilde{\boldsymbol{r}}(t) = +\infty$. Thus, parabolic and hyperbolic orbits are generally used for a satellite to escape from the gravitational attraction of Earth. For every point $\boldsymbol{y} \in \widetilde{\mathcal{Y}}$, if $0 \leqslant e(\boldsymbol{y}) < 1$, the orbit $\gamma_{\boldsymbol{y}}(t)$ on $\mathbb{R}^+$ is an ellipse, whose orientation is illustrated in Fig. 2.2. Moreover, it is easy to deduce the following

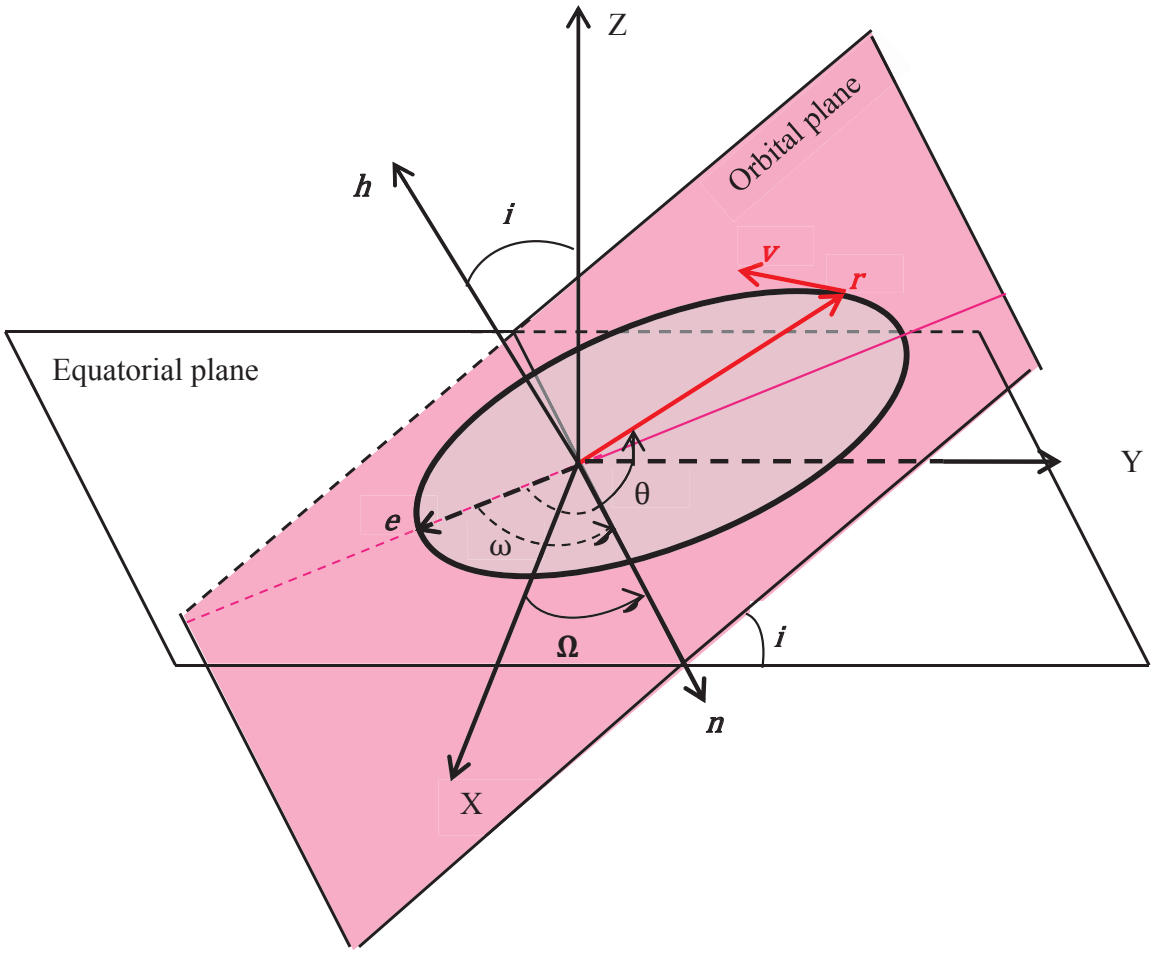

Figure 2.2 – The orientation of a 2-dimensional orbital plane in GICC and the geometric shape and orientation of an elliptic orbit on the orbital plane.

characterization of elliptic orbits.

Property 2.4. *Given every point $\boldsymbol{y} \in \widetilde{\mathcal{Y}}$, the mechanical energy E is negative if and only if $e(\boldsymbol{y}) < 1$.*

Thus, let us define the set

$$\mathcal{P} = \{\boldsymbol{y} \in \widetilde{\mathcal{Y}} \mid E < 0\}, \tag{2.11}$$

then for every point $(\boldsymbol{r}, \boldsymbol{v}) \in \mathcal{P}$, the associated orbit $\gamma_{\boldsymbol{y}}$ on $\mathbb{R}^+$ is periodic and the set $\mathcal{P}$ is called the periodic region in $\widetilde{\mathcal{Y}}$.

Definition 2.1 (Smallest period t_p)**.** *Given every point $\boldsymbol{y} \in \mathcal{P}$, we denote by*

$$t_p : \mathcal{P} \to \mathbb{R},\ \boldsymbol{y} \mapsto t_p(\boldsymbol{y}),$$

the smallest period of the orbit $\gamma_{\boldsymbol{y}}$ on $\mathbb{R}^+$.

According to Eq. (2.10), for every point $\boldsymbol{y} \in \mathcal{P}$, if $e(\boldsymbol{y}) \neq 0$, the associated orbit $\gamma_{\boldsymbol{y}}$ on $[0, t_p(\boldsymbol{y})]$ has its perigee point and apogee point at $\theta(t, \boldsymbol{y}) = 0$ and π, respectively. Thus, let

$$r_p : \mathcal{P} \to \mathbb{R},\ r_p(\boldsymbol{y}) = \frac{\| \boldsymbol{h} \|^2}{\mu_e(1 + e(\boldsymbol{y}))}, \tag{2.12}$$

$$r_a : \mathcal{P} \to \mathbb{R},\ r_a(\boldsymbol{y}) = \frac{\| \boldsymbol{h} \|^2}{\mu_e(1 - e(\boldsymbol{y}))}. \tag{2.13}$$

We say $r_p(\boldsymbol{y})$ and $r_a(\boldsymbol{y})$ are the perigee and apogee distances of the orbit $\gamma_{\boldsymbol{y}}$ on $[0, t_p(\boldsymbol{y})]$ if $e(\boldsymbol{y}) \neq 0$. Note that $r_a(\boldsymbol{y}) = r_p(\boldsymbol{y})$ if and only if $e(\boldsymbol{y}) = 0$, which corresponds to a circular orbit.

Property 2.5 (Minimum radius and maximum radius)**.** *Given every periodic orbit $(\widetilde{\boldsymbol{r}}(t), \widetilde{\boldsymbol{v}}(t)) = \gamma_{\boldsymbol{y}}(t)$ on $[0, t_p(\boldsymbol{y})]$ in $\mathcal{P}$, we have $r_p(\boldsymbol{y}) \leqslant \| \widetilde{\boldsymbol{r}}(t) \| \leqslant r_a(\boldsymbol{y})$ on $[0, t_p(\boldsymbol{y})]$. Thus, the perigee distance $r_p(\boldsymbol{y})$ and apogee distance $r_a(\boldsymbol{y})$ are the minimum radius and maximum radius of the orbit $(\widetilde{\boldsymbol{r}}(t), \widetilde{\boldsymbol{v}}(t))$ on $[0, t_p(\boldsymbol{y})]$.*

2.1.3 Admissible controlled trajectory of Σ_{sat}

For every initial point $\boldsymbol{x}_i = (\boldsymbol{y}_i, m_i) \in \widetilde{\mathcal{Y}} \times \mathbb{R}_+^*$ and measurable control function $\boldsymbol{\tau}(\cdot)$ taking values in $\mathcal{B}_{\tau_{\max}}$, we use $\Gamma(t, \boldsymbol{\tau}(t), \boldsymbol{x}_i)$ to denote the restriction to $\mathbb{R}_+$ of the solution of Σ_{sat} starting from $\boldsymbol{x}_i$. Let $\widetilde{t}_f \in \mathbb{R}^+$ be the maximum time such that solution $\Gamma(t, \boldsymbol{\tau}, \boldsymbol{x}_i)$ lies in $\mathcal{Y} \times \mathbb{R}_+^*$ and set $\mathcal{I}_\Gamma = [0, \widetilde{t}_f)$. The restriction of $\Gamma(t, \boldsymbol{\tau}, \boldsymbol{x}_i)$ to $\mathcal{I}_\Gamma$ is said to be controlled trajectory of Σ_{sat} starting from $\boldsymbol{x}_i$ and associated with $\boldsymbol{\tau}(\cdot)$.

Remark 2.1. *For every point $\boldsymbol{x}_i = (\boldsymbol{y}_i, m_i) \in \mathcal{P} \times \mathbb{R}_+^*$, let $(\boldsymbol{y}(t), m(t)) = \Gamma(t, \boldsymbol{0}, \boldsymbol{x}_i)$ on $\mathcal{I}_\Gamma$, we have that $\boldsymbol{y}(t) = \gamma_{\boldsymbol{y}_i}(t)$ and $m(t) = m_i$ for every $t \geqslant 0$, i.e., $\widetilde{t}_f = \infty$.*

Definition 2.2 (Controlled Keplerian motion)**.** *Given every initial point $\boldsymbol{x}_i = (\boldsymbol{y}_i, m_i) \in \mathcal{P} \times \mathbb{R}_+^*$ and measurable control function $\boldsymbol{\tau}(\cdot)$ taking values in $\mathcal{B}_{\tau_{\max}}$ with $\tau_{\max} > 0$, the corresponding motion of Σ_{sat} is called a controlled Keplerian motion.*

Let $r_c > 0$ and $M_0 > 0$ denote the radius of the surface of atmosphere around the Earth and the mass of a satellite without any fuel, respectively, then given every point $(\boldsymbol{y}, m) \in \mathcal{P} \times \mathbb{R}_+^*$ on the trajectories of Keplerian motions, it is required that $\| \boldsymbol{r} \| > r_c$ and $m > M_0$.

Definition 2.3 (Admissible region)**.** *We define the set*

$$\mathcal{A} = \{\boldsymbol{y} = (\boldsymbol{r}, \boldsymbol{v}) \in \mathcal{P} \mid \parallel \boldsymbol{r} \parallel > r_c\}, \tag{2.14}$$

the admissible region in $\mathcal{P}$ for Keplerian motion and/or controlled Keplerian motion.

Definition 2.4 (Admissible controlled trajectory)**.** *Given every $M_0 > 0$, we say the controlled trajectory $(\boldsymbol{y}(t), m(t)) = \Gamma(t, \boldsymbol{\tau}, \boldsymbol{y}_i, m_i)$ of Σ_{sat} on some finite intervals $[0, t_f] \subset \mathcal{I}_\Gamma$ with initial condition $(\boldsymbol{y}_i, m_i) \in \mathcal{A} \times \mathbb{R}^*_+$ is an admissible controlled trajectory if $\boldsymbol{y}(t) \in \mathcal{A}$ and $m(t) \geqslant M_0$ for $t \in [0, t_f]$.*

For every time interval $[0, t_f] \subset \mathcal{I}_\Gamma$, since $\dot{m}(t) \leqslant 0$, it follows $m(t_f) \leqslant m(t)$ on $[0, t_f]$. Thus, the inequality $m(t) \geqslant M_0$ can be ensured by $m(t_f) \geqslant M_0$.

2.1.4 Controlled problems in $\mathcal{A}$

For $\boldsymbol{y} \in \mathcal{A}$, let $(\widetilde{\boldsymbol{r}}(t), \widetilde{\boldsymbol{v}}(t)) = \gamma_{\boldsymbol{y}}(t)$ on $\mathbb{R}^+$. Then we have that the inequality $\parallel \widetilde{\boldsymbol{r}}(t) \parallel > r_c$ is satisfied on $\mathbb{R}^+$ if $r_p(\boldsymbol{y}) > r_c$. Thus, we define the set:

$$\mathcal{P}^+ \quad = \quad \{\boldsymbol{y} = (\boldsymbol{r}, \boldsymbol{v}) \in \mathcal{P} : r_p(\boldsymbol{y}) > r_c\}. \tag{2.15}$$

It is immediate to see that the periodic uncontrolled trajectory $\gamma(t, \boldsymbol{y})$ starting at any $\boldsymbol{y} \in \mathcal{P}^+$ remains in $\mathcal{P}^+$.

Let

$$\mathcal{P}^- \quad = \quad \{\boldsymbol{y} = (\boldsymbol{r}, \boldsymbol{v}) \in \mathcal{P} \mid \parallel \boldsymbol{r} \parallel > r_c,\ r_p(\boldsymbol{y}) < r_c < r_a(\boldsymbol{y})\}. \tag{2.16}$$

Then, for every point $\boldsymbol{y} \in \mathcal{P}^-$, there exists an interval $[t_1, t_2] \in [0, t_p(\boldsymbol{y})]$ such that $\parallel \widetilde{\boldsymbol{r}}(t) \parallel \leqslant r_c$ for $t \in [t_1, t_2]$. Thus, placing a satellite on a point $\boldsymbol{y} \in \mathcal{P}^-$, it can move out of the admissible region $\mathcal{A}$.

Definition 2.5 (Stable periodic region $\mathcal{P}^+$ and unstable periodic region $\mathcal{P}^-$ in $\mathcal{A}$)**.** *We say that the two sets $\mathcal{P}^+$ and $\mathcal{P}^-$ are the stable and unstable periodic regions, respectively.*

All the satellites periodically moving around the Earth are located in the stable periodic region $\mathcal{P}^+$. In order to fulfill observation or other mission requirements, a satellite is controlled to move from one point $\boldsymbol{y}_i$ in $\mathcal{P}^+$ to another point $\boldsymbol{y}_f$ in $\mathcal{P}^+$ by its control system.

Definition 2.6 (*Orbital Transfer Problem (OTP)*)**.** *We say that the problem of controlling a satellite from a point $\boldsymbol{y}_i$ in $\mathcal{P}^+$ to another point $\boldsymbol{y}_f$ in $\mathcal{P}^+$ is the orbital transfer problem, see Fig. 2.3a.*

For a typical space mission, in order to place a satellite into a stable orbit in $\mathcal{P}^+$, a rocket is used to carry the satellite from the surface of the Earth to a point $\boldsymbol{y}_i$ in $\mathcal{P}^-$, at which the rocket and the satellite are separated. From this moment on, the satellite is controlled by its own control system to be inserted into a stable orbit in $\mathcal{P}^+$.

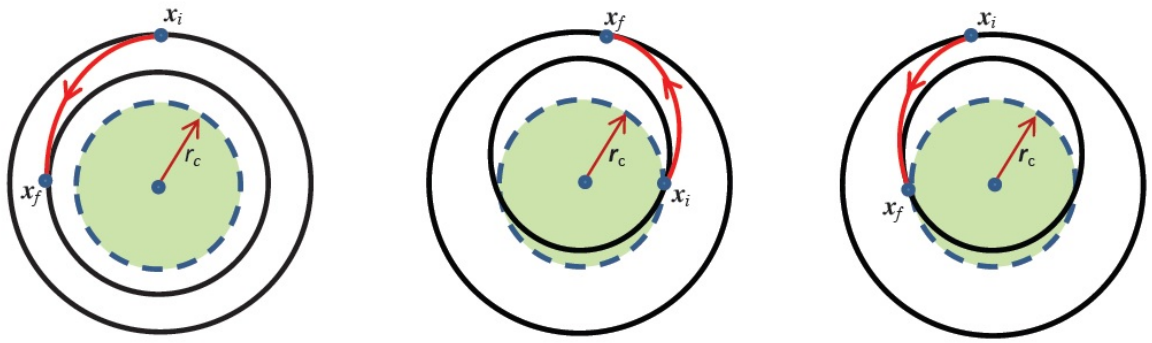

(a) OTP (b) OIP (c) DOP

Figure 2.3 – OTP, OIP, and DOP.

Definition 2.7 (*Orbital Insertion Problem (OIP)*)**.** *We say that the problem of controlling a satellite from an initial point $\boldsymbol{y}_i \in \mathcal{P}^-$ to a final point $\boldsymbol{y}_f \in \mathcal{P}^+$ is the orbit insertion problem, see Fig. 2.3b.*

After a satellite in the stable region $\mathcal{P}^+$ finishes its mission, it should be decelerated to return to the unstable region $\mathcal{P}^-$. Then, the satellite will coast into atmosphere such that the aerodynamic pressure will act as a control to control the satellite to fly to landing sites.

Definition 2.8 (*De-Orbit Problem (DOP)*)**.** *We say that the problem of controlling a satellite from an initial point $\boldsymbol{y}_i \in \mathcal{P}^+$ to a final point $\boldsymbol{y}_f \in \mathcal{P}^-$ is the de-orbit problem, see Fig. 2.3c.*

2.2 Prerequisite for controllability

According to the definition for controlled Keplerian motion in *Definition 2.2*, the controllability of Keplerian motion deals with the existence of admissible controlled trajectories for OTP, OIP, and DOP.

Definition 2.9 (Controllability for OTP)**.** *We say that the system Σ_{sat} is controllable for OTP if there exists $\tau_{\max} > 0$ so that, for every initial mass $m_i > 0$ and every initial and final points $(\boldsymbol{y}_i, \boldsymbol{y}_f) \in (\mathcal{P}^+)^2$, there exists a time $t_f \in \mathcal{I}_\Gamma$ and an admissible controlled trajectory $(\boldsymbol{y}(t), m(t)) = \Gamma(t, \boldsymbol{\tau}, \boldsymbol{y}_i, m_i)$ of Σ_{sat} on $[0, t_f]$ in $\mathcal{A} \times \mathbb{R}_+^*$ such that $\boldsymbol{y}(t_f) = \boldsymbol{y}_f$.*

Definition 2.10 (Controllability for OIP and DOP)**.** *We say that the system Σ_{sat} is controllable for OIP (DOP respectively) from any point $\boldsymbol{y}_i \in \mathcal{P}^-$ ($\boldsymbol{y}_i \in \mathcal{P}^+$ respectively) if for every initial mass $m_i > 0$ there exists $\tau_{\max} > 0$ so that, for every final point $\boldsymbol{y}_f \in \mathcal{P}^+$ ($\boldsymbol{y}_f \in \mathcal{P}^-$ respectively), there exists a time $t_f \in \mathcal{I}_\Gamma$ and an admissible controlled trajectory $(\boldsymbol{y}(t), m(t)) = \Gamma(t, \boldsymbol{\tau}, \boldsymbol{y}_i, m_i)$ of Σ_{sat} on $[0, t_f]$ in $\mathcal{A} \times \mathbb{R}_+^*$ such that $\boldsymbol{y}(t_f) = \boldsymbol{y}_f$.*

For every initial point $\boldsymbol{y}_i \in \mathcal{Y}$ and $\varepsilon > 0$, we use $\Gamma_\varepsilon(t, \boldsymbol{u}(t), \boldsymbol{y}_i)$ to denote the trajectory of Σ_ε in Eq. (2.4) associated with a measurable control $\boldsymbol{u}(\cdot) : [0, \bar{t}_f] \to \mathcal{B}_\varepsilon$ and we define $\bar{t}_f \in \mathbb{R}^+$ as the maximum time such that $\Gamma_\varepsilon(t, \boldsymbol{u}(t), \boldsymbol{y}_i)$ lies in $\mathcal{Y}$ on $[0, \bar{t}_f)$. Set $\overline{\mathcal{I}} = [0, \bar{t}_f)$. We refer to $\Gamma_\varepsilon(t, \boldsymbol{u}(t), \boldsymbol{y}_i)$ as the controlled trajectory of Σ_ε starting from $\boldsymbol{y}_i$ and corresponding to the control $\boldsymbol{u}(\cdot)$.

Remark 2.2. *Since $\gamma_{\boldsymbol{y}}(t) = \Gamma_\varepsilon(t, \mathbf{0}, \boldsymbol{y})$ on $\overline{\mathcal{I}}$, the uncontrolled trajectory $\Gamma_\varepsilon(t, \mathbf{0}, \boldsymbol{y})$ is periodic on $\mathbb{R}^+$ if $\boldsymbol{y} \in \mathcal{P}^+$.*

Lemma 2.1. *Fix $\varepsilon > 0$ and $\boldsymbol{x}_i = (\boldsymbol{y}_i, m_i) \in \mathcal{Y} \times \mathbb{R}^*_+$. Then, given every measurable control $\boldsymbol{u}(\cdot) : [0, t_f] \to \mathcal{B}_\varepsilon$, if $\tau_{\max} \geqslant \varepsilon m_i$, then there exists $M_0 > 0$ and an admissible controlled trajectory $(\boldsymbol{y}(t), m(t)) = \Gamma(t, \boldsymbol{\tau}, \boldsymbol{y}_i, m_i)$ of Σ_{sat} on $[0, t_f]$ in $\mathcal{A} \times [M_0, m_i]$ such that $\Gamma_\varepsilon(t, \boldsymbol{u}, \boldsymbol{y}_i) = \boldsymbol{y}(t)$ for every $t \in [0, t_f]$ and $m(t_f) \geqslant M_0$.*

Proof. Since $m(t) \leqslant m_i$ for each time $t \in [0, t_f]$ and $\tau_{\max} \geqslant \varepsilon m_i$, it follows that the thrust vector $\boldsymbol{\tau}(\cdot)$ on $[0, t_f]$ can take values in the set $\mathcal{B}_{\tau_{\max}}$ such that $\boldsymbol{\tau}(t)/m(t) = \boldsymbol{u}(t)$ for every time $t \in [0, t_f]$. Thus, let $(\boldsymbol{y}(t), m(t)) = \Gamma(t, \boldsymbol{\tau}, \boldsymbol{y}_i, m_i)$, we have $\Gamma_\varepsilon(t, \boldsymbol{u}, \boldsymbol{y}_i) = \boldsymbol{y}(t)$ for every time $t \in [0, t_f]$. Since along the trajectory $(\boldsymbol{y}(t), m(t)) = \Gamma(t, \boldsymbol{\tau}, \boldsymbol{y}_i, m_i)$ on $[0, t_f]$, we have $\boldsymbol{u}(t) = \boldsymbol{\tau}(t)/m(t)$, which implies that $\dot{m}(t) = -\beta \parallel \boldsymbol{u}(t) \parallel m(t)$. Thus, we obtain

$$\begin{aligned} m(t) &= m_i e^{-\beta \int_0^{t_f} \|\boldsymbol{u}(t)\| dt} \\ &> m_i e^{-\beta \varepsilon t_f}. \end{aligned} \tag{2.17}$$

Let $M_0 := m_i e^{-\beta \varepsilon t_f} > 0$. Then $m(t_f) \geqslant M_0$ and the lemma is proved. □

In order to study controllability, it is necessary to first show that the admissible region $\mathcal{A}$ is a connected subset of $\mathcal{P}$.

Lemma 2.2 (Connectedness of $\mathcal{A}$)**.** *The admissible region $\mathcal{A}$ is an arc-connected subset of $\mathcal{P}$, i.e., for every initial point $\boldsymbol{y}_i \in \mathcal{A}$ and every final point $\boldsymbol{y}_f \in \mathcal{A}$, there exists a continuous path $\boldsymbol{y}(\cdot) : [0, 1] \to \mathcal{A},\ \lambda \mapsto \boldsymbol{y}(\lambda)$ such that $\boldsymbol{y}(0) = \boldsymbol{y}_i$, and $\boldsymbol{y}(1) = \boldsymbol{y}_f$.*

Proof. We use the MEOE coordinates (cf. Definition A.2) to prove the result, i.e., it is enough to show that $\mathcal{Z}$ is arc-connected. Let us choose two point $\boldsymbol{z}_i$ and $\boldsymbol{z}_f$ in $\mathcal{Z}$ given by

$$\boldsymbol{z}_i = (P_i, e_{x_i}, e_{y_i}, h_{x_i}, h_{y_i}, l_i), \quad \boldsymbol{z}_f = (P_f, e_{x_f}, e_{y_f}, h_{x_f}, h_{y_f}, l_f),$$

with $\boldsymbol{y}_i = \boldsymbol{y}(\boldsymbol{z}_i)$ and $\boldsymbol{y}_f = \boldsymbol{y}(\boldsymbol{z}_f)$. We thus define the path $\boldsymbol{z} : [0, 1] \to \mathcal{Z}$ by

$$\boldsymbol{z}(\lambda) = (P(\lambda), e_x(\lambda), e_y(\lambda), h_x(\lambda), h_y(\lambda), l(\lambda)),$$

where

$$\begin{aligned} P(\lambda) &= [(1-\lambda) r_i + \lambda r_f][1 + e_x(\lambda)\cos(l(\lambda)) + e_y(\lambda)\sin(l(\lambda))], \\ e_x(\lambda) &= (1-\lambda) e_{x_i} + \lambda e_{x_f},\ e_y(\lambda) = (1-\lambda) e_{y_i} + \lambda e_{y_f}, \\ h_x(\lambda) &= (1-\lambda) h_{x_i} + \lambda h_{x_f},\ h_y(\lambda) = (1-\lambda) h_{h_i} + (1-\lambda) e_{x_i}, \\ l(\lambda) &= (1-\lambda) l_i + \lambda l_f, \end{aligned}$$

where $r_f = \parallel \boldsymbol{r}_f \parallel$ and $r_i = \parallel \boldsymbol{r}_i \parallel$. Note that $e_x(\lambda)^2 + e_y(\lambda)^2 < 1$ for each $\lambda \in [0, 1]$. Let $g(\lambda) = (P(\lambda), e_x(\lambda), e_y(\lambda), h_x(\lambda), h_y(\lambda), l(\lambda))$ on $[0, 1]$, we then have that $g(0) = \boldsymbol{z}_i$

and $g(1) = \boldsymbol{z}_f$. Consider the continuous function $\boldsymbol{y}(\lambda) = (\boldsymbol{r}(\boldsymbol{z}(\lambda)), \boldsymbol{v}(\boldsymbol{z}(\lambda)))$ for $\lambda \in [0,1]$. It follows that $\boldsymbol{y}(0) = \boldsymbol{y}_i$ and $\boldsymbol{y}(1) = \boldsymbol{y}_f$. It is immediate that $\boldsymbol{y}(\lambda) \in \mathcal{A}$ for $\lambda \in [0,1]$. Finally, since $P(\lambda) = (\boldsymbol{r}(\lambda) \times \boldsymbol{v}(\lambda))^2/\mu_e > 0$ and $0 \leqslant e = \sqrt{e_x(\lambda)^2 + e_y(\lambda)^2} < 1$, we have $\boldsymbol{r}(\lambda) \times \boldsymbol{v}(\lambda) \neq 0$ and $E(\lambda) = \frac{\boldsymbol{v}(\lambda)^2}{2} - \frac{\mu_e}{\|\boldsymbol{r}(\lambda)\|} < 0$ on $[0,1]$. This proves the lemma. □

We also need the following lemma.

Lemma 2.3 (Connectedness of $\mathcal{P}^+$)**.** *The set $\mathcal{P}^+$ is a connected subset of $\mathcal{A}$.*

Proof. Given every two points $\boldsymbol{y}_i \in \mathcal{P}^+$ and $\boldsymbol{y}_f \in \mathcal{P}^+$, using the same technique as in the proof of *Lemma 2.2*, let $\boldsymbol{y}(\lambda) = (\boldsymbol{r}(\boldsymbol{z}(\lambda)), \boldsymbol{v}(\boldsymbol{z}(\lambda)))$ on $[0,1]$, but we rewrite $P(\lambda)$ in the following form,

$$P(\lambda) = ((1-\lambda)r_{p_i} + \lambda r_{p_f})(1 + \sqrt{e_x(\lambda)^2 + e_y(\lambda)^2}),$$

where $r_{p_i} = r_p(\boldsymbol{y}_i)$ and $r_{p_f} = r_p(\boldsymbol{y}_f)$. Then, we have

$$r_p(\boldsymbol{y}(\lambda)) = \frac{P(\lambda)}{1 + \sqrt{e_x(\lambda)^2 + e_y(\lambda)^2}} = (1-\lambda)r_{p_i} + \lambda r_{p_f} > r_c.$$

Thus, $\boldsymbol{y}(\cdot)$ on $[0,1]$ takes values in $\mathcal{P}^+$ and this proves the lemma. □

2.3 Controllability for OTP

In this subsection, we first give a controllability property of Σ_ε for OTP, then, according to Lemma 2.1, we will establish the controllability of Σ_{sat} for OTP.

Definition 2.11. *For every controlled trajectory $\overline{\boldsymbol{y}}(\cdot) = \Gamma_\varepsilon(\cdot, \overline{\boldsymbol{u}}, \boldsymbol{y}_i)$ of Σ_ε (where $\varepsilon > 0$, $\overline{\boldsymbol{u}}(\cdot) : [0, t_f] \to \mathcal{B}_\varepsilon$ is measurable and $\boldsymbol{y}_i \in \mathcal{Y}$), we define*

$$\Sigma_\varepsilon^*(\overline{\boldsymbol{y}}) : \dot{\boldsymbol{\lambda}}(t) = A(t)\boldsymbol{\lambda}(t) + B(t)\boldsymbol{u}(t),$$

the linearized system along $\overline{\boldsymbol{y}}(\cdot)$ of Σ_ε on $[0, t_f]$, where

$$A(t) = \widetilde{\boldsymbol{f}}_{\boldsymbol{y}}(\overline{\boldsymbol{y}}(t), \overline{\boldsymbol{u}}(t)), \quad B(t) = \widetilde{\boldsymbol{f}}_{\boldsymbol{u}}(\overline{\boldsymbol{y}}(t), \overline{\boldsymbol{u}}(t)),$$

on $[0, t_f]$.

We first have a result of local controllability for the systems Σ_ε's around the periodic trajectories of the drift vector field.

Lemma 2.4. *Let $\overline{\boldsymbol{y}} \in \mathcal{P}^+$. Then, for every $\rho > 0$, there exists $\sigma > 0$ such that the following properties hold: $\mathcal{B}_\sigma(\overline{\boldsymbol{y}}) \subset \mathcal{P}^+$ and, for every $\boldsymbol{y} \in \mathcal{B}_\sigma(\overline{\boldsymbol{y}})$, there exists a controlled trajectory $\Gamma_\varepsilon(t, \boldsymbol{u}(t), \overline{\boldsymbol{y}})$ of Σ_ε such that*

$$\Gamma_\varepsilon(0, \boldsymbol{u}, \overline{\boldsymbol{y}}) = \overline{\boldsymbol{y}}, \quad \Gamma_\varepsilon(t_p(\overline{\boldsymbol{y}}), \boldsymbol{u}, \overline{\boldsymbol{y}}) = \boldsymbol{y},$$

and

$$\| \Gamma_\varepsilon(t, \boldsymbol{u}, \overline{\boldsymbol{y}}) - \Gamma_\varepsilon(t, \mathbf{0}, \overline{\boldsymbol{y}}) \| < \rho,$$

for $t \in [0, t_p(\overline{\boldsymbol{y}})]$.

Proof. According to Theorem 7 of Chapter 3 in Ref. [87], it suffices to prove the controllability of the linearized system $\Sigma^*_\varepsilon(\Gamma_\varepsilon(t, \mathbf{0}, \overline{\boldsymbol{y}}))$ along the periodic trajectory $\Gamma_\varepsilon(t, \mathbf{0}, \overline{\boldsymbol{y}})$ on the interval $[0, t_p(\overline{\boldsymbol{y}})]$. Then, the latter controllability would follow, according to Corollary 3.5.18 of Chapter 3 in Ref. [87], by the following rank condition: there exists a time $\tau \in [0, t_p(\overline{\boldsymbol{y}})]$ and a nonnegative integer k such that the rank of the matrix $[B_0(\tau), B_1(\tau), \cdots, B_k(\tau)]$ equals 6, where $B_{i+1}(t) = A(t)B_i(t) - \frac{d}{dt}B_i(t)$ for $i = 1, 2, \cdots$, and $B_0(t) = B(t)$. It therefore amounts to compute some $B_i(\cdot)$'s. The explicit expressions for matrices A and B in terms of $\boldsymbol{y}$ are

$$A = \widetilde{\boldsymbol{f}}_{\boldsymbol{y}} = \begin{bmatrix} \mathbf{0} & I_3 \\ -\frac{\mu}{\|\boldsymbol{r}\|^3} I_3 + 3\frac{\mu}{\|\boldsymbol{r}\|^5} \boldsymbol{r} \cdot \boldsymbol{r}^T & \mathbf{0} \end{bmatrix} \text{ and } B = \widetilde{\boldsymbol{f}}_{\boldsymbol{u}} = \begin{bmatrix} \mathbf{0} \\ I_3 \end{bmatrix}.$$

Since $B_0(t) = B(t)$, it follows that

$$\begin{aligned} B_1(t) &= A(t)B_0(t) - \frac{d}{dt}B_0(t) \\ &= A(t)B_0(t) = \begin{bmatrix} I_3 & \mathbf{0} \end{bmatrix}^T. \end{aligned}$$

Thus, we have that the rank of the matrix $[B_0(t), B_1(t)] = \begin{bmatrix} \mathbf{0} & I_3 \\ I_3 & \mathbf{0} \end{bmatrix}$ is equal to 6 for every time $t \in [0, t_p(\overline{\boldsymbol{y}})]$, proving the lemma. □

Proposition 2.1. *For $\varepsilon > 0$, the control system Σ_ε is controllable for OTP within $\mathcal{P}^+$, i.e., for every initial point $\boldsymbol{y}_i \in \mathcal{P}^+$ and final point $\boldsymbol{y}_f \in \mathcal{P}^+$, there exists a controlled trajectory $\Gamma_\varepsilon(t, \boldsymbol{u}, \boldsymbol{y}_i)$ of Σ_ε in $\mathcal{P}^+$ on a finite interval $[0, t_f] \subset \overline{\mathcal{I}}$ such that $\Gamma_\varepsilon(t_f, \boldsymbol{u}, \boldsymbol{y}_i) = \boldsymbol{y}_f$.*

Proof. Since the subset $\mathcal{P}^+$ is path-connected as is shown by *Proposition* 2.3, it follows that any two different points $\boldsymbol{y}_i$ and $\boldsymbol{y}_f$ in $\mathcal{P}^+$ are connected by a path $\boldsymbol{y} : [0, 1] \to \mathcal{P}^+,\ \lambda \mapsto \boldsymbol{y}(\lambda)$ such that $\boldsymbol{y}(0) = \boldsymbol{y}_i$ and $\boldsymbol{y}(1) = \boldsymbol{y}_f$. By compactness of the support of $\boldsymbol{y}(\cdot)$ in $\mathcal{P}^+$ there exists, for every $\sigma > 0$, a finite sequence of points $\boldsymbol{y}_0, \boldsymbol{y}_1, \cdots, \boldsymbol{y}_N$, on the support of $\boldsymbol{y}(\lambda)$ so that $\boldsymbol{y}_0 = \boldsymbol{y}_i$, $\boldsymbol{y}_n = \boldsymbol{y}_f$ and $\boldsymbol{y}_{j+1} \in \mathcal{B}_\sigma(\boldsymbol{y}_j)$, for $j = 0, 1, \cdots, N-1$. According to *Lemma* 2.4, for every $\rho > 0$, there exists $\sigma > 0$ small enough and a finite sequence of points $\boldsymbol{y}_0, \boldsymbol{y}_1, \cdots, \boldsymbol{y}_N$ as above such that, for $j = 0, 1, \cdots, N-1$, $\boldsymbol{y}_{j+1} \in \mathcal{B}_\sigma(\boldsymbol{y}_j)$ and one has a controlled trajectory $\Gamma_\varepsilon(t, \boldsymbol{u}_j, \boldsymbol{y}_j)$ on the interval $[0, t_p(\boldsymbol{y}_j)]$ such that

$$\Gamma_\varepsilon(0, \boldsymbol{u}_j, \boldsymbol{y}_j) = \boldsymbol{y}_j, \ \ \Gamma_\varepsilon(t_p(\boldsymbol{y}_j), \boldsymbol{u}_j, \boldsymbol{y}_j) = \boldsymbol{y}_{j+1},$$

and

$$\| \Gamma_\varepsilon(t, \boldsymbol{u}_j(t), \boldsymbol{y}_j) - \Gamma_\varepsilon(t, \mathbf{0}, \boldsymbol{y}_j) \| < \rho, \text{ for } t \in [0, t_p(\boldsymbol{y}_j)].$$

For $\sigma > 0$, let $\mathcal{W}_j \subset \mathcal{P}^+$ be an open neighborhood of $\boldsymbol{y}_j$ such that $\mathcal{B}_\sigma(\boldsymbol{y}_j) \subset \mathcal{W}_j$ for $j = 0, 1, \cdots, N$ and set $\mathcal{P}^+_{\mathcal{W}_j} = \{\Gamma_\varepsilon(t, 0, \mathcal{W}_j),\ t \geqslant 0\}$. For $\rho > 0$ small enough, the open set

$\mathcal{P}^+_{\mathcal{W}_j}$ is included in $\mathcal{P}^+$. By concatenating the $\Gamma_\varepsilon(\cdot, \boldsymbol{u}_j, \boldsymbol{y}_j)$ for $j = 0, 1, \cdots, N-1$, the initial point $\boldsymbol{y}_i$ can be steered to $\boldsymbol{y}_f$, proving the proposition. □

According to Lemma 2.1, and recalling the definition of controllability for OTPs in Definition 2.6, we obtain the following result of controllability:

Corollary 2.1. *For every $\mu_e > 0$, $\beta > 0$, $\tau_{\max} > 0$, the system Σ_{sat} is controllable for OTP.*

Note that $\mathcal{P}^+ \subset \mathcal{A}$, so the system Σ_{sat} is controllable for OTPs within $\mathcal{A}$ no matter what value of $\tau_{\max}$ the low-thrust control system can provide if the satellite takes high enough percent of total fuel, i.e., $(m_i - m_f)/m_i > 0$ is big enough. This result makes senses in engineering for electric thrust systems whose maximum thrust $\tau_{\max}$ is very small.

2.4 Controllability for OIP

We provide next a controllability criterion for OIP.

Lemma 2.5. *Assume that, for every point $(\boldsymbol{y}_i, m_i) \in \mathcal{P}^- \times \mathbb{R}^*_+$, there exists $\tau_{max} > 0$, a positive time $\bar{t} \in \mathcal{I}_\Gamma$, and a control $\widetilde{\boldsymbol{\tau}}(\cdot) : [0, \bar{t}] \to \mathcal{B}_{\tau_{\max}}$ such that along the controlled trajectory $(\widetilde{\boldsymbol{y}}, \widetilde{m}(t)) = \Gamma(t, \widetilde{\boldsymbol{\tau}}(t), \boldsymbol{y}_i, m_i)$ on $[0, \bar{t}]$, we have $\widetilde{\boldsymbol{y}}(t) \in \mathcal{A}$ on $[0, \bar{t}]$, $\widetilde{m}(\bar{t}) > 0$, and $r_p(\widetilde{\boldsymbol{y}}(\bar{t})) > r_c$. Then, the system Σ_{sat} is controllable for OIP from $(\boldsymbol{y}_i, m_i)$.*

Proof. Note that the assumption implies that there exists a control $\widetilde{\boldsymbol{\tau}}(\cdot) : [0, \bar{t}] \to \mathcal{B}_{\tau_{\max}}$ such that the admissible controlled trajectory $(\widetilde{\boldsymbol{y}}(t), \widetilde{m}(t)) = \Gamma(t, \widetilde{\boldsymbol{\tau}}, \boldsymbol{y}_i, m_i)$ in $\mathcal{A} \times [m(\bar{t}), m_i]$ on $[0, \bar{t}]$ steers $(\boldsymbol{y}_i, m_i)$ in $\mathcal{P}^- \times \mathbb{R}^*_+$ to some $(\boldsymbol{y}(\bar{t}), m(\bar{t}))$ in $\mathcal{P}^+ \times \mathbb{R}^*_+$. After arriving at $\boldsymbol{y}(\bar{t})$ in $\mathcal{P}^+$, according to Proposition 2.1, it follows that there exists an $M_0 \in (0, m(\bar{t})]$, a finite time $t_f \in \mathcal{I}_\Gamma$, and a control $\boldsymbol{\tau}(\cdot) : [0, t_f] \to \mathcal{B}_{\tau_{\max}}$ such that along the controlled trajectory $(\boldsymbol{y}(t), m(t)) = \Gamma(t, \boldsymbol{\tau}, \widetilde{\boldsymbol{y}}(\tau), \widetilde{m}(\tau))$ on $[0, t_f]$, we have $\boldsymbol{y}(t) \in \mathcal{A}$ on $[0, t_f]$, $\boldsymbol{y}(t_f) = \boldsymbol{y}_f$, and $m(t_f) > M_0$. □

One cannot have controllability for OIP for every value of $\tau_{\max} > 0$. Indeed, pick a point $(\boldsymbol{y}_i, m_i)$ in $\mathcal{P}^- \times \mathbb{R}^*_+$. For every control $\boldsymbol{\tau}(\cdot)$ taking values in $\mathcal{B}_{\tau_{\max}}$, the corresponding controlled trajectory $(\boldsymbol{y}(\cdot), m(\cdot)) = \Gamma(\cdot, \boldsymbol{\tau}, \boldsymbol{y}_i, m_i)$ converges to $\Gamma(\cdot, \mathbf{0}, \boldsymbol{y}_i, m_i)$ on $[0, t_p(\boldsymbol{y}_i)]$ as $\tau_{\max}$ tends to zero. Then, since $r_p(\boldsymbol{y}_i) < r_c$, there exists $t \in [0, t_p(\boldsymbol{y}_i)]$ such that $\| \boldsymbol{r}(t) \| < r_c$ implying that $(\boldsymbol{y}(\cdot), m(\cdot)) = \Gamma(\cdot, \boldsymbol{\tau}, \boldsymbol{y}_i, m_i)$ is not admissible for every control $\boldsymbol{\tau}(\cdot)$ taking values in $\mathcal{B}_{\tau_{\max}}$. For large values of $\tau_{\max}$, we can steer $(\boldsymbol{y}_i, m_i) \in \mathcal{P}^- \times \mathbb{R}^*_+$ to $(\boldsymbol{y}_f, m_f) \in \mathcal{P}^+ \times \mathbb{R}^*_+$ as described in the following lemma.

Lemma 2.6. *For every $\beta, \mu_e > 0$ and point $\boldsymbol{x}_i = (\boldsymbol{y}_i, m_i)$ in $\mathcal{P}^- \times \mathbb{R}^*_+$, there exists $\overline{\tau}_{\max} > 0$ such that the following holds:*

1) *if $\tau_{\max} > \overline{\tau}_{\max}$, there exists a control $\boldsymbol{\tau}(\cdot)$ taking values in $\mathcal{B}_{\tau_{\max}}$ and a positive time $\bar{t} \in \mathcal{I}_\Gamma$ such that, along the controlled trajectory $(\boldsymbol{y}(t), m(t)) = \Gamma(t, \boldsymbol{\tau}, \boldsymbol{y}_i, m_i)$ on $[0, \bar{t}]$, we have $\boldsymbol{y}(t) \in \mathcal{A}$ on $[0, \bar{t}]$, $m(\bar{t}) > 0$, and $r_p(\boldsymbol{y}(\bar{t})) > r_c$;*

2) *if* $\tau_{\max} \leqslant \overline{\tau}_{\max}$, *for every control* $\boldsymbol{\tau}(\cdot)$ *taking values in* $\mathcal{B}_{\tau_{\max}}$, *the controlled trajectory* $(\boldsymbol{y}(\cdot), m(\cdot)) = \Gamma(\cdot, \boldsymbol{\tau}, \boldsymbol{y}_i, m_i)$ *does not reach* $\mathcal{P}^+ \times \mathbb{R}^*_+$.

Proof. At the light of the remark preceding the lemma, it is enough to find a value of $\widetilde{\tau}_{\max}$ and a control $\boldsymbol{\tau}(\cdot)$ taking values in $\mathcal{B}_{\widetilde{\tau}_{\max}}$ steering $\boldsymbol{x}_i = (\boldsymbol{y}_i, m_i)$ to some point in $\mathcal{P}^+ \times \mathbb{R}^*_+$ along an admissible trajectory. We proceed as follows. Let $C_0 = \|\boldsymbol{r}_i\|^{1/2}\|\boldsymbol{v}_i\|$ which belongs to $(0, \sqrt{2\mu_e})$. Choose now the function $\boldsymbol{v}(\cdot)$ defined on some time interval $[0, \overline{T}]$ (with $\overline{T}$ to be fixed later) as follows: $\boldsymbol{v}(0) = \boldsymbol{v}_i$, $\dot{\boldsymbol{r}}(t) = \boldsymbol{v}(t)$ and

$$\boldsymbol{v}(t) = \frac{C_0}{(2\boldsymbol{r}(t))^{1/2}} \left(a_i \frac{\boldsymbol{r}(t)}{\|\boldsymbol{r}(t)\|} + b_i \frac{\boldsymbol{r}(t)^\perp}{\|\boldsymbol{r}(t)\|} \right), \ t \in [0, T].$$

Here $\boldsymbol{r}(t)^\perp$ denotes a continuous choice of vector perpendicular to $\boldsymbol{r}(t)$ in the 2D plane spanned by $\boldsymbol{r}_i$ and $\boldsymbol{v}_i$. (Implicitly, we assume with no loss of generality that $\boldsymbol{v}_i \neq 0$ with $a_i > 0$ and $b_i \neq 0$.) For simplicity, we assume next that $a_i = b_i = 1$. The curve $(\boldsymbol{r}(\cdot), \boldsymbol{v}(\cdot))$ defined previously can be explicitly integrated using polar coordinates for $\boldsymbol{r}(\cdot) = r(\cdot)\exp(i\theta(\cdot))$. One gets that, on $[0, T]$,

$$\dot{r}(t) = r(t)\dot{\theta}(t) = \left(\frac{C_0}{2r(t)} \right)^{1/2}.$$

After integration, one has for $t \in [0, T]$,

$$r(t) = (r_i^{3/2} + 3C_0 t/2)^{2/3}, \ \ \theta(t) = \theta_i + 2\ln(r_i^{3/2} + 3C_0 t/2)/3.$$

One also checks that $\boldsymbol{h}(t) = C_0(\frac{r(t)}{2})^{1/2}\boldsymbol{e}_i$, with $\boldsymbol{e}_i$ a constant vector of unit norm parallel to $\boldsymbol{r}_i \times \boldsymbol{v}_i$ and $\boldsymbol{L}(t) = (C_0^2/2 - \mu_e)\frac{\boldsymbol{r}(t)}{\|\boldsymbol{r}(t)\|}$. One deduces that $r_p(t) = C_1 r(t)^{1/2}$ for some positive constant C_1. One thus fixes $\overline{T}$ so that $r_p(\overline{T}) > r_c$. It remains to determine $\widetilde{\tau}_{\max}$ so that $(\boldsymbol{r}(t), \boldsymbol{v}(t))$ is part of a controlled admissible trajectory of system Σ_ε. One first integrates over $[0, T]$ the differential equation

$$\dot{m}(t) = -\beta\|\dot{\boldsymbol{v}}(t) + \frac{\mu_e}{r(t)^3}\boldsymbol{r}(t)\|m(t),$$

and then take $\boldsymbol{\tau}(t) = \left(\dot{\boldsymbol{v}}(t) + \frac{\mu_e}{r(t)^3}\boldsymbol{r}(t)\right) m(t)$ for $t \in [0, T]$. The final bound $\widetilde{\tau}_{\max}$ is simply the maximum of $\|\boldsymbol{\tau}(t)\|$ over $[0, T]$. □

As a combination of Lemmas 2.5 and 2.6, we obtain the following result.

Corollary 2.2. *For every* $\beta > 0$, $\mu_e > 0$, *and initial point* $(\boldsymbol{y}_i, m_i) \in \mathcal{P}^- \times \mathbb{R}^*_+$, *there exists a limiting value* $\overline{\tau}_{\max} > 0$ *depending on* $(\boldsymbol{y}_i, m_i)$ *such that the following properties hold:*

1) *if* $\tau_{\max} > \overline{\tau}_{\max}$, *the system* Σ_{sat} *is controllable for the OIP; and*

2) *if* $\tau_{\max} \leqslant \overline{\tau}_{\max}$, *the system* Σ_{sat} *is not controllable for the OIP.*

The limiting value $\overline{\tau}_{\max}$ can be computed by combining a shooting method and a bisection method as described in Section 2.6.

2.5 Controllability for DOP

Let us define a system $\widetilde{\Sigma}_{\text{sat}}$ associated to Σ_{sat} as

$$\widetilde{\Sigma}_{\text{sat}} : \begin{cases} \dot{\boldsymbol{r}}(t) = \boldsymbol{v}(t), \\ \dot{\boldsymbol{v}}(t) = -\frac{\mu_e}{\|\boldsymbol{r}(t)\|^3}\boldsymbol{r}(t) + \frac{\boldsymbol{\tau}(t)}{m(t)}, \\ \dot{m}(t) = +\beta \parallel \boldsymbol{\tau}(t) \parallel, \end{cases} \tag{2.18}$$

where all variables are the same as defined in Eq. (2.1). For every $\boldsymbol{x}_i \in \widetilde{\mathcal{Y}} \times \mathbb{R}^*_+$ and measurable control function $\boldsymbol{\tau}$ taking values in $\mathcal{B}_{\tau_{\max}}$ with $\tau_{\max} > 0$, we define by $\widetilde{\Gamma}(t, \boldsymbol{\tau}(t), \boldsymbol{x}_i)$ the corresponding trajectory of $\widetilde{\Sigma}_{\text{sat}}$ for some positive times.

Remark 2.3. *For every controlled trajectory* $(\boldsymbol{r}(t), \boldsymbol{v}(t), m(t)) = \Gamma(t, \boldsymbol{\tau}(t), \boldsymbol{x}_i)$ *of the system* Σ_{sat} *on some finite intervals* $[0, t_f] \subset \mathcal{I}_\Gamma$ *with* $(\boldsymbol{r}_f, \boldsymbol{v}_f, m_f) = \Gamma(t_f, \boldsymbol{\tau}(t_f), \boldsymbol{x}_i)$*, the trajectory* $(\widetilde{\boldsymbol{r}}(t), \widetilde{\boldsymbol{v}}(t), \widetilde{m}(t)) = \widetilde{\Gamma}(t, \boldsymbol{\tau}(t_f - t), \boldsymbol{r}_f, -\boldsymbol{v}_f, m_f)$ *of* $\widetilde{\Sigma}_{\text{sat}}$ *runs backward in time along the trajectory* $\Gamma(t, \boldsymbol{\tau}(t), \boldsymbol{x}_i)$ *on* $[0, t_f]$*, i.e.,*

$$(\widetilde{\boldsymbol{r}}(t), \widetilde{\boldsymbol{v}}(t), \widetilde{m}(t)) = (\boldsymbol{r}(t_f - t), -\boldsymbol{v}(t_f - t), m(t_f - t)) \text{ on } [0, t_f]. \tag{2.19}$$

As a consequence, according to Lemma 2.6 and Corollary 2.2, we obtain the following result.

Corollary 2.3. *For each* $\beta > 0$*,* $\mu_e > 0$*, and* $m_i > 0$*, given a point* $(\boldsymbol{r}_f, \boldsymbol{v}_f) \in \mathcal{P}^-$*, there exists a* $\overline{\tau}_{\max} > 0$ *depending on* $(\boldsymbol{r}_f, \boldsymbol{v}_f)$ *and* m_i *such that the following properties hold:*

1) *if* $\tau_{\max} > \overline{\tau}_{\max}$*, the system* Σ_{sat} *is controllable for the corresponding DOP; and*

2) *if* $\tau_{\max} \leqslant \overline{\tau}_{\max}$*, the system* Σ_{sat} *is not controllable for the corresponding DOP.*

2.6 Numerical Examples

In this section, we consider two numerical examples, one OIP and one DOP, to compute the limiting value $\overline{\tau}_{\max}$ in Corollaries 2.2 and 2.3, respectively. The gravitational constant μ_e in system Σ_{sat} (and/or $\widetilde{\Sigma}_{\text{sat}}$) equals 3986000.47 km^3/s^2, the radius of the Earth is $r_e = 6,374,004$ m, and we consider the vertical depth of atmosphere around the Earth is $90,000$ m, which means $r_c = r_e + 90,000$ m.

2.6.1 A numerical example for OIP

In order to be able to compute the limiting value $\overline{\tau}_{\max}$ in Corollary 2.2, we first define the following optimal control problem.

Definition 2.12 (*Optimal control problem (OCP) for OIP*). *Given every initial point* $(\boldsymbol{y}_i, m_i) \in \mathcal{P}^- \times \mathbb{R}^*_+$ *and* $\tau_{max} > 0$*, the optimal control problem for OIP consists of steering a satellite by* $\boldsymbol{\tau}(\cdot) \in \mathcal{B}_{\tau_{\max}}$ *on a time interval* $[0, t_f] \subset \mathcal{I}_\Gamma$ *along system* Σ_{sat} *such that, along the controlled trajectory* $(\boldsymbol{r}(t), \boldsymbol{v}(t), m(t)) = \Gamma(t, \boldsymbol{\tau}(t), \boldsymbol{y}_i, m_i)$*, the time* $t_f > 0$ *is the first occurrence for* $\| \boldsymbol{r}(t_f) \| = r_p(\boldsymbol{r}(t_f), \boldsymbol{v}(t_f))$*, i.e.,* $\| \boldsymbol{r}(t) \| > r_p(\boldsymbol{r}(t), \boldsymbol{v}(t))$ *on* $[0, t_f)$*, and that* $r_p(\boldsymbol{r}(t_f), \boldsymbol{v}(t_f))$ *is maximized, i.e., the cost functional is*

$$J = \int_0^{t_f} \frac{d}{dt} r_p(\boldsymbol{r}(t), \boldsymbol{v}(t)) dt. \tag{2.20}$$

Let $\widetilde{t}_f > 0$ be the optimal final time of the OCP for OIP, and let $(\widetilde{\boldsymbol{y}}(t), \widetilde{m}(t)) = \Gamma(t, \widetilde{\boldsymbol{\tau}}(t), \boldsymbol{y}_i, m_i)$ on $[0, \widetilde{t}_f]$ be the optimal controlled trajectory with the associated optimal control $\widetilde{\boldsymbol{\tau}}(t) \in \mathcal{B}_{\tau_{\max}}$ on $[0, \widetilde{t}_f]$. One can check, by using Pontryagin Maximum Principle as was done in Ref. [20], that $\| \widetilde{\boldsymbol{\tau}}(\cdot) \| = \tau_{max}$ on the whole interval $[0, \widetilde{t}_f]$. Thus, fixing the initial point $(\boldsymbol{y}_i, m_i) \in \mathcal{P}^- \times \mathbb{R}^*_+$, we have that the final time $\widetilde{t}_f$, the trajectory $(\widetilde{\boldsymbol{y}}(t), \widetilde{m}(t))$ at each time $t \in [0, \widetilde{t}_f]$, and the final perigee distance $r_p(\widetilde{\boldsymbol{y}}(\widetilde{t}_f))$ are functions of $\tau_{\max}$. Thus, let us define a function

$$s : \mathbb{R}_+ \to \mathbb{R}, \; s(\tau_{max}) = r_p(\widetilde{\boldsymbol{y}}(\widetilde{t}_f)) - r_c. \tag{2.21}$$

If $\overline{\tau}_{\max} > 0$ is the limiting value in Corollary 2.2, there must hold $s(\overline{\tau}_{\max}) = 0$. Thus, to compute the limiting value in Corollary 2.2, it amounts to find a $\overline{\tau}_{\max} > 0$ such that $s(\overline{\tau}_{\max}) = 0$. For every $\tau_{max} > 0$, using a shooting method as an inner loop to solve the OCP for OIP, we can obtain a value for $s(\tau_{max})$. Then, using a bisection method as an outer loop, one can obtain $\overline{\tau}_{\max} > 0$ such that $s(\overline{\tau}_{\max}) = 0$. According to Eq. (2.13) and the objective of the OCP for OIP, placing a satellite with the initial mass $m_i > 0$ on a point $(\boldsymbol{r}_i, \boldsymbol{v}_i) \in \mathcal{P}^-$, the optimal controlled trajectory lies on a 2-dimensional plane spanned by $\boldsymbol{r}_i$ and $\boldsymbol{v}_i$. Hence, the limiting value $\overline{\tau}_{\max}$ in Corollary 2.2 is determined only by $\| \boldsymbol{r}_i \|$, $\| \boldsymbol{v}_i \|$, and by the flight path angle $\eta_i \in [-\pi/2, \pi/2]$, i.e., the angle between the velocity vector $\boldsymbol{v}_i$ and local horizontal plane, defined by

$$\eta_i = \sin^{-1}\left(\frac{\boldsymbol{r}_i^T \boldsymbol{v}_i}{\| \boldsymbol{r}_i \| \| \boldsymbol{v}_i \|} \right).$$

Assume that a rocket carries a satellite, whose initial mass is $m_i = 150\ kg$, from the surface of the Earth to a point $\boldsymbol{y}_i = (\boldsymbol{r}_i, \boldsymbol{v}_i)$ in the unstable region $\mathcal{P}^-$ such that $\| \boldsymbol{r}_i \| = r_e + 110,000\ m$, $\| \boldsymbol{v}_i \| = 7879.5\ m/s$, and $\eta_i = 5^\circ$. The rocket and the satellite are separated at this point $\boldsymbol{y}_i$. Then, the satellite has to use its own engine to steer itself from the point $\boldsymbol{y}_i$ into the stable region $\mathcal{P}^+$. We can see from Figure 2.4 that the periodic orbit $\gamma_{\boldsymbol{y}_i}$ has collisions with the surface of the atmosphere around the Earth.

We choose the specific impulse of the engine fixed on the satellite as $I_{\text{sp}} = 2000$ s, which implies that $\beta = \frac{1}{I_{\text{sp}} g_0} = 5.102 \times 10^{-5}\ \text{m}^{-2}$ where $g_0 = 9.8\ \text{m}^2/\text{s}$. The computed result of the limiting value is $\overline{\tau}_{\max} = 8.052\ N$. Thus, in order to be able to insert the satellite from the point $\boldsymbol{y}_i$ into stable region $\mathcal{P}^+$, the maximum thrust of the engine has to be larger than $8.052\ N$. The optimal controlled trajectory of the corresponding OCP for OIP with $\overline{\tau}_{\max} = 8.052$ is

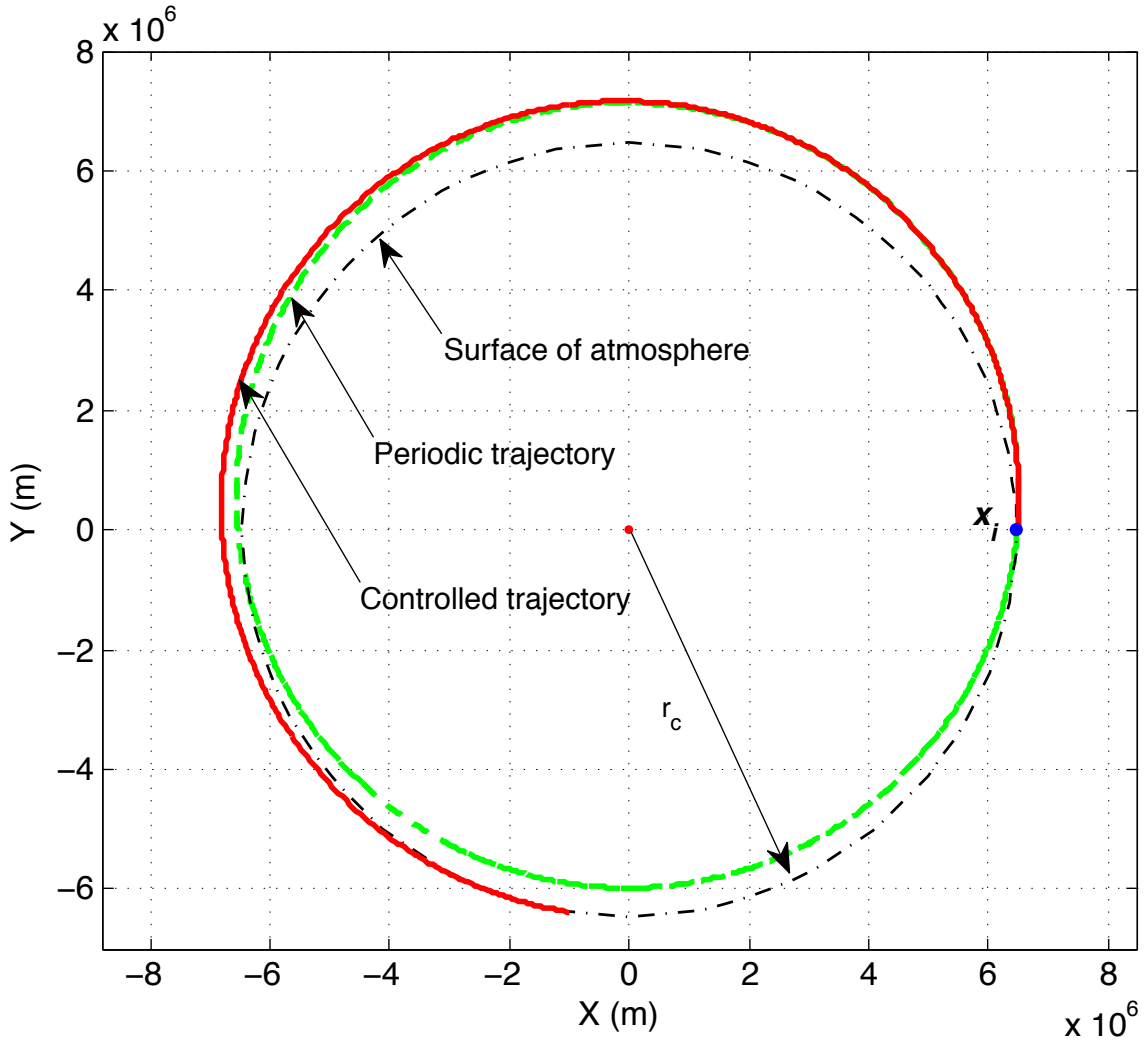

Figure 2.4 – The periodic orbital $\gamma_{\boldsymbol{y}_i}$ and the optimal controlled trajectory of the OCP for OIP with $\tau_{\max} = \overline{\tau}_{\max}$ starting from $\boldsymbol{y}_i$.

plotted in Figure 2.4 as well. To see the numerical results for different initial points, another two points $\boldsymbol{y}_1 = (\boldsymbol{r}_1, \boldsymbol{v}_1)$ and $\boldsymbol{y}_2 = (\boldsymbol{r}_2, \boldsymbol{v}_2)$ are chosen on the periodic orbit $\gamma_{\boldsymbol{y}_i}$ such that

$$\| \boldsymbol{r}_1 \| = r_e + 379,494\ m,\ \| \boldsymbol{v}_1 \| = 7,562\ m/s,\ \eta_1 = 4.3517^\circ,$$

$$\| \boldsymbol{r}_2 \| = r_e + 599,351\ m,\ \| \boldsymbol{v}_2 \| = 7,312\ m/s,\ \eta_2 = 3.0132^\circ.$$

Then, the limiting value of $\overline{\tau}_{\max}$ corresponding to the two initial points $\boldsymbol{y}_j$, $j = 1, 2$, are computed as $9.037\ N$ and $10.719\ N$, respectively. We see that the limiting values $\overline{\tau}_{\max}$ are different for different initial points on the same periodic orbit. The time history of radius $\| \boldsymbol{r}(t) \|$ and perigee distance $r_p(\boldsymbol{x}(t))$ along the optimal controlled trajectories starting from the initial points $\boldsymbol{y}_i$ and $\boldsymbol{y}_j$, $j = 1, 2$, are plotted in Figure 2.5. Since the three points $\boldsymbol{y}_i$ and $\boldsymbol{y}_j$, $j = 1, 2$ lie on the same periodic orbit $\gamma_{\boldsymbol{y}_i}$, r_p at initial time is the same, as shown in Figure 2.5.

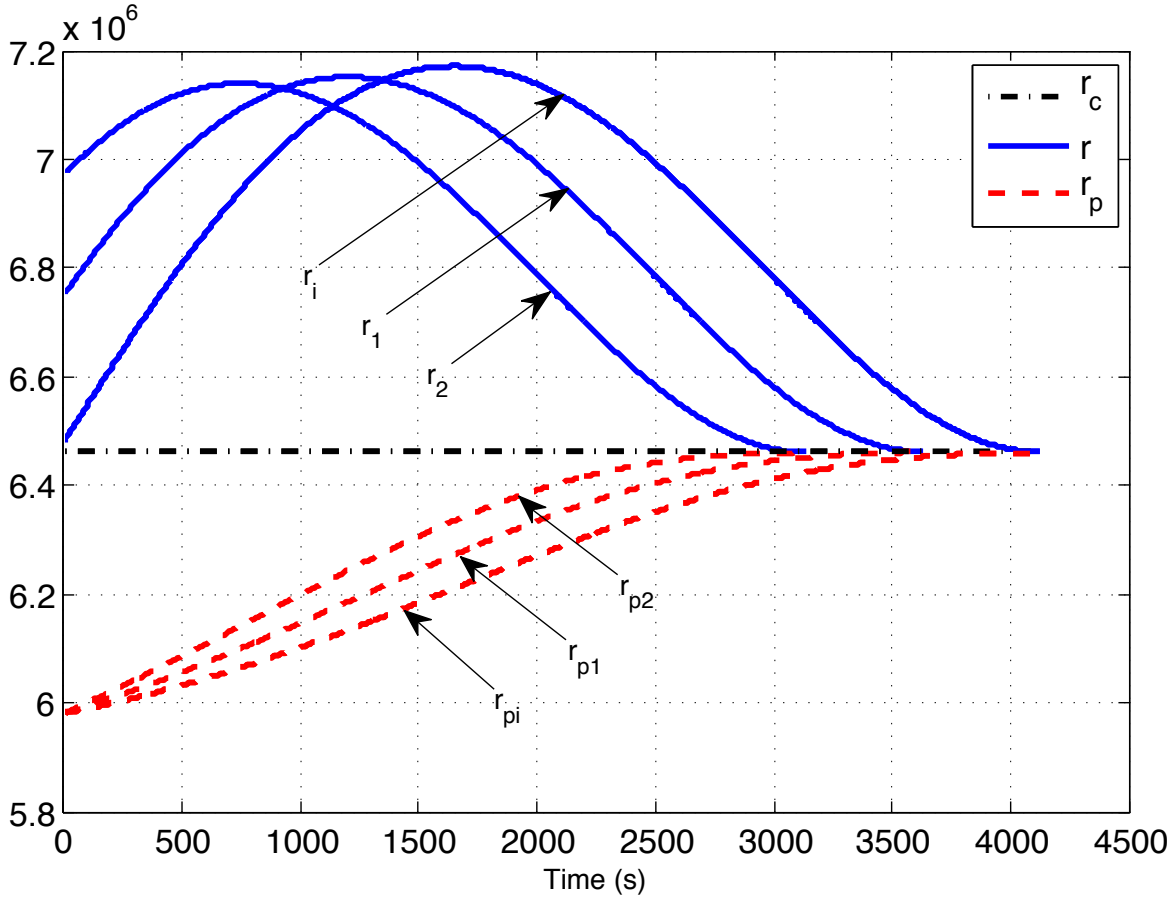

Figure 2.5 – The profile of $\| \boldsymbol{r} \|$ and r_p with respect to time for 3 different initial points, i.e., $\boldsymbol{y}_i$ and $\boldsymbol{y}_j$ $(j = 1, 2)$, for OIP; The subscripts, i, 1, and 2, correspond to the initial points $\boldsymbol{y}_i$, $\boldsymbol{y}_1$, and $\boldsymbol{y}_2$, respectively.

2.6.2 A numerical example for DOP

A DOP is a powered flight phase of a satellite in the region $\mathcal{A} \times \mathbb{R}^*_+$, during which a decelerating manoeuvre is performed so that the satellite will move to the desired final point $\boldsymbol{y}_f = (\boldsymbol{r}_f, \boldsymbol{v}_f) \in \mathcal{P}^-$ at the entry interface (EI). The condition at EI permits the satellite to have a subsequent safe entry flight in atmosphere to a landing site. A typical condition at EI, see Ref. [7], is given as:

$$\| \boldsymbol{r}_f \| = r_{EI}, \quad \| \boldsymbol{v}_f \| = V_{EI}, \quad \text{and} \quad \boldsymbol{r}_f^T \cdot \boldsymbol{v}_f = V_{EI} r_{EI} sin(\eta_{EI}), \tag{2.22}$$

where $r_{EI} = r_e + 122,000$ m, $V_{EI} = 7879.5\ m/s$, and $\eta_{EI} = -15^\circ$ denote the norm of position vector, the norm of velocity vector, and the flight path angle at EI, respectively. In order to compute the limiting value $\overline{\tau}_{\max}$ in *Corollary 2.3* for the DOP to a point $(\boldsymbol{r}_f, \boldsymbol{v}_f)$ in $\mathcal{P}^-$, we first define the below optimal control problem.

Definition 2.13 (*Optimal control problem (OCP) for DOP*)**.** *Given every final point* $\boldsymbol{y}_f =$

$(\boldsymbol{r}_f, \boldsymbol{v}_f) \in \mathcal{P}^-$ and $\tau_{max} > 0$, let $m_i > 0$ be the initial mass of a satellite, the optimal control problem for DOP consists of steering the satellite by $\boldsymbol{\tau}(\cdot) \in \mathcal{B}_{\tau_{\max}}$ on a time interval $[0, t_f] \subset \mathcal{I}_\Gamma$ subject to the system $\widetilde{\Sigma}_{\text{sat}}$ such that, along the controlled trajectory $(\boldsymbol{r}(t), \boldsymbol{v}(t), m(t)) = \widetilde{\Gamma}(t, \boldsymbol{\tau}(t), \boldsymbol{r}_f, -\boldsymbol{v}_f, m_f)$ ($m_f > 0$ is free) of System $\widetilde{\Sigma}_{\text{sat}}$, the time t_f is the first occurrence for $\| \boldsymbol{r}(t_f) \| = r_p(\boldsymbol{r}(t_f), \boldsymbol{v}(t_f))$, $m_i = m(t_f)$, and $r_p(\boldsymbol{r}(t_f), \boldsymbol{v}(t_f))$ is maximized, i.e., the cost functional is the same as Eq. (2.20).

Given every initial mass $m_i > 0$ and final point $(\boldsymbol{r}_f, \boldsymbol{v}_f)$ in $\mathcal{P}^-$, let $\bar{t}_f > 0$ be the optimal final time of the OCP for DOP, and let $(\overline{\boldsymbol{y}}(t), \overline{m}(t)) = \widetilde{\Gamma}(t, \overline{\boldsymbol{\tau}}(t), \boldsymbol{r}_f, -\boldsymbol{v}_f, m_f)$ be the optimal controlled trajectory associated to the control $\overline{\boldsymbol{\tau}}(t) \in \mathcal{B}_{\tau_{\max}}$ on $[0, \bar{t}_f]$. Then, the same as the OCP for OIP, the perigee distance $r_p(\overline{\boldsymbol{y}}(\bar{t}_f))$ is a function of $\tau_{\max}$. Let us define a function

$$\overline{s} : \mathbb{R}_+ \to \mathbb{R},\ \overline{s}(\tau_{\max}) = r_p(\overline{\boldsymbol{y}}(\bar{t}_f)) - r_c. \tag{2.23}$$

Then, according to Eq. (2.19), in order to compute the limiting value $\overline{\tau}_{\max}$ in *Corollary 2.3*, it suffices to combine a shooting method and a bisection method to compute the value $\overline{\tau}_{\max}$ such that $\overline{s}(\overline{\tau}_{\max}) = 0$.

What we developed in this chapter is applicable not only for low-thrust control systems but also for high-thrust control systems if only the thrust is finite. Thus, we consider the space shuttle's parameters in Refs. [11, 37]. The initial mass is $95,254.38\ kg$. The specific impulse of the engine is 313 s that means $\beta = 3.26 \times 10^{-4}$. The numerical result is $\overline{\tau}_{\max} = 14,004.62\ N$. Note that the propulsion for a space shuttle is provided by the orbital maneuvering system (OMS) engines, which produce a total vacuum thrust of $53,378.6\ N$, see Refs. [11, 37]. Thus, according to *Lemma 2.5*, for every initial point $\boldsymbol{y}_i$ in $\mathcal{P}^+$, the space shuttle can reach the EI condition in Eq.(2.22) by admissible controlled trajectories of the system Σ_{sat} if the satellite takes enough fuel. The periodic trajectory $\gamma_{\boldsymbol{y}_f}$ and associated optimal controlled trajectory with $\tau_{\max} = \overline{\tau}_{\max}$ are illustrated in Figure 2.6. The profile of $\| \boldsymbol{r} \|$ and r_p along optimal controlled trajectories for the DOP with $\tau_{max} = \overline{\tau}_{\max}$, $\overline{\tau}_{\max} + 100\ N$, and $\overline{\tau}_{\max} - 100\ N$, are illustrated in Figure 2.7. We can see from Figure 2.7 that the optimal controlled trajectory of the OCP for DOP with $\tau_{max} = \overline{\tau}_{\max} + 100$ N is an admissible controlled trajectory in $\mathcal{A}$ and the final point lies in $\mathcal{P}^+$. However, the optimal controlled trajectory of the OCP for DOP with $\tau_{max} = \overline{\tau}_{\max} - 100$ N cannot reach a point in $\mathcal{P}^+$ by admissible controlled trajectories of the system $\widetilde{\Sigma}_{\text{sat}}$.

2.7 Conclusion

In this chapter, the basic properties of the uncontrolled dynamics in two-body problem are represented, showing that the locus of the drift vector field describes a conic section. Then the controllability property for the Keplerian motion in the periodic region $\mathcal{P}$ is established. According to the state constraint that the radius of the Keplerian motion has to be larger than the radius of the surface of the atmosphere around the Earth, the periodic region is separated into two sets: $\mathcal{P}^+$ and $\mathcal{P}^-$. The controlled motion in the set $\mathcal{P}^+$ is the typical OTP and

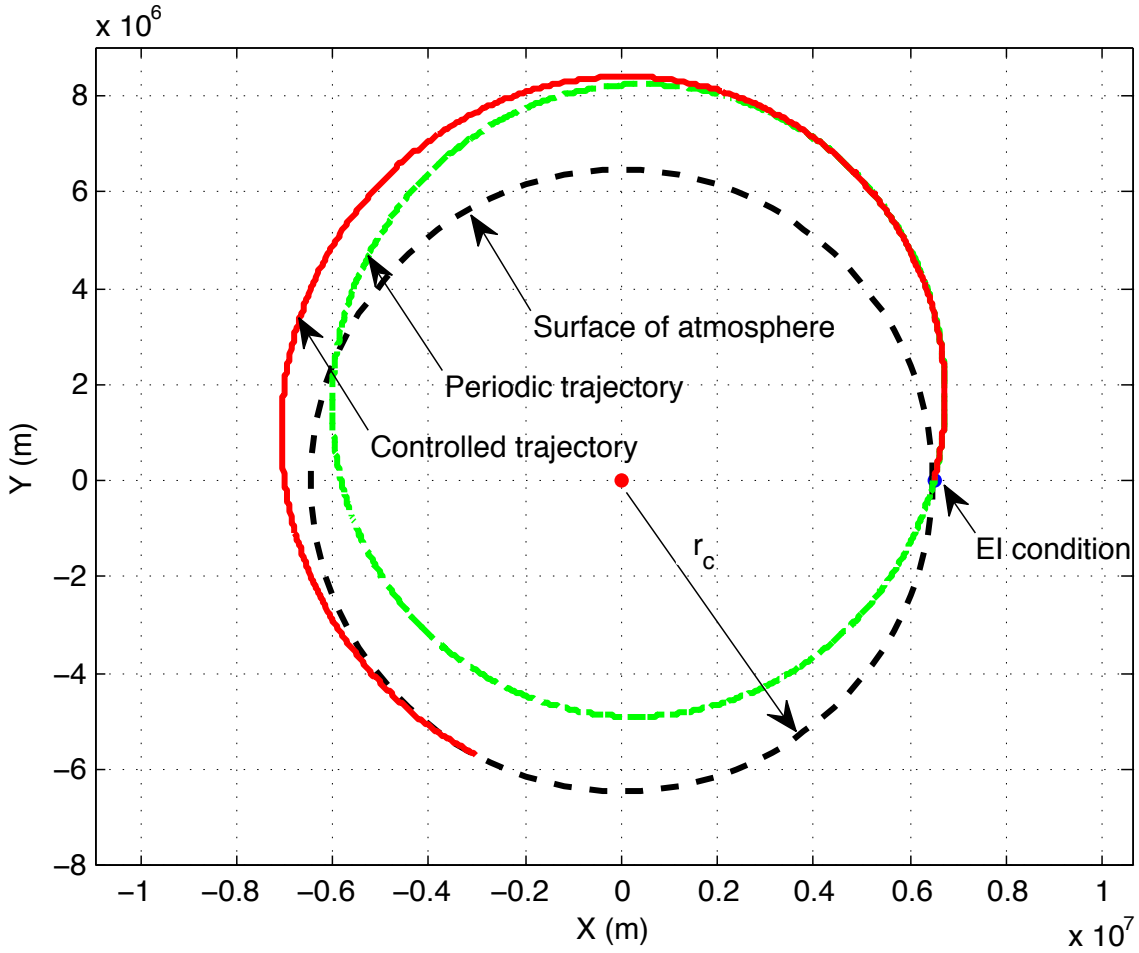

Figure 2.6 – The periodic trajectory $\gamma_{\boldsymbol{y}_f}$ determined by the EI condition in Eq.(2.22) and the optimal controlled trajectory of the OCP for DOP with $\tau_{max} = \overline{\tau}_{\max}$.

we obtain that the motion is controllable in the set $\mathcal{P}^+$ for every positive maximum thrust. Moreover, we obtain that there exist a limiting value of $\overline{\tau}_{max}$ depending on the initial point (the final point, respectively) such that the Keplerian motion for OIP (DOP, respectively) is controllable if and only if $\tau_{\max} > \overline{\tau}_{\max}$. Finally, two numerical examples are simulated to show that a shooting method and a bisection method can be combined to compute the limiting value $\overline{\tau}_{\max}$.

Recall that the drift vector field $\boldsymbol{f}_0$ in Eq. (1.4) for the CRTBP ($\mu \in (0,1)$) is recurrent[2] in an appropriate subregion $\mathcal{X}$ of state space. Thus, one can apply Lemma 2.4 and Proposition 2.1 to obtain that for every positive $\tau_{\max}$ there exists an admissible controlled trajectory of Σ in $\mathcal{X}$ connecting every two points in $\mathcal{X}$ (see [17] for establishing the controllability of Σ using another technique).

[2]Given a vector field $\boldsymbol{f}_0$, a point $\boldsymbol{x} \in \mathcal{X}$ is recurrent or positively Poisson stable for $\boldsymbol{f}_0$ if for any neighborhood $\mathcal{V} \subset \mathcal{X}$ of $\boldsymbol{x}$, for any positive T, there is $t > T$ such that $\exp(t\boldsymbol{f}_0(\boldsymbol{x}))$ is defined and belongs to $\mathcal{V}$. The vector field itself is said to be recurrent when it has a dense subset of recurrent points.

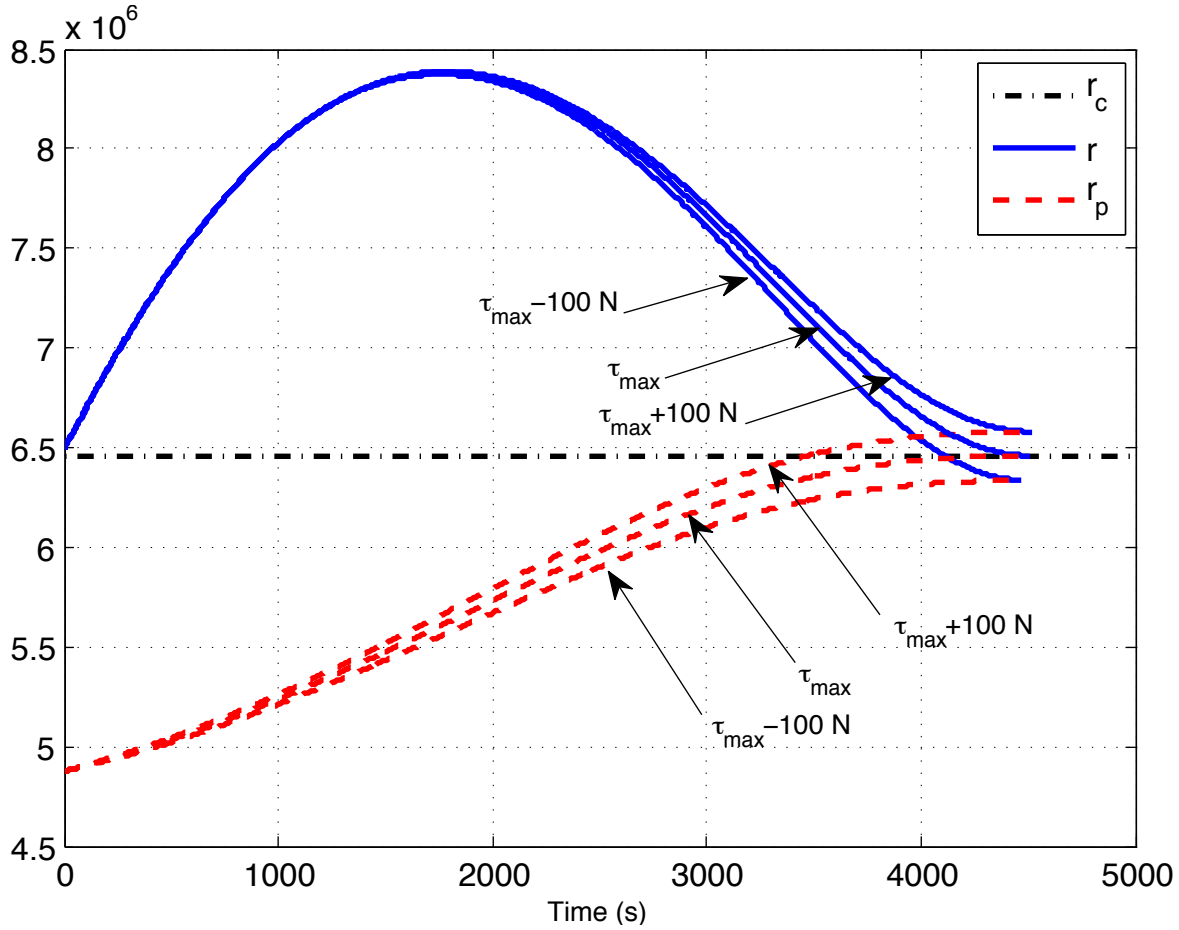

Figure 2.7 – The profile of $r = \| \boldsymbol{r} \|$ and r_p along the optimal controlled trajectory of the OCP for the DOP with $\tau_{max} = \overline{\tau}_{\max}$, $\overline{\tau}_{\max} + 100$ N, and $\overline{\tau}_{\max} - 100$ N.

Chapter 3

Sufficient conditions for L^1-extremals with fixed endpoints

In this chapter,[1] the sufficient conditions for nonsingular L^1-extremals with fixed endpoints are treated in detail. Although maximizing the final mass does not make sense anymore for the constant mass model ($\beta = 0$), the Lagrangian cost in Eq. (1.6) is still meaningful. Actually, as propellant is only a limited fraction of the total mass, one can expect this idealized constant mass model to capture the main features of Σ in Eq. (1.4). Henceforth, we shall assume $\beta = 0$ in this chapter such that the state $\boldsymbol{x}$ consists of position $\boldsymbol{r}$ and velocity $\boldsymbol{v}$ without mass m.

To avoid confusing the notations with those in the previous chapters, we reiterate that $\boldsymbol{x} = (\boldsymbol{r}, \boldsymbol{v})$ is the state valued in an open subset $\mathcal{X} \subset \mathbb{R}^n$ ($n = 6$ in this chapter), $\boldsymbol{u} := (\rho, \boldsymbol{\omega})$ is the control valued in $\mathcal{U} := [0, 1] \times \mathbb{S}^2$, $\boldsymbol{f}$ is a smooth vector field on $\mathcal{X}$ given by

$$\boldsymbol{f} : \mathcal{X} \times \mathcal{U} \to T_{\boldsymbol{x}}\mathcal{X}, \ \boldsymbol{f}(\boldsymbol{x}, \boldsymbol{u}) = \boldsymbol{f}_0(\boldsymbol{x}) + \rho \boldsymbol{f}_1(\boldsymbol{x}, \boldsymbol{\omega}),$$

where

$$\boldsymbol{f}_0(\boldsymbol{x}) = \begin{bmatrix} \boldsymbol{v} \\ \boldsymbol{h}(\boldsymbol{v}) + \boldsymbol{g}(\boldsymbol{r}) \end{bmatrix}$$

and

$$\boldsymbol{f}_1(\boldsymbol{x}, \boldsymbol{\omega}) = \begin{bmatrix} 0 \\ \tau_{\max}\boldsymbol{\omega}/m_0 \end{bmatrix},$$

and $f^0 : \mathcal{X} \times \mathcal{U} \to \mathbb{R}$ is a smooth cost function. We consider the following minimization problem with fixed endpoints and fixed final time t_f: Find $(\boldsymbol{x}, \boldsymbol{u}) : [0, t_f] \to \mathcal{X} \times \mathcal{U}$, $\boldsymbol{x}$ absolutely continuous, $\boldsymbol{u}$ measurable and bounded, such that

$$\dot{\boldsymbol{x}}(t) = \boldsymbol{f}(\boldsymbol{x}(t), \boldsymbol{u}(t)), \quad t \in [0, t_f] \text{ (a.e)},$$

$$\boldsymbol{x}(0) = \boldsymbol{x}_0, \quad \boldsymbol{x}(t_f) = \boldsymbol{x}_f,$$

[1] This chapter is based on the paper "L^1-minimization for mechanical systems" (with Jean-Baptiste Caillau and Yacine Chitour) appeared in [23].

and such that

$$\int_0^{t_f} f^0(\boldsymbol{x}(t), \boldsymbol{u}(t))dt$$

is minimized. The first order necessary conditions formulated by the Pontryagin Maximum Principle in Sect. 1.2 can be directly applied. Let $\boldsymbol{p} \in T^*_{\boldsymbol{x}}\mathcal{X}$ be the costate of $\boldsymbol{x}$. Recall that the abnormal extremals have been ruled out by Proposition 1.1, i.e., $p^0 = -1$. Then denote by $H(\boldsymbol{x}, \boldsymbol{p}, \boldsymbol{u})$ and $H(\boldsymbol{x}, \boldsymbol{p})$ the controlled Hamiltonian and maximum Hamiltonian, respectively.

Throughout this chapter, we assume that the nonsingular extremal $(\overline{\boldsymbol{x}}(\cdot), \overline{\boldsymbol{p}}(\cdot)) \in T^*\mathcal{X}$ on $[0, t_f]$ is computed based on the Pontryagin maximum principle and we say it is the reference extremal.

3.1 Parameterized family of extremals

Let

$$\overrightarrow{H} := \left(\frac{\partial H}{\partial \boldsymbol{p}}, -\frac{\partial H}{\partial \boldsymbol{x}}\right)$$

be the Hamiltonian vector field defined by Eqs. (1.7,1.8) and denote by $e^{t\overrightarrow{H}}(\boldsymbol{x}_0, \boldsymbol{p}_0)$ the corresponding Hamiltonian flow starting at $(\boldsymbol{x}_0, \boldsymbol{p}_0)$. For the sake of notational clarity, let $\overline{\boldsymbol{z}}_0 := (\overline{\boldsymbol{x}}(0), \overline{\boldsymbol{p}}(0))$ and $\mathcal{Z}_0 \subset T^*\mathcal{X}$ be an open neighborhood of $\overline{\boldsymbol{z}}_0$. Then, we denote by

$$(\boldsymbol{x}(t, \boldsymbol{z}_0), \boldsymbol{p}(t, \boldsymbol{z}_0)) : [0, t_f] \times \mathcal{Z}_0 \to T^*\mathcal{X},\ (t, \boldsymbol{z}_0) \mapsto e^{t\overrightarrow{H}}(\boldsymbol{z}_0),$$

the Hamiltonian flow starting at $\boldsymbol{z}_0 \in \mathcal{Z}_0$. Note that $(\overline{\boldsymbol{x}}(\cdot), \overline{\boldsymbol{p}}(\cdot)) = (\boldsymbol{x}(\cdot, \overline{\boldsymbol{z}}_0), \boldsymbol{p}(\cdot, \overline{\boldsymbol{z}}_0))$ on $[0, t_f]$. To avoid heavy notations, we also set $\gamma(t, \boldsymbol{p}_0) := e^{t\overrightarrow{H}}(\overline{\boldsymbol{x}}(0), \boldsymbol{p}_0)$ for $(t, \boldsymbol{p}_0) \in [0, t_f] \times T^*_{\boldsymbol{x}_0}\mathcal{X}$.

Definition 3.1 (Parameterized family $\mathcal{F}$ of extremals)**.** *Given the reference extremal $(\overline{\boldsymbol{x}}(\cdot), \overline{\boldsymbol{p}}(\cdot))$ on $[0, t_f]$, let $\mathcal{P}_0 \subset T^*_{\overline{\boldsymbol{x}}(0)}\mathcal{X}$ be an open neighborhood of $\overline{\boldsymbol{p}}(0)$. Then, we denote by*

$$\begin{aligned}\mathcal{F} \quad = \quad & \big\{(t, \boldsymbol{x}(t), \boldsymbol{p}(t)) \in \mathbb{R} \times T^*\mathcal{X} \mid \\ & (\boldsymbol{x}(t), \boldsymbol{p}(t)) = e^{t\overrightarrow{H}}(\overline{\boldsymbol{x}}(0), \boldsymbol{p}_0),\ t \in [0, t_f],\ \boldsymbol{p}_0 \in \mathcal{P}_0\big\},\end{aligned} \tag{3.1}$$

the $\boldsymbol{p}_0$-parameterized family of extremals around the reference one.

Define the projection from $\mathbb{R} \times T^*\mathcal{X}$ onto $\mathbb{R} \times \mathcal{X}$ by

$$\Pi_t : \mathbb{R} \times T^*\mathcal{X} \to \mathbb{R} \times \mathcal{X},\ \ (t, \boldsymbol{x}(t), \boldsymbol{p}(t)) \mapsto (t, \boldsymbol{x}(t)).$$

According to Agrachev's approach [2], the optimality of the reference extremal is related to the fold singularity of the projection $\Pi_t(\mathcal{F})$ through the notion of conjugate point (see Definition 1.3), as is shown by the typical picture for conjugate points in Fig. 3.1. We say the conditions ensuring the projection Π_t of $\mathcal{F}$ at each time $t \in (0, t_f]$ is a diffeomorphism is the *no-fold conditions* [63, 82]. In next paragraph, the no-fold conditions will be established.

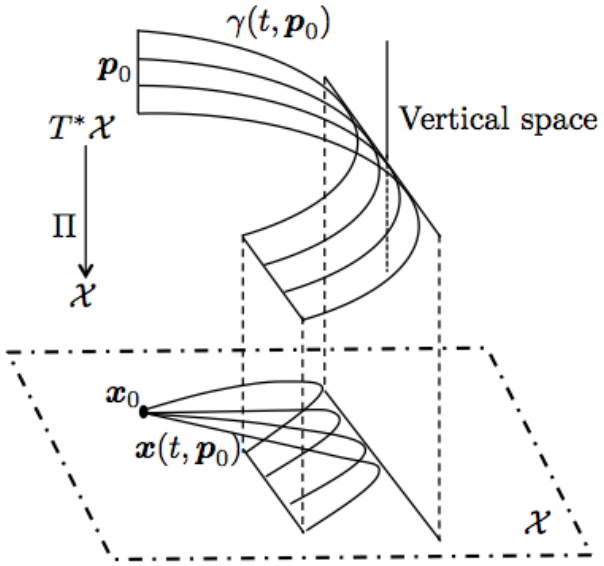

Figure 3.1 – A typical picture for a conjugate point (the fold singularity of the projection $\Pi_t(\mathcal{F})$). [2]

3.2 No-fold conditions for the projection of $\mathcal{F}$

Given the reference extremal $(\overline{\boldsymbol{x}}(\cdot), \overline{\boldsymbol{p}}(\cdot))$ on $[0, t_f]$, without loss of generality, let the positive integer k be the number of switching times $\bar{t}_i$ ($i = 1,\ 2,\ \cdots,\ k$) such that $0 = \bar{t}_0 < \bar{t}_1 < \bar{t}_2 < \cdots < \bar{t}_k < \bar{t}_{k+1} = t_f$.

Assumption 3.1. *Along the reference extremal $(\overline{\boldsymbol{x}}(\cdot), \overline{\boldsymbol{p}}(\cdot))$ on $[0, t_f]$, each switching point (at the switching time $\bar{t}_i \in (0, t_f)$) is assumed to be a regular one, i.e., $H_1(\overline{\boldsymbol{x}}(\bar{t}_i), \overline{\boldsymbol{p}}(\bar{t}_i)) = 0$ and $H_{01}(\overline{\boldsymbol{x}}(\bar{t}_i), \overline{\boldsymbol{p}}(\bar{t}_i)) \neq 0$.*

Note that the notation H_{01} is defined in Eq. (1.14). The condition $H_{01}(\overline{\boldsymbol{x}}(\bar{t}_i), \overline{\boldsymbol{p}}(\bar{t}_i)) \neq 0$ is called the *strict bang-bang Legendre* condition in [3]. As a result of Assumption 3.1, if the subset $\mathcal{Z}_0$ is small enough, the number of switching times on each extremal $(\boldsymbol{x}(\cdot, \boldsymbol{z}_0), \boldsymbol{p}(\cdot, \boldsymbol{z}_0))$ on $[0, t_f]$ for $\boldsymbol{z}_0 \in \mathcal{Z}_0$ remains equal to k, and we denote by

$$t_i : \mathcal{Z}_0 \to \mathbb{R}_+,\ \boldsymbol{z}_0 \mapsto t_i(\boldsymbol{z}_0), \tag{3.2}$$

the i-th switching time of the extremal $(\boldsymbol{x}(\cdot, \boldsymbol{z}_0), \boldsymbol{p}(\cdot, \boldsymbol{z}_0))$ for $\boldsymbol{z}_0 \in \mathcal{Z}_0$. Note that $\bar{t}_i = t_i(\overline{\boldsymbol{z}}_0)$. Let

$$\begin{aligned} \mathcal{F}_i \ := \ & \big\{(t, \boldsymbol{x}(t), \boldsymbol{p}(t)) \in \mathbb{R} \times T^*\mathcal{X} \mid \\ & (\boldsymbol{x}(t), \boldsymbol{p}(t)) = e^{t\overrightarrow{H}}(\overline{\boldsymbol{x}}_0, \boldsymbol{p}_0),\ t \in (t_{i-1}(\overline{\boldsymbol{x}}_0, \boldsymbol{p}_0), t_i(\overline{\boldsymbol{x}}_0, \boldsymbol{p}_0)],\ \boldsymbol{p}_0 \in \mathcal{P}_0\big\}, \end{aligned} \tag{3.3}$$

where $i = 1,\ 2,\ \cdots,\ k,\ k+1$. If the open neighborhood $\mathcal{P}_0$ is small enough, there holds

$$\mathcal{F} = \mathcal{F}_1 \cup \mathcal{F}_2 \cup \cdots \cup \mathcal{F}_k \cup \mathcal{F}_{k+1},$$

and

$$\mathcal{F}_i \cap \mathcal{F}_{i+1} = \varnothing,\ i = 1,\ 2,\ \cdots,\ k. \tag{3.4}$$

For the sake of notational clarity, let $\delta(t)$ be the determinant of the matrix $\partial \boldsymbol{x}(t, \overline{\boldsymbol{z}}_0)/\partial \boldsymbol{p}_0$ for $t \in [0, t_f]$, i.e.,

$$\delta(t) := \det\left[\frac{\partial \boldsymbol{x}}{\partial \boldsymbol{p}_0}(t, \overline{\boldsymbol{z}}_0)\right],\ t \in [0, t_f].$$

Note that $\delta(t)$ is piecewise continuous (see [63], e.g.).

Condition 3.1. *$\delta(t_f) \neq 0$ and $\delta(\cdot) \neq 0$ on each subinterval $(\bar{t}_i, \bar{t}_{i+1})$, $i = 0,\ 1,\ \cdots,\ k$.*

By restricting the subset $\mathcal{P}_0$ if necessary, this condition is sufficient to guarantee the projection Π_t of each subset $\mathcal{F}_i$ ($i = 1,\ 2,\ \cdots,\ k+1$) is a diffeomorphism (see, e.g., [2, 82]). However, this condition satisfied on each subinterval $(\bar{t}_{i-1}, \bar{t}_i)$ for $i = 1,\ 2,\ \cdots,\ k+1$ is not sufficient to guarantee that the projection Π_t of $\mathcal{F}$ is a diffeomorphism as well, as Fig. 3.2 shows that the composite flows may intersect with each other near the switching time $\bar{t}_i$. This is the typical

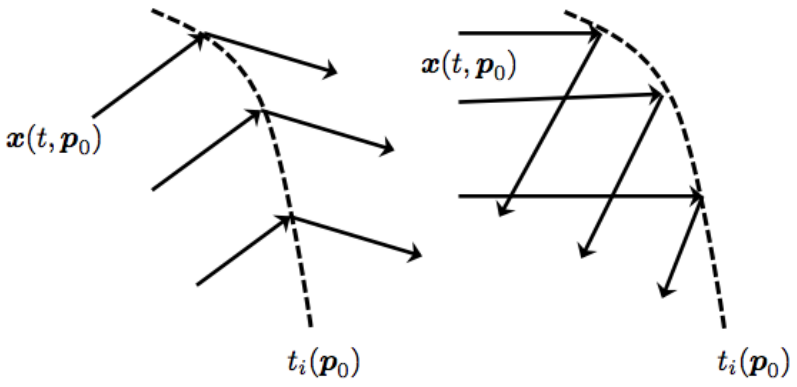

Figure 3.2 – Transversally crossing and fold singularity near switching surface [63, 82].

conjugate point behavior as can also be seen near the fold singularity for smooth projections.

Let

$$\Theta := \{(t, \boldsymbol{x}, \boldsymbol{p}) \in \mathbb{R} \times T^*\mathcal{X} \mid H_1(\boldsymbol{x}(t, \boldsymbol{z}_0), \boldsymbol{p}(t, \boldsymbol{z}_0)) = 0,\ t \in [0, t_f],\ \boldsymbol{z}_0 \in \mathcal{Z}_0\}$$

be the switching surface in $\mathbb{R} \times T^*\mathcal{X}$; one immediately gets that $\Theta_i := \mathcal{F}_i \cap \Theta$ is the set of all terminal points of $\mathcal{F}_i$ for $i = 1,\ 2,\ \cdots,\ k$. Note that the set $\Pi_t(\Theta_i)$ is of codimension one. With some abuses of notations, set $t_i(\boldsymbol{p}_0) := t_i(\overline{\boldsymbol{x}}(0), \boldsymbol{p}_0)$. As the mapping $(t, \boldsymbol{p}_0) \mapsto (t, \boldsymbol{x}(t_i(\boldsymbol{p}_0), \boldsymbol{p}_0))$ is a diffeomorphism from $\mathbb{R} \times \mathcal{P}_0$ onto $\Pi_t(\mathcal{F}_i)$ if Condition 3.1 holds, there

exists an inverse function $(t, \boldsymbol{x}) \mapsto \boldsymbol{p}_0(t, \boldsymbol{x})$ such that $\Pi_t(\Theta_i) = \{(t, \boldsymbol{x}) \in \mathbb{R} \times \mathcal{X} \mid \psi_i(t, \boldsymbol{x}) = 0\}$ with

$$\psi_i(t, \boldsymbol{x}) := t - t_i(\boldsymbol{p}_0(t, \boldsymbol{x})).$$

Clearly, the set $\Pi_t(\Theta_i)$ for $i = 1,\ 2,\ \cdots,\ k$ is the switching surface in $(t, \boldsymbol{x})$-space.

Denote the tangent vectors of the flows $t \mapsto (t, \overline{\boldsymbol{x}}(t))$ at $\bar{t}_i-$ and $\bar{t}_i+$ by $\boldsymbol{T}_i^- \in (\mathbb{R}^{n+1})^*$ and $\boldsymbol{T}_i^+ \in (\mathbb{R}^{n+1})^*$, respectively, i.e.,

$$\boldsymbol{T}_i^{\pm} := \frac{d}{dt}(\bar{t}_i\pm, \overline{\boldsymbol{x}}(\bar{t}_i\pm)) = (1, \dot{\overline{\boldsymbol{x}}}(\bar{t}_i\pm)). \tag{3.5}$$

Let the vector $\boldsymbol{N}_i \in \mathbb{R}^{n+1}$ be the normal vector of the switching surface $\Pi_t(\Theta_i)$ at $(\bar{t}_i, \overline{\boldsymbol{x}}(\bar{t}_i))$, i.e.,

$$\boldsymbol{N}_i := \nabla\psi_i(\bar{t}_i, \overline{\boldsymbol{x}}(\bar{t}_i)).$$

Remark 3.1. *By restricting the subset $\mathcal{P}_0$ if necessary, the projection Π_t of $\mathcal{F}$ at $\bar{t}_i$ is a diffeomorphism (respectively, a fold singularity) if the two vectors $\boldsymbol{T}_i^-$ and $\boldsymbol{T}_i^+$ point to the same side (respectively, the two different sides) of the switching surface $\Pi_t(\Theta_i)$ (see Fig. 3.2).*

Accordingly, one immediately gets that the projection Π_t of $\mathcal{F}$ around $\bar{t}_i$ is a diffeomorphism if

$$(\boldsymbol{T}_i^- \boldsymbol{N}_i)(\boldsymbol{T}_i^+ \boldsymbol{N}_i) > 0, \tag{3.6}$$

and it is a fold singularity if

$$(\boldsymbol{T}_i^- \boldsymbol{N}_i)(\boldsymbol{T}_i^+ \boldsymbol{N}_i) < 0. \tag{3.7}$$

The explicit expression for $\boldsymbol{N}_i = \nabla\psi_i(\bar{t}_i-, \boldsymbol{x}(\bar{t}_i-, \overline{\boldsymbol{z}}_0))$ is

$$\begin{aligned}
& \frac{d((\bar{t}_i-) - t_i(\overline{\boldsymbol{z}}_0))}{d(t, \boldsymbol{p}_0)} \left[\frac{d(\bar{t}_i-, \boldsymbol{x}(\bar{t}_i-, \overline{\boldsymbol{z}}_0))}{d(t, \boldsymbol{p}_0)}\right]^{-1} \\
= \ & (1, -\frac{dt_i(\overline{\boldsymbol{z}}_0)}{d\boldsymbol{p}_0}) \begin{bmatrix} 1 & 0 \\ \dot{\boldsymbol{x}}(\bar{t}_i-, \overline{\boldsymbol{z}}_0) & \frac{\partial \boldsymbol{x}}{\partial \boldsymbol{p}_0}(\bar{t}_i-, \overline{\boldsymbol{z}}_0) \end{bmatrix}^{-1} \\
= \ & (1, -\frac{dt_i(\overline{\boldsymbol{z}}_0)}{d\boldsymbol{p}_0}) \begin{bmatrix} 1 & 0 \\ -\left(\frac{\partial \boldsymbol{x}}{\partial \boldsymbol{p}_0}(\bar{t}_i-, \overline{\boldsymbol{z}}_0)\right)^{-1} \dot{\boldsymbol{x}}(\bar{t}_i-, \overline{\boldsymbol{z}}_0) & \left(\frac{\partial \boldsymbol{x}}{\partial \boldsymbol{p}_0}(\bar{t}_i-, \overline{\boldsymbol{z}}_0)\right)^{-1} \end{bmatrix} \\
= \ & \left[1 + \frac{dt_i(\overline{\boldsymbol{z}}_0)}{d\boldsymbol{p}_0}\left(\frac{\partial \boldsymbol{x}}{\partial \boldsymbol{p}_0}(\bar{t}_i-, \overline{\boldsymbol{z}}_0)\right)^{-1} \dot{\boldsymbol{x}}(\bar{t}_i-, \overline{\boldsymbol{z}}_0), -\frac{dt_i(\overline{\boldsymbol{z}}_0)}{d\boldsymbol{p}_0}\left(\frac{\partial \boldsymbol{x}}{\partial \boldsymbol{p}_0}(\bar{t}_i-, \overline{\boldsymbol{z}}_0)\right)^{-1}\right].
\end{aligned} \tag{3.8}$$

Substituting Eq. (3.5) into Eq. (3.8) leads to

$$\boldsymbol{T}_i^- \boldsymbol{N}_i = 1,$$

and

$$\boldsymbol{T}_i^+ \boldsymbol{N}_i = 1 + \frac{dt_i(\overline{\boldsymbol{z}}_0)}{d\boldsymbol{p}_0} \left(\frac{\partial \boldsymbol{x}}{\partial \boldsymbol{p}_0}(\bar{t}_i-, \overline{\boldsymbol{z}}_0) \right)^{-1} [\dot{\boldsymbol{x}}(\bar{t}_i-, \overline{\boldsymbol{z}}_0) - \dot{\boldsymbol{x}}(\bar{t}_i+, \overline{\boldsymbol{z}}_0)].$$

If $\Delta\rho_i := \overline{\rho}(\bar{t}_i+) - \overline{\rho}(\bar{t}_i-)$, we get

$$\dot{\boldsymbol{x}}(\bar{t}_i-, \overline{\boldsymbol{z}}_0) - \dot{\boldsymbol{x}}(\bar{t}_i+, \overline{\boldsymbol{z}}_0) = -\Delta\rho_i \boldsymbol{f}_1(\overline{\boldsymbol{x}}(\bar{t}_i), \overline{\boldsymbol{\omega}}(\bar{t}_i)).$$

By virtue of Lemma 2.6 in [63], we have

$$\frac{\partial \boldsymbol{x}}{\partial \boldsymbol{p}_0}(\bar{t}_i+, \overline{\boldsymbol{z}}_0) = \frac{\partial \boldsymbol{x}}{\partial \boldsymbol{p}_0}(\bar{t}_i-, \overline{\boldsymbol{z}}_0) - \Delta\rho_i \boldsymbol{f}_1(\overline{\boldsymbol{x}}(\bar{t}_i), \overline{\boldsymbol{\omega}}(\bar{t}_i)) \frac{dt_i(\overline{\boldsymbol{z}}_0)}{d\boldsymbol{p}_0}.$$

If $\delta(\bar{t}_i-) \neq 0$, taking determinants yields

$$\delta(\bar{t}_i+) = \delta(\bar{t}_i-) \det \left[I_n - \Delta\rho_i \left(\frac{\partial \boldsymbol{x}}{\partial \boldsymbol{p}_0}(\bar{t}_i-, \overline{\boldsymbol{z}}_0) \right)^{-1} \boldsymbol{f}_1(\overline{\boldsymbol{x}}(\bar{t}_i), \overline{\boldsymbol{\omega}}(\bar{t}_i)) \frac{dt_i(\overline{\boldsymbol{z}}_0)}{d\boldsymbol{p}_0} \right].$$

Since there holds

$$\det(I_n + \boldsymbol{a}\boldsymbol{b}^T) = 1 + \boldsymbol{a}^T \boldsymbol{b}$$

for every $\boldsymbol{a},\ \boldsymbol{b} \in \mathbb{R}^n$, one immediately gets

$$\begin{aligned} & I_n - \Delta\rho_i \left[\frac{\partial \boldsymbol{x}}{\partial \boldsymbol{p}_0}(\bar{t}_i-, \overline{\boldsymbol{z}}_0) \right]^{-1} \boldsymbol{f}_1(\overline{\boldsymbol{x}}(\bar{t}_i), \overline{\boldsymbol{\omega}}(\bar{t}_i)) \frac{dt_i(\overline{\boldsymbol{z}}_0)}{d\boldsymbol{p}_0} \\ = \ & 1 - \Delta\rho_i \frac{dt_i(\overline{\boldsymbol{z}}_0)}{d\boldsymbol{p}_0} \left[\frac{\partial \boldsymbol{x}}{\partial \boldsymbol{p}_0}(\bar{t}_i-, \overline{\boldsymbol{z}}_0) \right]^{-1} \boldsymbol{f}_1(\overline{\boldsymbol{x}}(\bar{t}_i), \overline{\boldsymbol{\omega}}(\bar{t}_i)). \end{aligned}$$

Therefore, Eq. (3.6) is satisfied if and only if there holds

$$\delta(\bar{t}_i-)\delta(\bar{t}_i+) > 0. \tag{3.9}$$

In an analogous way, Eq. (3.7) is satisfied if and only if there holds

$$\delta(\bar{t}_i-)\delta(\bar{t}_i+) < 0. \tag{3.10}$$

Remark 3.2. *Along the reference extremal, conjugate points can occur not only on each subinterval $(\bar{t}_{i-1}, \bar{t}_i)$, between switching times, if $\delta(t) = 0$ but also at each switching time $\bar{t}_i$ once Eq. (3.10) is satisfied.*

The fact that conjugate points can occur at switching times generalizes the conjugate point theory developed by the classical variational methods for totally smooth extremals (see, e.g., [13, 16, 57, 93]).

Condition 3.2. $\delta(\bar{t}_i-)\delta(\bar{t}_i+) > 0$ *for* $i = 1,\ 2,\ \cdots,\ k$.

According to the previous analysis, Conditions 3.1 and 3.2, once satisfied, are sufficient to guarantee the projection Π_t of the family $\mathcal{F}$ on $(0, t_f]$ is a diffeomorphism if the subset $\mathcal{P}_0$ is small enough. Thus, for broken extremals, the no-fold conditions consists of not only Condition 3.1 between switching times but also Condition 3.2 at switching times. By virtue of the *Shadow-price lemma*, the two no-fold conditions readily ensure the reference extremal to be a *relative optimum* (see, e.g., [82, Definition 5.3.2]). In the next paragraph, we will show that Conditions 3.1 and 3.2 are also sufficient for strong local optimality in $\mathcal{C}^0$-topology provided that each switching point is regular (cf. Assumption 3.1).

3.3 Sufficient conditions for strong local optimality

Definition 3.2 (Local optimality with fixed endpoints)**.** *An extremal trajectory $\overline{\boldsymbol{x}}(\cdot) : [0, t_f] \to \mathcal{X}$ associated with a measurable control $\overline{\boldsymbol{u}}(\cdot) = (\overline{p}(\cdot), \overline{\boldsymbol{\omega}}(\cdot)) : [0, t_f] \to \mathcal{U}$ is said to realize a weak local optimum in L^∞-topology (resp. strong local optimum in C^0-topology) if there exists an open neighborhood $\mathcal{W}_{\boldsymbol{u}} \subseteq \mathcal{U}$ of $\overline{\boldsymbol{u}}(\cdot)$ in L^∞-topology (resp. an open neighborhood $\mathcal{W}_{\boldsymbol{x}} \subseteq \mathcal{X}$ of $\overline{\boldsymbol{x}}(\cdot)$ in C^0-topology) such that for every admissible controlled trajectory $\boldsymbol{x}(\cdot) : [0, t_f] \to \mathcal{X}$ associated with a measurable control $\boldsymbol{u}(\cdot) = (\rho(\cdot), \boldsymbol{\omega}(\cdot)) : [0, t_f] \to \mathcal{W}_{\boldsymbol{u}}$ (resp. for every admissible controlled trajectory $\boldsymbol{x}(\cdot) : [0, t_f] \to \mathcal{W}_{\boldsymbol{x}}$ associated with a measurable control $\boldsymbol{u}(\cdot) = (\rho(\cdot), \boldsymbol{\omega}(\cdot)) : [0, t_f] \to \mathcal{U}$) with the same endpoints $\boldsymbol{x}(0) = \overline{\boldsymbol{x}}(0)$ and $\boldsymbol{x}(t_f) = \overline{\boldsymbol{x}}(t_f)$, there holds*

$$\int_0^{t_f} f^0(\boldsymbol{x}(t), \boldsymbol{u}(t))dt \geqslant \int_0^{t_f} f^0(\overline{\boldsymbol{x}}(t), \overline{\boldsymbol{u}}(t))dt.$$

It realizes a strict weak-local (resp. strong-local) optimum if the strict inequality holds.

From a Hamiltonian point of view, we will prove that Conditions 3.1 and 3.2 are sufficient for strong local optimality[2] provided that each switching point is regular.

Theorem 3.1. *Given the reference extremal $(\overline{\boldsymbol{x}}(\cdot), \overline{\boldsymbol{p}}(\cdot)) : [0, t_f] \to \mathcal{X}$ such that each switching point is regular (cf. Assumption 3.1), if Conditions 3.1 and 3.2 are satisfied, the reference extremal trajectory $\overline{\boldsymbol{x}}(\cdot)$ on $[0, t_f]$ realizes a strict minimum cost among all the admissible controlled trajectories $\boldsymbol{x}(\cdot) : [0, t_f] \to \mathcal{X}$ in a small tubular neighborhood of $\overline{\boldsymbol{x}}(\cdot)$ with the same endpoints $\boldsymbol{x}(0) = \overline{\boldsymbol{x}}(0)$ and $\boldsymbol{x}(t_f) = \overline{\boldsymbol{x}}(t_f)$.*

Proof. Without loss of generality, we assume there is only one switching time along the reference extremal, i.e., $k = 1$. We proceed in five steps.

Step 1. According to Condition 3.1, the matrix $\partial \boldsymbol{x}(t, \overline{\boldsymbol{z}}_0)/\partial \boldsymbol{p}_0$ is invertible for $t \in (0, t_1]$; one can then construct a Lagrangian perturbation $\mathcal{L}_0$ transverse to $T^*_{\boldsymbol{x}_0}\mathcal{X}$ containing $\overline{\boldsymbol{z}}_0$ such that $\partial \boldsymbol{x}(t, \overline{\boldsymbol{z}}_0)/\partial \boldsymbol{z}_0$ is invertible for $t \in [0, \bar{t}_1]$ with $\partial/\partial \boldsymbol{z}_0$ denoting the n partials with respect

[2] If a trajectory $\boldsymbol{x}(\cdot) : [0, t_f] \to \mathcal{X}$ realizes a strong local optimum, it automatically realizes a weak local one.

to $\boldsymbol{z}_0 \in \mathcal{L}_0$. (See Appendix B.) By restricting $\mathcal{L}_0$ if necessary, the mapping Π_t induces a diffeomorphism from

$$\mathcal{L}_1 := \{(t, \boldsymbol{z}(t)) \in \mathbb{R} \times T^*\mathcal{X} \mid \boldsymbol{z}(t) = e^{t\overrightarrow{H}}(\boldsymbol{z}_0),\ \boldsymbol{z}_0 \in \mathcal{L}_0,\ t \in [t_0, t_1(\boldsymbol{z}_0)]\}$$

onto its image. Similarly, Condition 3.1 implies that

$$\frac{\partial}{\partial \boldsymbol{p}_0}(\boldsymbol{x}_2(t - t_1(\boldsymbol{z}_0), \boldsymbol{z}_1(t_1(\boldsymbol{z}_0), \boldsymbol{z}_0)))|_{\boldsymbol{z}_0 = \overline{\boldsymbol{z}}_0}$$

is invertible for $t \in [\overline{t}_1, t_f]$. Restricting $\mathcal{L}_0$ again if necessary, one can assume that Π_t also induces a diffeomorphism from

$$\mathcal{L}_2 := \{(t, \boldsymbol{z}(t)) \in \mathbb{R} \times T^*\mathcal{X} \mid \boldsymbol{z}(t) = e^{t\overrightarrow{H}}(\boldsymbol{z}_0),\ \boldsymbol{z}_0 \in \mathcal{L}_0,\ t \in [t_1(\boldsymbol{z}_0), t_f]\}$$

onto its image.

Step 2. As $\mathcal{L}_0$ can be taken arbitrary close to $T^*_{\boldsymbol{x}_0}\mathcal{X}$, Condition 3.2 also indicates that every extremal trajectory $t \mapsto \boldsymbol{x}(t, \boldsymbol{z}_0)$ for $\boldsymbol{z}_0 \in \mathcal{Z}_0$ crosses the switching surface transversally. Thus, one can piece together the restrictions Π_t to $\mathcal{L}_1$ and $\mathcal{L}_2$ into a continuous bijection from $\mathcal{L}_1 \cup \mathcal{L}_2$ into $\Pi_t(\mathcal{L}_1 \cup \mathcal{L}_2)$. By restricting to a compact neighborhood of the graph of $\overline{\boldsymbol{z}}$, one may assume that Π_t induces a homeomorphism on its image.

Step 3. Let H^i, $i = 1, 2$, be the Hamiltonian on the field $\mathcal{L}_i$ and we denote $\alpha_i := \boldsymbol{p}d\boldsymbol{x} - H^i(\boldsymbol{z})dt$ the Poincaré-Cartan forms associated with H^i. To prove that α_1 is exact on $\mathcal{L}_1$, it is enough to prove that it is closed. Indeed, if $\gamma(s) := (t(s), \boldsymbol{z}_1(t(s), \boldsymbol{z}_0(s)))$ is a closed curve on $\mathcal{L}_1$, it retracts continuously on $\gamma_0 := (0, \boldsymbol{z}_0(s))$ so that, provided α_1 is closed,

$$\int_\gamma \alpha_1 = \int_{\gamma_0} \alpha_1 = \int_{\gamma_0} \boldsymbol{p}d\boldsymbol{x} = 0$$

because $\boldsymbol{z}_0(s)$ belongs to $\mathcal{L}_0$ that can be chosen such that $\boldsymbol{p}d\boldsymbol{x}$ is exact on it. (Compare [2, Chapter 17].) Similarly, to prove that α_2 is exact on $\mathcal{L}_2$, it suffices to prove that it is closed: If $\gamma(s) = (t(s), \boldsymbol{z}_2(t(s) - t_1(\boldsymbol{z}_0(s)), \boldsymbol{z}_1(t_1(\boldsymbol{z}_0(s)), \boldsymbol{z}_0(s))))$ is a closed curve in $\mathcal{L}_2$, it readily retracts continuously on the curve $\gamma_1(s) := (t_1(\boldsymbol{z}_0(s)), \boldsymbol{z}_1(t_1(\boldsymbol{z}_0(s)), \boldsymbol{z}_0(s)))$ in Θ, which retracts continuously on $\gamma_0(s) = (0, \boldsymbol{z}_0(s))$ again. Then, as $H^1 = H^2$ on Θ,

$$\int_\gamma \alpha_2 = \int_{\gamma_1} \alpha_2 = \int_{\gamma_1} \alpha_1 = \int_{\gamma_0} \alpha_1$$

that vanishes as before.

To prove that α_1 is closed, consider tangent vectors at $(t, \boldsymbol{z}) \in \mathcal{L}_1$; a parameterization of this tangent space is

$$(\delta t, \overrightarrow{H}^1(\boldsymbol{z})\delta t + \boldsymbol{z}_1'(t, \boldsymbol{z}_0)\delta \boldsymbol{z}_0), \quad (\delta t, \delta \boldsymbol{z}_0) \in \mathbb{R} \times T_{\boldsymbol{z}_0}\mathcal{L}_0$$

where $\boldsymbol{z}_0 \in \mathcal{L}_0$ is such that $\boldsymbol{z} = \boldsymbol{z}_1(t, \boldsymbol{z}_0)$. For two such vectors $\boldsymbol{v}_1$, $\boldsymbol{v}_2$,

$$\begin{aligned} d\alpha_1(t,\boldsymbol{z})(\boldsymbol{v}_1,\boldsymbol{v}_2) &= (d\boldsymbol{p}\wedge d\boldsymbol{x} - dH^1(\boldsymbol{z})dt)(\boldsymbol{v}_1,\boldsymbol{v}_2) \\ &= d\boldsymbol{p}\wedge d\boldsymbol{x}(\boldsymbol{z}_1'(t,\boldsymbol{z}_0)\delta\boldsymbol{z}_0^1, \boldsymbol{z}_1'(t,\boldsymbol{z}_0)\delta\boldsymbol{z}_0^2) \\ &= d\boldsymbol{p}\wedge d\boldsymbol{x}(\delta\boldsymbol{z}_0^1,\delta\boldsymbol{z}_0^2) \\ &= 0 \end{aligned}$$

because $\exp(t\overrightarrow{H}^1)$ is symplectic and $\mathcal{L}_0$ is Lagrangian. Regarding α_2, the tangent space at $(t,\boldsymbol{z}) \in \mathcal{L}_2$ is parameterized according to

$$(\delta t, \overrightarrow{H}^2\delta t + \boldsymbol{z}_2'(t - t_1(\boldsymbol{z}_0), \boldsymbol{z}_1(t_1(\boldsymbol{z}_0),\boldsymbol{z}_0))(I+\sigma(\boldsymbol{z}_0))\boldsymbol{z}_1'\delta\boldsymbol{z}_0)$$

with $(\delta t, \delta\boldsymbol{z}_0) \in \mathbb{R}\times T_{\boldsymbol{z}_0}\mathcal{L}_0$, and where $\boldsymbol{z}_0 \in \mathcal{L}_0$ is such that $\boldsymbol{z} = \boldsymbol{z}_2(t - t_1(\boldsymbol{z}_0), \boldsymbol{z}_1(t_1(\boldsymbol{z}_0),\boldsymbol{z}_0))$. For two such vectors $\boldsymbol{v}_1$, $\boldsymbol{v}_2$,

$$\begin{aligned} d\alpha_2(t,\boldsymbol{z})(\boldsymbol{v}_1,\boldsymbol{v}_2) &= (d\boldsymbol{p}\wedge d\boldsymbol{x} - dH^2(\boldsymbol{z})dt)(\boldsymbol{v}_1,\boldsymbol{v}_2) \\ &= d\boldsymbol{p}\wedge d\boldsymbol{x}((I+\sigma(\boldsymbol{z}_0))\boldsymbol{z}_1'(t,\boldsymbol{z}_0)\delta\boldsymbol{z}_0^1, (I+\sigma(\boldsymbol{z}_0))\boldsymbol{z}_1'(t,\boldsymbol{z}_0)\delta\boldsymbol{z}_0^2) \\ &= d\boldsymbol{p}\wedge d\boldsymbol{x}(\boldsymbol{z}_1'(t,\boldsymbol{z}_0)\delta\boldsymbol{z}_0^1, \boldsymbol{z}_1'(t,\boldsymbol{z}_0)\delta\boldsymbol{z}_0^2) \end{aligned}$$

because $\exp(t\overrightarrow{H}^2)$ is symplectic and because of the following lemma.

Lemma 3.1.

$$I + \sigma(\boldsymbol{z}_0) \in Sp(2n,\mathbb{R}).$$

Proof of the lemma. For any $\boldsymbol{z} \in \mathbb{R}^{2n}$,

$${}^t(I + J\boldsymbol{z}^t\boldsymbol{z})J(I + J\boldsymbol{z}^t\boldsymbol{z}) = J - \boldsymbol{z}^t\boldsymbol{z} + \boldsymbol{z}^t\boldsymbol{z} + \boldsymbol{z}(\underbrace{{}^t\boldsymbol{z}J\boldsymbol{z}}_{0})^t\boldsymbol{z} = J.$$

This proves the lemma because of

$$\sigma(\boldsymbol{z}_0) = \overrightarrow{H^1 - H^2}\frac{(H^1-H^2)'}{H_{12}}(\boldsymbol{z}_1(t_1(\boldsymbol{z}_0),\boldsymbol{z}_0)).$$

□

One then concludes as before that α_2 is closed using the fact that $\exp(t\overrightarrow{H})$ is symplectic and $\mathcal{L}_0$ is Lagrangian.

Step 4. Let $(\boldsymbol{x},\boldsymbol{u}) : [0,t_f] \to \mathcal{X}\times\mathcal{U}$ be an admissible pair. We first assume that $\boldsymbol{x}$ is of class $\mathcal{C}^1$ and that its graph has only one isolated contact with $\Pi_t(\Theta_1)$ at some point $(t_1, \boldsymbol{x}(t_1))$. For $\boldsymbol{x}$ close enough to $\overline{\boldsymbol{x}}$ in the $\mathcal{C}^0$-topology, this graph has a unique lift $t \mapsto (t, \boldsymbol{x}(t), \boldsymbol{p}(t))$ in $\mathcal{L}_1 \cup \mathcal{L}_2$ once the projection Π_t of $\mathcal{L}_1 \cup \mathcal{L}_2$ is a diffeomorphism. As a gluing at t_1 of two absolutely continuous functions, $\boldsymbol{z} := (\boldsymbol{x},\boldsymbol{p}) : [0,t_f] \to T^*\mathcal{X}$ is absolutely continuous.

Denote γ_1 and γ_2 the two pieces of this lift. Denote similarly $\overline{\gamma}_1$ and $\overline{\gamma}_2$ the pieces of the graph of the extremal $\overline{\boldsymbol{z}}$. One has

$$\begin{aligned}\int_0^{t_f} f^0(\boldsymbol{x}(t),\boldsymbol{u}(t))dt &= \left(\int_0^{t_1}+\int_{t_1}^{t_f}\right)(\boldsymbol{p}(t)\dot{\boldsymbol{x}}(t)-H(\boldsymbol{x}(t),\boldsymbol{p}(t),\boldsymbol{u}(t)))dt\\ &\geqslant \int_0^{t_1}(\boldsymbol{p}(t)\dot{\boldsymbol{x}}(t)-H^1(\boldsymbol{x}(t),\boldsymbol{p}(t)))dt\\ &+ \int_{t_1}^{t_f}(\boldsymbol{p}(t)\dot{\boldsymbol{x}}(t)-H^2(\boldsymbol{x}(t),\boldsymbol{p}(t)))dt\\ &= \int_{\gamma_1}\alpha_1+\int_{\gamma_2}\alpha_2 \end{aligned} \tag{3.11}$$

since $(t,\boldsymbol{z}(t))$ belongs to $\mathcal{L}_1$ for $t\in[0,t_1]$ (resp. to $\mathcal{L}_2$ for $t\in[t_1,t_f]$). By connectedness, there exists a smooth curve $\gamma_{12}\subset\Theta_1$ connecting $(\bar{t}_1,\overline{\boldsymbol{z}}(\bar{t}_1))$ to $(t_1,\boldsymbol{z}(t_1))$; having the same endpoints, γ_1 and $\overline{\gamma}_1\cup\gamma_{12}$ (resp. γ_2 and $-\gamma_{12}\cup\overline{\gamma}_2$) are homotopic. Since α_1 and α_2 are exact one forms on $\mathcal{L}_1$ and $\mathcal{L}_2$, respectively,

$$\begin{aligned}\int_{\gamma_1}\alpha_1+\int_{\gamma_2}\alpha_2 &= \int_{\overline{\gamma}_1\cup\gamma_{12}}\alpha_1+\int_{-\gamma_{12}\cup\overline{\gamma}_2}\alpha_2\\ &= \int_{\overline{\gamma}_1}\alpha_1+\int_{\overline{\gamma}_2}\alpha_2\\ &= \int_0^{t_f} f^0(\overline{\boldsymbol{x}}(t),\overline{\boldsymbol{u}}(t))dt \end{aligned} \tag{3.12}$$

since $H_1=H_2$ on Θ.

Step 5. Consider finally an admissible pair $(\boldsymbol{x},\boldsymbol{u})$, $\boldsymbol{x}$ close enough to $\overline{\boldsymbol{x}}$ in the $\mathcal{C}^0$-topology. One can find $\widetilde{\boldsymbol{x}}$ of class $\mathcal{C}^1$ arbitrarily close to $\boldsymbol{x}$ in the $W^{1,\infty}-topology$ such that $\widetilde{\boldsymbol{x}}(0)=\boldsymbol{x}_0$ and $\widetilde{\boldsymbol{x}}(t_f)=\boldsymbol{x}_f$. Moreover, as $\Pi_t(\Theta_1)$ is locally a smooth manifold, up to some $\mathcal{C}^1$-small perturbation one can assume that the graph of $\widetilde{\boldsymbol{x}}$ has only transverse intersections with $\Pi(\Theta_1)$. Let $\overline{\boldsymbol{z}}:(\widetilde{\boldsymbol{x}},\widetilde{\boldsymbol{p}})$ denote the associated lift; one has

$$f^0(\widetilde{\boldsymbol{x}}(t),\boldsymbol{u}(t))=(\widetilde{\boldsymbol{p}}(t)\dot{\widetilde{\boldsymbol{x}}}(t)-H(\widetilde{\boldsymbol{x}}(t),\widetilde{\boldsymbol{p}}(t),\boldsymbol{u}(t)))+\widetilde{\boldsymbol{p}}(t)(\boldsymbol{f}(\widetilde{\boldsymbol{x}}(t),\boldsymbol{u}(t))-\dot{\widetilde{\boldsymbol{x}}}(t)),$$

and the second term in the right-hand side can be made arbitrarily small when $\widetilde{\boldsymbol{x}}$ gets closer to $\boldsymbol{x}$ in the $W^{1,\infty}$-topology since $(t,\widetilde{\boldsymbol{z}}(t))=\Pi_t^{-1}(t,\widetilde{\boldsymbol{x}}(t))$ remains bounded by continuity of the inverse of Π_t. Let then $\varepsilon>0$; as a result of the previous discussion, there exists $\widetilde{\boldsymbol{x}}$ of class $\mathcal{C}^1$ with the same endpoints as $\boldsymbol{x}$ and whose graph has only isolated contacts with $\Pi_t(\Theta_1)$ such that

$$\int_0^{t_f} f^0(\boldsymbol{x}(t),\boldsymbol{u}(t))dt\geqslant\int_0^{t_f} f^0(\widetilde{\boldsymbol{x}}(t),\boldsymbol{u}(t))dt-\varepsilon,$$

and

$$\int_0^{t_f} f^0(\widetilde{\boldsymbol{x}}(t),\boldsymbol{u}(t))dt\geqslant\int_0^{t_f}(\widetilde{\boldsymbol{p}}(t)\dot{\widetilde{\boldsymbol{x}}}(t)-H(\widetilde{\boldsymbol{x}}(t),\widetilde{\boldsymbol{p}}(t),\boldsymbol{u}(t)))dt-\varepsilon.$$

One can extend straightforwardly the analysis of the previous step to finitely many contacts with $\Pi_t(\Theta_1)$, and bound below the integral in the right-hand side of the second inequality by the cost of the reference trajectory. As ε is arbitrary, this allows to conclude. □

3.4 Numerical examples for problems with fixed endpoints: the two-body case

We consider the two-body problem ($\mu = 0$ or 1) in dimension three. Two medium thrust cases are presented below; the final time is fixed to 1.6 times of the minimum time (case A), or to 1.3 times of the minimum time (case B), approximately, where already ensures a satisfying gain of consumption [31]. In order to have fixed endpoints to perform a conjugate point test according to the result in Sect. 3.3, the initial and final positions are fixed on the orbits (fixed longitude[3]).

3.4.1 Case A

The physical constants for numerical computations are listed in Tab. 3.1. Restricting to bang-

Table 3.1 – Case A. Summary of physical constants used for the numerical computation.

Gravitational constant μ of the Earth:			398600.47 Km^3s^{-2}
Mass of the spacecraft:	1500 Kg	Thrust:	20 Newtons
Initial perigee:	6643 Km	Final perigee:	42165 Km
Initial apogee:	46500 Km	Final apogee:	42165 deg
Initial inclination:	56 rad	Final inclination:	0 rad
Initial longitude:	π rad	Final longitude:	56.659 rad
Minimum time:	93.865 hours	Fixed final time:	147.28 hours
L^1 cost achieved (normalized):			52.638

bang (in the norm of the control) extremals, regularity of the switchings is easily verified numerically. Then one has to check the no-fold conditions (cf. Conditions 3.1 and 3.2) on the Jacobi fields. The optimal solution (see Fig. 3.3) and the Jacobi fields are computed using the `hampath` software [86]; as in [18, 31], a regularization by homotopy is used to capture the switching structure and initialize the computation of the bang-bang extremal by a single shooting method. We are then able to check Conditions 3.1 and 3.2 directly on this extremal by a simple sign test (including the jumps on the Jacobi fields at the regular switchings) on the determinant of the fields (see the numerical procedure in Appendix C). The piecewise continuous function $\delta(\cdot)$ is plotted in Fig. 3.4. An alternative approach would be to establish

[3]The definition of true longitude is given in Appendix A

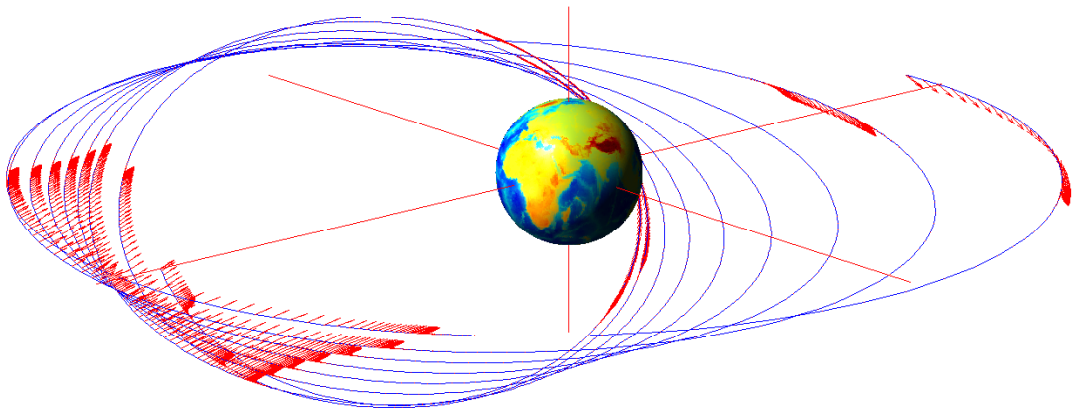

Figure 3.3 – Case A. L^1-minimum trajectory. The graph displays the trajectory (solid curve) as well as the action of the control (arrows). The initial orbit is strongly eccentric (the eccentricity equals 0.75) and strongly inclined (the inclination is 56 degrees). The geostationary target orbit around the Earth is reached at $t_f \simeq 147.28$ hours. The sparse structure of the control is clearly observed, with burn arcs concentrated around perigees and apogees (see [31]). The minimization leads to thrust only 35% of the time.

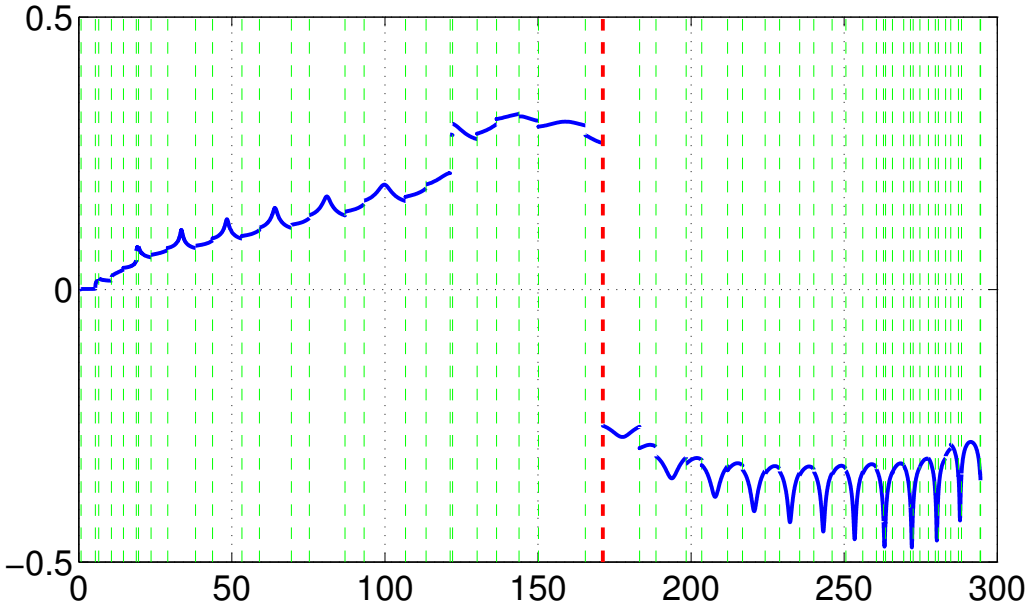

Figure 3.4 – Case A. Conjugate point test on the bang-bang L^1-extremal extended to $[0, 2t_f]$. The value of the determinant of Jacobi fields along the extremal is plotted against time. The first conjugate point occurs at $t_{1c} \approx 171.20$ hours $> t_f$; optimality of the reference extremal on $[0, t_f]$ follows. Jumps on the Jacobi fields are observed at each switching time, and conjugacy occurs at such a switching (sign change of the determinant).

a convergence result as in [85], and to verify the second order conditions on the sequence of regularized extremals. As underlined in Sect. 3.1, conjugate times may occur at or between switching times. On the example treated, no conjugate point is detected on $[0, t_f]$, ensuring a strong local optimum (cf. Theorem 3.1). The extremal is then extended up to $2\,t_f$, and a conjugate point is detected about $1.1\,t_f$, at a switching point (sign change occurring at the jump).

Remark 3.3. *As H_0 is the lift of a vector field, the determinant of Jacobi fields is either identically zero or non-vanishing along a cost arc ($\rho = 0$). (Compare with the case of polyhedral control set; see also Corollary 3.9 in [63].) Moreover, coming from the two-body case, the drift $\boldsymbol{f}_0$ is the symplectic gradient of the energy function,*

$$E(\boldsymbol{r}, \boldsymbol{v}) := \frac{1}{2}|\boldsymbol{v}|^2 - \frac{1}{|\boldsymbol{r}|^2}.$$

Accordingly, the $\delta\boldsymbol{x} = (\delta\boldsymbol{r}, \delta\boldsymbol{v})$ part of the Jacobi fields along an integral arc of $\overrightarrow{H}_0$ verifies

$$\delta\dot{\boldsymbol{x}}(t) = \overrightarrow{E}'(\overline{\boldsymbol{x}}(t))\delta\boldsymbol{x}(t),$$

so $\delta\boldsymbol{x}$ has a constant determinant along such an arc since the associated flow is symplectic. In particular, the disconjugacy condition (or Conditions 3.1 and 3.2) implies that the optimal solution starts with a burn arc.

3.4.2 Case B

In case B, we compute the transfer problem with a different inclination and a different maximum thrust (see Tab. 3.2). Using the same numerical method as in case A, the optimal

Table 3.2 – Case B. Summary of physical constants used for the numerical computation.

Gravitational constant μ of the Earth:			398600.47 Km^3s^{-2}
Mass of the spacecraft:	1500 Kg	Thrust:	10 Newtons
Initial perigee:	6643 Km	Final perigee:	42165 Km
Initial apogee:	46500 Km	Final apogee:	42165 Km
Initial inclination:	7 deg	Final inclination:	0 deg
Initial longitude:	π rad	Final longitude:	56.659 rad
Minimum time:	110.41 hours	Fixed final time:	147.28 hours
L^1 cost achieved (normalized):			67.617

solution is computed and displayed in Fig. 3.5. The piecewise continuous function $\delta(t)$ is computed by the numerical procedure in Appendix C. The extremal is then extended up to

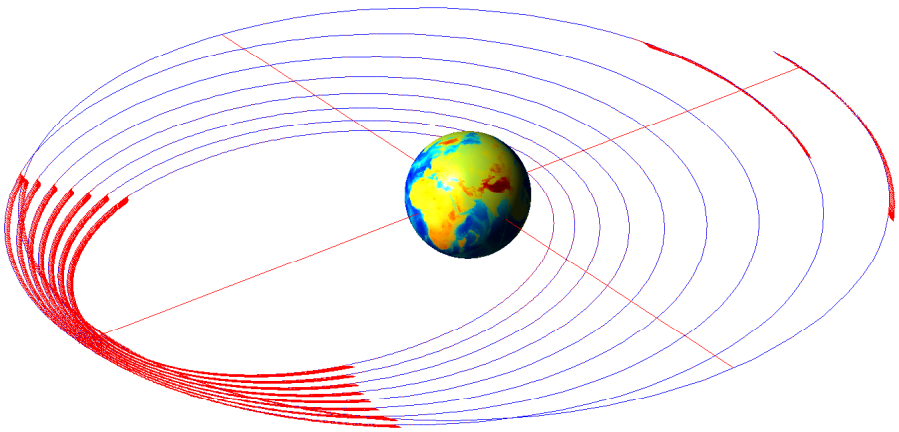

Figure 3.5 – Case B. L^1 minimum trajectory. The graph displays the trajectory (blue line), as well as the action of the control (red arrows). The initial orbit is strongly eccentric (0.75) and slightly inclined (7 degrees). The geostationary target orbit around the Earth is reached at $t_f \simeq 147.28$ hours. The sparse structure of the control is clearly observed, with burn arcs concentrated around perigees and apogees (see [31]). The minimization leads to thrust only 46% of the time. This percentage is higher than for case A (compared with Fig. 3.3), which is qualitatively consistent with the fact that the ratio of the final time vs. the minimum time is diminished in Case B.

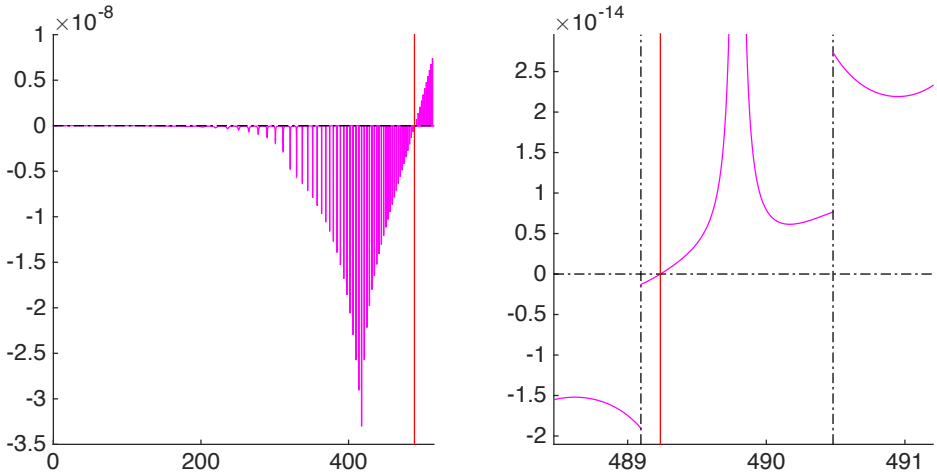

Figure 3.6 – Case B. Conjugate point test on a perturbed bang-bang L^1-extremal extended to $[0, 3.5\,t_f]$. The value of the determinant of Jacobi fields along the extremal is plotted against time (detail on the right subgraph). The endpoint conditions $\boldsymbol{x}_0$, $\boldsymbol{x}_f$ given in Tab. 3.1 are perturbed according to $\boldsymbol{x} \leftarrow \boldsymbol{x} + \Delta\boldsymbol{x}$, $|\Delta\boldsymbol{x}| \simeq 1e-5$, leading to conjugacy not at but between switching points—along a burn arc ($\rho = 1$). The first conjugate point occurs at $t_{1c} \simeq 489.23$ hours $> t_f$, ensuring again optimality of the reference extremal on $[0, t_f]$.

$3.5t_f$, and a conjugate point is detected about $3.2t_f$ at a switching point (see Fig. 3.7). A test on a perturbation of case B is provided in Fig. 3.6; by slightly changing the endpoint

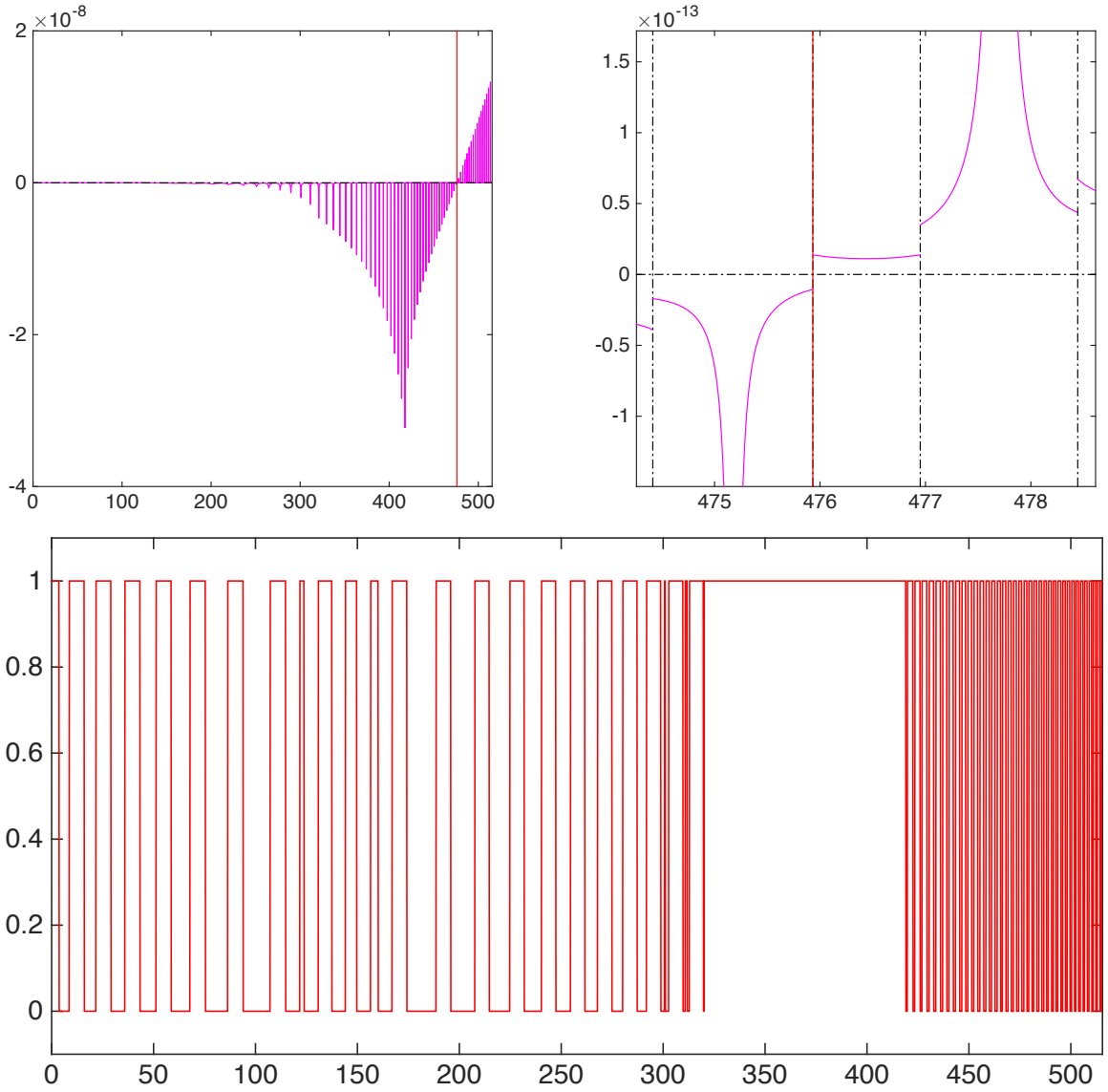

Figure 3.7 – Conjugate point test on the bang-bang L^1-extremal extended to $[0, 3.5t_f]$. The value of the determinant of Jacobi fields along the extremal is plotted against time on the upper left subgraph. The first conjugate point occurs at $t_{1c} \simeq 475.93$ hours $> t_f$; optimality of the reference extremal on $[0, t_f]$ follows. On the upper right subgraph, a zoom is provided to show the jumps on the Jacobi fields (then on their determinant) around the first conjugate time; several jumps are observed, the first one leading to a sign change at the conjugate time. Note that in accordance with Remark 3.3, the determinant must be constant along the cost arcs ($\rho = 0$) provided the symplectic coordinates $\boldsymbol{x} = (\boldsymbol{r}, \boldsymbol{v})$ are used; this is not the case here as the so called equinoctial elements [20] are used for the state—hence the slight change in the determinant. The bang-bang norm of the control, rescaled to belong to $[0, 1]$ and extended to $3.5\, t_f$, is portrayed on the lower graph. On the extended time span, there are already more than 70 switchings though the thrust is just a medium one. For low thrusts, hundreds of switchings occur.

conditions, one observes that conjugacy occurs not at a switching anymore, but along a burn (maximum-thrust) arc.

3.5 Conclusion

The sufficient second order conditions for bang-bang extremals with fixed endpoints are treated in detail. To establish such conditions, a parameterized family of extremals is constructed such that the reference extremal is embedded into a *field of extremals*. The projection behavior of the parameterized family is analyzed and two no-fold conditions (cf. Conditions 3.1 and 3.2) ensuring the projection is a local diffeomorphism are established. As a result, it is shown that conjugate points may occur not only on maximum-thrust arcs between switching times but also at switching times. Provided that the no-fold conditions are satisfied, a perturbation of Lagrangian submanifold is constructed such that its projection is a diffeomorphism and covers the graph of the reference trajectory in C^0-topology. By proving that the Poincaré-Cartan form $\boldsymbol{p}d\boldsymbol{x} - H\,dt$ is exact on the Lagrangian submanifold, it is shown that the no-fold conditions are sufficient to ensure a strong-local optimum for the reference extremal with fixed endpoints provided that each switching point is regular. Finally, two numerical examples in the two-body case ($\mu = 0$ or 1) are computed and the optimality of each trajectory is tested thanks to the second order conditions developed in this chapter.

Chapter 4

Sufficient conditions for L^1-extremals with variable target

The sufficient optimality conditions for broken extremals with fixed endpoints have been developed in Chapter 3. From the practical point of view, the boundary points may not be fixed but vary on a manifold. In this chapter[1], we shall establish the sufficient second-order conditions for the L^1-minimization with a general final condition defined by a smooth submanifold. The notations in this chapter are the same as those in Chapter 3 and we consider the following minimization problem with fixed final time t_f: Find $(\boldsymbol{x}, \boldsymbol{u}) : [0, t_f] \to \mathcal{X} \times \mathcal{U}$, $\boldsymbol{x}$ absolutely continuous, $\boldsymbol{u}$ measurable and bounded, such that

$$\dot{\boldsymbol{x}}(t) = \boldsymbol{f}(\boldsymbol{x}(t), \boldsymbol{u}(t)), \quad t \in [0, t_f] \text{ (a.e)},$$

$$\boldsymbol{x}(0) = \boldsymbol{x}_0, \quad \boldsymbol{x}(t_f) \in \mathcal{M},$$

where $\mathcal{M}$ is defined in Eq. (1.5), and such that

$$\int_0^{t_f} f^0(\boldsymbol{x}(t), \boldsymbol{u}(t))dt$$

is minimized. Note that $\mathcal{M}$ reduces to a singleton if $l = n$ where the optimality conditions have been addressed in the Chapter 3. In this chapter, we only consider the case of $l < n$.

Definition 4.1 (Local Optimality with variable target ($l < n$))**.** *Given a fixed final time $t_f > 0$, an extremal trajectory $\overline{\boldsymbol{x}}(\cdot) \in \mathcal{X}$ associated with the extremal control $\overline{\boldsymbol{u}}(\cdot) = (\overline{\rho}(\cdot), \overline{\boldsymbol{\omega}}(\cdot))$ in $\mathcal{U}$ on $[0, t_f]$ is said to be a weak-local optimum in L^∞-topology (resp. a strong-local optimum in C^0-topology) if there exists an open neighborhood $\mathcal{W}_{\boldsymbol{u}} \subseteq \mathcal{U}$ of $\overline{\boldsymbol{u}}(\cdot)$ in L^∞-topology (resp. an open neighborhood $\mathcal{W}_{\boldsymbol{x}} \subseteq \mathcal{X}$ of $\overline{\boldsymbol{x}}(\cdot)$ in C^0-topology) such that for every admissible controlled trajectory $\boldsymbol{x}(\cdot) \not\equiv \overline{\boldsymbol{x}}(\cdot)$ in $\mathcal{X}$ associated with the measurable control $\boldsymbol{u}(\cdot) = (\rho(\cdot), \boldsymbol{\omega}(\cdot))$ in $\mathcal{W}_{\boldsymbol{u}}$ on $[0, t_f]$ (resp. for every admissible controlled trajectory $\boldsymbol{x}(\cdot) \not\equiv \overline{\boldsymbol{x}}(\cdot)$ in $\mathcal{W}_{\boldsymbol{x}}$ associated with the measurable control $\boldsymbol{u}(\cdot) = (\rho(\cdot), \boldsymbol{\omega}(\cdot))$ in $\mathcal{U}$ on $[0, t_f]$) with the boundary conditions*

[1] This chapter is based on the paper "L^1-optimality conditions for the circular restricted three-body problem" to appear in [22].

$\boldsymbol{x}(0) = \overline{\boldsymbol{x}}(0)$ *and* $\boldsymbol{x}(t_f) \in \mathcal{M}$, *there holds*

$$\int_0^{t_f} f^0(\boldsymbol{x}(t), \boldsymbol{u}(t))dt \geqslant \int_0^{t_f} f^0(\overline{\boldsymbol{x}}(t), \overline{\boldsymbol{u}}(t))dt.$$

We say it is a strict weak-local (resp. strong-local) optimum if the strict inequality holds.

If $l < n$, to ensure the reference extremal trajectory $\overline{\boldsymbol{x}}(\cdot) : [0, t_f] \to \mathcal{X}$ is a strict strong-local optimum, in addition to the no-fold conditions (Conditions 3.1 and 3.2), an extra second-order condition (see, e.g., [15, 93]) is required to guarantee that every admissible controlled trajectory $\boldsymbol{x}_*(\cdot) : [0, t_f] \to \mathcal{X}$ in a small tubular neighborhood of $\overline{\boldsymbol{x}}(\cdot)$ on $[0, t_f]$, verifying the boundary conditions $\overline{\boldsymbol{x}}(0) = \boldsymbol{x}_*(0)$ and $\boldsymbol{x}_*(t_f) \in \mathcal{M}\backslash\{\overline{\boldsymbol{x}}(t_f)\}$, has a higher cost than the reference one.

4.1 Variation of the Poincaré-Cartan form on $\mathcal{M}$

Set

$$\Pi : T^*\mathcal{X} \to \mathcal{X},\ (\boldsymbol{x}, \boldsymbol{p}) \mapsto \boldsymbol{x},$$

and

$$\mathcal{N} := \big\{\boldsymbol{x} \in \mathcal{X} \mid \boldsymbol{x} = \Pi(\boldsymbol{x}(t_f, \boldsymbol{p}_0), \boldsymbol{p}(t_f, \boldsymbol{p}_0)),\ \boldsymbol{p}_0 \in \mathcal{P}_0\big\}. \tag{4.1}$$

Note that the mapping $\boldsymbol{p}_0 \mapsto \boldsymbol{x}(t_f, \boldsymbol{p}_0)$ on the sufficiently small subset $\mathcal{P}_0$ is a diffeomorphism if $\delta(t_f) \neq 0$, which indicates that the subset $\mathcal{N}$ is an open neighborhood of $\overline{\boldsymbol{x}}(t_f)$. Thus, in the case of $l < n$, the subset $\mathcal{M} \cap \mathcal{N}\backslash\{\overline{\boldsymbol{x}}(t_f\}$ is not empty if $\delta(t_f) \neq 0$. (See Fig 4.1.) For every sufficiently small subset $\mathcal{P}_0$, let us define by $\mathcal{Q}_0 \subseteq \mathcal{P}_0$ a subset of all $\boldsymbol{p}_0 \in \mathcal{P}_0$ satisfying $\Pi(\gamma(t_f, \boldsymbol{p}_0)) \in \mathcal{M} \cap \mathcal{N}$, i.e.,

$$\mathcal{Q}_0 := \big\{\boldsymbol{p}_0 \in \mathcal{P}_0 \mid \Pi(\gamma(t_f, \boldsymbol{p}_0)) \in \mathcal{M} \cap \mathcal{N}\big\}.$$

Note that for every $\boldsymbol{p}_0 \in \mathcal{Q}_0$ there holds $\boldsymbol{x}_0 = \Pi(\gamma(0, \boldsymbol{p}_0))$ and $\Pi(\gamma(t_f, \boldsymbol{p}_0)) \in \mathcal{M}$.

Remark 4.1. *For every* $\boldsymbol{p}_0 \in \mathcal{Q}_0$, *the extremal trajectory* $\boldsymbol{x}(\cdot, \boldsymbol{p}_0) = \Pi(\gamma(\cdot, \boldsymbol{p}_0))$ *on* $[0, t_f]$ *is an admissible controlled trajectory of the* L^1*-minimization problem.*

Definition 4.2. *Given the extremal* $(\overline{\boldsymbol{x}}(\cdot), \overline{\boldsymbol{p}}(\cdot))$ *on* $[0, t_f]$ *and a small* $\varepsilon > 0$, *let* $l < n$. *Then, we define by* $\boldsymbol{y} : [-\varepsilon, \varepsilon] \to \mathcal{M} \cap \mathcal{N},\ \eta \mapsto \boldsymbol{y}(\eta)$ *a twice continuously differentiable curve on* $\mathcal{M} \cap \mathcal{N}$ *such that* $\boldsymbol{y}(0) = \overline{\boldsymbol{x}}(t_f)$.

Lemma 4.1. *Given the extremal* $(\overline{\boldsymbol{x}}(\cdot), \overline{\boldsymbol{p}}(\cdot))$ *on* $[0, t_f]$ *such that each switching point is regular (cf. Assumption 3.1) and Conditions 3.1 and 3.2 are satisfied, let* $l < n$. *Then, if the subset* $\mathcal{P}_0$ *is small enough, for every smooth curve* $\boldsymbol{y}(\cdot) \in \mathcal{M} \cap \mathcal{N}$ *on* $[-\varepsilon, \varepsilon]$, *there exists a smooth path* $\eta \mapsto \boldsymbol{p}_0(\eta)$ *on* $[-\varepsilon, \varepsilon]$ *in* $\mathcal{Q}_0$ *such that* $\boldsymbol{y}(\cdot) = \Pi(\gamma(\cdot, \boldsymbol{p}_0(\cdot)))$ *on* $[-\varepsilon, \varepsilon]$.

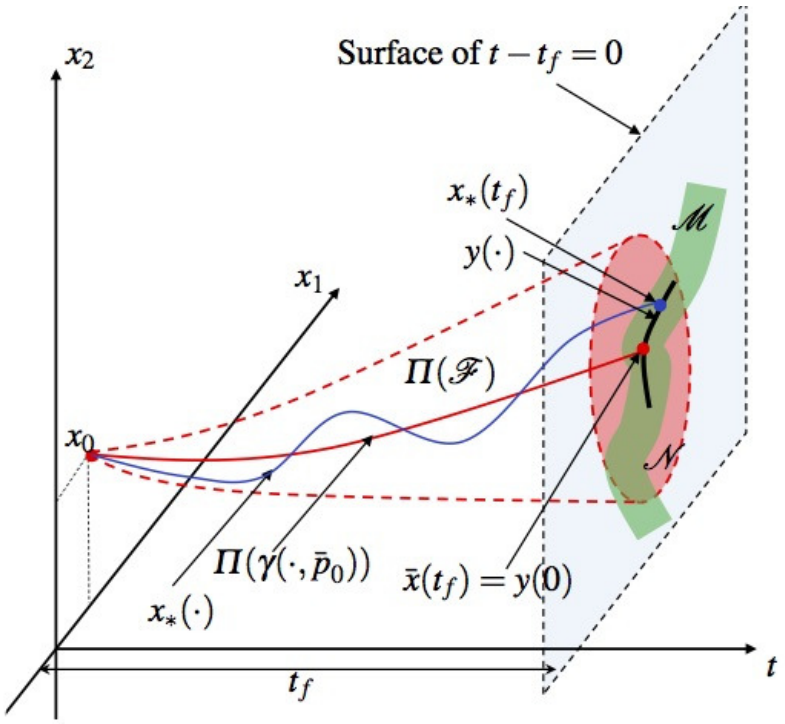

Figure 4.1 – The relationship between $\mathcal{N}$ and $\mathcal{M}$.

Proof. Note that the mapping $\boldsymbol{p}_0 \mapsto \boldsymbol{x}(t_f, \boldsymbol{p}_0)$ restricted to the subset $\mathcal{Q}_0$ is a diffeomorphism under the hypotheses of the lemma. Then, according to the *inverse function theorem*, the lemma is proved. □

Definition 4.3. *Let us define a path* $\boldsymbol{\lambda} : [-\varepsilon, \varepsilon] \to T^*_{\boldsymbol{y}(\cdot)}\mathcal{X},\ \eta \mapsto \boldsymbol{\lambda}(\eta)$ *in such a way that* $(\boldsymbol{y}(\cdot), \boldsymbol{\lambda}(\cdot)) = \gamma(\cdot, \boldsymbol{p}_0(\cdot))$ *on* $[-\varepsilon, \varepsilon]$. *Then, for every* $\xi \in [-\varepsilon, \varepsilon]$, *we define by* $J : [-\varepsilon, \varepsilon] \to \mathbb{R},\ \xi \mapsto J(\xi)$ *the integrand of the Poincaré-Cartan form* $\boldsymbol{p}d\boldsymbol{x} - H dt$ *along the extremal lift* $(\boldsymbol{y}(\cdot), \boldsymbol{\lambda}(\cdot))$ *on* $[0, \xi]$, *i.e.,*

$$J(\xi) = \int_0^\xi \boldsymbol{\lambda}(\eta)\boldsymbol{y}'(\eta) - H(\boldsymbol{y}(\eta), \boldsymbol{\lambda}(\eta))\frac{dt_f}{d\eta}d\eta,\ \xi \in [-\varepsilon, \varepsilon]. \tag{4.2}$$

Proposition 4.1. *In the case of* $l < n$, *given the extremal* $(\overline{\boldsymbol{x}}(\cdot), \overline{\boldsymbol{p}}(\cdot))$ *on* $[0, t_f]$ *such that each switching point is regular (cf. Assumption 3.1) and Conditions 3.1 and 3.2 are satisfied, assume* $\varepsilon > 0$ *is small enough. Then, the extremal trajectory* $\overline{\boldsymbol{x}}(\cdot)$ *on* $[0, t_f]$ *is a strict strong-local optimum (cf. Definition 4.1) if and only if there holds*

$$J(\xi) > J(0),\ \xi \in [-\varepsilon, \varepsilon]\backslash\{0\}, \tag{4.3}$$

for every smooth curve $\boldsymbol{y}(\cdot) \in \mathcal{M} \cap \mathcal{N}$ *on* $[-\varepsilon, \varepsilon]$.

Proof. Let us first prove that, under the hypotheses of this proposition, Eq. (4.3) is a sufficient condition for the strict strong-local optimality. Denote by $\boldsymbol{x}_*(\cdot)$ on $[0, t_f]$ (with its graph in $\Pi(\mathcal{L}_t)$) be an admissible controlled trajectory with the boundary conditions $\boldsymbol{x}_*(0) = \overline{\boldsymbol{x}}(0)$ and

$\boldsymbol{x}_*(t_f) \in \mathcal{M} \cap \mathcal{N}\backslash\{\overline{\boldsymbol{x}}(t_f)\}$. Let $(\rho_*(\cdot), \boldsymbol{\omega}_*(\cdot)) \in \mathcal{U}$ and $(\rho(\cdot, \boldsymbol{p}_0), \boldsymbol{\omega}(\cdot, \boldsymbol{p}_0)) \in \mathcal{U}$ on $[0, t_f]$ be the measurable control and the optimal control associated with $\boldsymbol{x}_*(\cdot)$ and $\boldsymbol{x}(\cdot, \boldsymbol{p}_0)$ on $[0, t_f]$, respectively. According to Definition 4.2 and Lemma 4.1, for every final point $\boldsymbol{x}_*(t_f) \in \mathcal{M} \cap \mathcal{N}\backslash\{\overline{\boldsymbol{x}}(t_f)\}$, there must exists a $\xi \in [-\varepsilon, \varepsilon]\backslash\{0\}$ and a smooth path $\boldsymbol{p}_0(\cdot) \in \mathcal{Q}_0$ associated with the smooth curve $\boldsymbol{y}(\cdot) \in \mathcal{M} \cap \mathcal{N}$ on $[-\varepsilon, \varepsilon]$ such that $\boldsymbol{y}(0) = \overline{\boldsymbol{x}}(t_f) = \Pi(\gamma(0, \boldsymbol{p}_0(\xi)))$ and $\boldsymbol{y}(\xi) = \boldsymbol{x}_*(t_f) = \Pi(\gamma(t_f, \boldsymbol{p}_0(\xi)))$. Since the trajectory $\boldsymbol{x}_*(\cdot)$ on $[0, t_f]$ has the same endpoints with the extremal trajectory $\boldsymbol{x}(\cdot, \boldsymbol{p}_0(\xi)) = \Pi(\gamma(\cdot, \boldsymbol{p}_0(\xi)))$ on $[0, t_f]$, according to Theorem 3.1, one obtains

$$\int_0^{t_f} \rho_*(t)dt \geqslant \int_0^{t_f} \rho(t, \boldsymbol{p}_0(\xi))dt, \tag{4.4}$$

where the equality holds if and only if $\boldsymbol{x}_*(\cdot) \equiv \boldsymbol{x}(\cdot, \boldsymbol{p}_0(\xi))$ on $[0, t_f]$.

Note that the four paths

1) $(\boldsymbol{x}_0, \boldsymbol{p}_0(\cdot))$ on $[0, \xi]$,

2) $\gamma(\cdot, \overline{\boldsymbol{p}}_0)$ on $[0, t_f]$,

3) $(\boldsymbol{x}(\cdot, \boldsymbol{p}_0(\xi)), \boldsymbol{p}(\cdot, \boldsymbol{p}_0(\xi))) = \gamma(\cdot, \boldsymbol{p}_0(\xi))$ on $[0, t_f]$, and

4) $(\boldsymbol{y}(\cdot), \boldsymbol{\lambda}(\cdot))$ on $[0, \xi]$

form a closed curve on the family $\mathcal{F}$. Since the integrand of the Poincaré-Cartan form $\boldsymbol{p}d\boldsymbol{x} - Hdt$ is exact on $\mathcal{F}$ (see [2, 23, 82]), one obtains

$$\begin{aligned} & J(\xi) + \int_0^{t_f} \big[\overline{\boldsymbol{p}}(t)\dot{\overline{\boldsymbol{x}}}(t) - H(\overline{\boldsymbol{x}}(t), \overline{\boldsymbol{p}}(t))\big]dt \\ = & \int_0^{t_f} \big[\boldsymbol{p}(t, \boldsymbol{p}_0(\xi))\dot{\boldsymbol{x}}(t, \boldsymbol{p}_0(\xi)) - H(\boldsymbol{x}(t, \boldsymbol{p}_0(\xi)), \boldsymbol{p}(t, \boldsymbol{p}_0(\xi)))\big]dt \\ + & \int_0^{\xi} \Big[\boldsymbol{p}_0(\eta)\frac{d\boldsymbol{x}_0}{d\eta} - H(\boldsymbol{x}_0, \boldsymbol{p}_0(\eta))\frac{dt_0}{d\eta}\Big]d\eta, \end{aligned} \tag{4.5}$$

where $t_0 = 0$. Since $\boldsymbol{x}_0$ is fixed, one obtains

$$\int_0^{\xi} \Big[\boldsymbol{p}_0(\eta)\frac{d\boldsymbol{x}_0}{d\eta} - H(\boldsymbol{x}_0, \boldsymbol{p}_0(\eta))\frac{dt_0}{d\eta}\Big]d\eta = 0$$

for every $\xi \in [-\varepsilon, \varepsilon]$. Then a combination of Eq. (4.5) with Eq. (4.4) leads to

$$\begin{aligned} \int_0^{t_f} \overline{\rho}(t)dt &= \int_0^{t_f} \big[\overline{\boldsymbol{p}}(t)\dot{\overline{\boldsymbol{x}}}(t) - H(\overline{\boldsymbol{x}}(t), \overline{\boldsymbol{p}}(t))\big]dt \\ &= -J(\xi) + \int_0^{t_f} \big[\boldsymbol{p}(t, \boldsymbol{p}_0(\xi))\dot{\boldsymbol{x}}(t, \boldsymbol{p}_0(\xi)) - H(\boldsymbol{x}(t, \boldsymbol{p}_0(\xi)), \boldsymbol{p}(t, \boldsymbol{p}_0(\xi)))\big]dt \\ &= -J(\xi) + \int_0^{t_f} \rho(t, \boldsymbol{p}_0(\xi))dt \\ &\leqslant -J(\xi) + \int_0^{t_f} \rho_*(t)dt. \end{aligned} \tag{4.6}$$

Since $J(0) = 0$, Eq. (4.3) implies the strict inequality

$$\int_0^{t_f} \overline{\rho}(t)dt < \int_0^{t_f} \rho_*(t)dt, \tag{4.7}$$

holds if $\xi \neq 0$ or $\boldsymbol{x}_*(t_f) \neq \overline{\boldsymbol{x}}(t_f)$. For the case of $\boldsymbol{x}_*(t_f) = \overline{\boldsymbol{x}}(t_f)$, Eq. (4.7) is satisfied as well according to Theorem 3.1, which proves that Eq. (4.3) is a sufficient condition.

Next, let us prove that Eq. (4.3) is a necessary condition. Assume Eq. (4.3) is not satisfied, i.e., there exists a smooth curve $\boldsymbol{y}(\cdot) \in \mathcal{M} \cap \mathcal{N}$ on $[-\varepsilon, \varepsilon]$ and a $\xi \in [-\varepsilon, \varepsilon]\backslash\{0\}$ such that $J(\xi) \leqslant J(0) = 0$. Then, according to Eq. (4.6), one obtains

$$\int_0^{t_f} \overline{\rho}(t)dt \geqslant \int_0^{t_f} \rho(t, \boldsymbol{p}_0(\xi))dt.$$

Note that the extremal trajectory $\Pi(\gamma(\cdot, \boldsymbol{p}_0(\xi)))$ is an admissible controlled trajectory of the L^1-minimization problem (cf. Remark 4.1). Thus, the proposition is proved. □

Proposition 4.2. *Given the extremal $(\overline{\boldsymbol{x}}(\cdot), \overline{\boldsymbol{p}}(\cdot))$ on $[0, t_f]$ such that each switching point is regular (cf. Assumption 3.1) and Conditions 3.1 and 3.2 are satisfied, let $l < n$. Then, if $\varepsilon > 0$ is small enough, the inequality $J''(0) \geqslant 0$ (resp. the strict inequality $J''(0) > 0$) for every smooth curve $\boldsymbol{y}(\cdot) \in \mathcal{M} \cap \mathcal{N}$ on $[-\varepsilon, \varepsilon]$ is a necessary condition (resp. a sufficient condition) for the strict strong-local optimality of the extremal trajectory $\overline{\boldsymbol{x}}(\cdot)$ on $[0, t_f]$.*

Proof. Since the final time t_f is fixed, Eq. (4.2) is reduced to

$$J(\xi) = \int_0^{\xi} \boldsymbol{\lambda}(\eta)\boldsymbol{y}'(\eta)d\eta.$$

Taking derivative of $J(\xi)$ with respect to ξ yields

$$J'(\xi) = \boldsymbol{\lambda}(\xi) \cdot \boldsymbol{y}'(\xi). \tag{4.8}$$

Note that $\boldsymbol{\lambda}(0) = \overline{\boldsymbol{p}}(t_f)$. Taking into account the transversality condition that $\overline{\boldsymbol{p}}(t_f) \perp d\phi(\overline{\boldsymbol{x}}(t_f))$, for every smooth curve $\boldsymbol{y}(\cdot) \in \mathcal{M} \cap \mathcal{N}$ on $[-\varepsilon, \varepsilon]$, we have $J'(0) = \boldsymbol{\lambda}(0)\boldsymbol{y}'(0) = 0$ since $\boldsymbol{y}'(0)$ is a tangent vector of the submanifold $\mathcal{M}$ at $\overline{\boldsymbol{x}}(t_f)$. Then, according to Proposition 4.1, this proposition is proved. □

4.2 Verifiable condition

Definition 4.4. *Given the extremal $(\overline{\boldsymbol{x}}(\cdot), \overline{\boldsymbol{p}}(\cdot))$ on $[0, t_f]$, denote by $\overline{\boldsymbol{\nu}} \in (\mathbb{R}^l)^*$ the vector of the Lagrangian multipliers of this extremal such that*

$$\overline{\boldsymbol{p}}(t_f) = \overline{\boldsymbol{\nu}} d\phi(\overline{\boldsymbol{x}}(t_f)).$$

Proposition 4.3. *In the case of $l < n$, given the extremal $(\overline{\boldsymbol{x}}(\cdot), \overline{\boldsymbol{p}}(\cdot))$ on $[0, t_f]$ such that each switching point is regular (cf. Assumption 3.1), assume Conditions 3.1 and 3.2 are satisfied. Then, the inequality $J''(0) \geqslant 0$ (resp. strict inequality $J''(0) > 0$) is satisfied for every smooth curve $\boldsymbol{y}(\cdot) \in \mathcal{M} \cap \mathcal{N}$ on $[-\varepsilon, \varepsilon]$ if and only if there holds*

$$\boldsymbol{\zeta}^T \left\{ \frac{\partial \boldsymbol{p}^T(t_f, \overline{\boldsymbol{p}}_0)}{\partial \boldsymbol{p}_0} \left[\frac{\partial \boldsymbol{x}(t_f, \overline{\boldsymbol{p}}_0)}{\partial \boldsymbol{p}_0} \right]^{-1} - \overline{\boldsymbol{\nu}} d^2\phi(\overline{\boldsymbol{x}}(t_f)) \right\} \boldsymbol{\zeta} \geqslant 0 \ (\text{resp. } > 0),$$

for every tangent vector $\boldsymbol{\zeta} \in T_{\overline{\boldsymbol{x}}(t_f)}\mathcal{M} \backslash \{0\}$.

Proof. Differentiating $J'(\xi)$ in Eq. (4.8) with respect to ξ yields

$$J''(\xi) \quad = \quad \boldsymbol{\lambda}'(\xi)\boldsymbol{y}'(\xi) + \boldsymbol{\lambda}(\xi)\boldsymbol{y}''(\xi). \tag{4.9}$$

Then, differentiating $\phi(\boldsymbol{y}(\xi))$ with respect to ξ yields

$$\begin{aligned} \frac{d}{d\xi}\phi(\boldsymbol{y}(\xi)) &= d\phi(\boldsymbol{y}(\xi))\boldsymbol{y}'(\xi) = 0, \\ \frac{d^2}{d\xi^2}\phi(\boldsymbol{y}(\xi)) &= [d^2\phi(\boldsymbol{y}(\xi))\boldsymbol{y}'(\xi)]\boldsymbol{y}'(\xi) + d\phi(\boldsymbol{y}(\xi))\boldsymbol{y}''(\xi) = 0. \end{aligned} \tag{4.10}$$

Since $(\overline{\boldsymbol{x}}(t_f), \overline{\boldsymbol{p}}(t_f)) = (\boldsymbol{y}(0), \boldsymbol{\lambda}(0))$, according to the definition of the vector $\overline{\boldsymbol{\nu}}$ in Definition 4.4, one immediately has $\boldsymbol{\lambda}(0) = \overline{\boldsymbol{\nu}} d\phi(\boldsymbol{y}(0))$. Thus, multiplying $\overline{\boldsymbol{\nu}}$ on both sides of Eq. (4.10) and fixing $\xi = 0$, we obtain

$$\begin{aligned} \overline{\boldsymbol{\nu}} \frac{d^2\phi(\boldsymbol{y}(0))}{d\xi^2} &= \boldsymbol{\lambda}(0)\boldsymbol{y}''(0) + \overline{\boldsymbol{\nu}} \left[d^2\phi(\boldsymbol{y}(0))\boldsymbol{y}'(0) \right] \boldsymbol{y}'(0) \\ &= \boldsymbol{\lambda}(0)\boldsymbol{y}''(0) + [\boldsymbol{y}'(0)]^T \left[\overline{\boldsymbol{\nu}} d^2\phi(\boldsymbol{y}(0)) \right] \boldsymbol{y}'(0) \\ &= 0. \end{aligned}$$

Substituting this equation into Eq. (4.9) yields

$$J''(0) = \boldsymbol{\lambda}'(0)\boldsymbol{y}'(0) - [\boldsymbol{y}'(0)]^T \left[\overline{\boldsymbol{\nu}} d^2\phi(\boldsymbol{y}(0)) \right] \boldsymbol{y}'(0). \tag{4.11}$$

Note that we have

$$\begin{aligned} \boldsymbol{y}'(\xi) &= \frac{d\boldsymbol{x}(t_f, \boldsymbol{p}_0(\xi))}{d\xi} = \frac{\partial \boldsymbol{x}(t_f, \boldsymbol{p}_0(\xi))}{\partial \boldsymbol{p}_0} [\boldsymbol{p}_0'(\xi)]^T, \\ [\boldsymbol{\lambda}'(\xi)]^T &= \frac{d\boldsymbol{p}^T(t_f, \boldsymbol{p}_0(\xi))}{d\xi} = \frac{\partial \boldsymbol{p}^T(t_f, \boldsymbol{p}_0(\xi))}{\partial \boldsymbol{p}_0} [\boldsymbol{p}_0'(\xi)]^T. \end{aligned} \tag{4.12}$$

Since the matrix $\partial \boldsymbol{x}(t_f, \boldsymbol{p}_0(\xi))/\partial \boldsymbol{p}_0$ is nonsingular if *Condition* 3.1 is satisfied, we have

$$[\boldsymbol{p}_0'(\xi)]^T = \left[\frac{\partial \boldsymbol{x}(t_f, \boldsymbol{p}_0(\xi))}{\partial \boldsymbol{p}_0} \right]^{-1} \boldsymbol{y}'(\xi).$$

Substituting this equation into Eq. (4.12) yields

$$[\boldsymbol{\lambda}'(\xi)]^T = \frac{\partial \boldsymbol{p}^T(t_f, \boldsymbol{p}_0(\xi))}{\partial \boldsymbol{p}_0} \left[\frac{\partial \boldsymbol{x}(t_f, \boldsymbol{p}_0(\xi))}{\partial \boldsymbol{p}_0}\right]^{-1} \boldsymbol{y}'(\xi).$$

Again, substituting this equation into Eq. (4.11) and taking into account $\overline{\boldsymbol{p}}_0 = \boldsymbol{p}_0(0)$ and $\overline{\boldsymbol{x}}(t_f) = \boldsymbol{y}(0)$, we eventually get that for every smooth curve $\boldsymbol{y}(\cdot) \in \mathcal{M} \cap \mathcal{N}$ on $[-\varepsilon, \varepsilon]$ there holds

$$J''(0) = [\boldsymbol{y}'(0)]^T \left\{\frac{\partial \boldsymbol{p}^T(t_f, \overline{\boldsymbol{p}}_0)}{\partial \boldsymbol{p}_0} \left[\frac{\partial \boldsymbol{x}(t_f, \overline{\boldsymbol{p}}_0)}{\partial \boldsymbol{p}_0}\right]^{-1} - \overline{\boldsymbol{\nu}} d^2\phi(\overline{\boldsymbol{x}}(t_f))\right\} \boldsymbol{y}'(0). \tag{4.13}$$

Note that the vector $\boldsymbol{y}'(0)$ can be an arbitrary vector in the tangent space $T_{\overline{\boldsymbol{x}}(t_f)}\mathcal{X}\backslash\{0\}$, one proves this proposition. □

Condition 4.1. *Given the extremal $(\overline{\boldsymbol{x}}(\cdot), \overline{\boldsymbol{p}}(\cdot))$ on $[0, t_f]$, let*

$$\boldsymbol{\zeta}^T \left\{\frac{\partial \boldsymbol{p}^T(t_f, \overline{\boldsymbol{p}}_0)}{\partial \boldsymbol{p}_0} \left[\frac{\partial \boldsymbol{x}(t_f, \overline{\boldsymbol{p}}_0)}{\partial \boldsymbol{p}_0}\right]^{-1} - \overline{\boldsymbol{\nu}} d^2\phi(\overline{\boldsymbol{x}}(t_f))\right\} \boldsymbol{\zeta} > 0,$$

be satisfied for every vector $\boldsymbol{\zeta} \in T_{\overline{\boldsymbol{x}}(t_f)}\mathcal{M}\backslash\{0\}$.

Then, as a combination *Propositions* 4.2 and 4.3, we eventually obtain the following result.

Theorem 4.1. *Given the extremal $(\overline{\boldsymbol{x}}(\cdot), \overline{\boldsymbol{p}}(\cdot))$ on $[0, t_f]$ such that every switching point is regular (cf. Assumption 3.1), let $l < n$. Then, if Conditions 3.1, 3.2, and 4.1 are satisfied, the extremal trajectory $\overline{\boldsymbol{x}}(\cdot)$ on $[0, t_f]$ realizes a strict strong-local optimality (cf. Definition 4.1).*

Consequently, in the case of $l < n$, *Conditions* 3.1, 3.2, and 4.1, once satisfied, are sufficient to guarantee a bang-bang extremal with regular switching points to be a strict strong-local optimum.

4.3 Numerical implementation for sufficient conditions

To test Conditions 3.1 and 3.2, it amounts to compute the matrix $\partial \boldsymbol{x}(t, \overline{\boldsymbol{z}}_0)/\partial \boldsymbol{p}_0$ on $[0, t_f]$. The numerical procedure for computing the matrix $\partial \boldsymbol{x}(t, \overline{\boldsymbol{p}}_0)/\partial \boldsymbol{p}_0$ is presented in Appendix C.

Once the extremal $(\overline{\boldsymbol{x}}(\cdot), \overline{\boldsymbol{p}}(\cdot)) = \gamma(\cdot, \overline{\boldsymbol{p}}_0)$ on $[0, t_f]$ is computed, according to Definition 4.4, the vector $\overline{\boldsymbol{\nu}}$ of Lagrangian multipliers in Condition 4.1 can be computed by

$$\overline{\boldsymbol{\nu}} = \overline{\boldsymbol{p}}(t_f) d\phi^T(\overline{\boldsymbol{x}}(t_f)) \left[d\phi(\overline{\boldsymbol{x}}(t_f)) d\phi^T(\overline{\boldsymbol{x}}(t_f))\right]^{-1}. \tag{4.14}$$

Definition 4.5. *We define by $\boldsymbol{C} \in \mathbb{R}^{n\times(n-l)}$ a full-rank matrix such that its columns form a basis of the tangent space $T_{\overline{\boldsymbol{x}}(t_f)}\mathcal{M}$.*

Then, one immediately gets that Condition 4.1 is satisfied if and only if there holds

$$\boldsymbol{C}^T \left\{ \frac{\partial \boldsymbol{p}^T(t_f, \overline{\boldsymbol{p}}_0)}{\partial \boldsymbol{p}_0} \left[\frac{\partial \boldsymbol{x}(t_f, \overline{\boldsymbol{p}}_0)}{\partial \boldsymbol{p}_0} \right]^{-1} - \overline{\boldsymbol{\nu}} d^2\phi(\overline{\boldsymbol{x}}(t_f)) \right\} \boldsymbol{C} \succ 0. \tag{4.15}$$

Note that the matrix $\boldsymbol{C}$ can be computed by a simple Gram–Schmidt process once the explicit expression of the matrix $d\phi(\overline{\boldsymbol{x}}(t_f))$ is derived. Thus, it suffices to compute the matrix $\partial \boldsymbol{x}(\cdot, \overline{\boldsymbol{p}}_0)/\partial \boldsymbol{p}_0$ on $[0, t_f]$ and the matrix $\partial \boldsymbol{p}^T(\cdot, \overline{\boldsymbol{p}}_0)/\partial \boldsymbol{p}_0$ at t_f in order to test *Conditions* 3.1, 3.2, and 4.1. (See Appendix C for the numerical procedure of computing the matrices $\partial \boldsymbol{x}(\cdot, \overline{\boldsymbol{p}}_0)/\partial \boldsymbol{p}_0$ and $\partial \boldsymbol{p}^T(\cdot, \overline{\boldsymbol{p}}_0)/\partial \boldsymbol{p}_0$ on $[0, t_f]$.)

4.4 Numerical example for problems with variable target: the three-body case

In this section, we consider the three-body problem modeled by Earth, Moon and a spacecraft. Since the orbits of the Earth and the Moon around their common center of mass are nearly circular (the eccentricity is around 5.49×10^{-2}), and since the mass of a spacecraft is negligible compared with that of the two celestial bodies, the CRTBP is valid (see, e.g., [91]). The physical parameters corresponding to the Earth-Moon system are $\mu = 1.2153 \times 10^{-2}$, $d_* = 384,400.00$ km, and $t_* = 3.7521 \times 10^5$ seconds (or 4.3427 days). The initial mass of the spacecraft is specified as $m_* = 500$ kg, the maximum thrust of the spacecraft engine is 1.0 N,

$$\tau_{max} = 1.0 \frac{t_*^2}{m_* d_*},$$

so that the initial maximum acceleration is 2.0×10^{-3} m^2/s. The spacecraft initially evolves on a circular geosynchronous Earth orbit (GEO) lying on the *XY*-plane such that the radius of the initial orbit is $r_g = 42,165.00$ km. When the spacecraft moves to the point on X-axis between the Earth and the Moon, i.e., $\| \boldsymbol{r}(0) \| = r_g/d_* - \mu$ (the initial state is fixed), we start to control the spacecraft to reach a circular orbit around the Moon with radius $r_m = 13,069.60$ km such that the L^1-norm of control is minimized at the fixed final time $t_f = 38.46$ days. Accordingly, the initial state $\boldsymbol{x}_0 = (\boldsymbol{r}_0, \boldsymbol{v}_0)$ is given as

$$\boldsymbol{r}_0 = (r_g/d_* - \mu, 0, 0)^T \text{ and } \boldsymbol{v}_0 = (0, v_g, 0)^T,$$

where v_g is the non-dimensional velocity taking the value such that, without any control, the spacecraft moves freely on the GEO, and an explicit expression of the function $\phi(\cdot)$ in

Eq. (1.5) therefore is

$$\phi(\boldsymbol{x}_f) = \begin{bmatrix} \frac{1}{2} \parallel \boldsymbol{r}(t_f) - [1-\mu, 0, 0]^T \parallel^2 - \frac{1}{2}(r_m/d_*)^2 \\ \frac{1}{2} \parallel \boldsymbol{v}(t_f) \parallel^2 - \frac{1}{2} v_m^2 \\ \boldsymbol{v}^T(t_f) \cdot (\boldsymbol{r}(t_f) - [1-\mu, 0, 0]^T) \\ \boldsymbol{r}^T(t_f) \cdot \mathbf{1}_Z \\ \boldsymbol{v}^T(t_f) \cdot \mathbf{1}_Z \end{bmatrix}, \tag{4.16}$$

where $\mathbf{1}_z = [0, 0, 1]^T$ denotes the unit vector of the Z-axis of the rotating frame *OXYZ* and v_m is the non-dimensional velocity taking the value such that the spacecraft, once steered to a point $\boldsymbol{x}_f$ with $\phi(\boldsymbol{x}_f) = 0$, will freely move on the final circular orbit around the Moon with radius r_m.

First, we compute the extremal $(\overline{\boldsymbol{x}}(\cdot), \overline{\boldsymbol{p}}(\cdot))$ on $[0, t_f]$. We search a zero of the shooting function corresponding to a two-point boundary value problem [68]. A simple shooting method does not allow one to solve this problem because one does not know *a priori* the structure of the optimal control. Moreover, the numerical computation of the shooting function and its differential may be intricate, as the function may not even be differentiable (typically at points corresponding to a change in the structure of the control strategy, that is a change in the number of switchings, here). We use a regularization procedure [18] that smoothes the controls discontinuities and get an energy-optimal trajectory first, then use a homotopy method to find the real trajectory with a bang-bang control. Note that both the initial point $\boldsymbol{x}_0$ and the final constraint submanifold $\mathcal{M}$ lie on the XY-plane, in order that the whole trajectory lies on the XY-plane as well. Fig. 4.2 illustrates the (non-dimensional) profile of the position vector $\boldsymbol{r}$ along the computed extremal trajectory. The profiles of ρ, $\parallel \boldsymbol{p}_v \parallel$, and H_1 with respect to time are shown in Fig. 4.3; we can see that the number of maximum-thrust arcs is 15 with 29 switching points and that the regularity condition in Assumption 3.1 at every switching point is satisfied. Since the extremal trajectory is computed thanks to necessary conditions, one has to check sufficient optimality conditions to make sure that it is at least locally optimal. According to what has been developed in Sect. 4, it suffices to check if *Conditions* 3.1, 3.2, and 4.1 are satisfied. Using Eqs. (C-1–C-4), one can compute $\delta(\cdot)$ on $[0, t_f]$. In order to have a clear view, the profile of $\delta(\cdot)$ on $[0, t_f]$ is rescaled by $\text{sgn}(\delta(\cdot)) * |\delta(\cdot)|^{1/12}$ (see Fig. 4.4). We can see that there exist no sign changes at switching points, and no zeros on smooth bang subarcs. Thus, Conditions 3.1 and 3.2 are satisfied along the computed extremal. To check Condition 4.1, differentiating $\phi(\cdot)$ in Eq. (4.16) yields

$$d\phi(\overline{\boldsymbol{x}}(t_f)) = \begin{bmatrix} \boldsymbol{r}(t_f) - [1-\mu, 0, 0]^T & \mathbf{0}_{3\times 1} & \boldsymbol{v}(t_f) & \mathbf{1}_Z & \mathbf{0}_{3\times 1} \\ \mathbf{0}_{3\times 1} & \boldsymbol{v}(t_f) & \boldsymbol{r}(t_f) - [1-\mu, 0, 0]^T & \mathbf{0}_{3\times 1} & \mathbf{1}_Z \end{bmatrix}^T \tag{4.17}$$

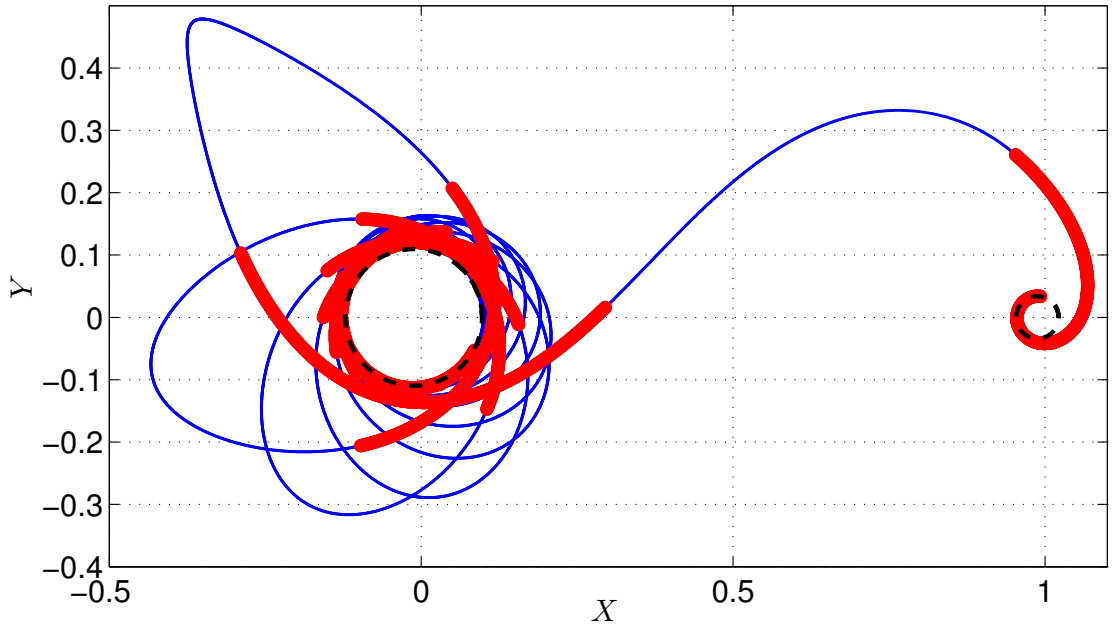

Figure 4.2 – Non-dimensional profile of the position vector $\boldsymbol{r}$ of the L^1-minimization trajectory in the rotating frame $OXYZ$. The thick curves are the maximum-thrust arcs, while the thin curves are the zero-thrust ones. The bigger dashed circle and the smaller one are the initial and final circular orbits around the Earth and the Moon, respectively.

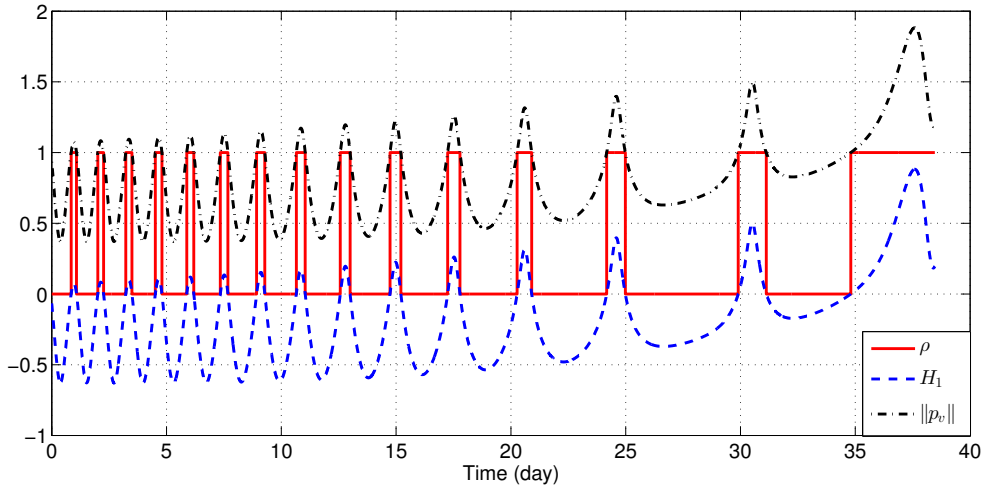

Figure 4.3 – Profiles of ρ, $\| \boldsymbol{p}_v \|$, and H_1 with respect to time along the L^1-minimization trajectory.

and

$$d^2\phi_1(\overline{\boldsymbol{x}}(t_f)) = \begin{pmatrix} I_3 & \mathbf{0}_3 \\ \mathbf{0}_3 & \mathbf{0}_3 \end{pmatrix}, \quad d^2\phi_2(\overline{\boldsymbol{x}}(t_f)) = \begin{pmatrix} \mathbf{0}_3 & \mathbf{0}_3 \\ \mathbf{0}_3 & I_3 \end{pmatrix},$$

$$d^2\phi_3(\overline{\boldsymbol{x}}(t_f)) = \begin{pmatrix} \mathbf{0}_3 & I_3 \\ I_3 & \mathbf{0}_3 \end{pmatrix}, \quad d^2\phi_4(\overline{\boldsymbol{x}}(t_f)) = d^2\phi_5(\overline{\boldsymbol{x}}(t_f)) = \mathbf{0}_6,$$

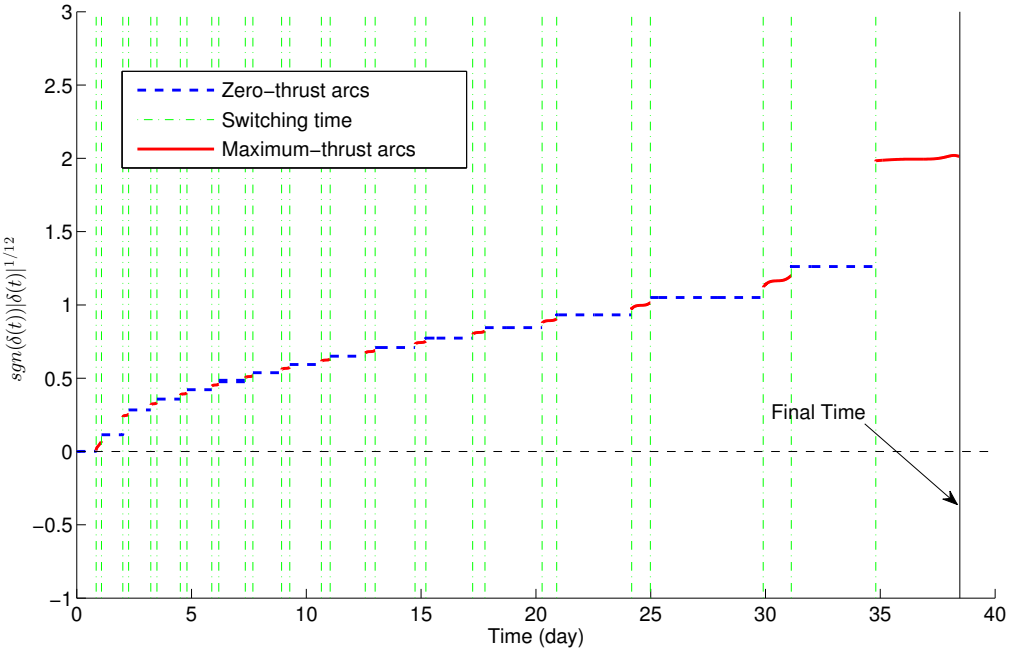

Figure 4.4 – The profile of $sgn(\delta(t))|\delta(t)|^{1/12}$ with respect to time along the L^1-minimization extremal for the CRTBP.

where $\phi_i(\cdot) : \mathcal{X} \to \mathbb{R},\ \boldsymbol{x} \mapsto \phi_i(\boldsymbol{x})$ for $i = 1,\ 2,\ \cdots,\ l$ are the elements of the vector-valued function $\phi(\boldsymbol{x})$. Then, substituting the values of $\overline{\boldsymbol{x}}(t_f)$ and $\overline{\boldsymbol{p}}(t_f)$ into Eq. (4.14), the vector $\overline{\boldsymbol{\nu}}$ can be computed. With the exception of the matrix $\boldsymbol{C}$, all quantities in Eq. (4.15) are obtained. One can use a Gram-Schmidt process to compute the matrix $\boldsymbol{C}$ associated with the matrix in Eq. (4.17). Substituting numerical values into Eq. (4.15), we eventually obtain

$$\boldsymbol{C}^T \left\{ \frac{\partial \boldsymbol{p}^T(t_f, \overline{\boldsymbol{p}}_0)}{\partial \boldsymbol{p}_0} \left[\frac{\partial \boldsymbol{x}(t_f, \overline{\boldsymbol{p}}_0)}{\partial \boldsymbol{p}_0} \right]^{-1} - \overline{\boldsymbol{\nu}} d^2\phi(\overline{\boldsymbol{x}}(t_f)) \right\} \boldsymbol{C} \approx 0.5292 \succ 0.$$

Thus, Condition 4.1 is satisfied. Fig. 4.5 shows the profile of $J(\cdot)$ with respect to $\boldsymbol{y}(\cdot) \in \mathcal{M} \cap \mathcal{N}$ in a small neighborhood of $\overline{\boldsymbol{x}}(t_f)$. One can clearly see that $J(\cdot) > J(0)$ on $[-\varepsilon, \varepsilon] \backslash \{0\}$. All the conditions in Theorem 4.1 are satisfied, So the computed L^1-minimization trajectory realizes a strict strong-local optimum in C^0-topology.

4.5 Conclusion

When the dimension of the target manifold is not zero, an extra second-order condition (cf. Condition 4.1) involving the geometry of the target manifold and the Jacobi fields is devised. This condition, once met, guarantees the variation of the cost functional on the target manifold is positive. Therefore, if the final point is not fixed but varies on the target manifold, the extra condition together with the no-fold conditions, i.e., Conditions 3.1 and 3.2, are sufficient for the strict strong-local optimality of a bang-bang extremal (cf. Theorem 4.1). Finally,

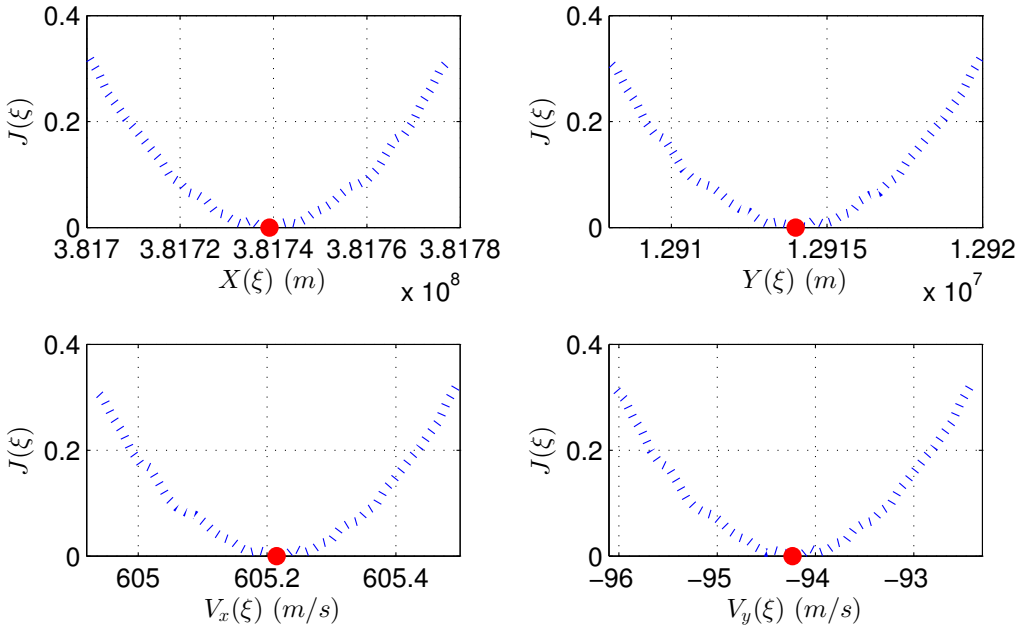

Figure 4.5 – Let $X(\xi)$ and $Y(\xi)$ be the projection of the position vector $\boldsymbol{r}(\xi)$ on X- and Y-axis of the rotating frame $OXYZ$, respectively, and let $V_x(\xi)$ and $V_y(\xi)$ be the projection of the velocity vector $\boldsymbol{v}(\xi)$ on X- and Y-axis of the rotating frame $OXYZ$, respectively. The figure plots the profiles $J(\xi)$ with respect to $X(\xi)$, $Y(\xi)$, $V_x(\xi)$, and $V_y(\xi)$. The dots on each plot denote $(J(0), \boldsymbol{y}(0))$.

approximating the Earth-Moon-spacecraft system by the CRTBP model, a transfer trajectory is computed by combining a shooting method with a continuation method. The optimality of the computed trajectory is tested thanks to the second order conditions developed.

Chapter 5

Neighboring optimal feedback control

Due to numerous unavoidable perturbations and errors, one cannot expect a spacecraft controlled by a precomputed optimal control (or nominal control) to exactly move on the corresponding precomputed optimal trajectory (or nominal trajectory) to a desired target. In this chapter, we shall establish the neighboring optimal feedback control, which is able to reduce the errors of final conditions. Indeed, the neighboring optimal optimal feedback control is one of the most important practical applications of optimal control theory (see [82, Chapter 5], e.g.). The classical way (see, e.g., [16, Chapter 6] and [33, Chapter 11]) to design the neighboring optimal control is to solve an accessory minimum problem by minimizing the second variation of the cost functional; a by-product is that it is impossible to construct the neighboring optimal feedback control if the typical Jacobi necessary condition is violated (see [48], e.g.). In those papers, a standing assumption is that the control function is continuous. Regarding the bang-bang case, the neighboring optimal control consists not only of the correction of thrust direction but also of switching times. In this chapter, the neighboring optimal control for L^1-minimization problem is constructed from the geometric point of view based on [82]. First, a parameterized family of neighboring extremals is constructed. Then, deriving the first-order term of the Taylor expansion of the parameterized neighboring extremals, the neighboring optimal feedback on the direction of thrust as well as on switching times are established.

5.1 Neighboring extremals

Throughout the chapter, we denote by $(\overline{\boldsymbol{x}}(\cdot), \overline{\boldsymbol{p}}(\cdot)) : [0, t_f] \to T^*\mathcal{X}$ and $\overline{\boldsymbol{u}}(\cdot) = (\overline{\rho}(\cdot), \overline{\boldsymbol{\tau}}(\cdot)) : [0, t_f] \to \mathcal{U}$ the nominal extremal and the nominal control, respectively, and we assume the nominal extremal is computed in advance.

Definition 5.1. *Let $\overline{\mathcal{W}} \subseteq T^*\mathcal{X}$ be a small tubular neighborhood of the nominal extremal $(\overline{\boldsymbol{x}}(\cdot), \overline{\boldsymbol{p}}(\cdot))$ on $[0, t_f]$, we say every Hamiltonian flow $e^{t\overrightarrow{H}}(\boldsymbol{x}_0, \boldsymbol{p}_0)$ on $[0, t_f]$, with the final condition:*

$$e^{t_f \overrightarrow{H}}(\boldsymbol{x}_0, \boldsymbol{p}_0) \in \{(\boldsymbol{x}, \boldsymbol{p}) \in T^*\mathcal{X} \mid \boldsymbol{x} \in \mathcal{M},\ \boldsymbol{p} \perp T^*_{\boldsymbol{x}}\mathcal{M}\},$$

is a neighboring extremal of the nominal one if it lies in $\overline{\mathcal{W}}$.

In the next paragraph, the neighboring extremals will be parameterized.

5.1.1 Parameterization of neighboring extremals

Assumption 5.1. *The matrix $\nabla\phi(\overline{\boldsymbol{x}}(t_f))$ is of full rank.*

As a result of this assumption, the manifold $\mathcal{M}$ is a local submersion. Then, let us define the Lagrangian submanifold $\mathcal{L}_f \subset T^*\mathcal{X}$ by

$$\mathcal{L}_f = \big\{(\boldsymbol{x},\boldsymbol{p}) \in T^*\mathcal{X} \mid \boldsymbol{x} \in \mathcal{M},\ \boldsymbol{p} \perp T^*_{\boldsymbol{x}}\mathcal{M}\big\}.$$

According to Definition 5.1, for every neighboring extremal $(\boldsymbol{x}(\cdot),\boldsymbol{p}(\cdot)) \in \overline{\mathcal{W}}$ on $[0,t_f]$, there holds $(\boldsymbol{x}(t_f),\boldsymbol{p}(t_f)) \in \mathcal{L}_f$. Assuming $\mathcal{N} \subset \mathcal{L}_f$ is a sufficiently small open neighborhood of $(\overline{\boldsymbol{x}}(t_f),\overline{\boldsymbol{p}}(t_f))$, there exists an invertible function $\boldsymbol{F} : \mathcal{N} \to \mathbb{R}^n$ such that both the function and its inverse $\boldsymbol{F}^{-1}$ are smooth, i.e., for every $\boldsymbol{q} \in \mathbb{R}^n$ there exists one and only one $(\boldsymbol{x},\boldsymbol{p}) \in \mathcal{N}$ such that $\boldsymbol{q} = \boldsymbol{F}(\boldsymbol{x},\boldsymbol{p})$. Let us define by

$$\gamma : [0,t_f] \times \boldsymbol{F}(\mathcal{N}) \to T^*\mathcal{X},\ \gamma(t,\boldsymbol{q}) = e^{t\overrightarrow{H}}(\boldsymbol{x},\boldsymbol{p})$$

the Hamiltonian flow with the final condition $\gamma(t_f,\boldsymbol{q}) = \boldsymbol{F}^{-1}(\boldsymbol{q})$, i.e., $\gamma(t_f,\boldsymbol{q}) \in \mathcal{N} \subset \mathcal{L}_f$ for every $\boldsymbol{q} \in \boldsymbol{F}(\mathcal{N})$. Then, if $\overline{\boldsymbol{q}} := \boldsymbol{F}(\overline{\boldsymbol{x}}(t_f),\overline{\boldsymbol{p}}(t_f))$, we have $(\overline{\boldsymbol{x}}(\cdot),\overline{\boldsymbol{p}}(\cdot)) = \gamma(\cdot,\overline{\boldsymbol{q}})$ on $[0,t_f]$.

Definition 5.2. *Given the nominal extremal $(\overline{\boldsymbol{x}}(\cdot),\overline{\boldsymbol{p}}(\cdot))$ on $[0,t_f]$, we denote by*

$$\mathcal{F}_{\boldsymbol{q}} = \big\{(t,\boldsymbol{x}(t),\boldsymbol{p}(t)) \in \mathbb{R} \times T^*\mathcal{X} \mid (\boldsymbol{x}(t),\boldsymbol{p}(t)) = \gamma(t,\boldsymbol{q}),\ t \in [0,t_f],\ \boldsymbol{q} \in \boldsymbol{F}(\mathcal{N})\big\}$$

the $\boldsymbol{q}$-parametrized family of neighboring extremals around the nominal one.

Obviously, once the tubular neighborhood $\overline{\mathcal{W}}$ is small enough, the graph of all the neighboring extremals is covered by the projection Π_t of $\mathcal{F}_{\boldsymbol{q}}$.

Definition 5.3 (Existence of neighboring extremals)**.** *Given the nominal extremal $(\overline{\boldsymbol{x}}(\cdot),\overline{\boldsymbol{p}}(\cdot))$ on $[0,t_f]$, we say that there exist neighboring extremals around this nominal one if and only if, for every infinitesimal deviation $\Delta\boldsymbol{x} \in \mathbb{R}^n$ and every time $t \in [0,t_f)$, there exists a $\boldsymbol{q}_* \in \boldsymbol{F}(\mathcal{N})$ such that $\overline{\boldsymbol{x}}(t) + \Delta\boldsymbol{x} = \Pi(\gamma(t,\boldsymbol{q}_*))$.*

Recall that the existence of neighboring extremals around the nominal one is a prerequisite to construct the neighboring optimal feedback control (see, e.g., [16, 48]). In the next paragraph, through analyzing the projection behavior of the family $\mathcal{F}_{\boldsymbol{q}}$ at each time $t \in [0,t_f)$, the conditions for the existence of neighboring extremals around a bang-bang nominal extremal will be presented.

5.1.2 Existence conditions for neighboring extremals

Hereafter, we denote by $t_0 \in [0, t_f)$ the current time and let $\boldsymbol{x}_* \in \mathcal{X}\backslash\mathcal{M}$ be the measured (or actual) state of the spacecraft at t_0. Generally speaking, there holds

$$\Delta\boldsymbol{x} := \boldsymbol{x}_* - \overline{\boldsymbol{x}}(t_0) \neq 0,$$

due to unavoidable perturbations and errors.

Assumption 5.2. *Let $t_m > 0$ be the minimum time to steer the system Σ by measurable controls $\boldsymbol{u}(\cdot) : [0, t_m] \to \mathcal{U}$ from the actual state $\boldsymbol{x}_* \in \mathcal{X}\backslash\mathcal{M}$ to $\mathcal{M}$. We assume that there exists at least one point $\boldsymbol{x}_f \in \mathcal{M}$ such that $t_f - t_0 \geqslant t_m$.*

As a combination of this assumption and the controllability results in Chapter 2, there exists at least one optimal trajectory $\boldsymbol{x}(\cdot) \in \mathcal{X}$ on $[t_0, t_f]$ such that $\boldsymbol{x}(t_0) = \boldsymbol{x}_*$ and $\boldsymbol{x}(t_f) \in \mathcal{M}$. (See [31] for the existence of optimal solution.)

Remark 5.1. *Given the nominal extremal $(\overline{\boldsymbol{x}}(\cdot), \overline{\boldsymbol{p}}(\cdot))$ on $[0, t_f]$ and a time $t_0 \in [0, t_f)$, denote by $\mathcal{O}_{t_0} \subset \mathcal{X}\backslash\mathcal{M}$ an infinitesimal open neighborhood of the point $\overline{\boldsymbol{x}}(t_0)$. Then, if the point $\overline{\boldsymbol{x}}(t_0)$ lies on the boundary of the domain $\Pi(\gamma(t_0, \boldsymbol{F}(\mathcal{N})))$ for a subset $\mathcal{N} \subset \mathcal{L}_f$, no matter how small the neighborhood $\mathcal{O}_{t_0}$ is, there are some $\boldsymbol{x}_* \in \mathcal{O}_{t_0}\backslash\{\overline{\boldsymbol{x}}(t_0)\}$ such that $\boldsymbol{x}_* \notin \Pi(\gamma(t_0, \boldsymbol{F}(\mathcal{N})))$.*

If the projection Π of $\mathcal{F}_{\boldsymbol{q}}$ at t_0 is a fold singularity, the point $\overline{\boldsymbol{x}}(t_0)$ lies on the boundary of the domain $\Pi(\gamma(t_0, \boldsymbol{F}(\mathcal{N})))$ for a sufficiently small subset $\mathcal{N}$, as is shown by the right plot in Fig. 5.1.

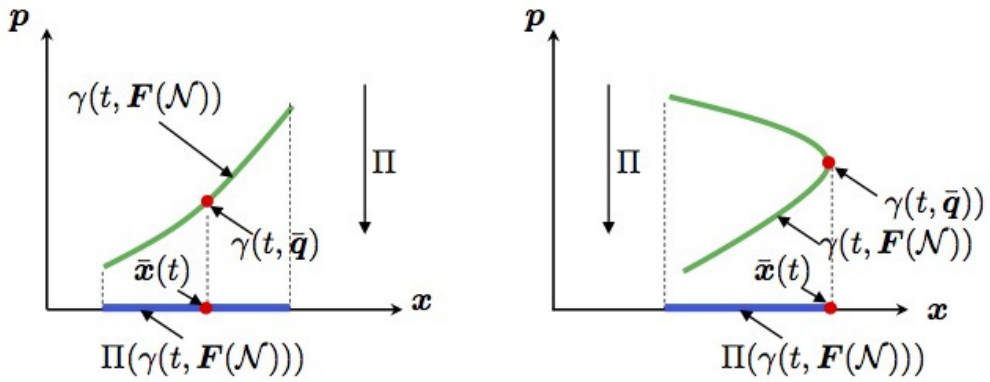

Figure 5.1 – The section of the family $\mathcal{F}_{\boldsymbol{q}}$ at a time $t \in [0, t_f)$.

Without loss of generality, we assume that, from the current time t_0 on, there exist $k \in \mathbb{N}$ switching times t_i $(i = 1, 2, \cdots, k)$ such that $t_0 < \bar{t}_1 < \bar{t}_2 < \cdots < \bar{t}_k < t_f$ along the nominal extremal $(\overline{\boldsymbol{x}}(\cdot), \overline{\boldsymbol{p}}(\cdot))$ on $[t_0, t_f]$.

Assumption 5.3. *Along the nominal extremal* $(\overline{\boldsymbol{x}}(\cdot), \overline{\boldsymbol{p}}(\cdot))$ *on* $[t_0, t_f]$*, each switching point* $(\overline{\boldsymbol{x}}(\bar{t}_i), \overline{\boldsymbol{p}}(\bar{t}_i))$ *is assumed to be a regular one, i.e.,* $H_1(\overline{\boldsymbol{x}}(\bar{t}_i), \overline{\boldsymbol{p}}(\bar{t}_i)) = 0$ *and* $H_{01}\overline{\boldsymbol{x}}(\bar{t}_i), \overline{\boldsymbol{p}}(\bar{t}_i)) \neq 0$ *for* $i = 1,\ 2,\ \cdots,\ k$.

For the sake of notational clarity, let $\delta_{\boldsymbol{q}}(t)$ be the determinant of the matrix $\partial \boldsymbol{x}(t, \overline{\boldsymbol{q}})/\partial \boldsymbol{q}$, i.e.,

$$\delta_{\boldsymbol{q}}(t) := \det\left[\frac{\partial \boldsymbol{x}}{\partial \boldsymbol{q}}(t, \overline{\boldsymbol{q}})\right],\ t \in [0, t_f].$$

According to the technique to establish the no-fold conditions in Chapter 3, one immediately gets that the projection Π of $\mathcal{F}_{\boldsymbol{q}}$ ceases to be a diffeomorphism if either $\delta_{\boldsymbol{q}}(t) = 0$ for $t \in (\bar{t}_i, \bar{t}_{i+1})$ or $\delta_{\boldsymbol{q}}(\bar{t}_i-)\delta_{\boldsymbol{q}}(\bar{t}_i+) < 0$ for $i = 1,\ 2,\ \cdots,\ k$. As a result of Remark 5.1, one obtains the following.

Remark 5.2. *Around the nominal extremal* $(\overline{\boldsymbol{x}}(\cdot), \overline{\boldsymbol{p}}(\cdot))$ *on* $[t_0, t_f]$*, there exist some deviations* $\Delta \boldsymbol{x}$ *with* $\|\Delta \boldsymbol{x}\| > 0$ *small enough such that* $\overline{\boldsymbol{x}}(t) + \Delta \boldsymbol{x} \neq \Pi(\gamma(t, \boldsymbol{q}))$ *for every* $\boldsymbol{q} \in \boldsymbol{F}(\mathcal{N})$ *if either* $\delta_{\boldsymbol{q}}(t) = 0$ *or* $\delta_{\boldsymbol{q}}(\bar{t}_i-)\delta_{\boldsymbol{q}}(\bar{t}_i+) < 0$.

This remark shows every neighboring extremal $\gamma(\cdot, \boldsymbol{q})$ for $\boldsymbol{q} \in \boldsymbol{F}(\mathcal{N})$ cannot pass through the point $\boldsymbol{x}_*$ at t_0 if either $\delta_{\boldsymbol{q}}(t) = 0$ or $\delta_{\boldsymbol{q}}(\bar{t}_i-)\delta_{\boldsymbol{q}}(\bar{t}_i+) < 0$. Recall that the classical variational method states that there exist no neighboring extremals if $\delta_{\boldsymbol{q}}(t) = 0$ since the gain matrix explodes in this case (see [16], e.g.). The geometric interpretation is that the equality $\delta_{\boldsymbol{q}}(t) = 0$ actually induces the lose of the diffeomorphism of $\Pi(\mathcal{F}_{\boldsymbol{q}})$. As a consequence, although the Jacobi necessary condition is satisfied, i.e., $\delta_{\boldsymbol{q}}(t) \neq 0$ for $t \in [t_0, t_f)$, there exist no neighboring extremals if the transversality condition at a switching time is violated, i.e., $\delta_{\boldsymbol{q}}(\bar{t}_i-)\delta_{\boldsymbol{q}}(\bar{t}_i+) < 0$.

Remark 5.3. *Given the nominal extremal* $(\overline{\boldsymbol{x}}(\cdot), \overline{\boldsymbol{p}}(\cdot)) = \gamma(\cdot, \overline{\boldsymbol{q}})$ *on* $[0, t_f]$ *and a point* $\boldsymbol{x}_* \in \mathcal{X}\backslash\mathcal{M}$ *such that the deviation* $\Delta \boldsymbol{x} = \boldsymbol{x}_* - \overline{\boldsymbol{x}}(t_0)$ *is small enough for* $t_0 \in [0, t_f)$*, assume Assumption 5.2 is satisfied. According to the inverse function theorem, there then exists a* $\boldsymbol{q}_* \in \boldsymbol{F}(\mathcal{N})$ *such that* $\boldsymbol{x}_* = \Pi(\gamma(t_0, \boldsymbol{q}_*))$ *if the mapping* $\boldsymbol{q} \mapsto \Pi(\gamma(t_0, \boldsymbol{q}))$ *on the domain* $\boldsymbol{F}(\mathcal{N})$ *is a diffeomorphism.*

Accordingly, the conditions that guarantee the projection Π of the family $\mathcal{F}_{\boldsymbol{q}}$ at each time $t \in [t_0, t_f)$ is a diffeomorphism are also sufficient for the existence of neighboring extremals. According to Chapter 3, if Assumption 5.3 is satisfied and the subset $\mathcal{N}$ is small enough, the mapping $\boldsymbol{q} \mapsto \boldsymbol{x}(t, \boldsymbol{q})$ is a diffeomorphism for each time $t \in [t_0, t_f)$ if $\delta_{\boldsymbol{q}}(t) \neq 0$ on $[0, t_f)$ and $\delta_{\boldsymbol{q}}(\bar{t}_i-)\delta_{\boldsymbol{q}}(\bar{t}_i+) > 0$ for $i = 1,\ 2,\ \cdots,\ k$. Then, we make the following assumption.

Assumption 5.4. $\delta_{\boldsymbol{q}}(t) \neq 0$ *for* $t \in [0, t_f)$ *and* $\delta_{\boldsymbol{q}}(\bar{t}_i-)\delta_{\boldsymbol{q}}(\bar{t}_i+) > 0$ *for* $i = 1, 2, \cdots, k$.

5.2 Neighboring optimal feedback control law

Due to unavoidable navigational errors and uncertainties in dynamical models, a spacecraft cannot be expected to exactly fly on the nominal trajectory $\overline{\boldsymbol{x}}(\cdot) = \Pi(\gamma(\cdot, \overline{\boldsymbol{q}}))$ on $[t_0, t_f]$. As

a result of Assumption 5.4, if the deviation $\Delta\boldsymbol{x}$ is small enough, there then exists $\boldsymbol{q}_* \in \boldsymbol{F}(\mathcal{N})$ such that $\overline{\boldsymbol{x}}(t_0) + \Delta\boldsymbol{x} = \boldsymbol{x}(t_0, \boldsymbol{q}_*)$. Obviously, a straightforward idea to generate the optimal control command is to recompute the new extremal $\gamma(\cdot, \boldsymbol{q}_*)$ on the interval $[t_0, t_f]$ such that, if no further perturbations occur, the spacecraft can be steered by the associated new optimal control function $\boldsymbol{u}(\gamma(\cdot, \boldsymbol{q}_*))$ on $[t_0, t_f]$ to fly to $\mathcal{M}$ at t_f. Although various numerical methods, e.g., direct methods [58, 79], indirect methods [17, 18, 31], and hybrid methods [67], are available in the literature, the onboard computers can hardly afford this computation in each guidance cycle, especially for the low-thrust orbital transfer problem with a long transfer time.

Next, the neighboring optimal feedback control law, which is the first-order term of the Taylor expansion of the new optimal control $\boldsymbol{u}(\gamma(\cdot, \boldsymbol{q}_*))$ on $[t_0, t_f]$, will be derived such that the spacecraft can be controlled to approximately move on the new extremal trajectory $\Pi(\gamma(\cdot, \boldsymbol{q}_*))$ on $[t_0, t_f]$.

5.2.1 Neighboring optimal feedback on switching times

Note that $t_i(\boldsymbol{q}_*)$ is exactly the i-th switching time of the new extremal $\gamma(\cdot, \boldsymbol{q}_*)$ on $[t_0, t_f]$. Set $\Delta\boldsymbol{q} := \boldsymbol{q}_* - \overline{\boldsymbol{q}}$. Then the Taylor expansion of $t_i(\boldsymbol{q}_*)$ is

$$\Delta t_i := t_i(\boldsymbol{q}_*) - t_i(\overline{\boldsymbol{q}}) = \frac{dt_i(\overline{\boldsymbol{q}})}{d\boldsymbol{q}}\Delta\boldsymbol{q}^T + O_{t_i}(|\Delta\boldsymbol{q}|^2), \tag{5.1}$$

where $O_{t_i}(|\Delta\boldsymbol{q}|^2)$ is the sum of second and higher order terms. Note that there holds

$$H_1(\boldsymbol{x}(t_i(\boldsymbol{q}), \boldsymbol{q}), \boldsymbol{p}(t_i(\boldsymbol{q}), \boldsymbol{q})) \equiv 0$$

for every $\boldsymbol{q} \in \boldsymbol{F}(\mathcal{N})$. Differentiating the identity $H_1(\boldsymbol{x}(t_i(\boldsymbol{q}), \boldsymbol{q}), \boldsymbol{p}(t_i(\boldsymbol{q}), \boldsymbol{q})) \equiv 0$ with respect to $\boldsymbol{q}$ yields

$$\begin{aligned}
0 &= \frac{\partial H_1(\gamma(t_i(\boldsymbol{q}), \boldsymbol{q}))}{\partial \boldsymbol{x}^T}\left(\dot{\boldsymbol{x}}(t_i(\boldsymbol{q}), \boldsymbol{q})\frac{dt_i(\boldsymbol{q})}{d\boldsymbol{q}} + \frac{\partial \boldsymbol{x}(t_i(\boldsymbol{q}), \boldsymbol{q})}{\partial \boldsymbol{q}}\right) \\
&+ \frac{\partial H_1(\gamma(t_i(\boldsymbol{q}), \boldsymbol{q}))}{\partial \boldsymbol{p}^T}\left(\dot{\boldsymbol{p}}(t_i(\boldsymbol{q}), \boldsymbol{q})\frac{dt_i(\boldsymbol{q})}{d\boldsymbol{q}} + \frac{\partial \boldsymbol{p}(t_i(\boldsymbol{q}), \boldsymbol{q})}{\partial \boldsymbol{q}}\right) \\
&= \dot{H}_1(\gamma(t_i(\boldsymbol{q}), \boldsymbol{q}))\frac{dt_i(\boldsymbol{q})}{d\boldsymbol{q}} + \frac{\partial H_1(\gamma(t_i(\boldsymbol{q}), \boldsymbol{q}))}{\partial \boldsymbol{x}^T}\frac{\partial \boldsymbol{x}(t_i(\boldsymbol{q}), \boldsymbol{q})}{\partial \boldsymbol{q}} \\
&+ \frac{\partial H_1(\gamma(t_i(\boldsymbol{q}), \boldsymbol{q}))}{\partial \boldsymbol{p}^T}\frac{\partial \boldsymbol{p}(t_i(\boldsymbol{q}), \boldsymbol{q})}{\partial \boldsymbol{q}}.
\end{aligned} \tag{5.2}$$

Since $\dot{H}_1(\overline{\boldsymbol{x}}(t_i), \overline{\boldsymbol{p}}(t_i)) \neq 0$ by Assumption 5.3, one obtains

$$\begin{aligned}
\frac{dt_i(\overline{\boldsymbol{q}})}{d\boldsymbol{q}} &= -\Big[\frac{\partial H_1(\overline{\boldsymbol{x}}(t_i), \overline{\boldsymbol{p}}(t_i))}{\partial \boldsymbol{x}^T}\frac{\partial \boldsymbol{x}(t_i, \overline{\boldsymbol{q}})}{\partial \boldsymbol{q}} \\
&\quad + \frac{\partial H_1(\overline{\boldsymbol{x}}(t_i), \overline{\boldsymbol{p}}(t_i))}{\partial \boldsymbol{p}^T}\frac{\partial \boldsymbol{p}(t_i, \overline{\boldsymbol{q}})}{\partial \boldsymbol{q}}\Big]/\dot{H}_1(\overline{\boldsymbol{x}}(t_i), \overline{\boldsymbol{p}}(t_i)),
\end{aligned} \tag{5.3}$$

where the two vectors

$$\frac{\partial H_1}{\partial \boldsymbol{x}^T}(\overline{\boldsymbol{x}}(t_i),\overline{\boldsymbol{p}}(t_i)) = \overline{\boldsymbol{p}}^T(t_i)\frac{\partial \boldsymbol{f}_1}{\partial \boldsymbol{x}}(\overline{\boldsymbol{x}}(t_i),\boldsymbol{\omega}(\overline{\boldsymbol{x}}(t_i),\overline{\boldsymbol{p}}(t_i))),$$

$$\frac{\partial H_1}{\partial \boldsymbol{p}^T}(\overline{\boldsymbol{x}}(t_i),\overline{\boldsymbol{p}}(t_i)) = \boldsymbol{f}_1^T(\overline{\boldsymbol{x}}(t_i),\boldsymbol{\omega}(\overline{\boldsymbol{x}}(t_i),\overline{\boldsymbol{p}}(t_i))),$$

can be directly computed once the nominal extremal $\gamma(\cdot,\overline{\boldsymbol{q}})$ on $[t_0,t_f]$ is given. For every sufficiently small $\Delta\boldsymbol{x}$ and every time $t_0 \in [0,t_f)$, one has the following the Taylor expansion

$$\begin{aligned}\Delta\boldsymbol{q}^T &:= \boldsymbol{q}_*^T - \overline{\boldsymbol{q}}^T \\ &= \left[\frac{\partial \boldsymbol{x}(t_0,\overline{\boldsymbol{q}})}{\partial \boldsymbol{q}}\right]^{-1}\Delta\boldsymbol{x} + O_{\boldsymbol{q}}(|\Delta\boldsymbol{x}|^2),\end{aligned} \tag{5.4}$$

where $O_{\boldsymbol{q}}(|\Delta\boldsymbol{x}|^2)$ denotes the sum of second and higher order terms. For notational clarity, let us define a matrix-valued function $S:[t_0,t_f]\to\mathbb{R}^{n\times n}$ as

$$S(t) = \frac{\partial \boldsymbol{p}}{\partial \boldsymbol{q}}(t,\overline{\boldsymbol{q}})\left[\frac{\partial \boldsymbol{x}}{\partial \boldsymbol{q}}(t,\overline{\boldsymbol{q}})\right]^{-1}. \tag{5.5}$$

Set

$$\delta\boldsymbol{x}_i := \frac{\partial \boldsymbol{x}}{\partial \boldsymbol{q}}(t_i,\overline{\boldsymbol{q}})\left[\frac{\partial \boldsymbol{x}}{\partial \boldsymbol{q}}(t_0,\overline{\boldsymbol{q}})\right]\Delta\boldsymbol{x}.$$

It is clear that $\delta\boldsymbol{x}_i$ is the first order term of the Taylor series of $\boldsymbol{x}(t_i,\boldsymbol{q}_*)-\overline{\boldsymbol{x}}(t_i)$. Substituting Eq. (5.4) and Eq. (5.3) into Eq. (5.1), one gets

$$\begin{aligned}\Delta t_i = &- \left[\frac{\partial H_1(\overline{\boldsymbol{x}}(t_i),\overline{\boldsymbol{p}}(t_i))}{\partial \boldsymbol{x}^T} + \frac{\partial H_1(\overline{\boldsymbol{x}}(t_i),\overline{\boldsymbol{p}}(t_i))}{\partial \boldsymbol{p}^T}S(t_i)\right]\delta\boldsymbol{x}_i/\dot{H}_1(\overline{\boldsymbol{x}}(t_i),\overline{\boldsymbol{p}}(t_i)) \\ &+ \frac{dt_i(\overline{\boldsymbol{q}})}{d\boldsymbol{q}}O_{\boldsymbol{q}}(|\Delta\boldsymbol{x}|^2) + O_{t_i}(|\Delta\boldsymbol{q}|^2).\end{aligned}$$

Let

$$\delta t_i := -\left[\frac{\partial H_1(\overline{\boldsymbol{x}}(t_i),\overline{\boldsymbol{p}}(t_i))}{\partial \boldsymbol{x}^T} + \frac{\partial H_1(\overline{\boldsymbol{x}}(t_i),\overline{\boldsymbol{p}}(t_i))}{\partial \boldsymbol{p}^T}S(t_i)\right]\delta\boldsymbol{x}_i/\dot{H}_1(\overline{\boldsymbol{x}}(t_i),\overline{\boldsymbol{p}}(t_i)) \tag{5.6}$$

be the first-order term of the Taylor series of Δt_i. Then, if $\Delta\boldsymbol{x}$ is infinitesimal, it suffices to use $t_i+\delta t_i$ as the neighboring optimal feedback on switching times.

5.2.2 Neighboring optimal feedback on thrust direction

Set $(\Delta\boldsymbol{p}_r,\Delta\boldsymbol{p}_v,\Delta p_m) := \Delta\boldsymbol{p} := \boldsymbol{p}(t_0,\boldsymbol{q}_*)-\boldsymbol{p}(t_i,\overline{\boldsymbol{q}})$. Note that the maximum condition in Eq. (1.12) gives a natural feedback on thrust direction, i.e., if $\|\overline{\boldsymbol{p}}_v(t_0)+\Delta\boldsymbol{p}_v\|\neq 0$, the optimal thrust direction on the new extremal $\gamma(\cdot,\boldsymbol{q}_*)$ at t_0 is

$$\boldsymbol{\omega}(\boldsymbol{x}_*,\overline{\boldsymbol{p}}(t_0)+\Delta\boldsymbol{p}) = \frac{\overline{\boldsymbol{p}}_v(t_0)+\Delta\boldsymbol{p}_v}{\|\overline{\boldsymbol{p}}_v(t_0)+\Delta\boldsymbol{p}_v\|}.$$

The Taylor expansion of $\boldsymbol{p}(t_0, \boldsymbol{q}_*)$ around $\overline{\boldsymbol{q}}$ is

$$\Delta \boldsymbol{p} = \boldsymbol{p}(t_0, \boldsymbol{q}_*) - \boldsymbol{p}(t_0, \overline{\boldsymbol{q}}) = \frac{\partial \boldsymbol{p}}{\partial \boldsymbol{q}}(t_0, \overline{\boldsymbol{q}}) \Delta \boldsymbol{q}^T + O_{\boldsymbol{p}}(|\Delta \boldsymbol{q}|^2), \tag{5.7}$$

where $O_{\boldsymbol{p}}(|\Delta \boldsymbol{q}|^2)$ is the sum of second and higher order terms. Substituting Eq. (5.4) into Eq. (5.7) leads to

$$\Delta \boldsymbol{p} = S(t_0) \Delta \boldsymbol{x} + \frac{\partial \boldsymbol{p}(t_0, \overline{\boldsymbol{q}})}{\partial \boldsymbol{q}} O_{\boldsymbol{q}}(|\Delta \boldsymbol{x}|^2) + O_{\boldsymbol{p}}(|\Delta \boldsymbol{q}|^2). \tag{5.8}$$

Denote by $S_1 \in \mathbb{R}^{3\times 7}$ the first three rows, $S_2 \in \mathbb{R}^{3\times 7}$ the forth to sixth rows, and $S_3 \in (\mathbb{R}^7)^*$ the last row of the gain matrix S such that

$$S = \begin{bmatrix} S_1 \\ S_2 \\ S_3 \end{bmatrix}.$$

Let

$$\delta \boldsymbol{p}_v := S_2(t_0) \Delta \boldsymbol{x},$$

be the first order term of the Taylor series of $\Delta \boldsymbol{p}_v$. It suffices to use $\delta \boldsymbol{p}_v$ to replace $\Delta \boldsymbol{p}_v$ if $\Delta \boldsymbol{x}$ is infinitesimal. Consequently, assuming that the deviation $\Delta \boldsymbol{x}$ is infinitesimal and that $\|\overline{\boldsymbol{p}}_v(t_0) + \delta \boldsymbol{p}_v\| \neq 0$, we can use

$$\boldsymbol{\omega}(\boldsymbol{x}_*, \overline{\boldsymbol{p}}(t_0) + \delta \boldsymbol{p}(t_0)) = \frac{\overline{\boldsymbol{p}}_v(t_0) + \delta \boldsymbol{p}_v}{\|\overline{\boldsymbol{p}}_v(t_0) + \delta \boldsymbol{p}_v\|}, \tag{5.9}$$

as the neighboring optimal feedback on the thrust direction.

5.3 Numerical implementation

Once the perturbation $\Delta \boldsymbol{x}$ is measured at $t_0 \in [0, t_f)$, it amounts to compute the two matrices $\partial \boldsymbol{x}(t_0, \overline{\boldsymbol{q}})/\partial \boldsymbol{q}$ and $\partial \boldsymbol{p}(t_0, \overline{\boldsymbol{q}})/\partial \boldsymbol{q}$ in order to compute the neighboring optimal feedback in Eq. (5.6) and Eq. (5.9).

5.3.1 Differential equations

It follows from the classical results about solutions to ordinary differential equations that the trajectory $(\boldsymbol{x}(\cdot, \boldsymbol{q}), \boldsymbol{p}(\cdot, \boldsymbol{q}))$ and its time derivative $(\dot{\boldsymbol{x}}(\cdot, \boldsymbol{q}), \dot{\boldsymbol{p}}(\cdot, \boldsymbol{q}))$ between switching times are continuously differentiable with respect to $\boldsymbol{q}$. Thus, taking derivative of Eq. (1.7) with respect to $\boldsymbol{q}$ on each subinterval $(\bar{t}_i, \bar{t}_{i+1})$ yields the following homogeneous linear matrix

differential equations

$$\begin{bmatrix} \frac{d}{dt}\frac{\partial \boldsymbol{x}}{\partial \boldsymbol{q}}(t,\overline{\boldsymbol{q}}) \\ \frac{d}{dt}\frac{\partial \boldsymbol{p}}{\partial \boldsymbol{q}}(t,\overline{\boldsymbol{q}}) \end{bmatrix} = \begin{bmatrix} H_{\boldsymbol{px}}(\overline{\boldsymbol{x}}(t),\overline{\boldsymbol{p}}(t)) & H_{\boldsymbol{pp}}(\overline{\boldsymbol{x}}(t),\overline{\boldsymbol{p}}(t)) \\ -H_{\boldsymbol{xx}}(\overline{\boldsymbol{x}}(t),\overline{\boldsymbol{p}}(t)) & -H_{\boldsymbol{xp}}(\overline{\boldsymbol{x}}(t),\overline{\boldsymbol{p}}(t)) \end{bmatrix} \begin{bmatrix} \frac{\partial \boldsymbol{x}}{\partial \boldsymbol{q}}(t,\overline{\boldsymbol{q}}) \\ \frac{\partial \boldsymbol{p}}{\partial \boldsymbol{q}}(t,\overline{\boldsymbol{q}}) \end{bmatrix}. \tag{5.10}$$

Recall that the two matrices $\partial \boldsymbol{x}(\cdot,\overline{\boldsymbol{q}})/\partial \boldsymbol{q}$ and $\partial \boldsymbol{p}(\cdot,\overline{\boldsymbol{q}})/\partial \boldsymbol{q}$ are discontinuous at each switching time $\bar{t}_i$ ($i = 1, 2, \cdots, k$). By virtue of [63, Lemma 2.6], the updating formulas for the two matrices at each switching time $\bar{t}_i$ are

$$\begin{cases} \frac{\partial \boldsymbol{x}}{\partial \boldsymbol{q}}(\bar{t}_i+,\overline{\boldsymbol{q}}) = \frac{\partial \boldsymbol{x}}{\partial \boldsymbol{q}}(\bar{t}_i-,\overline{\boldsymbol{q}}) - \Delta\rho_i \frac{\partial H_1(\gamma(\bar{t}_i,\overline{\boldsymbol{q}}))}{\partial \boldsymbol{p}} \frac{dt_i(\overline{\boldsymbol{q}})}{d\boldsymbol{q}}, \\ \frac{\partial \boldsymbol{p}}{\partial \boldsymbol{q}}(\bar{t}_i+,\overline{\boldsymbol{q}}) = \frac{\partial \boldsymbol{p}}{\partial \boldsymbol{q}}(\bar{t}_i-,\overline{\boldsymbol{q}}) + \Delta\rho_i \frac{\partial H_1(\gamma(\bar{t}_i,\overline{\boldsymbol{q}}))}{\partial \boldsymbol{x}} \frac{dt_i(\overline{\boldsymbol{q}})}{d\boldsymbol{q}}, \end{cases} \tag{5.11}$$

where $\Delta\rho_i = \overline{\rho}(t_i+) - \overline{\rho}(t_i-)$ and $dt_i(\overline{\boldsymbol{q}})/d\boldsymbol{q}$ can be computed by using Eq. (5.3).

Once the final conditions are given, one can use Eq. (5.10) and Eq. (5.11) to compute the two matrices $\partial \boldsymbol{x}(\cdot,\overline{\boldsymbol{q}})/\partial \boldsymbol{q}$ and $\partial \boldsymbol{p}(\cdot,\overline{\boldsymbol{q}})/\partial \boldsymbol{q}$ on the whole interval $[t_0, t_f]$. In the next paragraph, the procedure for computing the values of the final matrices $\partial \boldsymbol{x}(t_f,\overline{\boldsymbol{q}})/\partial \boldsymbol{q}$ and $\partial \boldsymbol{p}(t_f,\overline{\boldsymbol{q}})/\partial \boldsymbol{q}$ will be presented.

5.3.2 Final conditions

Typically, the sweep variables are used to compute the final values $\partial \boldsymbol{x}(t_f,\overline{\boldsymbol{q}})/\partial \boldsymbol{q}$ and $\partial \boldsymbol{p}(t_f,\overline{\boldsymbol{q}})/\partial \boldsymbol{q}$ (see [16, 82], e.g.). In fact, the row vectors of the matrix

$$\begin{bmatrix} \partial \boldsymbol{x}(t_f,\overline{\boldsymbol{q}})/\partial \boldsymbol{q} \\ \partial \boldsymbol{p}(t_f,\overline{\boldsymbol{q}})/\partial \boldsymbol{q} \end{bmatrix}$$

form a set of basis vectors of the tangent space $T_{\overline{\boldsymbol{z}}_f}\mathcal{L}_f$ with $\overline{\boldsymbol{z}}_f = (\overline{\boldsymbol{x}}(t_f), \overline{\boldsymbol{p}}(t_f))$. Therefore, to compute the final values $\partial \boldsymbol{x}(t_f,\overline{\boldsymbol{q}})/\partial \boldsymbol{q}$ and $\partial \boldsymbol{p}(t_f,\overline{\boldsymbol{q}})/\partial \boldsymbol{q}$, it amounts to compute a basis of $T_{\overline{\boldsymbol{z}}_f}\mathcal{L}_f$.

Final conditions for the case of $l = n$

If $l = n$, the final state is fixed since the submanifold $\mathcal{M}$ reduces to a singleton. Thus, in the case of $l = n$, one can simply set $\boldsymbol{q} = \boldsymbol{p}^T(t_f)$, which indicates

$$\frac{\partial \boldsymbol{x}}{\partial \boldsymbol{q}}(t_f,\overline{\boldsymbol{q}}) = 0_n \text{ and } \frac{\partial \boldsymbol{p}}{\partial \boldsymbol{q}}(t_f,\overline{\boldsymbol{q}}) = I_n, \tag{5.12}$$

where 0_n and I_n denote the zero and identity matrix of $\mathbb{R}^{n\times n}$, respectively.

Final conditions for the case of $0 < l < n$

Note that $\Pi(\mathcal{N}) \subset \Pi(\mathcal{L}_f)$ and $\Pi(\mathcal{L}_f) = \mathcal{M}$. Thus, the subset $\Pi(\mathcal{N})$ is diffeomorphic to

$\mathbb{R}^{n-l}$. In analogy with parameterizing neighboring extremals, if the subset $\mathcal{N}$ is small enough and if $l < n$, there exists an invertible function $\boldsymbol{F}_1 : \Pi(\mathcal{N}) \to \mathbb{R}^{n-l}$ such that both the function and its inverse $\boldsymbol{F}_1^{-1}$ are smooth. According to Eq. (1.10), for every $(\boldsymbol{x}, \boldsymbol{p}) \in \mathcal{N}$, there exists a $\boldsymbol{\nu} \in (\mathbb{R}^l)^*$ such that

$$\boldsymbol{p} = \boldsymbol{\nu} \nabla \phi(\boldsymbol{x}). \tag{5.13}$$

Let us define a function $\boldsymbol{F}_2 : \mathcal{N} \to (\mathbb{R}^l)^*$, $(\boldsymbol{x}, \boldsymbol{p}) \mapsto \boldsymbol{F}_2(\boldsymbol{x}, \boldsymbol{p})$ as

$$\boldsymbol{F}_2(\boldsymbol{x}, \boldsymbol{p}) = \boldsymbol{p}^T \nabla \phi^T(\boldsymbol{x}) [\nabla \phi(\boldsymbol{x}) \nabla \phi^T(\boldsymbol{x})]^{-1},$$

such that $\boldsymbol{\nu} = \boldsymbol{F}_2(\boldsymbol{x}, \boldsymbol{p})$. By Assumption 5.1, if the subset $\mathcal{N}$ is small enough, the function $\boldsymbol{F}_2$ is a diffeomorphism from the domain $\mathcal{N}$ onto its image. Thus, it is enough to set $\boldsymbol{F} = (\boldsymbol{F}_1, \boldsymbol{F}_2)$ such that $\boldsymbol{q} = (\boldsymbol{q}_1, \boldsymbol{\nu})$. Let

$$\overline{\boldsymbol{q}}_1 := \boldsymbol{F}_1(\overline{\boldsymbol{x}}(t_f)),$$

then we have $\overline{\boldsymbol{q}} = (\overline{\boldsymbol{q}}_1, \overline{\boldsymbol{\nu}})$ where

$$\overline{\boldsymbol{\nu}} := \overline{\boldsymbol{p}}^T(t_f) \nabla \phi^T(\overline{\boldsymbol{x}}(t_f)) \left[\nabla \phi(\overline{\boldsymbol{x}}(t_f)) \nabla \phi^T(\overline{\boldsymbol{x}}(t_f)) \right]^{-1}$$

denotes the vector of the Lagrangian multipliers for the nominal extremal $\gamma(\cdot, \overline{\boldsymbol{q}})$ on $[0, t_f]$. A direct calculation leads to

$$\begin{aligned} \frac{\partial \boldsymbol{x}}{\partial \boldsymbol{q}}(t_f, \overline{\boldsymbol{q}}) &= \left[\frac{\partial \boldsymbol{x}}{\partial \boldsymbol{q}_1}(t_f, \overline{\boldsymbol{q}}), \frac{\partial \boldsymbol{x}}{\partial \boldsymbol{\nu}}(t_f, \overline{\boldsymbol{q}}) \right], & (5.14) \\ \frac{\partial \boldsymbol{p}}{\partial \boldsymbol{q}}(t_f, \overline{\boldsymbol{q}}) &= \left[\frac{\partial \boldsymbol{p}(t_f, \overline{\boldsymbol{q}})}{\partial \boldsymbol{q}_1}, \frac{\partial \boldsymbol{p}(t_f, \overline{\boldsymbol{q}})}{\partial \boldsymbol{\nu}} \right] \\ &= \left[\sum_{i=1}^{l} \overline{\nu}_i \nabla^2 \phi_i(\boldsymbol{x}(t_f, \overline{\boldsymbol{q}})) \frac{\partial \boldsymbol{x}(t_f, \overline{\boldsymbol{q}})}{\partial \boldsymbol{q}_1}, \nabla \phi^T(\boldsymbol{x}(t_f, \overline{\boldsymbol{q}})) \right], & (5.15) \end{aligned}$$

where $\phi_i : \mathcal{X} \to \mathbb{R}$ and $\overline{\nu}_i \in \mathbb{R}$ for $i = 1, 2, \cdots, l$ are the elements of the vector-valued function $\phi(\boldsymbol{x})$ and the vector $\overline{\boldsymbol{\nu}}$, respectively. Since $\boldsymbol{x}(t_f, \boldsymbol{q})$ is not a function of $\boldsymbol{\nu}$, there holds

$$\frac{\partial \boldsymbol{x}(t_f, \overline{\boldsymbol{q}})}{\partial \boldsymbol{\nu}} = \boldsymbol{0}_{n \times l}. \tag{5.16}$$

Taking the differentiation of $\phi(\boldsymbol{x}(t_f, \boldsymbol{q})) = 0$ with respect to $\boldsymbol{q}_1$ leads to

$$\nabla \phi(\boldsymbol{x}(t_f, \overline{\boldsymbol{q}})) \frac{\partial \boldsymbol{x}(t_f, \overline{\boldsymbol{q}})}{\partial \boldsymbol{q}_1} = 0. \tag{5.17}$$

Once the matrix $\nabla \phi(\boldsymbol{x}(t_f, \overline{\boldsymbol{q}}))$ is given, one can compute the full-rank matrix $\partial \boldsymbol{x}(t_f, \overline{\boldsymbol{q}}) / \partial \boldsymbol{q}_1$ by a Gram-Schmidt orthogonalization.

All the necessary quantities for computing the final conditions are now available for $l <$

n. Therefore, one can compute the gain matrix S by integrating Eq. (5.10) from the above conditions backward between switching times and by using Eq. (5.11) to update the boundary condition at each switching.

5.3.3 Riccati differential equation

Note that one has to solve a $2 \times n^2$ order of differential equations in order to compute the gain matrix $S(t)$ if using Eq. (5.10) and Eq. (5.11). Next, based on [82], the differential equations of the gain matrix $S(t)$ will be derived such that only n^2 order of differential equations are required to solve.

According to Eq. (5.5), we have

$$S(t)\frac{\partial \boldsymbol{x}}{\partial \boldsymbol{q}}(t, \overline{\boldsymbol{q}}) = \frac{\partial \boldsymbol{p}}{\partial \boldsymbol{q}}(t, \overline{\boldsymbol{q}}),$$

for $t \in [\bar{t}_i, \bar{t}_{i+1}]$ with $i = 0, 1, \cdots, k$. Differentiating this equation with respect to time yields

$$\dot{S}(\cdot)\frac{\partial \boldsymbol{x}}{\partial \boldsymbol{q}}(\cdot, \overline{\boldsymbol{q}}) + S(\cdot)\frac{\partial \dot{\boldsymbol{x}}}{\partial \boldsymbol{q}}(\cdot, \overline{\boldsymbol{q}}) = \frac{\partial \dot{\boldsymbol{p}}}{\partial \boldsymbol{q}}(\cdot, \overline{\boldsymbol{q}}),$$

on $[\bar{t}_i, \bar{t}_{i+1}]$. Substituting Eq. (5.10) into this equation, we hence obtain

$$\begin{aligned} \dot{S}(\cdot) &= -H_{\boldsymbol{xx}}(\overline{\boldsymbol{x}}(\cdot), \overline{\boldsymbol{p}}(\cdot)) - H_{\boldsymbol{xp}}(\overline{\boldsymbol{x}}(\cdot), \overline{\boldsymbol{p}}(\cdot))S(\cdot) \\ &\quad -S(\cdot)H_{\boldsymbol{px}}(\overline{\boldsymbol{x}}(\cdot), \overline{\boldsymbol{p}}(\cdot)) - S(\cdot)H_{\boldsymbol{pp}}(\overline{\boldsymbol{x}}(\cdot), \overline{\boldsymbol{p}}(\cdot))S(\cdot), \end{aligned} \tag{5.18}$$

on $[\bar{t}_i, \bar{t}_{i+1}]$. According to Eq. (5.11), the gain matrix $S(\cdot)$ is discontinuous at each switching time $\bar{t}_i$. Assuming the matrix $\partial \boldsymbol{x}(\bar{t}_i-, \overline{\boldsymbol{q}})/\partial \boldsymbol{q}$ is nonsingular and multiplying $\left[\partial \boldsymbol{x}(\bar{t}_i-, \overline{\boldsymbol{q}})/\partial \boldsymbol{q}\right]^{-1}$ on the latter equation of Eq. (5.11), one obtains

$$\begin{aligned} S(\bar{t}_i-) &= \frac{\partial \boldsymbol{p}}{\partial \boldsymbol{q}}(\bar{t}_i-, \overline{\boldsymbol{q}}) \left[\frac{\partial \boldsymbol{x}}{\partial \boldsymbol{q}}(\bar{t}_i-, \overline{\boldsymbol{q}})\right]^{-1} \\ &= \left[\frac{\partial \boldsymbol{p}}{\partial \boldsymbol{q}}(\bar{t}_i+, \overline{\boldsymbol{q}}) - \Delta\rho_i \frac{\partial \boldsymbol{f}_1}{\partial \boldsymbol{x}}(\overline{\boldsymbol{x}}(\bar{t}_i), \overline{\boldsymbol{\omega}}(\bar{t}_i))\overline{\boldsymbol{p}}(\bar{t}_i)\frac{dt_i(\overline{\boldsymbol{q}})}{d\boldsymbol{q}}\right] \\ &\times \left[\frac{\partial \boldsymbol{x}}{\partial \boldsymbol{q}}(\bar{t}_i+, \overline{\boldsymbol{q}}) + \Delta\rho_i \boldsymbol{f}_1(\overline{\boldsymbol{x}}(\bar{t}_i), \overline{\boldsymbol{\omega}}(\bar{t}_i))\frac{dt_i(\overline{\boldsymbol{q}})}{d\boldsymbol{q}}\right]^{-1} \\ &= \left\{S(\bar{t}_i+) - \Delta\rho_i \frac{\partial \boldsymbol{f}_1}{\partial \boldsymbol{x}}(\overline{\boldsymbol{x}}(\bar{t}_i), \overline{\boldsymbol{\omega}}(\bar{t}_i))\overline{\boldsymbol{p}}(\bar{t}_i)\frac{dt_i(\overline{\boldsymbol{q}})}{d\boldsymbol{q}}\left[\frac{\partial \boldsymbol{x}}{\partial \boldsymbol{q}}(\bar{t}_i+, \overline{\boldsymbol{q}})\right]^{-1}\right\} \\ &\times \frac{\partial \boldsymbol{x}}{\partial \boldsymbol{q}}(\bar{t}_i+, \overline{\boldsymbol{q}}) \left[\frac{\partial \boldsymbol{x}}{\partial \boldsymbol{q}}(\bar{t}_i+, \overline{\boldsymbol{q}}) + \Delta\rho_i \boldsymbol{f}_1(\overline{\boldsymbol{x}}(\bar{t}_i), \overline{\boldsymbol{\omega}}(\bar{t}_i))\frac{dt_i(\overline{\boldsymbol{q}})}{d\boldsymbol{q}}\right]^{-1}. \end{aligned} \tag{5.19}$$

Let us define a vector-valued function $R(\bar{t}_i) : \mathbb{R}_+ \to (\mathbb{R}^n)^*$ as

$$R(\bar{t}_i) = \frac{dt_i(\overline{\boldsymbol{q}})}{d\boldsymbol{q}} \left[\frac{\partial \boldsymbol{x}}{\partial \boldsymbol{q}}(\bar{t}_i+, \overline{\boldsymbol{q}}) \right]^{-1}.$$

Substituting this equation into Eq. (5.3) yields

$$R(\bar{t}_i) = -\left[\frac{\partial H_1(\overline{\boldsymbol{x}}(\bar{t}_i), \overline{\boldsymbol{p}}(\bar{t}_i))}{\partial \boldsymbol{x}^T} + \frac{\partial H_1(\overline{\boldsymbol{x}}(\bar{t}_i), \overline{\boldsymbol{p}}(\bar{t}_i))}{\partial \boldsymbol{p}^T} S(\bar{t}_i+) \right] / \dot{H}_1(\overline{\boldsymbol{x}}(\bar{t}_i), \overline{\boldsymbol{p}}(\bar{t}_i)).$$

Given a nonsingular matrix $\boldsymbol{A} \in \mathbb{R}^{n\times n}$ and two vectors $\boldsymbol{b} \in \mathbb{R}^n$ and $\boldsymbol{c} \in \mathbb{R}^n$, if the matrix $\boldsymbol{A} + \boldsymbol{b}\boldsymbol{c}^T$ is nonsingular, the equation

$$\left(\boldsymbol{A} + \boldsymbol{b}\boldsymbol{c}^T\right)^{-1} = \boldsymbol{A}^{-1} - \frac{\boldsymbol{A}^{-1}\boldsymbol{b}\boldsymbol{c}^T\boldsymbol{A}^{-1}}{1 + \boldsymbol{c}^T\boldsymbol{A}^{-1}\boldsymbol{b}}, \tag{5.20}$$

is satisfied (see, e.g., [82, Lemma 6.1.4]). Thus, if the matrix $\partial \boldsymbol{x}(\bar{t}_i+, \overline{\boldsymbol{q}})/\partial \boldsymbol{q}$ is nonsingular, taking into account Eq. (5.20), one gets

$$\begin{aligned} & \frac{\partial \boldsymbol{x}}{\partial \boldsymbol{q}}(\bar{t}_i+, \overline{\boldsymbol{q}}) \left[\frac{\partial \boldsymbol{x}}{\partial \boldsymbol{q}}(\bar{t}_i+, \overline{\boldsymbol{q}}) + \Delta\rho_i \boldsymbol{f}_1(\overline{\boldsymbol{x}}(\bar{t}_i), \overline{\boldsymbol{\omega}}(\bar{t}_i)) \frac{dt_i(\overline{\boldsymbol{q}})}{d\boldsymbol{q}} \right]^{-1} \\ = \; & I_n - \Delta\rho_i \frac{\boldsymbol{f}_1(\overline{\boldsymbol{x}}(\bar{t}_i), \overline{\boldsymbol{\omega}}(\bar{t}_i)) R(\bar{t}_i)}{1 + \Delta\rho_i R(\bar{t}_i) \boldsymbol{f}_1(\overline{\boldsymbol{x}}(\bar{t}_i), \overline{\boldsymbol{\omega}}(\bar{t}_i))}. \end{aligned} \tag{5.21}$$

Substituting this equation into Eq. (5.19), we eventually obtain the result

$$\begin{aligned} S(t_i-) \;=\; & \left[S(t_i+) - \Delta\rho_i \frac{\partial \boldsymbol{f}_1}{\partial \boldsymbol{x}}(\overline{\boldsymbol{x}}(t_i), \overline{\boldsymbol{\omega}}(t_i)) \overline{\boldsymbol{p}}(t_i) R(t_i) \right] \\ & \left[I_n - \Delta\rho_i \frac{\boldsymbol{f}_1(\overline{\boldsymbol{x}}(t_i), \overline{\boldsymbol{\omega}}(t_i)) R(t_i)}{1 + \Delta\rho_i R(t_i) \boldsymbol{f}_1(\overline{\boldsymbol{x}}(t_i), \overline{\boldsymbol{\omega}}(t_i))} \right]. \end{aligned} \tag{5.22}$$

This formula provides the required boundary condition for Eq. (5.18) on the interval $[\bar{t}_{i-1}, \bar{t}_i]$. Then, the gain matrix $S(\cdot)$ can be propagated further backward by integrating the Riccati differential equation in Eq. (5.18). Note that $S(t_f) = \infty$ since the matrix $\partial \boldsymbol{x}(t_f, \overline{\boldsymbol{q}})/\partial \boldsymbol{q}$ is singular. One can use Eq. (5.10) to integrate backward from t_f on a short interval $[t_s, t_f]$ with $t_s < t_f$. Then, substitute the corresponding values into the matrix $S(t_s)$, one can use Eq. (5.18) and Eq. (5.22) to get $S(\cdot)$ on $[0, t_s]$.

Once the matrix $S(\cdot)$ on $[0, t_f)$ is computed offline and stored in the onboard computer, the online computation is left to compute Eq. (5.6) and Eq. (5.9) by interpolating the sampled gain matrices stored in the onboard computer.

Remark 5.4. *This chapter is a preliminary step to derive the neighboring optimal feedback on thrust direction and switching times and to present a geometric interpretation between the sufficient conditions and the existence of neighboring extremals. So, the computational and operational issues in practice for storing and interpolating the gain matrix is not discussed here.*

5.4 Numerical examples for neighboring optimal control

The NOC derived in this chapter is applied to orbital transfer problems in the two-body problem and two cases (case A and case B) are simulated.

5.4.1 Case A: Constant mass model

For case A, we consider that the parameters are the same as those in Tab. 3.2. The nominal trajectory and control have been computed (see Fig. 3.5). Perturbations on the initial state and on the propulsive parameters are considered. Each perturbed component of the initial state is subject to a normal distribution ($X \sim N(\mu, \sigma^2)$) where the mean value μ and the 3σ-value are presented in Tab. 5.1. According to [73], the thrust magnitude (or the acceleration) is

Table 5.1 – Case A: Statistical information for the perturbations.

Initial state:	X	Y	Z	V_x	V_y	V_z
μ:	-46,500.0 km	0	0	0	-1,452.98 m/s	-178.51 m/s
3σ:	10 km	10 km	10 km	50 m/s	50 m/s	50 m/s

subject to small fluctuations, which has been modelled through a trigonometric series with random coefficients

$$\tau_{\max}(t) = \tau_{\max}^{nom}\left(1 + \sum_{k=1}^{5} a_k \sin(2k\pi t) + \sum_{k=1}^{5} a_{k+5}\cos(2k\pi t)\right), \tag{5.23}$$

where $\tau_{\max}^{nom} > 0$ is the nominal maximum thrust. The coefficients $\{a_k\}_{k=1,\cdots,10}$ have a random Gaussian distribution centered around zero and with a 3σ value of $0.02\tau_{\max}^{nom}$.

A *Monte Carlo* campaign (with 100 runs) is performed to show the statistical information on the accuracy of the NOC. The statistical information for the errors on the final conditions are presented in Tab. 5.2. Moreover, the time evolutions of the errors on semi-major axis,

Table 5.2 – Case A: Statistical information for the errors on final conditions.

Final errors:	δa (m)	δe	δi (deg)
μ:	- 15.35	1.33×10^{-4}	4.32×10^{-6}
σ:	-90.98	3.75×10^{-4}	9.93×10^{-6}

inclination, and eccentricity are portrayed in Figs. 5.2–5.4, respectively, showing that the errors tend to zero at the final time.

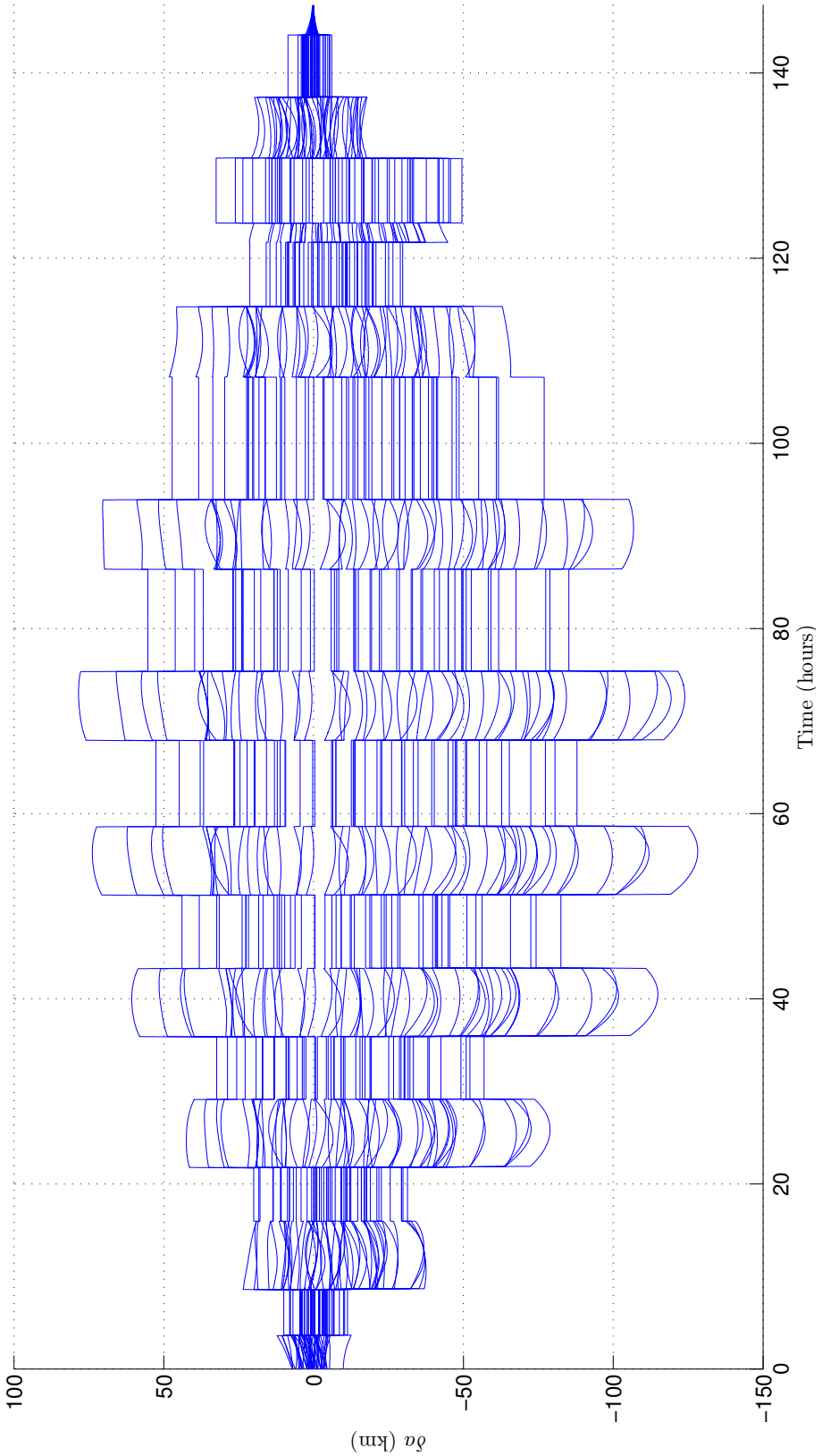

Figure 5.2 – Evolution of errors on semi-major axis for Monte Carlo campaigns.

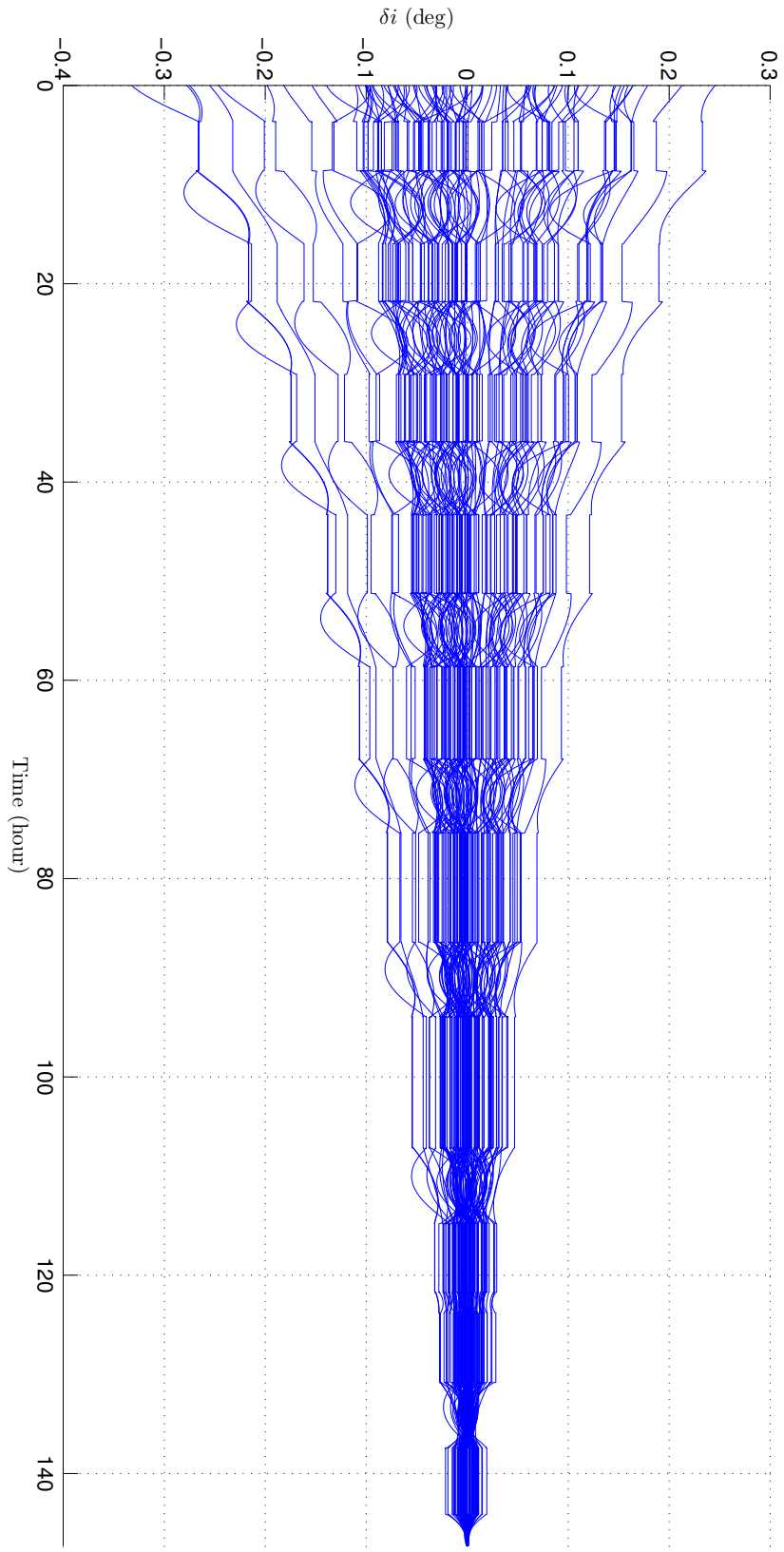

Figure 5.3 – Evolution of errors on inclination for Monte Carlo campaigns.

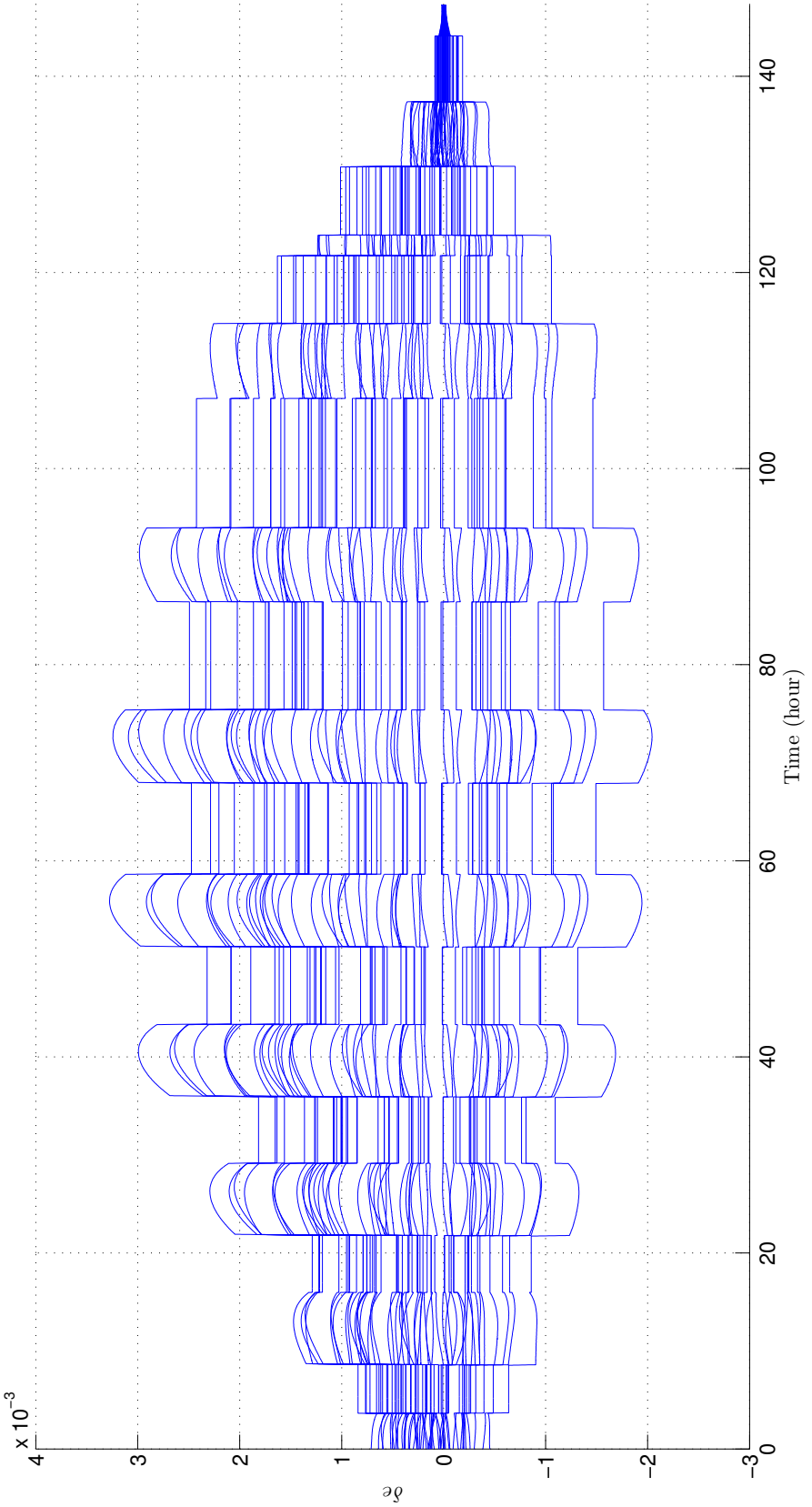

Figure 5.4 – Evolution of errors on eccentricity for Monte Carlo campaigns.

5.4.2 Case B: Varying mass model

For case B, the physical parameters for numerical computations are listed in Tab. 5.3. Denote

Table 5.3 – Physical parameters for computing the nominal trajectory for the NOC.

Earth gravitational constant μ_e:	398600.47 km^3/s^2
Gravity at sea level g_0:	9.80 m/s^2
Initial mass m_0:	1500.00 kg
Specific impulse value I_{sp}:	2000.00 s
Maximum thrust $\tau_{\max}$:	10.00 N
Fixed final time t_f:	157.88 hours

by a, e, i, ω, Ω, f the semi-major axis, the eccentricity, the inclination, the argument of periapsis, the argument of ascending node, and the true anomaly of the classical orbital elements (COE's). The conditions for initial and final orbits are presented in Tab. 5.4 in terms of the COE's. In order to achieve a stable numerical computation [19], we use the *modified*

Table 5.4 – The initial and final conditions in terms of the COE's.

COE	Initial conditions	Final conditions
a	26,571.429 km	42,165.000 km
e	0.750	0
i	30.000 deg	0
ω	0	Undefined
Ω	0	Undefined
f	π	Undefined

equatorial orbital elements (MEOE),

$$\begin{aligned} P &= a(1-e^2), \\ e_x &= e\cos(\omega+\Omega), \\ e_y &= e\sin(\omega+\Omega), \\ h_x &= \tan(i/2)\cos(\Omega), \\ h_y &= \tan(i/2)\sin(\Omega), \\ l &= f+\omega+\Omega, \end{aligned}$$

to compute the optimal solution. Note that the initial true longitude is $l_0 = \pi$ (see Tab. 5.4). Let the final true longitude be $l_f = 9 \times 2\pi$.

The 3-dimensional position vector $\boldsymbol{r}(\cdot)$ on $[0, t_f]$ is plotted in Fig. 5.5, showing that all

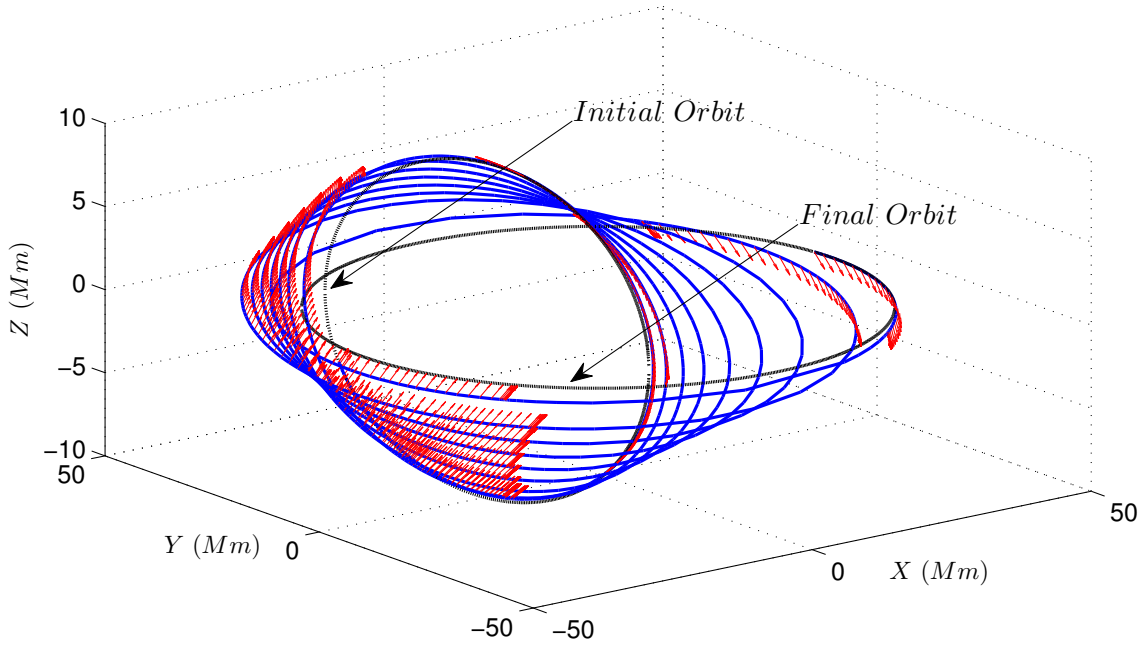

Figure 5.5 – The 3-dimensional trajectory $\boldsymbol{r}(\cdot)$ on $[0, t_f]$ for the low-thrust multi-burn fuel-optimal orbital transfer problem in a Cartesian coordinate system. The arrows denote the thrust direction on burn arcs.

the burn arcs occur around the apogees and perigees.

Remark 5.5. *Note that $\beta > 0$ as I_{sp} takes a finite value (see Tab. 5.3). Thus, the L^1-solution realizes a minimum fuel consumption.*

To see the regularity conditions, the profiles of $\rho(\cdot)$, $H_1(\cdot)$, and $\|\boldsymbol{p}_v(\cdot)\|$ with respect to time on $[0, t_f]$ are plotted in Fig. 5.6. It is seen from that figure that the number of burn arcs along the fuel-optimal trajectory is 13 with 24 switching points and that each switching point is regular (cf. Assumption 5.3). The profiles of semi-major axis a, eccentricity e, and inclination i along the low-thrust fuel-optimal trajectory are reported in Fig. 5.7.

With the exception the final mass m_f, all other final states are fixed if we use the *MEOE* as states such that $\boldsymbol{x} = (P, e_x, e_y, h_x, h_y, l, m)^T$ and $\boldsymbol{p} = (p_p, p_{e_x}, p_{e_y}, p_{h_x}, p_{h_y}, p_l, p_m)^T$. Thus, applying Eqs. (5.14–5.17), we get the following final condition:

$$\frac{\partial \boldsymbol{x}}{\partial \boldsymbol{q}}(t_f, \overline{\boldsymbol{q}}) = \begin{pmatrix} \mathbf{0}_6 & \mathbf{0}_{6\times 1} \\ \mathbf{0}_{1\times 6} & 1 \end{pmatrix} \text{ and } \frac{\partial \boldsymbol{p}}{\partial \boldsymbol{q}}(t_f, \overline{\boldsymbol{q}}) = \begin{pmatrix} I_6 & \mathbf{0}_{6\times 1} \\ \mathbf{0}_{1\times 6} & 0 \end{pmatrix}. \tag{5.24}$$

Starting from this final condition, we propagate Eq. (5.10) backward and use the updating formulas in Eq. (5.11) at each switching time to compute the matrices $\partial \boldsymbol{x}(\cdot, \overline{\boldsymbol{q}})/\partial \boldsymbol{q}$ and $\partial \boldsymbol{p}(\cdot, \overline{\boldsymbol{q}})/\partial \boldsymbol{q}$ on $[0, t_f]$.

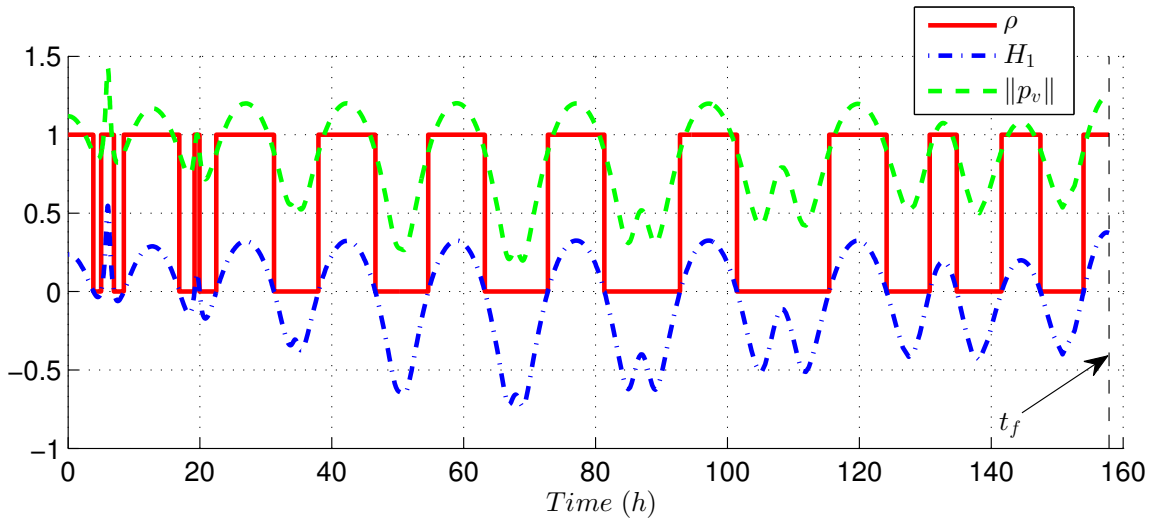

Figure 5.6 – The profiles of $\rho(\cdot)$, $H_1(\cdot)$, and $\| \boldsymbol{p}_v(\cdot) \|$ with respect to time on $[0, t_f]$ along the low-thrust multi-burn fuel-optimal trajectory.

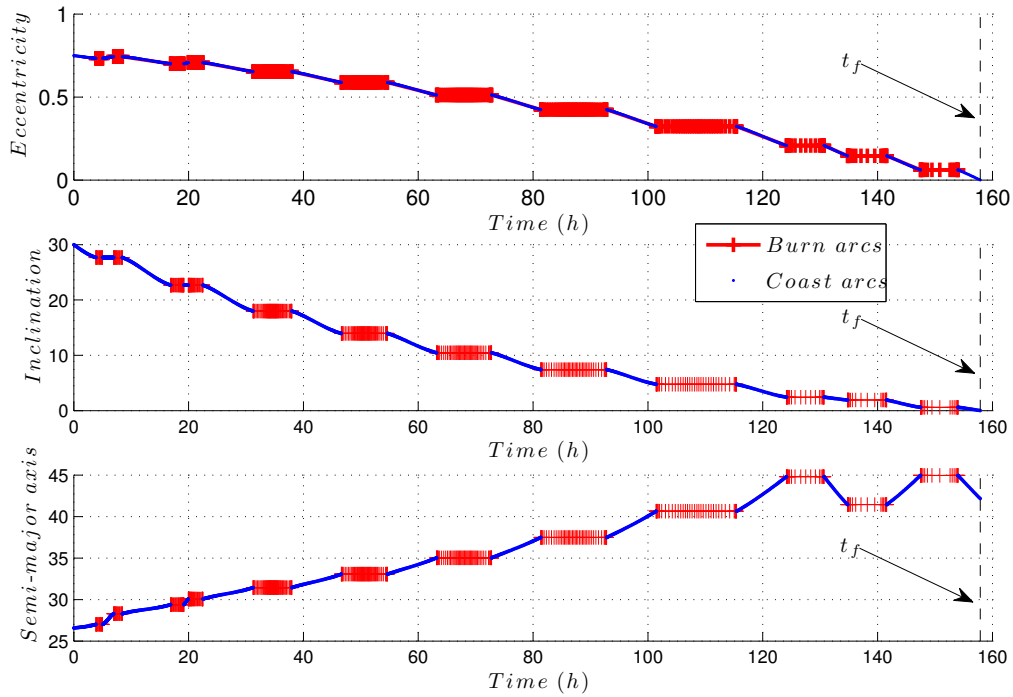

Figure 5.7 – The profiles of eccentricity e, inclination i, and semi-major axis a against time along the low-thrust multi-burn fuel-optimal trajectory.

To have a clear view, the profile of $\text{sgn}(\delta_{\boldsymbol{q}}(\cdot)) \times |\delta_{\boldsymbol{q}}(\cdot)|^{1/20}$ instead of $\delta_{\boldsymbol{q}}(\cdot)$ on $[0, t_f]$ is plotted in Fig. 5.8. Note that the function $\text{sgn}(\delta_{\boldsymbol{q}}(\cdot)) \times |\delta|^{1/20}$ on $[0, t_f]$ can capture the sign property of $\delta_{\boldsymbol{q}}(\cdot)$ on $[0, t_f]$. We can clearly see from this figure that $\delta_{\boldsymbol{q}}(t) \neq 0$ for $t \in [0, t_f)$ and $\delta_{\boldsymbol{q}}(\bar{t}_i-)\delta_{\boldsymbol{q}}(\bar{t}_i+) > 0$ at each switching time. According to [82], the low-thrust multi-burn

fuel-optimal trajectory on $[0, t_f]$ realizes a relative optimum. (See [82] for detailed definition of relative optimum.) In addition, for every sufficiently small deviation $\Delta\boldsymbol{x}$ from the nominal trajectory $\overline{\boldsymbol{x}}(\cdot)$ at every time $t_0 \in [0, t_f)$, there exists a neighboring extremal $(\boldsymbol{x}(\cdot), \boldsymbol{p}(\cdot))$ with its graph in $\mathcal{F}_{\boldsymbol{q}}$ such that $\boldsymbol{x}(t_0) = \overline{\boldsymbol{x}}(t_0) + \Delta\boldsymbol{x}$. Thus, one can construct the neighboring optimal feedback control around the nominal trajectory. In order to see the occurrence of

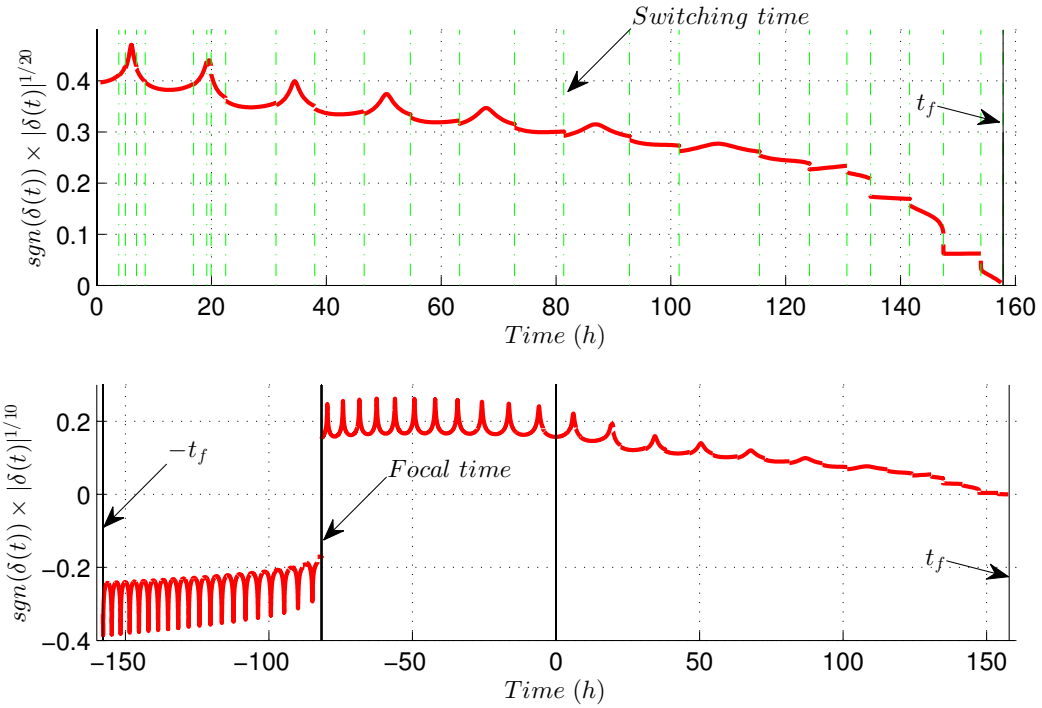

Figure 5.8 – The top plot is the profile of $\text{sgn}(\delta_{\boldsymbol{q}}(t)) \times |\delta_{\boldsymbol{q}}(t)|^{1/20}$ on $[0, t_f]$ and the bottom plot is the profile of $\text{sgn}(\delta_{\boldsymbol{q}}(t)) \times |\delta_{\boldsymbol{q}}(t)|^{1/10}$ on $[-t_f, t_f]$.

focal points or to see the sign change of $\delta_{\boldsymbol{q}}(t)$, the profile of $\text{sgn}(\delta_{\boldsymbol{q}}(\cdot)) \times |\delta_{\boldsymbol{q}}(\cdot)|^{1/10}$ on the extended time interval $[-t_f, t_f]$ is plotted in the bottom subplot of Fig. 5.8. Apparently, there exists a sign change of $\delta_{\boldsymbol{q}}(t)$ at the switching time $t_c \approx -81.716$ h. Thus, a focal point occurs at t_c, which implies that the nominal extremal $(\overline{\boldsymbol{x}}(\cdot), \overline{\boldsymbol{p}}(\cdot))$ on $[t_0, t_f]$ is not optimal any more if $t_0 < t_c$. In addition, as is shown by Remark 5.2, it is impossible to construct the NOC once $t_0 < t_c$.

Perturbations on the initial state and on the propulsive parameters are considered. Each perturbed component of the initial state is subject to a normal distribution where the mean value μ and the 3σ-value are presented in Tab. 5.5. Note that the perturbations on the initial mass are not considered since the corresponding perturbations are equivalent to those on the thrust magnitude or on the acceleration. The perturbations on thrust magnitude on burn arcs are subject to Eq. (5.23). Then, a *Monte Carlo* simulation (including 100 runs) is performed to show the statistical information on final conditions. The statistical information for the errors of final conditions is presented in Tab. 5.6, showing that the standard deviation is reduced from 10 km at initial time to 0.45 km at the final time in terms of semi-major axis. In addition,

Table 5.5 – Case B: Statistical information for the perturbations.

State:	P	e_x	e_y	h_x	h_y	l
μ:	11,625.0 km	0.75	0	0.26795	0	π
3σ:	10 km	0.001	0.001	0.001	0.001	0.001

Table 5.6 – Case B: Statistical information for the errors on final conditions.

Errors:	δa (m)	δe	δi (deg)
μ:	90.11	9.25×10^{-6}	1.39×10^{-4}
σ:	451.69	7.59×10^{-6}	1.08×10^{-4}

the standard deviations in terms of the inclination and the eccentricity are small enough. Figs. 5.9–5.11 portray the time evolutions of the errors on semi-major axis, inclination, and eccentricity, respectively, showing that the corresponding errors tend to zero at the final time.

5.5 Conclusion

In this chapter, the neighboring optimal feedback control for the L^1-minimization problem with fixed final time is established. The crucial step is to construct a parameterized family of neighboring extremals around a nominal extremal. A geometric interpretation is given to show that the projection of the parameterized family is a fold singularity if the Jacobi necessary condition is violated. As a result, it is concluded that it is impossible to construct the neighboring optimal control for the bang-bang case if either the Jacobi necessary condition between switching times or a transversality condition at switching times is violated. On the contrary, there exist neighboring extremals around the nominal one such that any sufficiently small deviated state can be passed by a neighboring extremal if the generalized disconjugacy conditions between and at switching times are satisfied.

The neighboring optimal feedback control is exactly the first-order term of the Taylor expansion of the extremal control corresponding to the parameterized neighboring extremal. Results show that the differential equation of gain matrix between switching times is more or less the same as the Riccati differential equation of [16]. However, the gain matrix is discontinuous at each switching time. So, the gain matrix has to be updated by an extra formula at each switching. Finally, two fixed-time finite-thrust orbital transfer problems are computed and Monte Carlo tests are performed to show that the neighboring optimal feedback control significantly reduces the errors of final conditions.

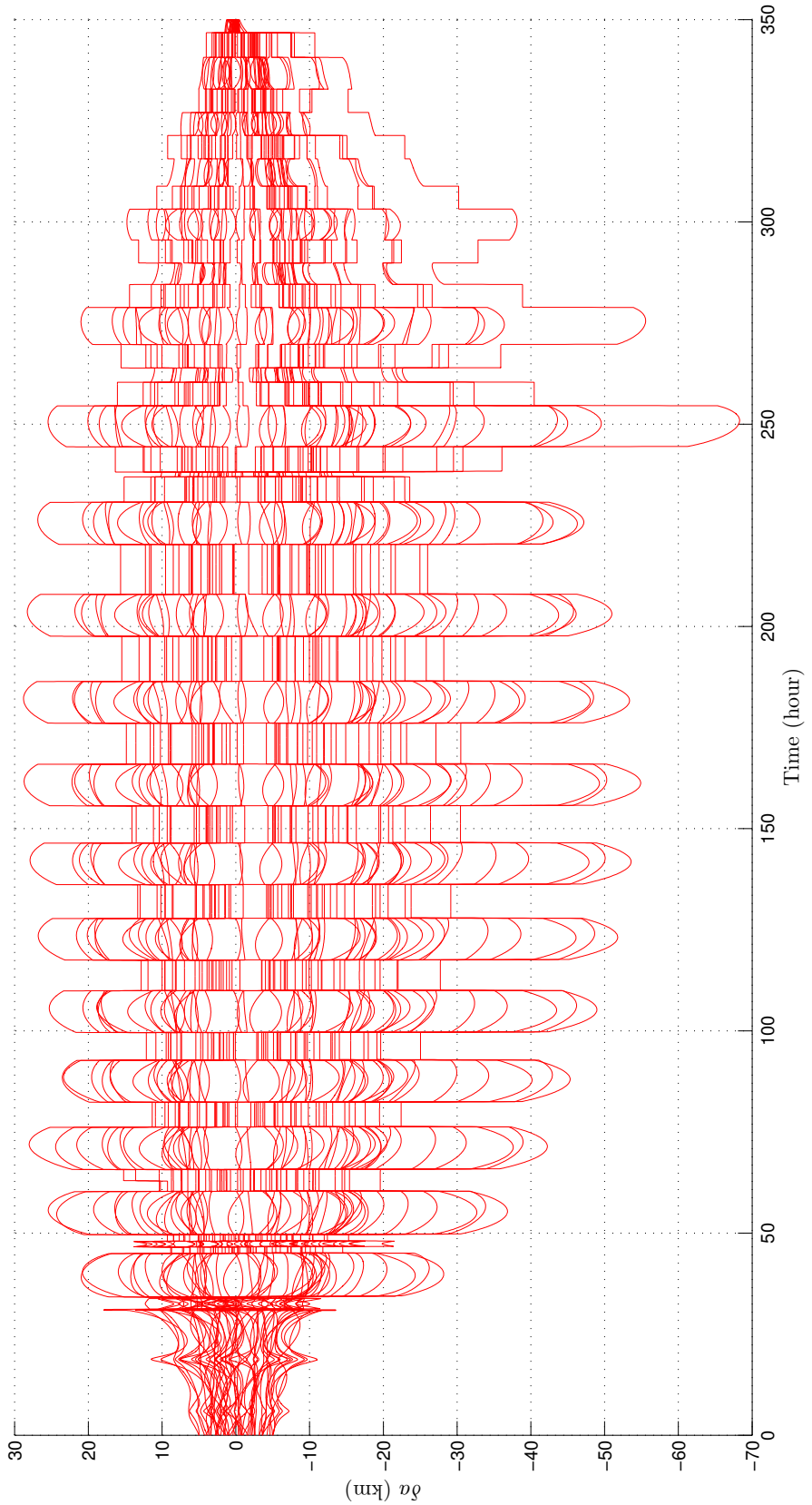

Figure 5.9 – Case B: Evolution of errors on semi-major axis for Monte Carlo campaigns.

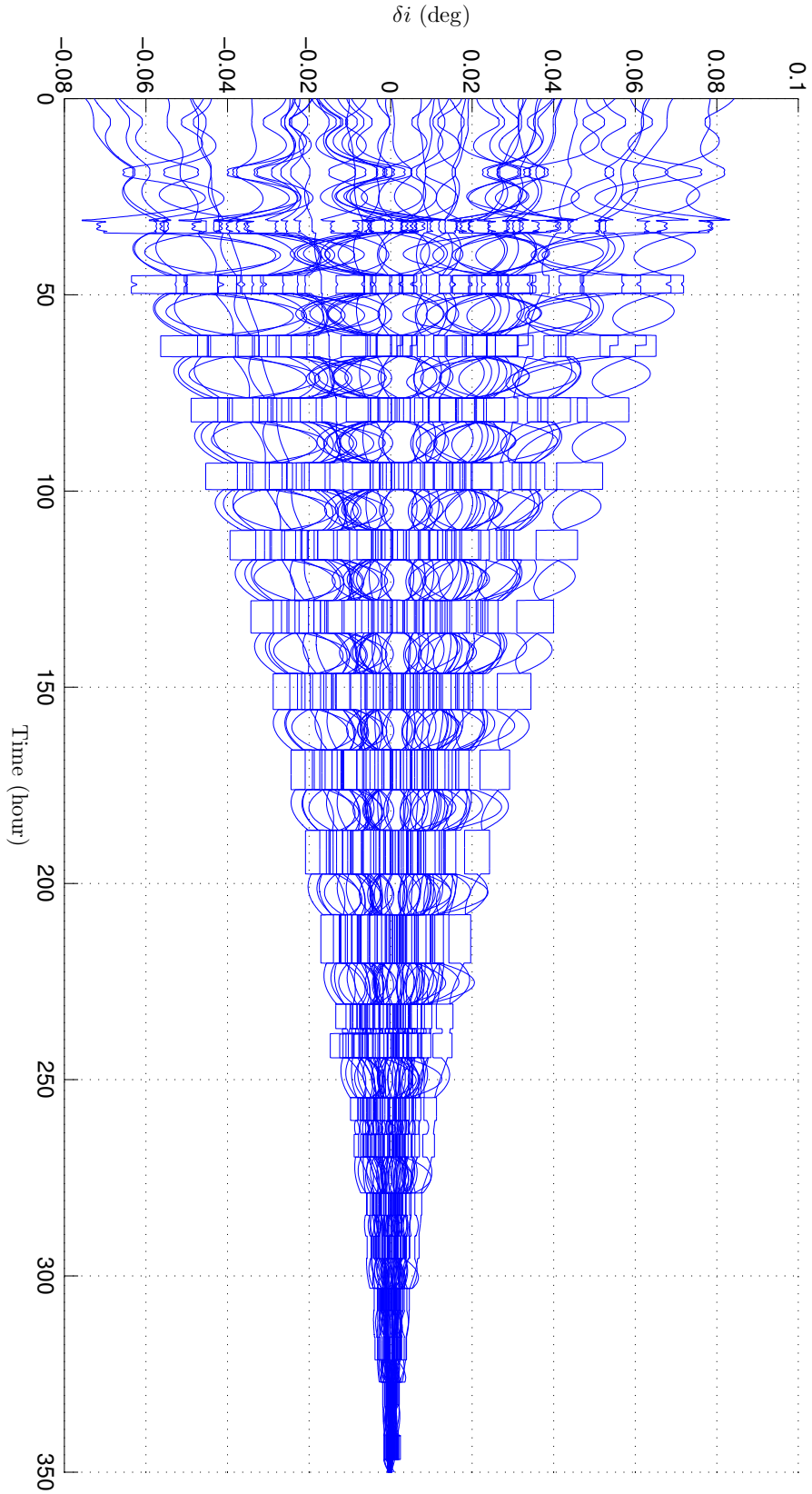

Figure 5.10 – Case B: Evolution of errors on inclination for Monte Carlo campaigns.

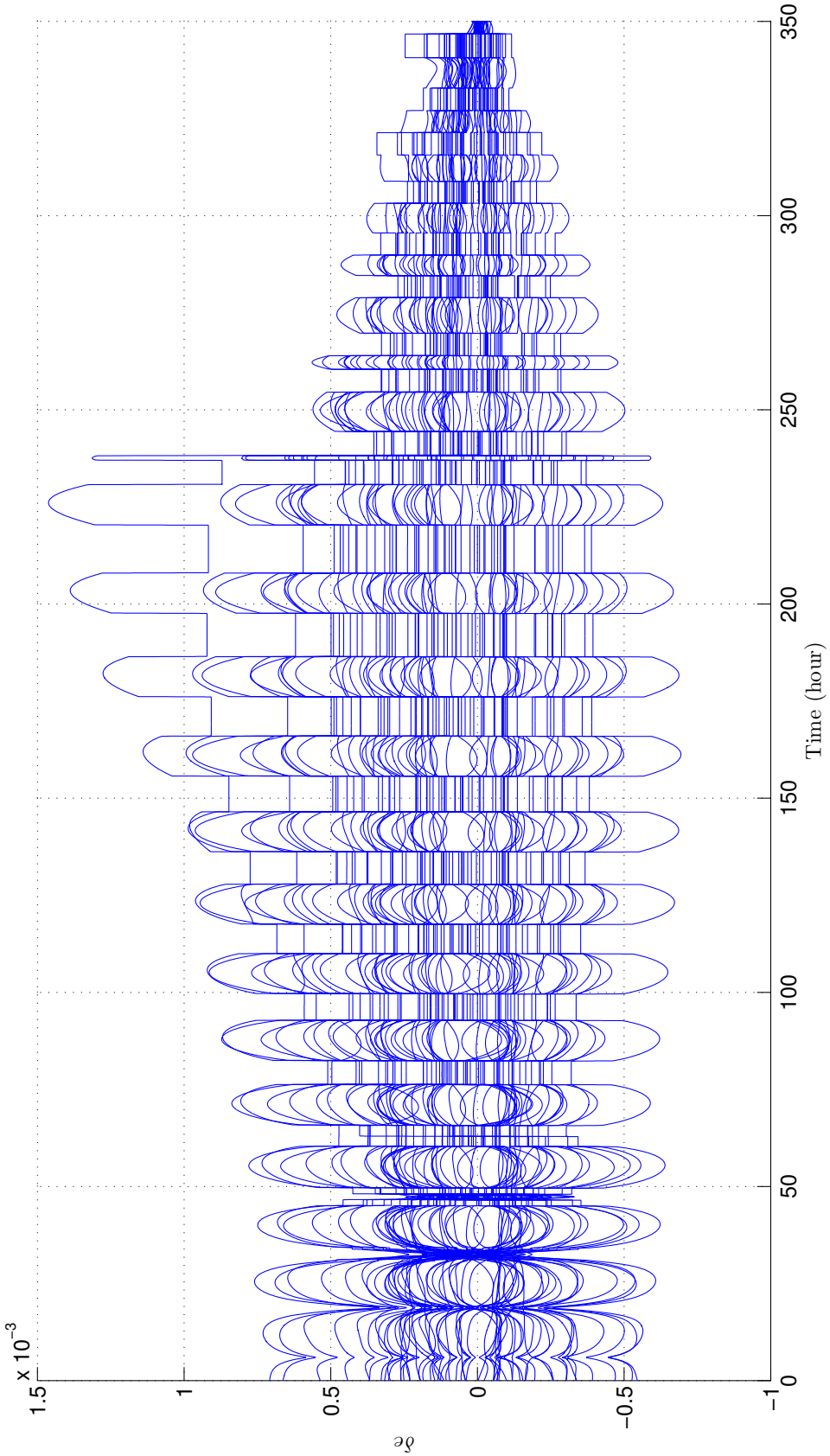

Figure 5.11 – Case B: Evolution of errors on eccentricity for Monte Carlo campaigns.

Chapter 6

Research summary and future directions

6.1 Research summary

This thesis is concerned with the L^1-minimization for the translational motion of a spacecraft controlled by finite-thrust propulsion systems and subject to the gravitation of multiple celestial bodies. The applications into the circular restricted three-body problem have been treated in detail. First order necessary conditions have been derived by using the Pontryagin maximum principle, revealing the existence of bang-bang and singular controls. Singular extremals have been analyzed, recalling the existence of the Fuller (or chattering) phenomena according to the theorems developed by Marchal [53] and Zelikin and Borisov [95, 96].

The first contribution of this work is that the controllability for the Keplerian motion ($\mu = 0$ or 1) with low-thrust control systems has been addressed (cf. Chapter 2) by using some geometric techniques of [34, 87]. Since the drift vector field for the circular restricted three-body problem, where $\mu \in (0, 1)$, is recurrent, the theorems established in Chapter 2 shows that the controllability of the CRTBP with low-thrust control systems holds as well in some appropriate subregion of state space [17]. Moreover, taking into account some state constraints, it is shown that the Keplerian motion is controllable if and only if the maximum thrust is bigger than a limiting value. This result makes sense for de-orbit problems and orbital insertion problems where one has to make sure the satellite moves outside of the atmosphere around the Earth.

The second contribution of this work is that the sufficient second order conditions for strong-local optimality in C^0-topology were established in Chapters 3 and 4. To establish the sufficient conditions, a parameterized family of extremals has been constructed such that the reference extremal can be embedded into a *field of extremals*. By studying the projection behavior of the parameterized family, two "no-fold conditions" ensuring the projection of the field is a local diffeomorphism have been devised (see Conditions 3.1 and 3.2). If the endpoints are fixed, the two no-fold conditions are sufficient to guarantee the reference extremal is a strong-local optimum in C^0-topology provided that each switching point is regular (cf. Theorem 3.1). Regarding the scenario that the target point is not fixed but varies on a mani-

fold, an extra condition (cf. Condition 4.1) involving the geometry of the target manifold and the Jacobi fields has been established for the strong-local optimality. It is concluded that the extra condition together with the two no-fold conditions are sufficient to guarantee the strong-local optimum of the reference extremal (cf. Theorem 4.1). Since those three conditions are related to the Jacobi fields, the numerical test of the sufficient conditions eventually turns to computing the Jacobi fields. The associated numerical procedure is detailed in Appendix C.

The last part of the research aims at establishing neighboring optimal feedback control law for the L^1-minimization (cf. Chapter 5). The neighboring optimal control is a classical topic in optimal control and dates back to the work of, e.g., Bryson [16], Kelley [39], and Breakwell [13]. Since the optimal control function for the L^1-minimization exhibits a bang-bang behavior, the neighboring optimal feedback consist not only of the correction of thrust direction but also of the correction of switching times. Unlike the classical variational method to solve an accessory minimum problem, the neighboring optimal feedback control in this work has been established by deriving the first order term of the Taylor expansion of the extremal control corresponding to a parameterized family of neighboring extremals.

6.2 Future directions

In this work, the time interval is considered fixed, the mass of the satellite is considered as a constant, and the constraints are active only at boundary points. Therefore, the following possible extensions are identified:

Sufficient optimality conditions for fuel-optimal problems: The L^1-minimization is equivalent to maximizing the final mass if $\beta > 0$; that is the important fuel-optimal control problem in astronautics. Once the mass is not constant but varying ($\beta > 0$), the state $\boldsymbol{x}$ consists of not only $\boldsymbol{r}$ and $\boldsymbol{v}$ but also m. Note that

$$\frac{d}{dt}\frac{\partial m}{\partial \boldsymbol{p}_0}(t, \overline{\boldsymbol{p}}_0) = -\beta \frac{\partial \rho(t, \overline{\boldsymbol{p}}_0)}{\partial \boldsymbol{p}_0} \equiv 0$$

since $\rho(t, \boldsymbol{p}_0)$ for $t \in [0, t_f]$ is a piecewise constant along every nonsingular extremal. Thus, the matrix $\partial \boldsymbol{x}(t, \overline{\boldsymbol{p}}_0)/\partial \boldsymbol{p}_0$ is singular on $[0, t_1]$ as $\partial m(0, \overline{\boldsymbol{p}}_0)/\partial \boldsymbol{p}_0 = 0$. Consequently, the inequality $\delta(t) \neq 0$ in Condition 3.1 cannot be used to test conjugate points any more. Therefore, a natural extension of this work is to establish numerically verifiable no-fold conditions for mass varying model.

Sufficient optimality conditions for free-time problems: Once the final time t_f is left free, there holds $H(\boldsymbol{x}(\cdot), \boldsymbol{p}(\cdot)) \equiv 0$ on $[0, t_f]$ for every minimizing extremal $(\boldsymbol{x}, \boldsymbol{p}) \in T^*\mathcal{X}$. Thus, every minimizing extremal lies in the codimension one manifold

$$\mathcal{H} := \{(\boldsymbol{x}, \boldsymbol{p}) \in T^*\mathcal{X} \mid H(\boldsymbol{x}, \boldsymbol{p}) = 0\}.$$

As a result, there holds

$$\operatorname{rank}\left[\partial \boldsymbol{x}(t, \overline{\boldsymbol{p}}_0)/\partial \boldsymbol{p}_0\right] \leqslant n-1$$

for $t \in [0, t_f]$ (see [9]). Again, the inequality $\delta(t) \neq 0$ in Condition 3.1 cannot be used to test conjugate points for free-time problems. Therefore, an extension of this work would be to establish the numerically verifiable no-fold conditions for free-time problem.

Sufficient optimality conditions for optimal control problems with path constraints: In this research, the sufficient optimality conditions have been established for optimal control problems with constraints of boundary points only. Many practical problems of engineering or scientific interest can be formulated in the framework of optimal control problems with state space constraints. Examples come from various disciplines, e.g., the space shuttle re-entry problem. Despite of its importance, there still exists a large gap between the theories of necessary and sufficient conditions for optimality for optimal control problems with state space constraints. The literature on sufficient conditions for optimality for optimal control problems with state space constraints is limited. A natural extension of this work would be to establish such conditions for the optimal control problems with path constraints.

Sufficient optimality conditions for singular extremals: The sufficient optimality conditions for singular extremals have not been considered in this research although the existence of singular extremals is presented. Restricting the order of singular extremals to one, the sufficient conditions for bang-singular extremals have been studied by Poggiolini and Stefani [72] from the Hamiltonian point of view. A possible extension of this work is to establish the sufficient second order optimality conditions for second order singular extremals.

Neighboring optimal feedback control for free-time problems: Once the final time t_f is left free, the neighboring optimal feedback control consists of not only the correction of the thrust direction and the switching times but also the correction of the final time. Moreover, the conditions for the existence of neighboring extremals would be different from Conditions 3.1 and 3.2. Therefore, a future work would be to consider the neighboring optimal feedback control for free-time problems.

Neighboring optimal feedback control with path constraints: The computation of solutions for optimal control problems with state constraints is much more difficult than that for optimal control problems without state constraints. Therefore, the applications of the optimal control problems with state constraints demand for a theory of neighboring extremals.

Neighboring optimal feedback control for singular extremals: Since the order of the singular extremals is of order two, a variation at endpoints may induce the occurrence of chattering or Fuller phenomena (see [12], e.g.). It is necessary to analyze under what conditions the chattering phenomena occur when dealing with neighboring optimal feedback control for singular extremals. Moreover, the efficient computation of chattering solutions is an open problem (see, e.g., [32, 69]).

Appendix A

Modified equinoctial orbital elements

In this appendix, we provide two sets of coordinates for points in the periodic region $\mathcal{P}$ (see, e.g., [94] for all the results given here).

Definition A.1 (*Classical orbital elements (COE)*). *For $\boldsymbol{x} = (\boldsymbol{r}, \boldsymbol{v}) \in \mathcal{P}$, define the following functions:*

$$a(\boldsymbol{x}) = -\frac{\mu}{2E}, \tag{A-1}$$

$$i(\boldsymbol{x}) = \cos^{-1} \frac{\| \boldsymbol{h}^T \cdot \mathbf{1}_z \|}{\| \boldsymbol{h} \| \| \mathbf{1}_z \|}, \tag{A-2}$$

$$\omega(\boldsymbol{x}) = \cos^{-1} \frac{\| \boldsymbol{L}^T \cdot \boldsymbol{n} \|}{\| \boldsymbol{L} \| \| \boldsymbol{n} \|}, \tag{A-3}$$

$$\Omega(\boldsymbol{x}) = \cos^{-1} \frac{\| \mathbf{1}_x^T \cdot \boldsymbol{n} \|}{\| \mathbf{1}_x \| \| \boldsymbol{n} \|}, \tag{A-4}$$

where $\mathbf{1}_x = [1, 0, 0]^T$, $\boldsymbol{n} = \mathbf{1}_z \times \boldsymbol{h}$ with $\mathbf{1}_z = [0, 0, 1]^T$. The quantity $a(\boldsymbol{x})$ is called the semi-major axis of the orbit $\gamma_{\boldsymbol{x}}$ whose shape is thus determined by $a(\boldsymbol{x})$ and $e(\boldsymbol{x})$. The angles $i(\boldsymbol{x})$, $\omega(\boldsymbol{x})$ and $\Omega(\boldsymbol{x})$ are called the inclination of the orbit $\gamma_{\boldsymbol{x}}$, the argument of perigee of the orbit $\gamma_{\boldsymbol{x}}$ and the right ascension of the ascending node of the orbit $\gamma_{\boldsymbol{x}}$, respectively. Then, the variables $(a(\boldsymbol{x}), e(\boldsymbol{x}), i(\boldsymbol{x}), \omega(\boldsymbol{x}), \Omega(\boldsymbol{x}), \theta(\boldsymbol{x}))$ are called the classical orbital elements of the orbit $\gamma_{\boldsymbol{x}}$.

(Note that the set of COEs is singular if $e = 0$ and $i = 0, \pi$.)

Definition A.2 (*M*odified equinoctial orbital elements (MEOE)). *For $\boldsymbol{x} \in \mathcal{P}$, define the following functions:*

$$P(\boldsymbol{x}) = a(\boldsymbol{x})(1 - e(\boldsymbol{x})^2)/\mu, \tag{A-5}$$

$$e_x(\boldsymbol{x}) = e(\boldsymbol{x}) \cos(\omega(\boldsymbol{x}) + \Omega(\boldsymbol{x})), \tag{A-6}$$

$$e_y(\boldsymbol{x}) = e(\boldsymbol{x}) \sin(\omega(\boldsymbol{x}) + \Omega(\boldsymbol{x})), \tag{A-7}$$

$$h_x(\boldsymbol{x}) = \tan(i(\boldsymbol{x})/2) \cos(\Omega(\boldsymbol{x})), \tag{A-8}$$

$$h_y(\boldsymbol{x}) = \tan(i(\boldsymbol{x})/2) \sin(\Omega(\boldsymbol{x})), \tag{A-9}$$

$$l(\boldsymbol{x}) = \omega(\boldsymbol{x}) + \Omega(\boldsymbol{x}) + \theta(\boldsymbol{x}), \tag{A-10}$$

where $(a(\boldsymbol{x}), e(\boldsymbol{x}), i(\boldsymbol{x}), \omega(\boldsymbol{x}), \Omega(\boldsymbol{x}), \theta(\boldsymbol{x}))$ *are the COE defined previously. Then the* 6*-tuple* $\boldsymbol{z} = (P, e_x, e_y, h_x, h_y, l) \in \mathbb{R}^5 \times \mathbb{S}$ *gathers the so-called modified equinoctial orbit elements (MEOE), Moreover, we also have that*

$$\boldsymbol{r} = \frac{P}{CW}\begin{bmatrix} (1 + h_x^2 - h_y^2)\cos l + 2h_x h_y \sin l \\ (1 - h_x^2 + h_y^2)\sin l + 2h_x h_y \cos l \\ 2h_x \sin l - 2h_y \cos l \end{bmatrix}, \tag{A-11}$$

$$\boldsymbol{v} = \frac{\sqrt{\mu/P}}{C}\begin{bmatrix} 2h_x h_y(e_x + \cos l) - (1 + h_x^2 - h_y^2)(e_y + \sin l) \\ -2h_x h_y(e_y + \sin l) + (1 - h_x^2 + h_y^2)(e_x + \cos l) \\ 2h_x(e_x + \cos l) + 2h_y(e_y + \sin l) \end{bmatrix}, \tag{A-12}$$

where $C = 1 + h_x^2 + h_y^2$ *and* $W = 1 + e_x \cos l + e_y \sin l$*. Note that* $e = \sqrt{e_x^2 + e_y^2}$ *and* $P = \boldsymbol{h}^2/\mu$*. Thus, let us define the set*

$$\mathcal{Z} = \big\{\boldsymbol{z} \in \mathbb{R}^5 \times \mathbb{S} : P > 0 \text{ and } 0 \leqslant e_x^2 + e_y^2 < 1\big\},$$

then the transformation $(\boldsymbol{r}, \boldsymbol{v}) : \mathcal{Z} \to \mathcal{P},\ \boldsymbol{z} \mapsto (\boldsymbol{r}(\boldsymbol{z}), \boldsymbol{v}(\boldsymbol{z}))$ *is a covering map. Hence* $\mathcal{P}$ *is arc-connected if* $\mathcal{Z}$ *is.*

Appendix B

Sufficient conditions in the smooth case

Consider the same minimization problem as in Chapter 3. Suppose that

Assumption B.1. *The reference extremal is normal.*

Having fixed p^0 to -1, we make a stronger assumption that the maximized Hamiltonian is well defined and smooth, and set

$$h(\boldsymbol{z}) := \max_{\mathcal{U}} H(\boldsymbol{z}, \cdot), \quad \boldsymbol{z} \in T^*\mathcal{X}.$$

Scholium B.1. *For almost all* $t \in [0, t_f]$,

$$h'(\overline{\boldsymbol{z}}(t)) = \frac{\partial H}{\partial \boldsymbol{z}}(\overline{\boldsymbol{z}}(t), \overline{\boldsymbol{u}}(t)), \quad \nabla^2 h(\overline{\boldsymbol{z}}(t)) - \nabla^2_{\boldsymbol{zz}} H(\overline{\boldsymbol{z}}(t), \overline{\boldsymbol{u}}(t)) \geqslant 0.$$

Proof. For a.a. $t \in [0, t_f]$, $h(\overline{\boldsymbol{z}}(t)) - H(\overline{\boldsymbol{z}}(t), \overline{\boldsymbol{u}}(t)) = 0$, while

$$h(\boldsymbol{z}) - H(\boldsymbol{z}, \overline{\boldsymbol{u}}) \geqslant 0, \quad \boldsymbol{z} \in T^*\mathcal{X},$$

by definition of h. Applying the first and second order necessary conditions for optimality on $T^*\mathcal{X}$ at $\boldsymbol{z} = \overline{\boldsymbol{z}}$ gives the result. □

We make the following assumption on the smooth reference extremal.

Assumption B.2. *The matrix* $\partial \boldsymbol{x}(t, \overline{\boldsymbol{z}}_0)/\partial \boldsymbol{p}_0$ *is invertible for* $t \in (0, t_f]$.

Theorem B.1. *Under Assumptions B.1 and B.2, the reference trajectory is a* C^0*-local optimizer among all trajectories with the same endpoints.*

The disconjugacy condition (cf. Assumption B.2) can be numerically verified, e.g., by a rank test while integrating the variational system along the reference extremal. For the sake of completeness, we provide a proof that essentially goes along the lines of [2, Chapter 21]. Note that no Legendre type assumption is needed, though.

Proof. For S_0 symmetric of order n, $L_0 := \{\delta \boldsymbol{x}_0 = S_0 \delta \boldsymbol{p}_0\}$ is a Lagrangian subspace of $T_{\overline{\boldsymbol{z}}_0}(T^*\mathcal{X})$. Denote by $\delta \boldsymbol{z} = (\delta \boldsymbol{x}, \delta \boldsymbol{p})$ the solution of the linearized system

$$\delta \dot{\boldsymbol{z}}(t) = \overrightarrow{h}'(\overline{\boldsymbol{z}}(t)) \delta \boldsymbol{z}(t), \quad \delta \boldsymbol{z}(0) = (S_0, I),$$

and set $\delta\widetilde{\boldsymbol{z}}(t) = (\delta\widetilde{\boldsymbol{x}}(t), \delta\widetilde{\boldsymbol{p}}(t)) := \Phi_t^{-1}\delta\boldsymbol{z}(t)$ where Φ_t is the fundamental solution of the linearized system

$$\dot{\Phi}_t = \frac{\partial\overrightarrow{H}}{\partial\boldsymbol{z}}(\overline{\boldsymbol{z}}(t), \overline{\boldsymbol{u}}(t))\Phi_t, \quad \Phi_0 = I.$$

As $\delta\boldsymbol{p}(0) = \delta\widetilde{\boldsymbol{p}}(0) = I$,

$$S(t) := \delta\widetilde{\boldsymbol{x}}(t)\delta\widetilde{\boldsymbol{p}}(t)^{-1}$$

is well defined for small enough $t \geqslant 0$. Since

$$L_t := \left(e^{t\overrightarrow{h}}\right)'(\overline{\boldsymbol{z}}(t))(L_0) \quad \text{and} \quad \Phi_t^{-1}(L_t)$$

are Lagrangian as images of L_0 through linear symplectic mappings, $S(t)$ must by symmetric.

Lemma B.1. *$\dot{S}(t) \geqslant 0$.*

Proof of the lemma. Let $t_1 > 0$ such that $S(t_1)$ is well defined, and let $\xi \in \mathbb{R}^n$. Set

$$\xi_0 := \delta\widetilde{\boldsymbol{p}}(t_1)^{-1}\xi \quad \text{and} \quad \delta\widetilde{\boldsymbol{z}}_1(t) := \delta\widetilde{\boldsymbol{z}}(t)\xi_0.$$

Then $\delta\widetilde{\boldsymbol{z}}_1(t_1) = (S(t_1)\xi, \xi)$, and $\delta\widetilde{\boldsymbol{x}}_1(t) = S(t)\delta\widetilde{\boldsymbol{p}}_1(t)$. Differentiating the previous relation and using $S(t)$ symmetry leads to

$$(\dot{S}(t)\delta\widetilde{\boldsymbol{p}}_1(t)|\delta\widetilde{\boldsymbol{p}}_1(t)) = \omega(\delta\widetilde{\boldsymbol{z}}_1(t), \delta\dot{\widetilde{\boldsymbol{z}}}_1(t)).$$

Differentiating now

$$\delta\widetilde{\boldsymbol{z}}_1(t) = \Phi_t^{-1}\delta\boldsymbol{z}(t)\xi_0,$$

one gets

$$\begin{aligned}\delta\dot{\widetilde{\boldsymbol{z}}}_1(t) &= \Phi_t^{-1}(\overrightarrow{h}'(\overline{\boldsymbol{z}}(t)) - \frac{\partial\overrightarrow{H}}{\partial\boldsymbol{z}}(\overline{\boldsymbol{z}}(t), \overline{\boldsymbol{u}}(t)))\Phi_t\delta\widetilde{\boldsymbol{z}}(t)\\ &= J^t\Phi_t(\underbrace{\nabla^2 h(\overline{\boldsymbol{z}}(t)) - \nabla^2_{\boldsymbol{zz}}H(\overline{\boldsymbol{z}}(t), \overline{\boldsymbol{u}}(t))}_{\geqslant 0})\Phi_t\delta\widetilde{\boldsymbol{z}}_1(t).\end{aligned}$$

(J denotes the standard symplectic matrix.) Evaluating at $t = t_1$, one eventually gets $(\dot{S}(t_1)\xi|\xi) \geqslant 0$. □

For $S_0 = 0$, there is $\eta > 0$ such that $S(t)$ is well defined on $[0, \eta]$, which remains true for $S_0 > 0$ with $|S_0| > 0$ small enough. By the lemma before, $S_t > 0$ on $[0, \eta]$. In particular, it is an invertible matrix, which ensures that $\Phi_t^{-1}(L_t)$ is transversal to $\ker\Pi'(\overline{\boldsymbol{z}}_0)$ ($\Pi : T^*\mathcal{X} \to \mathcal{X}$ being the canonical projection), that is L_t is transversal to $\ker\Pi'(\overline{\boldsymbol{z}}(t))$ by virtue of the following lemma.

Lemma B.2. *$\Phi_t(\ker\Pi'(\overline{\boldsymbol{z}}_0)) = \ker\Pi'(\overline{\boldsymbol{z}}(t))$.*

Proof of the lemma. Note that in the linearized system defining Φ_t,

$$\begin{aligned}\delta\dot{\boldsymbol{x}}(t) &= \nabla^2_{\boldsymbol{xp}} H(\overline{\boldsymbol{z}}(t), \overline{\boldsymbol{u}}(t))\delta\boldsymbol{x},\\ \delta\dot{\boldsymbol{p}}(t) &= -\nabla^2_{\boldsymbol{xx}} H(\overline{\boldsymbol{z}}(t), \overline{\boldsymbol{u}}(t))\delta\boldsymbol{x} - \nabla^2_{\boldsymbol{px}}(\overline{\boldsymbol{z}}(t), \overline{\boldsymbol{u}}(t))\delta\boldsymbol{p},\end{aligned}$$

the equation on $\delta\boldsymbol{x}$ is linear. Hence $\delta\boldsymbol{x}(0) = 0$ implies $\delta\boldsymbol{x} \equiv 0$. □

By restricting $|S_0|$ if necessary, Assumption B.2 allows to assume that $\delta\boldsymbol{x}(t)$ remains invertible for $t \in [\eta, t_f]$, so transversality of L_t holds on $[0, t_f]$. As a result, one can devise a Lagrangian submanifold $\mathcal{L}_0 \subset T^*\mathcal{X}$ whose tangent space at $\overline{\boldsymbol{z}}_0$ is L_0; then

$$\mathcal{L} := \{(t, \boldsymbol{z}) \in \mathbb{R} \times T^*\mathcal{X} \mid (\exists \boldsymbol{z}_0 \in \mathcal{L}_0) : t \in (-\varepsilon, t_f + \varepsilon) \text{ s.t. } \boldsymbol{z} = e^{t\overrightarrow{h}}(\boldsymbol{z}_0)\}$$

is well defined for ε small enough, and such that $\Pi_t : \mathbb{R} \times T^*\mathcal{X} \to \mathbb{R} \times \mathcal{X}$ induces a diffeomorphism from $\mathcal{L}$ onto its image. One can moreover choose $\mathcal{L}_0$ such that $\boldsymbol{p}d\boldsymbol{x}$ is not only closed but an exact on $\mathcal{L}$. This, together with Assumption B.1, allows to conclude as usual that the reference trajectory is optimal with respect to C^0-neighboring trajectories with the same endpoints. □

Appendix C

Numerical implementation of the Jacobi field computation

It follows from the classical results about solutions to ODEs that the extremal trajectory $(\boldsymbol{x}(t,\boldsymbol{p}_0),\boldsymbol{p}(t,\boldsymbol{p}_0))$ and its time derivative are continuously differentiable with respect to $\boldsymbol{p}_0$ on (t_i,t_{i+1}) for $i=0,1,\cdots,k$. Thus, taking derivative of Eq. (1.7) with respect to $\boldsymbol{p}_0$ on each segment (t_i,t_{i+1}), we obtain

$$\begin{bmatrix} \frac{d}{dt}\frac{\partial \boldsymbol{x}}{\partial \boldsymbol{p}_0}(t,\overline{\boldsymbol{p}}_0) \\ \frac{d}{dt}\frac{\partial \boldsymbol{p}^T}{\partial \boldsymbol{p}_0}(t,\overline{\boldsymbol{p}}_0) \end{bmatrix} = \begin{bmatrix} H_{\boldsymbol{px}}(\overline{\boldsymbol{x}}(t),\overline{\boldsymbol{p}}(t)) & H_{\boldsymbol{pp}}(\overline{\boldsymbol{x}}(t),\overline{\boldsymbol{p}}(t)) \\ -H_{\boldsymbol{xx}}(\overline{\boldsymbol{x}}(t),\overline{\boldsymbol{p}}(t)) & -H_{\boldsymbol{xp}}(\overline{\boldsymbol{x}}(t),\overline{\boldsymbol{p}}(t)) \end{bmatrix} \begin{bmatrix} \frac{\partial \boldsymbol{x}}{\partial \boldsymbol{p}_0}(t,\overline{\boldsymbol{p}}_0) \\ \frac{\partial \boldsymbol{p}^T}{\partial \boldsymbol{p}_0}(t,\overline{\boldsymbol{p}}_0) \end{bmatrix}. \tag{C-1}$$

Since the initial point $\boldsymbol{x}_0$ is fixed, one can obtain the initial conditions as

$$\frac{\partial \boldsymbol{x}}{\partial \boldsymbol{p}_0}(0,\overline{\boldsymbol{p}}_0)=\mathbf{0}_n \text{ and } \frac{\partial \boldsymbol{p}^T}{\partial \boldsymbol{p}_0}(0,\overline{\boldsymbol{p}}_0)=I_n, \tag{C-2}$$

where $\mathbf{0}_n$ and I_n denote the zero and identity matrix of $\mathbb{R}^{n\times n}$, respectively. Note that the two matrices $\partial \boldsymbol{x}(\cdot,\overline{\boldsymbol{p}}_0)/\partial \boldsymbol{p}_0$ and $\partial \boldsymbol{p}^T(\cdot,\overline{\boldsymbol{p}}_0)/\partial \boldsymbol{p}_0$ are discontinuous at each switching time t_i. Comparing with [23, 63, 82], the update formulas for the two matrices $\partial \boldsymbol{x}(\cdot,\overline{\boldsymbol{p}}_0)/\partial \boldsymbol{p}_0$ and $\partial \boldsymbol{p}^T(\cdot,\overline{\boldsymbol{p}}_0)/\partial \boldsymbol{p}_0$ at each switching time t_i can be written as

$$\frac{\partial \boldsymbol{x}}{\partial \boldsymbol{p}_0}(t_i+,\overline{\boldsymbol{p}}_0) = \frac{\partial \boldsymbol{x}}{\partial \boldsymbol{p}_0}(t_i-,\overline{\boldsymbol{p}}_0) - \Delta\rho_i \boldsymbol{f}_1(\boldsymbol{x}(t_i),\boldsymbol{\omega}(t_i))dt_i(\overline{\boldsymbol{p}}_0), \tag{C-3}$$

$$\frac{\partial \boldsymbol{p}^T}{\partial \boldsymbol{p}_0}(t_i+,\overline{\boldsymbol{p}}_0) = \frac{\partial \boldsymbol{p}^T}{\partial \boldsymbol{p}_0}(t_i-,\overline{\boldsymbol{p}}_0) + \Delta\rho_i \frac{\partial \boldsymbol{f}_1}{\partial \boldsymbol{x}}(\boldsymbol{x}(t_i),\boldsymbol{\omega}(t_i)\boldsymbol{p}^T(t_i)dt_i(\overline{\boldsymbol{p}}_0), \tag{C-4}$$

where $\Delta\rho_i=\rho(t_i+)-\rho(t_i-)$. With the exception of $dt_i(\overline{\boldsymbol{p}}_0)$, every requested quantity can be explicitly computed. For every $\boldsymbol{p}_0\in\mathcal{P}$ there holds

$$H_1(\boldsymbol{x}(t_i(\boldsymbol{p}_0),\boldsymbol{p}_0),\boldsymbol{p}(t_i(\boldsymbol{p}_0),\boldsymbol{p}_0))=0. \tag{C-5}$$

Taking into account $\dot{H}_1(\boldsymbol{x}(t), \boldsymbol{p}(t)) = H_{01}(\boldsymbol{x}(t), \boldsymbol{p}(t))$ and differentiating Eq. (C-5) with respect to $\boldsymbol{p}_0$ yields

$$\begin{aligned} 0 &= H_{01}(\boldsymbol{x}(t_i, \boldsymbol{p}_0), \boldsymbol{p}(t_i, \boldsymbol{p}_0)) dt_i(\boldsymbol{p}_0) + \boldsymbol{p}(t_i, \boldsymbol{p}_0) \frac{\partial \boldsymbol{f}_1}{\partial \boldsymbol{x}}(\boldsymbol{x}(t_i, \boldsymbol{p}_0), \boldsymbol{\omega}(t_i, \boldsymbol{p}_0)) \frac{\partial \boldsymbol{x}(t_i, \boldsymbol{p}_0)}{\partial \boldsymbol{p}_0} \\ &+ \boldsymbol{f}_1^T(\boldsymbol{x}(t_i, \boldsymbol{p}_0), \boldsymbol{\omega}(t_i, \boldsymbol{p}_0)) \frac{\partial \boldsymbol{p}^T(t_i, \boldsymbol{p}_0)}{\partial \boldsymbol{p}_0}. \end{aligned}$$

By virtue of Assumption 3.1, there holds $H_{01}(\overline{\boldsymbol{x}}(t_i), \overline{\boldsymbol{p}}(t_i)) \neq 0$ for $i = 1, 2, \cdots, k$. Thus, we obtain

$$\begin{aligned} dt_i(\overline{\boldsymbol{p}}_0) &= -\Big[\boldsymbol{p}(t_i, \overline{\boldsymbol{p}}_0) \frac{\partial \boldsymbol{f}_1}{\partial \boldsymbol{x}}(\boldsymbol{x}(t_i, \boldsymbol{p}_0), \boldsymbol{\omega}(t_i, \boldsymbol{p}_0)) \frac{\partial \boldsymbol{x}(t_i, \overline{\boldsymbol{p}}_0)}{\partial \boldsymbol{p}_0} \\ &+ \boldsymbol{f}_1^T(\boldsymbol{x}(t_i, \overline{\boldsymbol{p}}_0), \boldsymbol{\omega}(t_i, \overline{\boldsymbol{p}}_0)) \frac{\partial \boldsymbol{p}^T(t_i, \overline{\boldsymbol{p}}_0)}{\partial \boldsymbol{p}_0}\Big] / H_{01}(\overline{\boldsymbol{x}}(t_i), \overline{\boldsymbol{p}}(t_i)). \end{aligned}$$

Therefore, in order to compute the two matrices $\partial \boldsymbol{x}(\cdot, \overline{\boldsymbol{p}}_0)/\partial \boldsymbol{p}_0$ and $\partial \boldsymbol{p}^T(\cdot, \overline{\boldsymbol{p}}_0)/\partial \boldsymbol{p}_0$ on $[0, t_f]$, it is sufficient to choose the initial condition in Eq. (C-2), then to numerically integrate Eq. (C-1) between switching times and to use Eq. (C-3) and Eq. (C-4) to update the Jacobi fields at each switching time.

Bibliography

[1] H. H. Afshari, A. B. Novinzadeh, and J. Roshanian. Determination of nonlinear optimal feedback law for satellite injection problem using neighboring optimal control. *American Journal of Applied Sciences*, 6(3):430–438, 2009.

[2] A. A Agrachev and Y. L Sachkov. *Control Theory from the Geometric Viewpoint*, volume 87 of *Encyclopedia of Mathematical Sciences*. Springer-Verlag, Berlin, 2004.

[3] A. A Agrachev, G. Stefani, and P. Zezza. Strong optimality for a bang-bang trajectory. *SIAM Journal of Control and Optimization*, 41(4):1991–2041, 2002.

[4] V. V Beletsky. *Essays on the motion of celestial bodies*. Birkhäuser, 1999.

[5] B. Berret, C. Darlot, F. Jean, T. Pozzo, C. Papaxanthis, and J.-P Gauthier. The inactivation principle: Mathematical solutions minimizing the absolute work and biological implications for the planning of arm movements. *PLoS Comput. Biol.*, 4(10), 2008.

[6] J.-M Bismut. *Hypoelliptic Laplacian and orbital integrals*. Princeton University Press, 2011.

[7] M. C. Boldwin and P. Lu. Optimal deorbit guidance. *Journal of Guidance, Control, and Dynamics*, 35(1):93–103, 2012.

[8] B. Bonnard, J.-B Caillau, and E. Trélat. Geometric optimal control of elliptic keplerian orbits. *Discrete Contin. Dyn. Syst. Ser. B*, 5(4):929–956, 2005.

[9] B. Bonnard, J.-B Caillau, and E. Trélat. Second-order optimality conditions in the smooth case and applications in optimal control. *ESAIM Control Optimization and Calculus of Variation*, 13(2):207–236, 2007.

[10] B. Bonnard and M. Chyba. *Singular Trajectories and Their Role in Control Theory*. Springer, 2003.

[11] T. J Brand, D. W Brown, and J. P Higgins. Space shuttle gnc equation document no. 124. unified powered flight guidance. Technical Report 9-10268, NASA, 1973.

[12] J. V Breakwell and J. F Dixon. Minimum-fuel rocket trajectories involving intermediate-thrust arcs. *Journal of Optimization Theory and Applications*, 17(5/6):465–479, 1975.

[13] J. V Breakwell and Y. C Ho. On the conjugate point condition for the control problem. *International Journal of Engineering Science*, 2:565–579, 1965.

[14] J. V. Breakwell, J. L. Speyer, and A. E. Bryson. Optimization and control of nonlinear systems using the second variation. *SIAM Journal on Control*, 1(2), 1963.

[15] R. G Brusch and T. L Vincent. Numerical implementation of a second-order variable endpoint condition. *AIAA Journal*, 8(12):2230–2235, 1970.

[16] A. E. Bryson and Y. C. Ho. *Applied Optimal Control*. Blaisdell, Waltham, Mass., 1969.

[17] J.-B Caillau and B. Daoud. Minimum time control of the restricted three-body problem. *SIAM Journal of Control and Optimization*, 50(6):3178–3202, 2012.

[18] J.-B Caillau, B. Daoud, and J. Gergaud. Minimum fuel control of the planar circular restricted three-body problem. *Celestial Mechanics and Dynamical Astronomy*, 114:137–150, 2012.

[19] J.-B Caillau, J. Gergaud, and J. Noailles. 3d geosynchronous transfer of a satellite: Continuation on the thrust. *Journal of Optimization Theory and Applications*, 118(3):541–565, 2003.

[20] J.-B Caillau and J. Noailles. Coplanar control of a satellite around the earth. *ESAIM Control Optim. and Calc. Var.*, 6:239–258, 2001.

[21] A. J Calise, N. Melamed, and S. Lee. Design and evaluation of a three-dimensional optimal ascent guidance algorithm. *Journal of Guidance, Control, and Dynamics*, 21(6):867–875, 1998.

[22] Z. Chen. L^1-optimality conditions for the circular restricted three-body problem. *Celestial Mechanics and Dynamical Astronomy*, (to appear), 2016.

[23] Z. Chen, J.-B Caillau, and Y. Chitour. L^1-minimization for mechanical systems. *SIAM Journal on Control and Optimization*, 54(3):1245–1265, 2016.

[24] Z. Chen and Y. Chitour. Controllability of keplerian motion with low-thrust control systems. In M. Bergounioux, J.-B. Caillau, T. Haberkorn, G. Peyré, and C. Schnörr, editors, *In Variational methods in imaging, geometric control and related fields.*, volume 18 of *Radon series on Computational and Applied Mathematics*. De Gruyter, September 2016.

[25] C.-H. Chuang, T. D Goodson, L. A Ledsinger, and J. Hanson. Optimality and guidance for plannar multiple-burn orbital transfers. *Journal of Guidance, Control, and Dynamics*, 23(2):241–250, 1996.

[26] H. D Curtis. *Orbital mechanics for engineering students*. Elsevier, 2005.

[27] I. Ekeland. Discontinuités de champs hamiltoniens et existence de solutions optimales en calcul des variations. *Publ. Math. Inst. Hautes Études Sci*, 47:5–32, 1977.

[28] M. Flies and M. Hazewinkel, editors. *Envelopes, Conjugate Points and Optimal Bang-Bang Extremals*, Dordrecht, the Netherlands, 1987. in Proc. 1985 Paris Conf. on Nonlinear Systems, Reidel Publishers.

[29] R. E Foerster and I. Flügge-Lotz. A neighboring optimal feedback control scheme for systems using discontinuous control. *Journal of Optimization Theory and Applications*, 8(5):367–395, 1971.

[30] A. T Fuller. The absolute optimality of a nonlinear control system with integral-square-error criterion. *Journal of Electronics and Control*, 17(1):301–317, 1964.

[31] J. Gergaud and T. Haberkorn. Homotopy method for minimum consumption orbital transfer problem. *ESAIM: Control, Optimization and Calculus of Variations*, 12:294–310, 2006.

[32] R. Ghezzi, M. Caponigro, B. Piccoli, and E. Trélat. Regularization of chattering phenomena via bounded variation controls. In *NetCo 2014*, Tours, France, 2014.

[33] D. G. Hull. *Optimal Control Theory for Applications*. Mechanical Engineering Series. Springer-Verlag, 2003.

[34] F. Jean. *Control of nonholonomic systems: From sub-Riemannian geometry to motion planning*. Springer, 2014.

[35] D. J Jezewski. Optimal analytical multiburn trajectories. *AIAA Journal*, 10(5):680–685, 1972.

[36] J.-W Jo and J. E Prussing. Procedure for applying second-order conditions in optimal control problems. *Journal of Guidance, Control, and Dynamics*, 23(2):241–250, 2000.

[37] B. K Joosten. Descent guidance and mission planning for space shuttle. In *Space Shuttle Technology Conference*, pages 113–124, 1985.

[38] V. Jurdjevic. *Geometric Control Theory*. Cambridge University Press, 1997.

[39] H. J. Kelley. Guidance theory and extremal fields. *IRE Transation on Automatic Control*, AC-7(5):75–82, 1962.

[40] H. J Kelley. An optimal guidance approximation theory. *IEEE Trans.*, AC-9:375–380, 1964.

[41] H. J Kelley, R. E Kopp, and A. G Moyer. *Singular Extremals*, volume 1 of *Optimization–Theory and Applications*. Academic Press, New York, 1966.

[42] A. L Kornhauser and P. M Lion. Optimal deterministic guidance for bounded-thrust spacecrafts. *Celestial Mechanics*, 5:261–281, 1972.

[43] B. Kugelmann and H. J Pesch. New general guidance method in constrained optimal control, part 1: Numerical method. *Journal of Optimization Theory and Applications*, 67(3):421–446, 1990.

[44] B. Kugelmann and H. J Pesch. New general guidance method in constrained optimal control, part 2: Application to space shuttle guidance. *Journal of Optimization Theory and Applications*, 67(3):437–446, 1990.

[45] I. Kupka. Geometric theory of extremals in optimal control problems i: The fold and maxwell case. *Trans. Amer. Math. Soc.*, 299(1):225–243, 1987.

[46] D. F Lawden. Optimal intermediate-thrust arcs in a gravitational field. *Acta Astronautica*, 8:106–123, 1961.

[47] D. F Lawden. *Optimal Trajectories for Space Navigation*. Butterworth, London, 1963.

[48] I. Lee. Optimal trajectory, guidance, and conjugate points. *Information and Control*, 8:589–606, 1965.

[49] P. Lu. A general nonlinear guidance law. In *AIAA Paper*, number 94–3632, August 1994.

[50] P. Lu, B. Griffin, G. Dukeman, and F. Chavez. Rapid optimal multi-burn ascent planning and guidance. *Journal of Guidance, Control, and Dynamics*, 31(6):1156–1164, 2008.

[51] P. Lu and B. Pan. Highly constrained optimal launch ascent guidance. *Journal of Guidance, Control, and Dynamics*, 33(3):756–767, 2010.

[52] P. Lu, H. Sun, and B. Tsai. Closed-loop endoatmospheric ascent guidance. *Journal of Guidance, Control, and Dynamics*, 26(2):283–294, 2003.

[53] C. Marchal. Chattering arcs and chattering controls. *Journal of Optimization Theory and Applications*, 11(5):441–486, 1973.

[54] H. Maurer and N. P Osmolovskii. Second order sufficient conditions for time-optimal bang-bang control problems. *SIAM Journal on Control and Optimization*, 42(6):2239–2263, 2004.

[55] J. E Mcintyre. Neighboring optimal terminal control with discontinuous forcing functions. *AIAA Journal*, 4(1):141–148, 1966.

[56] D. Mcneal. *Neighboring Optimal Control of Nonlinear Systems Using Bounded Control*. PhD thesis, Stanford University, Aero-Astronautcs Sudaar, 1967.

[57] P. M Mermau and W. F Powers. Conjugate point properties for linear quadratic problems. *Journal of Mathematical Analysis and Applications*, 55:418–433, 1976.

[58] G. Mingotti, F. Topputo, and F. Bernelli-Zazzera. Low-energy, low-thrust transfers to the moon. *Celestial Mechanics and Dynamical Astronomy*, 105(1–3):61–74, 2009.

[59] BepiColombo mission:. sci.esa.int/bepicolombo.

[60] Lisa Pathfinder mission:. sci.esa.int/lisa-pathfinder.

[61] D. S. Naidu. *Aeroassisted Orbital Transfer: Guidance and Control Strategies*. Springer-Verlag, New York, 1994.

[62] D. S. Naidu, J. L. Hibey, and C. D Charalambous. Neighboring optimal guidance for aeroassisted orbital transfers. *in Aerospace and Electronic Systems, IEEE Transaction on*, 29(3):656–665, 1993.

[63] J. Noble and H. Schättler. Sufficient conditions for relative minima of broken extremals in optimal control theory. *Journal of Mathematical Analysis and Applications*, 269:98–128, 2002.

[64] N. P Osmolovskii and H. Maurer. Equivalence of second order optimality conditions for bang-bang control problems, part 1: Main results. *Control Sybernet*, 34(3):927–950, 2005.

[65] N. P Osmolovskii and H. Maurer. Equivalence of second order optimality conditions for bang-bang control problems, part 2: Proofs, variational derivatives and representations. *Control Sybernet*, 36(1):5–45, 2007.

[66] N. P Osmolovskii and H. Maurer. *Applications to Regular and Bang-Bang Control: Second-Order Necessary and Sufficient Optimality Conditions in Calculus of Variations and Optimal Control*. Advances in Decision and Control. 2014.

[67] M. T Ozimek and K. C Howell. Low-thrust transfers in the earth-moon system, including applications to libration point orbits. *Journal of Guidance, Control, and Dynamics*, 33(2):533–549, 2010.

[68] B. Pan, Z. Chen, P. Lu, and B. Gao. Reduced transversality conditions for optimal space trajectories. *Journal of Guidance, Control, and Dynamics*, 36(5):1289–1300, 2013.

[69] C. Park. Necessary conditions for the optimality of singular arcs of spacecraft trajectories subject to multiple gravitational bodies. *Advances in Space Research*, 51:2125–2135, 2013.

[70] H. J. Pesch. Neighboring optimum guidance of a space-shuttle-orbiter-type vehicle. *Journal of Guidance, Control, and Dynamics*, 3(5):386–391, 1980.

[71] L. Poggiolini and G. Stefani. State-local optimality of a bang-bang trajectory: a hamiltonian approach. *Systems & Control Letters*, 53:269–279, 2004.

[72] L. Poggiolini and G. Stefani. Sufficient optimality conditions for a bang-singular extremal in the minimum time problem. *Control and cybernetics*, 37(2), 2008.

[73] M. Pontani, G. Cecchetti, and P. Teofilatto. Variable-time-domain neighboring optimal guidance applied to space trajectories. *Acta Astronautica*, 115:102–120, 2015.

[74] M. Pontani, G. Cecchetti, and P. Teofilatto. Variable-time-domain neighboring optimal guidance, part 1: Algorithm structure. *Journal of Optimization Theory and Applications*, 166:76–92, 2015.

[75] M. Pontani, G. Cecchetti, and P. Teofilatto. Variable-time-domain neighboring optimal guidance, part 2: Application to lunar descent and soft landing. *Journal of Optimization Theory and Applications*, 166:93–114, 2015.

[76] L. S Pontryagin, V. G Boltyanski, R. V Gamkrelidze, and E. F Mishchenko. *The Mathematical Theory of Optimal Processes (Russian)*. English translation: Interscience, 1962.

[77] J. E Prussing and S. L Sandrik. Second-order necessary conditions and sufficient conditions applied to continuous-thrust trajectories. *Journal of Guidance, Control, and Dynamics*, 28(4):812–816, 2005.

[78] H. M Robbins. Optimality of intermediate-thrust arcs of rocket trajectories. *AIAA Journal*, 3(6):1094–1098, 1965.

[79] S. D Ross and D. J Scheeres. Multiple gravity assists, capture, and escape in the restricted three-body problem. *SIAM Journal of Applied Dynamics and Systems*, 6(3):576–596, 2007.

[80] A. V Sarychev. The index of second variation of a control system. *Mat. Sb.*, 41:338–401, 1982.

[81] A. V Sarychev. First and second-order sufficient optimality conditions for bang-bang controls. *SIAM Journal on Control and Optimization*, 35(1):315–340, 1997.

[82] H. Schättler and U. Ledzewicz. *Geometric Optimal Control: Theory, Methods, and Examples*. Springer, 2012.

[83] H. Seywald and E. M Cliff. Neighboring optimal control based feedback law for the advanced launch system. *Journal of Guidance, Control, and Dynamics*, 17(6):1154–1162, 1994.

[84] I. Shafieenejad, A. B. Novinzadeh, and R. Shisheie. Analytical mathematical feedback guidance scheme for low-thrust orbital plane change manoeuvres. *Mathematical and Computer Modelling*, 58(11–12):1714–1726, 2013.

[85] C. Silva and E. Trélat. Asymptotic approach on conjugate points for minimal time bang-bang controls. *Systems and Control Letters*, 59:720–733, 2010.

[86] Hampath software:. hampath.org.

[87] E. D Sontag. *Mathematical control theory*. Springer, 1998.

[88] J. L. Speyer and A. E. Bryson. A neighboring optimum feedback control scheme based on extimated time-to-go with application to reentry flight paths. *AIAA Journal*, 6(5), 1968.

[89] H. J Sussmann. Geometry and optimal control in mathematical control theory. In J. Baillieul and J. C Willems, editors, *Dedicated to Roger W. Brockett on his 60th birthday*. Springer, 1998.

[90] H. J Sussmann. Résultats récents sur les courbes optimalse in quelques aspects de la théori du controle. In *Journée Annuelle de la Société Mathématique de France*, 2000.

[91] V. Szebehely. *Theory of Orbits: The Restricted Problem of Three Bodies*. Academic Press, Massachusetts, 1967.

[92] G. Vossen and H. Maurer. On L^1-minimization in optimal control and applications to robotics. *Optimal Control Applications and Methods*, 59:301–321, 2006.

[93] L. J Wood. Second-order optimality conditions for the bolza problem with endpoints variable. *Journal of Aircraft*, 11(4):212–221, 1974.

[94] O. Zarrouati. *Trajectories Spatiales*. CNES Cepadues, 1987.

[95] M. I Zelikin and V. F Borisov. *Theory of Chattering Control with Applications to Astronautics, Robotics, Economics, and Engineering*. Birkhäuser, 1994.

[96] M. I Zelikin and V. F Borisov. Optimal chattering feedback control. *Journal of Mathematical Sciences*, 114(3):1227–1344, 2003.

université PARIS-SACLAY | École doctorale de mathématiques Hadamard (EDMH)

Titre :.....Minimisation L^1 en Mécanique Spatiale..... .....

Mots clés : contrôle optimal, extrémales brisées, conditions suffisantes, mécanique spatiale

Résumé : Une question importante en mécanique spatiale est de contrôler le mouvement d'un satellite soumis à la gravitation de corps célestes de telle sorte que certains indices de performance soient minimisés. Dans cette thèse, nous nous intéressons à la minimisation de la norme L^1 du contrôle pour le problème circulaire restreint des trois corps (ce coût modélise la consommation de l'engin spatial). Les conditions nécessaires à l'optimalité sont obtenues en utilisant le principe du maximum de Pontryagin, révélant l'existence de contrôles bang-bang et singuliers. En dimension finie, le problème de minimisation L^1 est bien connu pour générer des solutions où le contrôle a des propriétés de parcimonie ; les contrôles bang-bang traduisent cette même propriété, alors que l'existence de contrôles singuliers est une spécificité de la dimension infinie. En s'appuyant sur les résultats de Marchal et Zelikin, la présence du phénomène de Fuller est mise en évidence par l'analyse des extrémales singulières. La contrôlabilité pour le problème à deux corps (un cas dégénéré du problème circulaire restreint des trois corps) avec un contrôle prenant des valeurs dans une boule euclidienne est établie, puis facilement étendue au problème des trois corps, le champ de vecteurs correspondant à la dérive étant récurrent. En conséquence, si les trajectoires contrôlées admissibles restent dans un compact fixé, l'existence des solutions du problème de minimisation L^1 peut être obtenue par une combinaison du théorème de Filippov et une procédure appropriée de convexification. Les questions de contrôlabilité sous contraintes d'état sont également abordées. Bien que le principe du maximum de Pontryagin permette d'identifier les candidats à être solutions du problème de minimisation L^1, il ne peut garantir que ces candidats soient localement optimaux, sauf si certaines conditions d'optimalité suffisantes sont satisfaites. Dans cette thèse, l'idée cruciale pour obtenir de telles conditions pour des extrémales brisées est de plonger celles-ci dans un champ d'extrémales, en utilisant le point de vue d'Ekeland et Kupka ("compétition entre hamiltoniens"). En l'absence de singularité pli, deux types de conditions sont proposées. Dans le cas de points terminaux fixés, ces conditions sont suffisantes pour garantir que l'extrémale de référence est localement minimisante tant que chaque point de commutation est régulier. Si le point terminal n'est pas fixe mais appartient à une sous-variété lisse, une condition suffisante supplémentaire impliquant la géométrie de cette variété cible est établie. L'application au calcul d'extrémales voisines en minimisation L^1 est finalement considérée.

Université Paris-Saclay
Espace Technologique / Immeuble Discovery
Route de l'Orme aux Merisiers RD 128 / 91190 Saint-Aubin, France

université PARIS-SACLAY | École doctorale de mathématiques Hadamard (EDMH)

Title :.....L^1-Minimization for Space Mechanics.....

Keywords : optimal control; broken extremals; sufficient conditions ; space mechanics

Abstract : An important question in space mechanics is to control the motion of a satellite in the gravitational field of celestial bodies, in order that prescribed performance indices are minimized. In this work, we are interested in minimizing the L^1 norm of the control for the circular restricted three-body problem. (This cost models theconsumption of the spacecraft.) Necessary conditions for optimality are obtained thanks to Pontryagin maximum principle, revealing the existence of both bang and singular controls. In finite dimension, minimizing L^1 norms is well known to generate parsimonious solutions; bang controls account for this property whereas the existence of singular ones is a peculiarity of the infinite dimensional setting. Building upon Marchal and Zelikin results, the occurence of the Fuller phenomenon is related to singular extremals of order two. The controllability of the two-body problem (a degenerate subcase of the three-body problem) with a control valued in a Euclidean ball is established, then easily extended to the restricted three-body case by using the recurrence of the drift on a appropriate submanifold. As a result, provided that the trajectories remain into a fix compact subset, existence of solution for the L^1 minimization problem is obtained by combining Filippov's theorem with a suitable convexification procedure. Controllabilty under specific state constraints is also addressed. Although the maximum principle allows to select candidates to be L^1 minimizers, it cannot guarantee that these candidates are locally optimal unless sufficient optimality conditions hold. In this work, the idea to obtain such conditions for broken extremals is to embed these into a field of extremals, using moreover Ekeland and Kupka point of view ("competing Hamiltonians"). In the absence of fold singularity, two types of conditions are devised. In the case of fixed endpoints, these conditions are sufficient for local optimality whenever switching points are regular ones. When the terminal point lies on a whole submanifold, an additional condition involving the geometry of this target manifold has to be taken into account.These results are eventually applied to the computation of neighbouring extremals for L^1 minimization.

Université Paris-Saclay
Espace Technologique / Immeuble Discovery
Route de l'Orme aux Merisiers RD 128 / 91190 Saint-Aubin, France